VOLUME 123 NUMBER 3

# THE ASTROPHYSICAL JOURNAL

AN INTERNATIONAL REVIEW OF SPECTROSCOPY AND ASTRONOMICAL PHYSICS

MAY 1956

PROPORTIONALITY OF NEBULAR RED SHIFTS TO WAVE LENGTH
*R. Minkowski and O. C. Wilson* 373
ON THE H AND K EMISSION IN DWARF STARS *Daniel M. Popper* 377
A SPECTROPHOTOMETRIC ANALYSIS OF THE BRIGHTEST HERBIG-HARO OBJECT *Karl-Heinz Böhm* 379
COMPLEX LINES IN THE SPECTRUM OF RW CEPHEI
*Paul W. Merrill and Olin C. Wilson* 392
THE RADIAL VELOCITY OF DQ CEPHEI = HD 199908
*J. Sahade, O. Struve, O. C. Wilson, and V. Zebergs* 399
ON THE LUMINOSITIES, MOTIONS, AND SPACE DISTRIBUTION OF THE NEARER NORTHERN O–B5 STARS *A. Blaauw* 408
SIX-COLOR PHOTOMETRY OF STARS. VIII. THE COLORS OF 409 STARS OF DIFFERENT SPECTRAL TYPES *Joel Stebbins and Gerald E. Kron* 440
VARIATIONS IN THE STELLAR LUMINOSITY FUNCTION. VIII. A SUMMARY OF RESULTS *S. W. McCuskey* 458
CORRELATION PROBLEMS IN THE STUDY OF THE BRIGHTNESS OF THE MILKY WAY *Alladi Ramakrishnan and S. K. Srinivasan* 479
ON THE OPTICAL PROPERTIES OF INTERSTELLAR DUST *John R. Platt* 486
NONTHERMAL RADIO EMISSION OF THE GALAXY AND THE ORIGIN OF COSMIC RADIATIONS *C. Y. Fan* 491
THE EQUILIBRIUM OF A SELF-GRAVITATING INCOMPRESSIBLE FLUID SPHERE WITH A MAGNETIC FIELD. I *Kevin H. Prendergast* 498
THE EXTERNAL ELECTRIC FIELD OF A ROTATING MAGNET *George Backus* 508
MODEL ATMOSPHERES FOR A-TYPE STARS *Kiyotsu Osawa* 513
CLASSIFICATION OF EMISSION LINES λ 5694 AND λ 5446 IN THE SOLAR CORONA *F. Rohrlich* 521
CORONAL TEMPERATURE DETERMINATION FROM EMISSION LINES
*Donald E. Billings, Sabine Hirsch, and Carlos Varsavsky* 532
THE HELIUM EQUILIBRIUM IN PROMINENCES AND THE CHROMOSPHERE *Harold Zirin* 536
AN INVESTIGATION OF FAINT LINES IN THE SOLAR SPECTRUM BETWEEN 5000 A AND 6000 A *Romuald Zalubas* 544
NOTES
ON THE SPACE REDDENING OF DELTA CEPHEI AND ETA AQUILAE *Daniel L. Harris III* 549
POLARIZATION IN THE JET OF MESSIER 87 *W. Baade* 550
ABSTRACTS OF ASTROPHYSICAL JOURNAL SUPPLEMENT SERIES
STELLAR SPECTRA IN MILKY WAY REGIONS. V. A REGION IN MONOCEROS. VI. A REGION IN CAMELOPARDALIS *S. W. McCuskey* 552
ANNOUNCEMENT 552
ERRATA 552
INDEXES 553

THE UNIVERSITY OF CHICAGO PRESS
CHICAGO, ILLINOIS, U.S.A.

May 1956 Vol. 123, No. 3

# THE ASTROPHYSICAL JOURNAL

## AN INTERNATIONAL REVIEW OF SPECTROSCOPY AND ASTRONOMICAL PHYSICS

Founded in 1895 by George E. Hale and James E. Keeler

Published in Collaboration with the American Astronomical Society

S. CHANDRASEKHAR
*Managing Editor*

A. BLAAUW
*Associate Editor*

Yerkes Observatory of the University of Chicago

EDITORIAL BOARD

HAROLD F. WEAVER (1956-60)
Berkeley Astronomical Department
University of California

MARTIN SCHWARZSCHILD (1954-58)
Princeton University Observatory

LEO GOLDBERG (1955-59)
The Observatory of the University of Michigan

HORACE W. BABCOCK (1953-57)
Mount Wilson Observatory of the Carnegie Institution of Washington

G. HERZBERG (1952-56)
National Research Council, Ottawa

---

**The Astrophysical Journal** is published bimonthly by the University of Chicago at the University of Chicago Press, 5750 Ellis Avenue, Chicago 37, Illinois, during January, March, May, July, September, and November. ¶Two volumes are published per year, one beginning with the January issue and the other beginning with the July issue. On all orders from the United States and its possessions the subscription price is $7.50 per volume or $15.00 per year; the price of single copies is $3.50. ¶On all orders from Canada the subscription price is $8.00 per volume or $16.00 per year; the price of single copies is $3.65. On all orders from all other countries the subscription price is $8.25 per volume or $16.50 per year; the price of single copies is $3.75. (Orders for service of less than a volume will be charged at the single-copy rate.) ¶Subscriptions are payable in advance. Please make all remittances payable to The University of Chicago Press, in United States currency or its equivalent by postal or express money orders or bank drafts. (Exception: members of The American Astronomical Society must send their subscriptions and remittances to the Treasurer of the Society.)

**The following is an authorized agent:**

For the British Commonwealth, except North America and Australasia: The Cambridge University Press, Bentley House, 200 Euston Road, London, N.W. 1, England. Prices of yearly subscriptions and of single copies may be had on application.

**Claims for missing numbers** should be made within the month following the regular month of publication. The publishers expect to supply missing numbers free only when losses have been sustained in transit, and when the reserve stock will permit.

**Business correspondence** should be addressed to The University of Chicago Press, Chicago 37, Illinois.

**Communications** for the editors and manuscripts should be addressed to: S. Chandrasekhar, Editor of THE ASTROPHYSICAL JOURNAL, Yerkes Observatory, Williams Bay, Wisconsin.

**Line drawings and photographs** should be made by the author, and all marginal notes such as co-ordinates, wave lengths, etc., should be included in the cuts. It will not be possible to set up such material in type.

**One copy of the corrected galley proof** should be returned as soon as possible to the editor, Yerkes Observatory, Williams Bay, Wisconsin. Authors should take notice that the manuscript will not be sent to them with the proof.

**The cable address** is "Observatory, Williamsbay, Wisconsin."

**The articles in this journal** are indexed in the *International Index to Periodicals*, New York, N.Y.

**Applications for permission to quote** from this journal should be addressed to The University of Chicago Press, and will be freely granted.

**Microfilms of complete journal volumes** are available to regular subscribers only and may be obtained at the end of the year. Orders and inquiries should be addressed to University Microfilms, 313 North First Street, Ann Arbor, Michigan.

**Notice to subscribers:** If you change your address, please notify us and your local postmaster immediately.

Entered as second-class matter, July 31, 1940, at the Post-Office at Chicago, Ill., under the Act of March 3, 1879.
Acceptance for mailing at special rate of postage provided for in United States Postal Act of October 3, 1917, Section 1103, amended February 28, 1925.
Copyright 1956 by the University of Chicago.

[PRINTED IN U.S.A.]

# THE ASTROPHYSICAL JOURNAL

AN INTERNATIONAL REVIEW OF SPECTROSCOPY AND ASTRONOMICAL PHYSICS

VOLUME 123 MAY 1956 NUMBER 3


## PROPORTIONALITY OF NEBULAR RED SHIFTS TO WAVE LENGTH


R. MINKOWSKI AND O. C. WILSON

Mount Wilson and Palomar Observatories

Carnegie Institution of Washington, California Institute of Technology



*Received January 30, 1956*



ABSTRACT

Measures of the red shift $c\delta\lambda/\lambda_0$ for the colliding galaxies Cygnus A give the value 16812 ± 9 km/sec for the mean wave length 3830 A and 16798 ± 7 km/sec for the mean wave length 6472 A. The relative change in the red shift with wave length is less than $3 \times 10^{-4}$ per 1000 A. Combination of the optical results with those by Lilley and McClain for the 21-cm hydrogen line shows that the relative change is less than $3 \times 10^{-9}$ per 1000 A.


Since the discovery of the nebular red shift, its wave-length dependence has been investigated at various times. The result of these investigations has always been that the red shift is proportional to wave length, as is to be expected if the shift is due to a Doppler effect caused by a recession of the galaxies. The relevant data for three galaxies are given in historical order in Table 1. The second column gives the quantity $v = c\delta\lambda/\lambda_0$, which is expected to be independent of wave length if the shift is a Doppler effect. The third and fourth columns give the variation $\Delta v = c[(\delta\lambda_1/\lambda_{1,0}) - (\delta\lambda_2/\lambda_{2,0})]$ reduced to a wave-length range of 1000 A and its mean error. In the fifth and sixth columns are given the relative change $\Delta v/v$ per 1000 A and its mean error. These data have been derived from least-squares solutions of the observed red shifts in the spectral range stated in the last column. The data for the brightest galaxy in the Leo cluster and for NGC 1275 are by Humason (1931); those for NGC 4151 by Wilson (1949). At no time have the observations indicated a significant deviation from proportionality between red shift and wave length.

Rather precise measures are available for near-by bright galaxies, such as NGC 224. A large part of the radial velocities of such objects may be due to their peculiar motions; this is certainly true for those galaxies whose velocities, corrected for galactic rotation, are negative. Such galaxies are unsuitable for an investigation of the wave-length dependence of the red shift. The dispersion among peculiar nebulae has been estimated by Hubble (1936) to be of the order of 200 km/sec. The significance of the result obtained for NGC 4151 is therefore probably not destroyed by the peculiar motion of this galaxy.

A much more precise test has become possible by the discovery of a pair of galaxies in collision which are to be identified with the strong radio source Cygnus A (Baade and Minkowski 1954). The spectrum of this object contains strong emission lines, so that a

precise determination of the red shift of 16800 km/sec seemed to be possible. The faintness of the object ($m_{ph} = 17.9$) does not permit the use of high dispersion. Two exposures in the violet and three exposures in the red were obtained with the nebular spectrograph at the prime focus of the 200-inch telescope; the relevant data are given in Table 2. Essentially higher dispersions than those used would have led to prohibitive exposure time. The gain in accuracy would have been small, since the lines have a width of about 500 km/sec. Each plate was measured twice, once by each of the authors. The results are given in Table 3, which contains the individual values and the mean value of $c\delta\lambda/\lambda_0$ for each line. The wave lengths of the lines used are those determined by Bowen (1955). The two lines of the [O II] doublet λ 3726.04/3728.80 are not resolved. The wave length of the blend depends on the intensity ratio of the lines, which varies with the electron density of the gas (Osterbrock 1955; Seaton 1955) from 1:2 at high density to 1.5:1 at low density. The average density of the gas in galaxies is very low, and we have therefore

TABLE 1

WAVE-LENGTH DEPENDENCE OF RED SHIFT FROM PREVIOUS INVESTIGATIONS

| Galaxy | $c\delta\lambda/\lambda_0$ (km/sec) | $\Delta v$ (km/sec) | m.e. (km/sec) | $\Delta v/v$ | m.e. | Range (A) |
|---|---|---|---|---|---|---|
| NGC 1275 | + 5200 | − 41 | ±228 | 0.0078 | ±0.043 | 3727–4861 |
| Leo cluster | +19700 | −422 | ±366 | .021 | ± .019 | 3933–4340 |
| NGC 4151 | + 967 | + 2.2 | ± 1.0 | 0.0023 | ±0.001 | 3425–6583 |

TABLE 2

LIST OF EXPOSURES

| Plate No. | Exposure (hours) | Dispersion (A/mm) | Range |
|---|---|---|---|
| N 260 | 5.5 | 170 | 3600–4400 |
| N 265 | 6.5 | 170 | 3600–4400 |
| N 261 | 5.5 | 215 | 6500–7000 |
| N 262 | 5.5 | 215 | 6500–7000 |
| N 263 | 7 | 215 | 6500–7000 |

assumed that the wave length of the blend is λ 3727.70, the limit for low density. From the entries in Table 3 the mean value 16812 km/sec, with a mean error of ±9 km/sec, is found for the mean wave length 3830 A of the lines in the blue region. Some doubt exists whether the [O I] line 6363.82 should be disregarded or not in forming the mean for the red region. This line was found difficult to measure because of the presence of [Fe X] λ 6374. If the line is used, the mean value of the red shift for the mean wave length of the red region λ 6472 becomes 16791 km/sec, with a mean error of ±9 km/sec. If the line is disregarded, the mean value becomes 16798 km/sec, with a mean error of ±7 km/sec. This second value seems to deserve more confidence. The mean value of the red shift then is 16805 km/sec. The variation of the red shift per 1000 A becomes

$$\Delta v = 5.2 \text{ km/sec} \pm 6.1 \text{ km/sec (m.e.)},$$

and the corresponding relative change per 1000 A is

$$\frac{\Delta v}{v} = 0.00031 \pm 0.00036 \text{ (m.e.)}.$$

This establishes the proportionality between red shift and wave length with about eight times higher precision than that obtained for NGC 4151.

Three doublets are represented by the measured lines. In Table 4 are given the doublet separations for zero velocity, the separation expected for a red shift of 16805 km/sec, and the observed separations. The agreement between expected and observed separations is satisfactory, except possibly for the [O I] doublet containing $\lambda$ 6363.82, which should probably be disregarded, as mentioned above. Within the relatively low accuracy with which the doublet separations could be determined, they increase in the same way as the wave lengths themselves and do not admit an intrinsic change of the separation.

TABLE 3

MEASURED VALUES OF $c\delta\lambda/\lambda_0$

| PLATE NO. | $\lambda_0$ | | | | | | | | | |
|---|---|---|---|---|---|---|---|---|---|---|
| | [Ne V] 3425.87 | | [O II] 3727.70 | | [Ne III] 3868.76 | | [Ne III] 3967.47 | | Hδ 4101.74 | |
| | OCW | RM | OCW | RM | OCW | RM | OCW | RM | OCW | RM |
| N 260 | 16797 | 16830 | 16833 | 16842 | 16825 | 16805 | 16827 | 16867 | ... | 16820 |
| N 265 | 16772 | 16795 | 16776 | 16846 | 16832 | 16800 | 16829 | 16823 | 16748 | 16786 |
| Mean | 16798 | | 16824 | | 16816 | | 16836 | | 16785 | |

| PLATE NO. | $\lambda_0$ | | | | | | | | | |
|---|---|---|---|---|---|---|---|---|---|---|
| | [O I] 6300.31 | | [O I] 6363.82 | | [N II] 6548.06 | | Hα 6562.82 | | [N II] 6583.37 | |
| | OCW | RM | OCW | RM | OCW | RM | OCW | RM | OCW | RM |
| N 261 | 16765 | 16778 | 16719 | 16761 | 16801 | 16807 | 16784 | 16790 | 16843 | 16796 |
| N 262 | 16820 | 16777 | 16719 | 16795 | 16835 | 16817 | 16754 | 16736 | 16814 | 16760 |
| N 263 | 16827 | 16830 | 16812 | 16753 | 16811 | 16827 | 16806 | 16810 | 16812 | 16776 |
| Mean | 16800 | | 16761 | | 16813 | | 16780 | | 16800 | |

TABLE 4

DOUBLET SEPARATIONS (IN A)

| Doublet | $\Delta\lambda_0$ | $\Delta\lambda$ Expected | $\Delta\lambda$ Observed |
|---|---|---|---|
| [Ne III] $^3P_n-{}^1D$ | 98.71 | 104.24 | $104.64\pm0.34$ |
| [O I] $^3P_n-{}^1D$ | 63.51 | 67.01 | $66.08\pm0.41$ |
| [N II] $^3P_n-{}^1D$ | 35.31 | 37.29 | $36.94\pm0.66$ |

Quite recently Lilley and McClain (1956) have observed the red shift of the 21-cm line of neutral hydrogen in Cygnus A appearing as an absorption line on the background of the nonthermal radio radiation of the object. Their value of 16700 km/sec, with an estimated uncertainty of $\pm 50$ km/sec according to a private communication, agrees satisfactorily with the red shift determined in the optical region. If radio and optical values are combined, the variation in the red shift per 1000 A becomes

$$\Delta v = 5 \times 10^{-5} \text{ km/sec} \pm 3 \times 10^{-5} \text{ km/sec},$$

and the corresponding relative change per 1000 A is

$$\frac{\Delta v}{v} = 3 \times 10^{-9} \pm 2 \times 10^{-9}.$$

Actually, the 21-cm line is due to a transition between fine-structure levels of hydrogen. The result for the 21-cm line therefore also confirms with high accuracy that the fine-structure separation remains unaffected by the red shift.

Some uncertainty exists concerning the quantitative significance of the result of the comparison of optical and radio data. The optical data obviously refer to ionized gas in the object, the radio data to neutral gas in front of the object observed in projection against those parts of the object which emit nonthermal radio radiation. Since different parts of the object are involved, the observed velocities will be affected by differential motions and need not be exactly equal. An indication of this is possibly that the 21-cm line has a width of about 800 km/sec, about twice that of the optical lines. A complicated structure of the line should occur if either the neutral gas or the nonthermal emission or both are distributed nonuniformly in the system. Actually, the 21-cm results suggest at least the possibility that the 21-cm line is double. A doubling of the line is to be expected if the nonthermal radiation is emitted in two far outlying parts of the object as the radiointerferometric results by Jennison and Das Gupta (1953) indicate.

## REFERENCES

Baade, W., and Minkowski, R. 1954, *Ap. J.*, **119**, 206.
Bowen, I. S. 1955, *Ap. J.*, **121**, 306.
Hubble, E. 1936, *Ap. J.*, **84**, 270.
Humason, M. L. 1931, *Ap. J.*, **74**, 123. The result for NGC 1275 is derived from the unpublished detailed data which Dr. Humason has kindly made available.
Jennison, R. C., and Das Gupta, M. K. 1953, *Nature*, **172**, 996 and 1030.
Lilley, A. E., and McClain, E. F. 1956, *Ap. J.*, **123**, 172.
Osterbrock, D. 1955, *Ap. J.*, **60**, 175.
Seaton, J. M. 1954, *Ann. d'ap.*, **17**, 74.
Wilson, O. C. 1949, *Pub. A.S.P.*, **61**, 132.

# ON THE H AND K EMISSION IN DWARF STARS*

DANIEL M. POPPER
Department of Astronomy, University of California, Los Angeles
*Received January 23, 1956*

ABSTRACT

Spectrograms of five main-sequence stars with H and K emission failed to show variations of emission-line intensity over a 5-year period, with the exception of a single spectroscopic flare of one of the stars.

This investigation consists of a search for cyclic variations in the intensity of H and K emission lines in the spectra of main-sequence stars. If such emission lines were produced to an appreciable degree in regions of prominence-like activity at the surface of a star, variations of activity would cause variations in emission-line intensity. The activity would have to be on a considerably larger scale than at the surface of the sun for the emission lines to show in the spectrum of the star as a whole. The determination of such a basic quantity as the period of variation for a number of main-sequence stars could afford a valuable clue to the fundamental cause of solar activity. There is no observational evidence for variations in H and K emission other than the occasional stellar "flares" and the statement by Joy and Wilson (1949) that "the intensity of the emission is probably variable to a considerable extent in many stars."

The stars to be observed were chosen from the list of Joy and Wilson (1949) to satisfy the following criteria: Except for the emission lines, they should be apparently normal main-sequence stars, not members of spectroscopic binary systems or associated with known dark matter. The stars should be bright enough that the region of H and K is well exposed on spectrograms of 2 hours' or less exposure with the Cassegrain spectrographs of the 60- and 100-inch telescopes, dispersions about 50 A/mm at H and K. The emission lines should be strong enough to be visible with this dispersion. The stars should be far enough north to be observable through most of the year but not so far north ($\delta > 64°$) as to be out of reach of the 100-inch.

The observations were continued as opportunity offered for a period of about 5 years (1950–1954). The observing list is given in Table 1. With the exception of HD 115953, the spectral classifications are on the MK system, 61 Cyg A and B having been used as standards. The effort was made to keep the density of exposures as nearly equal as possible from plate to plate so that moderate changes in emission-line intensity could be detected by visual inspection, although photometric standards were impressed on each plate. In order to carry out visual comparisons carefully and conveniently, a simple comparison microscope was constructed.

As previously reported (Popper 1953) and shown in Figure 1, HD 234677 showed a spectroscopic "flare" on July 21, 1953. With this single exception, visual comparison of the spectrograms shows no definite intensity changes of H and K emission; i.e., the results of the investigation are essentially negative. Photometry of the spectrograms has not been thought worthwhile because of the great amount of work involved and because of the relatively low accuracy of photographic spectrophotometry of this kind.

The conclusion to be drawn from this investigation is that H and K emission lines in the spectra of main-sequence stars near type M0 are not produced in regions of prominence-like activity or, if they are so produced, the activity is not variable to an appreciable degree.

* This investigation was made possible by a co-operative arrangement with the Mount Wilson and Palomar Observatories.

The lack of variation reported here is in agreement with the result of O. C. Wilson (1954), who compared H and K emission intensities in the spectra of a number of stars obtained with higher dispersion at two epochs separated by 13 years. Feast and Thackeray (1954) likewise found no variation in the K-type dwarf $\epsilon$ Ind observed over two seasons. Although the discovery of cyclic activity in stars other than the sun may be expected to lead to results of considerable importance, its detection appears to be an exceptionally difficult observational problem. Other approaches than the abortive one attempted herein might be a study of variations of frequency of flares in individual stars or of variations in "patchiness" on the surfaces of stars.

TABLE 1

STARS OBSERVED FOR VARIATION IN H AND K EMISSION

| STAR | $m_p$ | SPECTRUM | NO. OF SPECTROGRAMS | |
|---|---|---|---|---|
| | | | 60-Inch | 100-Inch |
| HD 88230 = 20 C 564 | 6.8 | K7 V | 15 | 21 |
| HD 115953 = ADS 8862 A | 8.8 | dM2 | 8 | 12 |
| HD 234677 = GC 25394 | 8.3 | K6 V | 8 | 11 |
| 61 Cyg A | 5.6 | K5 V | 10 | 8 |
| 61 Cyg B | 6.3 | K7 V | 11 | 9 |

It is of interest that the spectroscopic flare occurred in the only star of the observed group that normally shows hydrogen lines in emission, H$\epsilon$ emission being observed on all spectrograms of HD 234677 and H$\alpha$ appearing on coudé plates. As nearly as can be determined from the literature, all late K- or M-type dwarfs that have flared show hydrogen emission in their normal spectra. Other stars with H and K emission found to have hydrogen lines also in emission are $\xi$ Boo B, dK5 (weak H$\epsilon$ emission on coudé plates, H$\alpha$ in absorption), and the spectroscopic binary HD 224085, dK2 (H$\epsilon$ emission on Cassegrain spectrograms, H$\alpha$ emission on coudé plates).

Dr. E. C. Yowell obtained many of the spectrograms upon which this investigation is based.

REFERENCES

Feast, M. W., and Thackeray, A. D. 1954, *M.N.*, **114**, 635.
Joy, A. H., and Wilson, R. E. 1949, *Ap. J.*, **109**, 319.
Popper, D. M. 1953, *Pub. A.S.P.*, **65**, 278.
Wilson, O. C. 1954, *Proc. Nat. Sci. Found. Conference on Stellar Atmospheres*, p. 155.

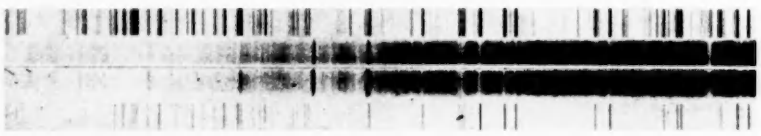

FIG. 1.—Spectrograms of HD 234677. *Above:* March 4, 1950; *below:* July 21, 1953. The spectroscopic flare occurred on the latter date.

# A SPECTROPHOTOMETRIC ANALYSIS OF THE BRIGHTEST HERBIG-HARO OBJECT*

KARL-HEINZ BÖHM†
Lick Observatory, University of California
*Received December 23, 1955*

ABSTRACT

Relative intensities of the emission lines in the spectrum of the brightest Herbig-Haro Object have been determined from three spectrograms taken by Herbig in January, 1955, with the nebular spectrograph of the Crossley reflector. These plates cover the wave-length region λλ 3700–6800. The color index appropriate to the very faint underlying continuum has been estimated as $B-V=+1.3$ mag. for the region λλ 4200–5400, after correction for space reddening.

The most consistent explanation of the intensities of the forbidden lines (except the (Fe II] and [Fe III] lines, for which no transition probabilities and excitation cross-sections are available) can be given if a mean electron temperature of $T_e = 7500°$, a mean electron density of $N_e = 1.3 \times 10^4$ cm$^{-3}$, and a color excess $E_{(B-V)} = 0.4$ mag. are assumed. This color excess agrees with that of the neighboring star BD−6°1253. From the surface brightness in H8, a value of $N_e = 2.5 \times 10^3$ cm$^{-3}$ is derived. The difference between the two values of $N_e$ is probably due to a nonuniform density distribution in the nebula. The rather low value of $T_e$ excludes an interpretation of the relatively high ionization as due to electron impact. Therefore, the most obvious means of explaining the ionization is to assume a strong radiation field in the far ultraviolet. If the radiation is produced by a "central star" (of solar dimensions) in the nebula, a radiation temperature of 24000° for $\lambda < 353$ is required to explain the observed ratio of O II to O III. The observed ratio of the sum of the intensities of all forbidden lines to the intensity of Hβ leads to a radiation temperature of 29000° for $\lambda < 916$. It is shown that this ultraviolet radiation excess cannot be produced by accretion heating. The numerical results are still subject to considerable uncertainty, because of our lack of information about density fluctuations in these objects.

## I. INTRODUCTION

In 1951 Herbig described several peculiar nebulous objects lying in a heavily obscured area in Orion, whose spectra are in some respects intermediate between those of planetary nebulae and ordinary T Tauri stars. Their spectra showed rather strong Balmer lines, strong lines of [O I], [O II], and [S II], faint lines of [Fe II], [Fe III], [O III], and [Ne III], as well as the permitted lines H and K of Ca II and Mg I λ 4571. Herbig emphasized the similarity of the spectra of these objects to that of the nebula closely surrounding T Tauri, which was discovered by Burnham (see Herbig 1950). Herbig found starlike condensations in each object and showed that these "central stars" had approximately the luminosity of K- or M-type dwarfs. He considered it more probable that these objects were late-type dwarfs than that they were very subluminous blue stars. If this is the case, then some unknown mechanism of interaction between a late-type dwarf and the nebular material would be required in order to explain the comparatively high ionization in these nebulae.

Later Haro (1952), on the basis of direct photographs in the infrared, drew the conclusion that the "central stars" (if they were stellar) must be hot blue objects of very low luminosity. Recently Ambarzumian (1954) has suggested that these peculiar nebulous objects,[1] which are obviously in some way associated with the T Tauri stars, should be considered as representing the early stages of newly formed T Tauri stars. Therefore, it

* *Contributions from the Lick Observatory*, Ser. II, No. 58.

† Present address: Institut für Theoretische Physik und Sternwarte, Kiel, Germany.

[1] We follow Ambarzumian in the practice of calling these nebulae "Herbig-Haro Objects"; Herbig (1952) called them "Objects of group D."

seemed of some importance to investigate the physical state of these nebulae and their central stars. To this end, a quantitative analysis has been made of the emission-line spectrum of the brightest of these objects, located near NGC 1999 and called Object No. 1 by Herbig (1951). It is No. 11*a* in the list of Haro (1953). The object was described by Herbig (1951) as looking like "a slightly diffuse star with a very short curved nebulous tail extending for 5″ in p.a. 308°." Its visual magnitude is about 17.2 (see Sec. III).

The organization of the paper is as follows: in Section II the spectrophotometric data for Object No. 1 are given. A mean electron temperature, $T_e$, and a mean electron density of the nebula, $N_e$, are derived in Section III from the relative intensities (corrected for space reddening) of the forbidden lines. This value of $N_e$ is then compared with the electron density derived from the surface brightness in H8. After a demonstration that the ionization in the nebula probably cannot be due to electron impact (but is probably produced by radiation in the far ultraviolet), the strength of the radiation field of the exciting source beyond the O II ionization limit ($\lambda < 353$) is derived in Section IV from the O II–O III ionization equilibrium. The radiation temperature of the central star beyond the Lyman limit is computed from the electron temperature and the ratio

TABLE 1

SPECTROGRAMS* OF HERBIG'S OBJECT NO. 1

| Plate No. | Date 1955 | Exposure Time (min.) | Emulsion | Wratten Filters Used for Calibration |
|---|---|---|---|---|
| CS-1958 | Jan. 24 | 127 | 103*a*-F(3) | 50, 62, 71A |
| CS-1966 | Jan. 28 | 152 | 103*a*-D | 18A, 50, 62 |
| CS-1970 | Jan. 29 | 88 | II*a*-O (baked) | 18A, 50 |

* The spectra were not widened.

of the sum of the intensities of all forbidden lines to the intensity of H$\beta$. Finally, some considerations regarding possible sources for the excess of ultraviolet radiation are presented. The numerical results given in Section III are still subject to considerable uncertainty, because the methods applied there do not satisfactorily take into account the effects of stratification and of possible fluctuations in density and electron temperature. The importance of such fluctuations in the case of the planetary nebulae has become more and more evident during the last years (see, e.g., Aller and White [1949] and, with regard to the theory, Zanstra [1953]). Unfortunately, the Herbig-Haro Objects are too faint and not extended enough to permit observations that could give information about density fluctuations, except to the extent discussed in Section III.

## II. SPECTROPHOTOMETRIC DATA

Three new spectrograms of Object No. 1 were obtained for this investigation by Dr. G. H. Herbig[2] with the nebular spectrograph of the Crossley reflector of the Lick Observatory. They cover the wave-length region from $\lambda$ 3700 to $\lambda$ 6800. The dispersion is 430 A/mm at H$\gamma$. The observational details are given in Table 1. The seventh-magnitude star HD 16397 of type dG0, for which six-color photoelectric data have been published by Stebbins and Whitford (1945), was used as a comparison star on all three plates. The energy distribution in the spectrum of this star was obtained by comparing its six-color magnitudes with those of HR 483 (spectral type G2 V) for which a comparison with the

[2] I am very much indebted to Dr. Herbig for taking these spectrograms.

sun has recently been made by Stebbins and Kron.[3] For the sun the energy distribution given by Minnaert (1924) from a reduction of Abbott's 1920–1922 measurements was used. The errors involved in the comparison of HD 16397 with the sun should be small, since the spectral types of the three stars employed (HD 16397, HR 483, and the sun) are very similar.

Microphotometer tracings of all emission lines appearing on the spectrograms of Object No. 1 were made both parallel and at right angles to the direction of dispersion. (The monochromatic images of the nebula on the plates are too small to permit successive runs parallel to the dispersion.) When tracing parallel to the dispersion, the projected microphotometer slit length was made equal to the length of the shortest monochromatic images. For the tracings across the spectrum, the projected slit length was made equal to the width of the narrowest monochromatic images.

First, preliminary intensities were derived from the parallel tracings only. The intensities were determined from curves of the blackening versus intensity for the different wave lengths and the known energy distribution in the spectrum of the comparison star, with allowance for the effects of the change of dispersion with wave length in the spectrum of the comparison star and for selective extinction in the earth's atmosphere. (The mean extinction factors determined for Mount Hamilton by D. M. Popper [1938] were used for the latter purpose.)

These preliminary intensities were corrected in the following way for the different extensions of the monochromatic images at right angles to the dispersion: If $I\ (x, y)$ is the intensity in an emission line as a function of the co-ordinates $x$ (parallel to the dispersion) and $y$ (perpendicular to $x$), the total (relative) intensity of the line was found by multiplying $\int I\ dx$ by the "effective length" of the line: $\int I\ dy / I_0$, where $I_0$ is the intensity in the center of the line. This procedure would be strictly correct only if $I\ (x, y) = f_1(x)\ f_2(y)$, but it is probably entirely satisfactory for the determination of approximate line intensities for such faint and not very extended objects. The final intensities are given in Table 2.

In addition to the emission lines, the spectrum of Object No. 1 shows a faint continuum. Whether this belongs to a central star or to the nebula itself cannot be decided at present. The color of this continuous spectrum was determined by tracing across the spectrum at wave lengths that are relatively free of emission lines and then comparing the results with those for the comparison star. Tracings were made at λλ 4200, 4500, and 4800 on the II*a*-O plate and at λ 4500 and λ 5400 on the 103*a*-D plate. The derived color index of the continuum, without correction for reddening, is +1.7 mag. on the $(B - V)$ system. The reddening correction derived in Section III from the emission lines reduces this color index to +1.3 mag. On account of the extreme faintness of the continuum, especially on the D plate, this value for the color of the continuum is rather uncertain, and it can be considered only as a very rough estimate. It is quite certain, however, that the energy distribution in this continuum is not that of a blue (O- or B-type) star.

## III. ELECTRON TEMPERATURE AND ELECTRON DENSITY IN THE NEBULA

A priori, one knows nothing about the excitation and ionization mechanisms in the Herbig-Haro Objects. But from the observed fact that none of the ions that show forbidden lines exhibit any permitted lines, it may be concluded that the population of the metastable levels is mainly caused by electron impact (see, e.g., Wurm 1937). In such a case the intensity ratio of two forbidden multiplets is a function only of the electron temperature, $T_e$, the electron density, $N_e$, the excitation cross-sections, and the transition probabilities, $A_{nm}$. All the forbidden lines observed in the Herbig-Haro Objects except those of [Fe II] correspond to transitions between the three lowest terms of an

[3] I should like to thank Dr. Stebbins and Dr. Kron very much for making their results available to me in advance of publication.

TABLE 2

EMISSION-LINE INTENSITIES IN HERBIG'S OBJECT NO. 1

| λ | Identification | No. Plates on Which Intensity Was Determined | Intensity* | Intensity Corrected for Space Reddening*† |
|---|---|---|---|---|
| 3726 | [O II] | 3 | 116 | 192 |
| 3729 | | | | |
| 3835 | H9 | 1 | 5 | 8 |
| 3868 | [Ne III] | 2 | 6 | 9 |
| 3889 | H8 | 1 | 7 | 11 |
| 3933 | Ca II | 3 | 8 | 12 |
| 3968 | [Ne III] | 3 | 18 | 26 |
| 3968 | Ca II | | | |
| 3970 | Hε | | | |
| 4068 | [S II] | 3 | 43 | 59 |
| 4076 | | | | |
| 4101 | Hδ | 3 | 14 | 19 |
| 4177 | [Fe II] | 1 | 2 | 3 |
| 4244 | [Fe II] | 3 | 6 | 8 |
| 4245 | | | | |
| 4287 | [Fe II] | 2 | 8 | 10 |
| 4340 | Hγ | 3 | 34 | 42 |
| 4359‡ | [Fe II] | 3 | 11 | 13 |
| 4414 | [Fe II] | 3 | 7 | 8 |
| 4416 | | | | |
| 4475 | [Fe II] | 2 | 4 | 5 |
| 4571 | Mg I | 2 | 5 | 6 |
| 4658 | [Fe III] | 3 | 4 | 4 |
| 4861 | Hβ | 3 | 100 | 100 |
| 4959 | [O III] | 3 | 15 | 14 |
| 5006 | [O III] | 3 | 43 | 40 |
| 5199 | [N I] | 1 | 9 | 8 |
| 5201 | § | | | |
| 5577 | [O I] | 1 | ≤6 | ≤5 |
| 6300 | [O I] | 2 | 429 | 289 |
| 6364 | | | | |
| 6548 | [N II] | 1 | 890 | 580 |
| 6563 | Hα | | | |
| 6584 | [N II] | | | |
| 6717 | [S II] | 1 | 568 | 353 |
| 6731 | | | | |

* The intensity of Hβ has been set equal to 100.

† The assumption regarding space reddening is discussed in Sec. III.

‡ λ 4359 may be disturbed slightly by Hg I λ 4358 from city lights.

§ This line seems to be somewhat more diffuse than the other faint lines.

‖ λ 5577 is strongly disturbed by the night-sky line at the same wave length. As the night-sky line extends over the whole width of the spectrum, whereas the lines of the nebula cover only a small fraction of it, the intensity of λ 5577 was determined by taking a microphotometer tracing along the night-sky line and then attributing the intensity increase in the center of the spectrum to nebular emission. This procedure gives only an upper limit for the intensity, because the intensity increase is probably due partly to the nebular continuum.

ion. These terms will be denoted as 1, 2, and 3 in order of increasing excitation. Then it follows from the condition of statistical equilibrium (Menzel, Aller, and Hebb 1941; Seaton 1954) that

$$\frac{I_{21}}{I_{31}}=\frac{E_{21}\Omega(1,2)}{E_{31}A_{31}\Omega(1,3)}\,e^{E_{32}/kT_e} \times\frac{(A_{31}+A_{32})+8.54\times10^{-6}\{[\Omega(1,3)+\Omega(2,3)]/\omega_3T_e^{1/2}\}N_e}{1+8.54\times10^{-6}[\Omega(1,2)/A_{21}\omega_2T_e^{1/2}]\{[\Omega(1,3)+\Omega(2,3)]/\Omega(1,3)\}N_e}, \tag{1}$$

if we recognize that $\Omega(1,3)/\Omega(1,2)\ll 1$, which is true in all cases of interest.[4] Corresponding equations can, of course, be derived for $I_{21}/I_{32}$ and $I_{31}/I_{32}$. The meaning of the symbols is as follows: $I_{nm}$ is the intensity of the forbidden line corresponding to the transition $n\rightarrow m$; $E_{nm}$ is the energy difference in ergs between the terms $n$ and $m$; $\omega_n$ is the statistical weight of the term $n$; and $\Omega(m,n)$ are the collision strengths as defined by Hebb and Menzel (1940). They are related to the so-called "deactivation coefficients," $a_{nm}$, by the well-known equation

$$a_{nm}=8.54\times10^{-6}\frac{\Omega(m,n)}{\omega_nT_e^{1/2}}, \tag{2}$$

where $a_{nm}N_eN_n$ is the number of electron impacts per cubic centimeter and per second leading to the transition $n\rightarrow m$; $a_{nm}$ and the corresponding excitation coefficients are connected by Milne's equation (1928),

$$\frac{a_{mn}}{a_{nm}}=\frac{\omega_n}{\omega_m}\,e^{-E_{nm}/kT_e}. \tag{3}$$

If the intensity ratios $I_{21}/I_{31}$, $I_{21}/I_{32}$, and $I_{31}/I_{32}$ for two different ions can be observed, in principle $T_e$ and $N_e$ may be computed, provided that the collision strengths and the transition probabilities are known. In the present case, only $I_{21}/I_{31}$ for S II has been observed, and a lower limit can be set for $I_{21}/I_{32}$ of O I. For neutral atoms, $\Omega(m,n)$ changes rather rapidly with $T_e$ (Seaton 1954). Therefore, it is more convenient to use the $a_{nm}$ coefficients directly. This gives

$$\frac{I_{21}}{I_{32}}=\frac{E_{21}A_{21}a_{21}\omega_2}{E_{32}A_{32}a_{31}\omega_3}\,e^{E_{32}/kT_e}\,\frac{(A_{31}+A_{32})+(a_{32}+a_{31})N_e}{A_{21}+[a_{21}+(a_{32}a_{21}/a_{31})]N_e}. \tag{4}$$

An additional equation containing $N_e$ and $T_e$ may be obtained by a procedure suggested by Seaton (1954). Since the ionization potentials and the photoionization cross-sections for O I and N I are nearly equal[5] (furthermore, in our case, double ionization is small), the following relation holds approximately:[6]

$$\frac{N(\text{O I})}{N(\text{O II})}=\frac{N(\text{N I})}{N(\text{N II})}. \tag{5}$$

[4] It should be noted that some of the approximations made by Seaton (1954) cannot be made here, for we do not know anything about the range in which $T_e$ and $N_e$ are to be expected.

[5] According to eq. (10), it is also to be expected that the collisional cross-sections for ionization should not differ very much.

[6] Dr. Aller has kindly pointed out to me that relation (5) is often not fulfilled in planetary nebulae. But in most planetaries double ionization of oxygen and nitrogen plays a very important role. If, as in the Herbig-Haro Objects, this is not the case, it seems reasonable to accept Seaton's conclusions, unless one doubts the correctness of the photoionization cross-sections given by Bates (1946).

This equation leads to one that is independent of the abundance ratio of O to N:

$$\frac{I(\lambda 6300+\lambda 6363)\,I(\lambda 6548+\lambda 6584)}{I(\lambda 5199)\,I(\lambda 3727)} = \frac{E_{21}^{(\mathrm{O\,I})}E_{21}^{(\mathrm{N\,II})}A_{21}^{(\mathrm{O\,I})}A_{21}^{(\mathrm{N\,II})}}{E_{21}^{(\mathrm{N\,I})}E_{21}^{(\mathrm{O\,II})}A_{21}^{(\mathrm{N\,I})}A_{21}^{(\mathrm{O\,II})}}\,\frac{a_{21}^{(\mathrm{O\,I})}a_{21}^{(\mathrm{N\,II})}}{a_{21}^{(\mathrm{N\,I})}a_{21}^{(\mathrm{O\,II})}}\,\frac{\omega_2^{(\mathrm{O\,I})}\omega_1^{(\mathrm{N\,I})}\omega_2^{(\mathrm{N\,II})}\omega_1^{(\mathrm{O\,II})}}{\omega_1^{(\mathrm{O\,I})}\omega_2^{(\mathrm{N\,I})}\omega_1^{(\mathrm{N\,II})}\omega_2^{(\mathrm{O\,II})}}\left[\frac{A_{21}^{(\mathrm{N\,I})}+a_{21}^{(\mathrm{N\,I})}N_e}{A_{21}^{(\mathrm{O\,I})}+a_{21}^{(\mathrm{O\,I})}N_e}\right] \quad (6)$$

$$\times\left[\frac{A_{21}^{(\mathrm{O\,II})}+a_{21}^{(\mathrm{O\,II})}N_e}{A_{21}^{(\mathrm{N\,II})}+a_{21}^{(\mathrm{N\,II})}N_e}\right]\exp\left\{\frac{1}{kT_e}\left[-E_{21}^{(\mathrm{O\,I})}-E_{21}^{(\mathrm{N\,II})}+E_{21}^{(\mathrm{N\,I})}+E_{21}^{(\mathrm{O\,II})}\right]\right\}.$$

Transitions from and to term 3 are neglected. This procedure is justified by the fact that auroral ($3\rightarrow 2$) and transauroral ($3\rightarrow 1$) lines of O I, N I, O II, and N II are very faint compared with the nebular ($2\rightarrow 1$) lines of these ions.

For the application of equation (6) one must separate the contribution of [N II] λ 6548 and λ 6584 from the intensity of Hα. It is not possible to do this directly, for the dispersion of the present spectrograms is too low. Therefore, the observed intensities of Hβ to H9, together with the theory of the Balmer decrement, were used to find the intensity of Hα. Under all assumptions that have been made about space reddening (see below), the measured Balmer decrement lies between Menzel's case B and the case of collisional excitation in an optically thick nebula (Chamberlain 1953).[7] By use of the observed Balmer decrement, an interpolation between these theoretical cases yields the theoretical intensity of Hα. By subtraction of this value from the measured intensity of Hα + λ 6548 + λ 6584, the intensity due to the [N II] lines alone is obtained.

This step may easily introduce an uncertainty of about a factor of 2 in the intensity of λ 6548 + λ 6584. But fortunately the derived $T_e$ is not very sensitive to such intensity changes. Even if the intensity of λ 6548 + λ 6584 were lower by a factor of 4 than derived here, $T_e$ would be increased by only 1500°, and $N_e$ would be decreased by 30 per cent. The results might be seriously affected in case a selective mechanism exists that would increase the intensity of Hα without influencing the decrement of the other Balmer lines. Such a process, the charge transfer between $H^-$ and $H^+$, has been recently discussed by Bates and Lewis (1955). But it is very improbable that this particular process plays any important role under nebular conditions. Furthermore, the other curves of $T_e$ versus $N_e$ (see Fig. 1) lead to about the same values of $T_e$ and $N_e$.

Equation (1) applied to S II, relation (4) applied to O I, and equation (6) yield two equations and one inequality for the determination of $N_e$ and $T_e$. The observed intensities are taken from Table 2. The $a_{nm}$ and $\Omega(m, n)$ values are those given by Seaton (1953, 1954), and the $A_{nm}$ values are those derived by Garstang (1951, 1952) and Pasternack (1940), as corrected by Seaton (1954). The solution of this system of equations has been found graphically. The three $N_e = f(T_e)$-curves have been computed by a trial-and-error method.

The whole computation has been carried out under three different assumptions about the interstellar reddening: (1) there is no reddening; (2) a color excess of $E_{(B-V)} = 0.4$ mag. is appropriate; this is the color excess of the star BD−6°1253 in the neighboring NGC 1999 as determined by Greenstein (1948) and by Herbig and Eggen (unpublished); (3) the value of $E_{(B-V)}$ is 0.8 mag., obtained from the assumption that the Balmer decrement is formed according to Menzel's case B. Table 3 shows the most important observed intensity ratios as corrected according to these various assumptions.

Assumption 3 leads to a contradiction in the system of equations: the application of equation (4) to O I shows that for no value of $N_e$ can $T_e$ be higher than 12700°. On the other hand, the solution of equations (1) and (6) under the third assumption gives

[7] For the definition of case B see Baker, Menzel, and Aller (1938).

$T_e > 20000°$ and $N_e \approx 1.1 \times 10^4$ cm$^{-3}$. Consequently, the assumption of heavy reddening can be excluded.

Assumption 1 leads to $T_e = 5200°$ and $N_e = 1.1 \times 10^4$ cm$^{-3}$, while assumption 2 gives $T_e = 7500°$ and $N_e = 1.3 \times 10^4$ cm$^{-3}$. It is considered that assumption 2 (i.e., that Object No. 1 has the same reddening as BD$-6°1253$) is the most probable, and the corresponding values of $T_e$ and $N_e$ have been used in the computations to follow.

The graphical solution of the equations under assumption 2 is given in Figure 1. In order to check whether the other features of the forbidden-line spectrum can also be explained by these values of $T_e$ and $N_e$, curves of $T_e$ versus log $N_e$ have been computed also for the observed intensity ratios $I$ ([S II], $\lambda 6717 + \lambda 6731$)/$I$ ([O II], $\lambda 3726 +$ $\lambda 3729$) and $I$([O III], $\lambda 4959 + \lambda 5006$)/$I$([Ne III], $\lambda 3868 + \lambda 3968$) under the assumptions of normal cosmic abundance ratios (Unsöld 1942; Aller 1953*a;* Traving 1955) and that the degrees of ionization are given by

$$\frac{N(\text{O II})}{N(\text{O})} = \frac{N(\text{S II})}{N(\text{S})}; \qquad \frac{N(\text{O III})}{N(\text{O})} = \frac{N(\text{Ne III})}{N(\text{Ne})}.$$

The second assumption is probably correct only to the right order of magnitude (see, e.g., the degree of ionization for planetaries given by Aller and Menzel [1945] and Aller [1954]). But the curves for $I$([S II], $\lambda 6717 + \lambda 6731$)/$I$([O II], $\lambda 3726 + \lambda 3729$) and $I$([O III], $\lambda 4959 + \lambda 5006$)/$I$([Ne III], $\lambda 3868 + \lambda 3968$) show at least that there is, in principle, no difficulty in explaining the rather considerable strengths of the [S II] lines as an effect of low $T_e$ and that there is no indication that $T_e$ in the O III region is appreciably different from that in the regions of lower ionization. The first point is further illustrated by the data in Table 4, which shows the ratio $I$([S II], $\lambda 6717 + \lambda 6731$)/$I$([O II], $\lambda 3726 + \lambda 3729$) as a function of $T_e$ and log $N_e$.

A further problem is the interpretation of the low-excitation permitted lines like H and K of Ca II and Mg I $\lambda 4571$. We first compare the intensity of Mg I $\lambda 4571$ with that of the [O I] multiplet $\lambda 6300 + \lambda 6363$, assuming that the Mg I line is also produced by electron impact. By the neglect of transitions to higher terms, it is found that, for $T_e = 7500°$,

$$\frac{I_{21}^{(\text{O I})}}{I_{21}^{(\text{Mg I})}} = 0.14 \, \frac{A_{21}^{(\text{O I})} a_{21}^{(\text{O I})} N_1^{(\text{O I})}}{A_{21}^{(\text{Mg I})} a_{21}^{(\text{Mg I})} N_1^{(\text{Mg I})}} \, \frac{A_{21}^{(\text{Mg I})} + a_{21}^{(\text{Mg I})} N_e}{A_{21}^{(\text{O I})} + a_{21}^{(\text{O I})} N_e}, \tag{7}$$

TABLE 3*

LINE-INTENSITY RATIOS CORRECTED FOR THREE DIFFERENT COLOR EXCESSES ACCORDING TO DIFFERENT ASSUMPTIONS ABOUT REDDENING

| ION | LINES | $E_{(B-V)}$ (mag.) | | |
|---|---|---|---|---|
| | | 0.0 | 0.4 | 0.8 |
| [S II]/[S II] | I ($\lambda 6717+\lambda 6731$)/I ($\lambda 4068+\lambda 4076$) | 13.2 | 6.0 | 2.4 |
| [S II]/[O II] | I ($\lambda 6717+\lambda 6731$)/I ($\lambda 3726+\lambda 3729$) | 4.9 | 1.8 | 0.6 |
| [O I]/[N I] | I ($\lambda 6300+\lambda 6363$)/I ($\lambda 5199$) | 48 | 36 | 26 |
| [O I]/[O I] | I ($\lambda 6300+\lambda 6363$)/I ($\lambda 5577$) | $\geq 71$ | $\geq 58$ | $\geq 46$ |
| [O III]/[Ne III] | I ($\lambda 4959+\lambda 5006$)/I ($\lambda 3868+\lambda 3968$) | 6.4 | 4.5 | 2.4 |
| [N II]/[O II] | I ($\lambda 6548+\lambda 6584$)/I ($\lambda 3726+\lambda 3729$) | (2.3) | (1) | ($\leq$ 0.2) |

* The ratio $I$ ([N II], $\lambda 6548 + \lambda 6584$)/$I$([O II], $\lambda 3726 + \lambda 3729$) has been derived by the method described in the text. In the case of $E_{(B-V)} = 0.8$ mag., only an upper limit for this ratio can be obtained, as the measured $I(\text{H}\alpha + \lambda 6548 + \lambda 6584)$ is nearly equal to the predicted $I(\text{H}\alpha)$. The upper limit has been derived under the assumption of an uncertainty of 30 per cent in the measured $I(\text{H}\alpha + \lambda 6548 + \lambda 6584)$.

where $N_1$ is the number of atoms in the ground state. Probably $a_{21}^{(O\,I)}$ and $a_{21}^{(Mg\,I)}$ are of the same order of magnitude. Oxygen is about ten times as abundant as magnesium. Furthermore, for [O I] and Mg I, it is known that $A_{21} \gg N_e a_{21}$, if the derived value of $N_e = 1.3 \times 10^4$ cm$^{-3}$ is used. Therefore, there would be no difficulty in producing comparable intensities for these [O I] and Mg I lines, provided that one could show that under certain conditions a rather large number of neutral magnesium atoms can exist in the H II region. It might be that this is a consequence of the peculiarities of the radiation field derived in the next section.

It is certainly not possible to explain the intensity of the H and K lines of Ca II in a similar manner, for calcium is less abundant than oxygen by a factor of about 200. The only possible explanation of the strength of the H and K lines seems to be that they

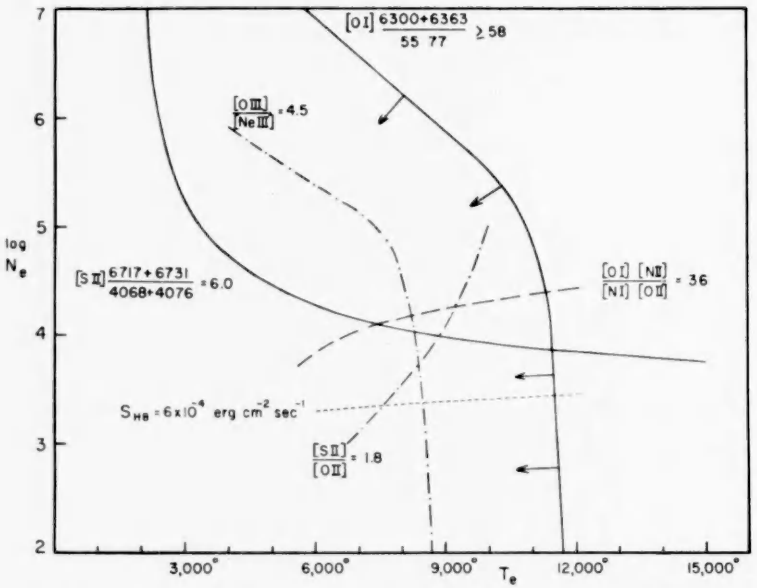


FIG. 1.—The relationships between log $N_e$ and $T_e$ that correspond to the observed intensity ratios of forbidden lines and to the observed surface brightness in H8.

TABLE 4

$\{I$ ([S II], λ 6717+λ 6731)$\}/\{I$ ([O II], λ 3726+λ 3729)$\}$ AS FUNCTION OF $T_e$ AND LOG $N_e$

| LOG $N_e$ | $T_e$ | | | | |
|---|---|---|---|---|---|
| | 5000° | 6000° | 7000° | 8000° | 9000° |
| 3 | 4.7 | 2.6 | 1.7 | 1.3 | 0.96 |
| 4 | 10.1 | 5.4 | 3.4 | 2.4 | 1.8 |
| 5 | 25.4 | 13.4 | 8.3 | 5.7 | 4.0 |

are formed in regions of much higher density. The existence of such regions of higher density may also explain why the observed Balmer decrement is somewhat steeper than in Menzel's case B.

Independently of the preceding considerations, $N_e$ can be derived from the surface brightness of the nebula in a Balmer line. H8 was selected for this purpose, because it is the highest-level Balmer line for which a fairly reliable intensity measurement can be made. It is advisable to use as high a member of the Balmer series as possible, since the differences between the $b_n$'s of Menzel's case B and the case of collisional excitation in an optically thick nebula become appreciably smaller for the higher Balmer lines.

The surface brightness in H8 was determined in the following way: Herbig (unpublished) has compared Object No. 1 with neighboring stars on Crossley direct photographs taken in the wave-length interval λλ 5200–5800, which contains no strong emission lines. Approximate photographic magnitudes are known for the comparison stars and a reasonable assumption as to their color indices leads to an estimation of the integrated "photovisual" magnitude of Object No. 1 as 17.0–17.5 mag. For purposes of calculation the mean value of 17.2 mag. is adopted.

If strong emission lines such as Hβ and λ 6300 and λ 6363 are not excluded by the use of such a restricted spectral region, the object appears considerably brighter.

The total energy of the continuum between λ 5200 and λ 5800 was compared to that of H8, and it was found that

$$\frac{I_{H8}}{\int_{\lambda 5200}^{\lambda 5800} I_\lambda d\lambda} = 0.05 .$$

From direct photographs, it is found that Object No. 1 on the present spectrograms *effectively* extends over 33 square seconds of arc; this value includes allowance for the fact that about one-quarter of the nebula is cut off by the slit jaws of the spectrograph. Now the sun has a visual surface brightness of $-19.7$ mag. per square minute of arc (de Vaucouleurs 1949) and emits $5.3 \times 10^9$ ergs cm$^{-2}$ sec$^{-1}$ in the whole spectral range between λ 5200 and λ 5800 (Minnaert 1924). From these data we find the surface brightness of Object No. 1 in H8 as $S_{H8} = 6 \times 10^{-4}$ erg cm$^{-2}$ sec$^{-1}$. This value includes correction for space absorption, obtained from the relationship between absorption and reddening in the Orion aggregate given by Sharpless (1952).

Under the assumption of complete ionization of hydrogen, we have (corresponding expressions are given by Menzel and Aller [1941])

$$N_e^2 = \frac{3 S_{H8} T_e^{3/2}}{r K} \frac{n'^3 n^3}{b_8 g} \frac{e^{-1.57 \times 10^5 / n^2 T_e}}{2hR}, \tag{8}$$

where $K = 3.26 \times 10^{-6}$, $n' = 2$, $n = 8$, $R$ is Rydberg's constant, $h$ is Planck's constant, and $g$ is the Gaunt factor. The radius of Object No. 1 is $r$, for which a value of 1400 astronomical units or $2.1 \times 10^{16}$ cm was used. This value follows from a distance of 500 parsecs for the Orion aggregate. The corresponding curve of $T_e$ versus log $N_e$ is also given in Figure 1. The value of $N_e$ derived from $S_{H8}$ in this manner is about five times lower than the value of $N_e$ obtained from the forbidden-line intensities. This can be easily explained as a consequence of nonuniform electron density. A similar effect occurs in some planetary nebulae, according to Aller (1954) and Seaton (1954).

## IV. IONIZATION IN THE NEBULA

The low electron temperature ($T_e \approx 7500°$) shows that the ionization cannot be caused mainly by electron impact. This conclusion can be demonstrated as follows:

Consider the ionization equilibrium of O II and O III. If radiation ionization were negligible, the following equation would be valid for two consecutive stages of ionization:

$$\frac{x}{1-x} = \frac{S}{\alpha}, \tag{9}$$

since three-body recombinations can be neglected under nebular conditions. The degree of ionization is $x$, and $S$ is defined by setting the number of ionizations by impact per cubic centimeter per second equal to $N(1-x)N_e S$, while $\alpha$ is defined by setting the number of radiative recombinations per cubic centimeter per second equal to $NxN_e\alpha$. In a semiclassical approximation, $S$ is given by (see Woolley and Stibbs 1953; Böhm 1954)

$$S = \frac{12\pi e^4 f}{(2\pi m)^{1/2}(kT_e)^{3/2}} \frac{K_2(h\nu_0/kT_e)}{h\nu_0/kT_e}. \tag{10}$$

The oscillator strength for the transition from the ground state to the continuum is $f$; $\nu_0$ is the frequency corresponding to the ionization limit; $K_2$ is the well-known second exponential integral; and $\alpha(T)$ for O II has been given by Bates, Buckingham, Massey, and Unwin (1939) and has been graphically extrapolated to higher temperatures.[8] For O III, $\alpha$ has been estimated by assuming that it is proportional to $Z^2$ (Kramers 1923).

From equation (9) it is found that an electron temperature of about 32000° would be required to explain the observed ratio $N(\text{O III})/N(\text{O II}) = 5.6 \times 10^{-2}$ (see below). This is in obvious contradiction to the electron temperature of 7500° derived in the preceding section. Consequently, the most obvious means of explaining the observed ionization seems to be a strong source of radiation that is effective only in the far ultraviolet.

In order to get some information about the required radiation field, let us consider again the ionization equilibrium of O II and O III. Since $T_e$ and $N_e$ are known, one can compute the number $N_1$ of O ions in the ground state (which is nearly equal to the total number of ions considered) from the observed surface brightness $S_{21}$. Again neglecting transitions to and from higher levels, we find

$$N_1 = \frac{3S_{21}(A_{21} + a_{21}N_e)}{r\,A_{21}E_{21}(\omega_2/\omega_1)\,a_{21}N_e} \exp\left(\frac{E_{21}}{kT_e}\right). \tag{11}$$

The $N_e$-value derived from the forbidden-line spectrum was used, but $r$ was reduced by a factor of 5 in order to make allowance for the nonuniform density distribution indicated in the preceding section. The computed ion densities are $N(\text{O III}) = 0.10$ cm$^{-3}$ and $N(\text{O II}) = 1.8$ cm$^{-3}$. If it is assumed that the ionization is caused by radiation from some source (the "central star") in the center of the nebula, the condition of ionization equilibrium is

$$N(\text{O II})\,\bar{\kappa}_\nu N_{ph} = \alpha N(\text{O III})\,N_e, \tag{12}$$

where

$$N_{ph} = W\int_{\nu_0}^{\infty} \frac{4\pi I_\nu}{h\nu}\,d\nu$$

is the number of photons with $\nu > \nu_0$ passing 1 cm$^2$/sec and

$$\bar{\kappa}_\nu = \frac{\int_{\nu_0}^{\infty} \kappa_\nu (I_\nu/\nu)\,d\nu}{\int_{\nu_0}^{\infty} (I\nu/\nu)\,d\nu}$$

[8] Such a procedure has been successful even to $T_e = 10^{8}$° (Woolley and Allen 1948).

is a kind of mean absorption coefficient per O II atom for $\nu > \nu_0$, and $W$ is the dilution factor; for Herbig's Object No. 1, $W = 2.8 \times 10^{-12}$. This value is derived by assuming that the diameter of the O III region is of the same order of magnitude as the diameter of the whole nebula and that the central star has the same diameter as the sun. The quantity $\bar{\kappa}_\nu$ has been taken equal to $\kappa_\nu$ at the ionization limit, for $I_\nu/\nu$ probably decreases rapidly with increasing $\nu$ and because $\kappa_\nu$ for O II changes slowly with frequency (Bates 1946). A value of $\kappa_\nu = 8.1 \times 10^{-18}$ cm$^2$ (Bates 1946) at the ionization limit of O II has been used in the computation. In order to get an estimate of the radiation temperature, it is necessary to compare the derived value of

$$\int_{\nu_0}^{\infty} \frac{4\pi I_\nu}{h\nu}\, d\nu = 5.2 \times 10^{19} \text{ cm}^{-2} \text{ sec}^{-1}$$

with

$$\int_{\nu_0}^{\infty} \frac{4\pi I_\nu}{h\nu}\, d\nu = \frac{8\pi k^3}{c^2 h^3} T^3 \int_{x_0}^{\infty} \frac{x^2}{e^x - 1}\, dx \qquad \left(x = \frac{h\nu}{kT}\right), \tag{13}$$

which is the corresponding expression for black-body radiation. For the evaluation of the foregoing integral, the asymptotic expansion given by Zanstra (1927) has been used. The value obtained for the radiation temperature for $\lambda < \lambda_0$ ($\lambda_0 = \lambda\,353$) is $T_{\text{rad}} \approx 24000°$.

Finally, it is possible to obtain some information about the radiation temperature for $\lambda < 916$, shortward of the Lyman limit, by the use of some recent results of Aller (1953*b*). From consideration of the equilibrium between the energy gain of electrons due to photoionization and the energy losses due to free-free transitions and collisional excitation, one gets a relation between $T_{\text{rad}}$, $T_e$, and the ratio of the sum of the intensities of all forbidden lines to the intensity of, for example, H$\beta$. In the present case $\Sigma I_F / I_{H\beta} = 10.6$. With $T_e = 7500°$, it is found that $T_{\text{rad}} = 29000°$ (for the appropriate formulae and a table covering a large range of $T_e$, see Aller's paper). This result is independent of the dilution factor to a first approximation.

At present it does not seem possible to reach definite conclusions about the source responsible for the excess of ultraviolet radiation. It can easily be shown that the excess cannot be radiation arising from accretion heating (for a recent discussion of this effect see Mestel [1954]). The reasoning is as follows: The most favorable condition for accretion is that in which the star is at rest relative to the nebula. In this case the rate of accretion is given, according to Bondi (1952), by

$$\frac{dM}{dt} = 2\pi\Lambda\,(GM)^2 c_\infty^{-3} \rho_\infty, \tag{14}$$

where $M$ is the mass of the star (which has been assumed to be one solar mass), $G$ is the gravitational constant, $c_\infty$ is the velocity of sound at infinity, $\rho_\infty$ is the density of the nebula at a large distance from the star, and $\Lambda$ is a constant of the order of unity.

The fact that contradicts the assumption that accretion may play any important role for the Herbig-Haro Objects is the observed value of the radius of the luminous part of the nebula: 1400 a.u. This radius is two orders of magnitude larger than the "accretion radius"

$$r_{\text{acc}} = \frac{2GM}{c_\infty^2} = 14.3 \text{ a.u.}$$

It has been emphasized that under such conditions the accretion rate will be cut down to a very small value according to the high value of $c_\infty^3$ in equation (14) (Schatzman

1953; Mestel 1954). In our case, with $T_e = 7500°$, $N_e = 2.5 \times 10^3$ cm$^{-3}$, and H completely ionized, we get an accretion rate from equation (14) of only

$$\frac{dM}{dt} = 3.4 \times 10^{14} \text{ gm/sec}.$$

An upper limit for the emission of ultraviolet quanta beyond the Lyman limit by accretion heating is given by (Mestel 1954)

$$N_{ph} = \frac{\frac{1}{2}\left[\frac{2}{5}\left(dM/dt\right)(1/m_{\mathrm{H}})\right]}{4\pi R^2},$$

where $R$ is the radius of the central star and $m_{\mathrm{H}}$ is the mass of the hydrogen atom. This expression gives for our object

$$N_{ph} = 6.6 \times 10^{14} \text{ cm}^{-2} \text{ sec}^{-1}.$$

It has been shown that the number of ultraviolet quanta beyond the Lyman limit actually emitted by the central star is equal to that emitted by a black body at $T = 29000°$. At this temperature,

$$N_{ph} = 2.9 \times 10^{23} \text{ cm}^{-2} \text{ sec}^{-1}.$$

These estimates clearly exclude the possibility of accretion heating playing any important role for the excitation and ionization of these peculiar nebulae.

Consequently, it seems probable that the source which emits the ultraviolet radiation lies in the central star itself. Whether some kind of extremely strong convective zone near the surface of the star could produce an extended "chromosphere" emitting so strongly in the ultraviolet remains to be investigated.

I am very much indebted to Dr. G. H. Herbig for suggesting a detailed investigation of this object and for many very stimulating discussions, especially about the empirical aspects of the problems discussed here. Furthermore, I am grateful to Dr. Herbig and to Dr. L. H. Aller for reading the manuscript and for making many helpful suggestions. I am also indebted to Dr. J. L. Greenstein for critical and helpful comments and to Dr. L. Biermann for an interesting discussion about some theoretical aspects of the problem. I am greatly indebted to Dr. C. D. Shane for making my stay at the Lick Observatory possible and to the Deutsche Forschungsgemeinschaft for a travel grant to the United States.

## REFERENCES

Aller, L. H. 1953*a*, *Astrophysics* (New York: Ronald Press Co.), Vol. 1.
———. 1953*b*, *Ap. J.*, **118**, 547.
———. 1954, *ibid.*, **120**, 401.
Aller, L. H., and Menzel, D. H. 1945, *Ap. J.*, **102**, 239.
Aller, L. H., and White, M. 1949, *A.J.*, **54**, 181.
Ambarzumian, V. A. 1954, *Comm. Burakan Obs.*, No. 13.
Baker, J. G., Menzel, D. H., and Aller, L. H. 1938, *Ap. J.*, **88**, 422.
Bates, D. R. 1946, *M.N.*, **106**, 432.
Bates, D. R., Buckingham, R. A., Massey, H. G. W., and Unwin, J. J. 1939, *Proc. R. Soc. London*, *A*, **170**, 322.
Bates, D. R., and Lewis, J. T. 1955, *Proc. Phys. Soc. London*, *A*, **68**, 173.
Böhm, K. H. 1954, *Zs. f. Ap.*, **35**, 179.
Bondi, H. 1952, *M.N.*, **112**, 195.
Chamberlain, J. W. 1953, *Ap. J.*, **117**, 387.
Garstang, R. H. 1951, *M.N.*, **111**, 115.
———. 1952, *Ap. J.*, **115**, 506.
Greenstein, J. L. 1948, *Ap. J.*, **107**, 375.

Haro, G. 1952, *Ap. J.*, **115**, 572.
———. 1953, *ibid.*, **117**, 73.
Hebb, M. H., and Menzel, D. H. 1940, *Ap. J.*, **92**, 408.
Herbig, G. H. 1950, *Ap. J.*, **111**, 11.
———. 1951, *ibid.*, **113**, 697.
———. 1952, *J.R.A.S. Canada*, **46**, 222.
Kramers, H. A. 1923, *Phil. Mag.*, **46**, 836.
Menzel, D. H., and Aller, L. H. 1941, *Ap. J.*, **93**, 195.
Menzel, D. H., Aller, L. H., and Hebb, M. H. 1941, *Ap. J.*, **93**, 230.
Mestel, L. 1954, *M.N.*, **114**, 437.
Milne, E. A. 1928, *M.N.*, **88**, 493.
Minnaert, M. 1924, *B.A.N.*, **2**, 75.
Pasternack, S. 1940, *Ap. J.*, **92**, 129.
Popper, D. M. 1938, Dissertation, University of California.
Schatzman, E. 1953, *Gas Dynamics of Cosmic Clouds* (Cambridge: North Holland Publishing Co., Amsterdam, 1955).
Seaton, M. J. 1953, *Proc. R. Soc. London, A*, **218**, 400.
———. 1954, *M.N.*, **114**, 154.
Sharpless, S. 1952, *Ap. J.*, **116**, 251.
Stebbins, J., and Whitford, A. E. 1945, *Ap. J.*, **102**, 318.
Traving, G. 1955, *Zs. f. Ap.*, **36**, 1.
Unsöld, A. 1942, *Zs. f. Ap.*, **21**, 22.
Vaucouleurs, G. de. 1949, *Ann. d'ap.*, **12**, 287.
Woolley, R. v.d. R., and Stibbs, D. W. 1953, *The Outer Layers of a Star* (Oxford: Clarendon Press).
Wurm, K. 1937, *Zs. f. Ap.*, **14**, 321.
Zanstra, H. 1927, *Pub. Dom. Ap. Obs. Victoria*, **4**, 256.
———. 1953, *Gas Dynamics of Cosmic Clouds* (Cambridge: North Holland Publishing Co., Amsterdam, 1955).

# COMPLEX LINES IN THE SPECTRUM OF RW CEPHEI

PAUL W. MERRILL AND OLIN C. WILSON
Mount Wilson and Palomar Observatories
Carnegie Institution of Washington, California Institute of Technology
*Received December 27, 1955*

ABSTRACT

The spectrum of this extreme supergiant M-type star observed with dispersion of 9 A/mm shows many absorption lines apparently with two components separated by a narrow central maximum. The maximum is probably actual emission superposed on an absorption line considerably widened by turbulence. In certain lines, especially the resonance lines of Ca I, Cr I, Mn I, and Sr II, the shortward component is greatly reinforced by the absorption of an upper expanding shell of gas. Shortward of λ 4000 A there appear numerous narrow emission lines, chiefly of Fe I and Ti I, without accompanying dark lines. The peculiar relative intensities of these lines are probably due to strong differential absorption. The spectrum is compared with that of α Orionis.

RW Cephei, HD 212466 (1900 $\alpha$ $22^h19^m4$, $\delta + 55°28'$), is an irregular red supergiant variable star with a range in photographic magnitude from 8.4 to 9.1. Its spectrum was classified M0:I*a*-O by Phillip C. Keenan (1942), who remarked: "In the spectrum of RW Cep all lines are stronger than normal, and the enhancement of the lines sensitive to luminosity is so great as to make it appear probable that this star has the greatest absolute brightness of any of those studied here, with the exception of VV Cep."

Two high-dispersion spectrograms of RW Cephei obtained with the 200-inch telescope on November 14, 1954 (Pc 1855), and on September 2, 1955 (Pc 2248), both on the II*a*-O emulsion (baked before exposure), show many extraordinary features. The photographed spectrum extends in the third order of the grating, dispersion 9.0 A/mm, from λ 3700 to λ 5200 A, and in the second order, 13.5 A/mm, from λ 4500 to λ 5400 A. Much of the range from λ 4400 to λ 5100 A is overexposed, while below about λ 3950 A the continuous spectrum becomes too weak for satisfactory measurement of absorption lines.

## ABSORPTION LINES

The remarkable profiles of certain absorption lines are illustrated by tracings in Figure 1. Many lines show two components of minima or intensity separated by a fairly well-defined central maximum. The two minima, called the "shortward" and the "longward" components, yield radial velocities differing, on the average, by 43 km/sec (0.6 A at λ 4200 A). Measured displacements and estimated intensities of 42 lines are recorded in Table 1.

For the strong resonance lines of Ca I, Cr I, Mn I, and Sr II the estimated intensity of the shortward component averages about four times that of the longward component, making the lines very unsymmetrical. In Fe I the average ratio is 0.7 for ground-level lines and about the same for other lines. A few lines of Ti I indicate that the ratio is about 1.4 regardless of excitation potential. In general, the separation between the absorption components tends to increase with intensity, but there is considerable scatter. The exceptionally large separation of λ 4227 of Ca I is due to the unusual width of the longward component. Note, in Table 1, that this component yields a much smaller negative displacement than that of any other line, while the shortward component yields an average displacement.

Many absorption lines, some of them strong and fairly wide, show no distinct central maxima. This is especially true in the spectral region longward of H$\beta$. In this region, bisection of about fifty lines gave, with considerable scatter, a mean displacement of

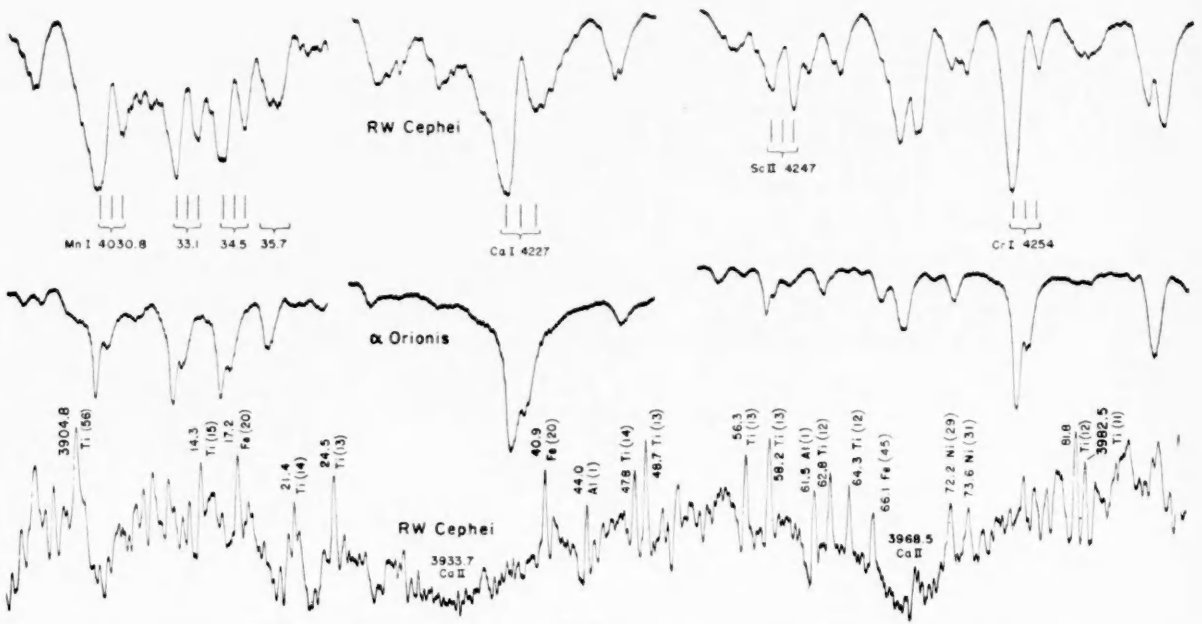


FIG. 1.—Tracings of spectra. Upper and lower rows are of RW Cephei, plate Pc 1855 taken by O. C. Wilson, November 14, 1954. Center row is of α Orionis, plate Ce 2434, taken by W. S. Adams, October 13, 1940.

TABLE 1

DOUBLE ABSORPTION LINES IN THE SPECTRUM OF RW CEPHEI

| λ (A) | Ident. | E.P. (ev) | Shortward Component | | Central Maximum | Longward Component | |
|---|---|---|---|---|---|---|---|
| | | | Int. | Rad. Vel. (km/sec) | Rad. Vel. (km/sec). | Int. | Rad. Vel. (km/sec) |
| 4005.25 | Fe I | 1.5 | 3 | −80 | −57 | 4 | −36 |
| 30.76 | Mn I | 0.0 | 12 | −83 | −56 | 3 | −37 |
| 33.07 | Mn I | 0.0 | 8 | −85 | −56 | 3 | −36 |
| 34.49 | Mn I | 0.0 | 6 | −85 | −59 | 3 | −40 |
| 41.36 | Mn I | 2.1 | 4 | −84 | −55 | 3 | −41 |
| 71.74 | Fe I | 1.5 | 2 | −79 | −58 | 3 | −37 |
| 77.71 | Sr II | 0.0 | 8 | −88 | −55 | 3 | −33 |
| 4143.87 | Fe I | 1.5 | 3 | −82 | −62 | 4 | −39 |
| 4202.03 | Fe I | 1.5 | 2 | −82 | −59 | 3 | −38 |
| 26.73 | Ca I | 0.0 | 24 | −81 | −48 | 6 | −11 |
| 46.83 | Sc II | 0.3 | 4 | −82 | −60 | 5 | −40 |
| 50.79 | Fe I | 1.5 | 10 | −85 | −64 | 6 | −43 |
| 54.35 | Cr I | 0.0 | 20 | −88 | −57 | 4 | −36 |
| 58.32 | Fe I | 0.0 | 4 | −81 | −61 | 6 | −42 |
| 60.48 | Fe I | 2.4 | 4 | −81 | −58 | 6 | −38 |
| 71.76 | Fe I | 1.5 | (7 | −83) | −57 | 6 | −35 |
| 74.80 | Cr I | 0.0 | 14 | −86 | −56 | 3 | −35 |
| 89.72 | Cr I | 0.0 | 10 | −84 | −58 | 2 | −38 |
| 94.13 | Fe I | 1.5 | 3 | −79 | −58 | 6 | −37 |
| 4300.57 | Ti I | 0.8 | 4 | −78 | −59 | 3 | −44 |
| 75.93 | Fe I | 0.0 | 8 | −95 | −64 | 4 | −42 |
| 83.55 | Fe I | 1.5 | 4 | −82 | −58 | 4 | −38 |
| 4404.71 | Fe I | 1.5 | 4 | −80 | −59 | (7 | −31) |
| 15.12 | Fe I | 1.5 | 4 | −76 | −61 | 2 | −44 |
| 27.31 | Fe I | 0.0 | 3 | −74 | −60 | 4 | −42 |
| 61.65 | Fe I | 0.0 | 4 | −77 | −59 | 6 | −40 |
| 66.57 | Fe I | 0.0 | 2 | −76 | −61 | 5 | −42 |
| 82.17 | Fe I | 0.0 | 2 | −80 | −60 | 5 | −38 |
| 89.74 | Fe I | 0.0 | 4 | −77 | −59 | 6 | −45 |
| 94.57 | Fe I | 2.2 | 1 | −80 | −61 | 3 | −44 |
| 4518.02 | Ti I | 0.8 | 4 | −84 | −59 | 5 | −37 |
| 22.80 | Ti I | 0.8 | 5 | −81 | −58 | 3 | −39 |
| 28.61 | Fe I | 2.2 | 1 | −73 | −60 | 4 | −43 |
| 54.03 | Ba II | 0.0 | 5 | −87 | −62 | 3 | −44 |
| 63.76 | Ti II | 1.2 | 3 | −82 | −64 | 5 | −41 |
| 71.10 | Mg I | 0.0 | 3 | −82 | −63 | (6 | −36) |
| 71.97 | Ti II | 1.6 | (6 | −93) | −64 | 4 | −31 |
| 4934.09 | Ba II | 0.0 | 7 | −81 | −60 | 6 | −39 |
| 5012.07 | Fe I | 0.9 | 3 | −71 | −58 | 5 | −45 |
| 14.18 | Ti I | 0.0 | 6 | −81 | −55 | 3 | −34 |
| 22.87 | Ti I | 0.8 | 5 | −83 | −67 | 3 | −42 |
| 64.65 | Ti I | 0.0 | 4 | −93 | −62 | 6 | −35 |
| Mean | | | | (−82) | −59.2 | | (−39) |

−54 km/sec. If these lines are formed chiefly in the reversing layer, this value may be an approximation to the radial velocity of the star. Shortward of Hβ the displacements are even more scattering, some lines giving about the same displacement as that obtained from the longward component of double lines (Table 1).

## EMISSION LINES

Measured displacements of the narrow maximum between the two absorption components of each line are included in Table 1. This maximum appears to be something more than a narrow section of the original continuous spectrum remaining after absorption components have reduced the intensity on either side; it is probably formed, at least in part, by some actual emission superposed on a wide absorption line. We will return to this point in the "Discussion."

Shortward of λ 4000 A, superposed on the weak continuous spectrum (interrupted, of course, by numerous absorption lines), there appear many narrow maxima which look like emission lines (see Fig. 1 and Table 2). More than 60 of them have been identified with lines of neutral metals as follows: Fe I, 23; Ti I, 21; Ni I, 7; Co I, 6; V I, 5; Mg I, 2; Al I, 2; and Sc I, 1. Although many of the emission lines are weak, the measured displacements are quite consistent (Table 2), yielding a mean value of −58.8 km/sec.

All the Fe I lines thus far found to be bright are in the wave-length region near 3900 A and are in multiplets (20), (21), and (22), whose lower term is $a^5F$, excitation potential 0.9 ev, and in (45), lower term $a^3F$, E.P. 1.5 ev; these lower terms are the first two above the ground term. It is significant that lines from the ground term are not in the list of well-defined bright lines (Table 2), although some of them are complex with weak maxima between two absorption components. All lines of multiplets (20), (22), and (45) are accounted for, but the intensities show an astonishing lack of correlation with the normal laboratory values. Lines of laboratory intensity 10 or 20 are as strong in the star as those of intensity 100 or 200. It is perhaps noteworthy that lines of greatest relative weakening in the star are marked "r" or "R" (reversed) in the laboratory list.

The Ti I emission lines are mostly in multiplets (12), (13), (14), and (17) from the ground level. Discrepancies with laboratory intensities are in the same sense as in Fe I (i.e., strong and weak lines are more nearly equal than in the laboratory) but are less striking because the range in laboratory intensities is not so great as in Fe I. Figure 1 shows that H and K of Ca II are very broad absorption lines without strong emission components. The exposure is too weak to reveal possible details of the central structure. Our observations suggest that emission lines are less conspicuous shortward from λ 3700 A than between λ 3700 and λ 4000 A, but additional spectrograms will be required to settle this important point.

Differences between the two spectrograms, which were taken nearly 10 months apart, are minor. In a few absorption lines, small changes in structure are noticeable. Emission lines of Ti I have about the same intensities on both plates; emission lines of other elements are weaker on the second plate. In a number of double absorption lines the maxima between the two components appear to be lower on the second plate. Differences in displacements also are slight. Mean values of the differences are in Table 3. In forming Tables 1 and 2 the small differences in Table 3 were disregarded; the data are the means of all available measurements in both orders on both plates.

## DISCUSSION

The complex lines of RW Cephei appear to be formed by contributions from three stellar levels.

A. *Reversing layer.*—Absorption lines from the reversing layer are widened, probaby chiefly by turbulence, to an amount corresponding to a total velocity spread of about 80 km/sec. If other causes of widening are present, the range of turbulent velocities would,

TABLE 2

EMISSION LINES IN THE SPECTRUM OF RW CEPHEI

| LABORATORY | | | RW CEPHEI | | LABORATORY | | | RW CEPHEI | |
|---|---|---|---|---|---|---|---|---|---|
| λ | Element* | Mult. | Int. | Rad. Vel. (km/sec) | λ | Element* | Mult. | Int. | Rad. Vel. (km/sec) |
| 3653.50 | Ti | 19 | 1 | −56 | 3873.95 | Co | 18 | B1 | |
| 3717.39 | Ti | 17 | 2? | (−43) | 75.08 | V | 7 | 1 | −59 |
| 27.62 | Fe | 21 | 1 | −60 | 76.04 | Fe | 22 | 1 | −61 |
| 29.81 | Ti | 17 | 1.5 | −53 | 76.83 | Co | 17 | 1 | −60 |
| 41.06 | Ti | 17 | 3 | −58 | 78.02 | Fe | 20 | 2 | −64 |
| 52.86 | Ti | 17 | Tr | −56 | 87.05 | Fe | 20 | 4 | −59 |
| 53.62 | Ti | 17 | 2 | −58 | 88.52 | Fe | 45 | 4 | −62 |
| 71.65 | Ti | 17 | 5 | −57 | 98.01 | Fe | 20 | 1 | −62 |
| 75.57 | Ni | 33 | 1.5 | −62 | 3902.95 | Fe | 45 | 1 | −61 |
| 83.53 | Ni | 30 | 2 | −58 | 04.78 | Ti | 56 | 6 | −57 |
| 3807.14 | Ni | 33 | Tr | −58 | 09.89 | V | 7 | 1 | (−56) |
| 12.96 | Fe | 22 | Tr | −59 | 09.93 | Co | 3 | | (−59) |
| 14.53 | Fe | 22 | 1 | −57 | 11.81 | Sc | 8 | 1 | −56 |
| 15.84 | Fe | 45 | 1 | −56 | 14.33 | Ti | 15 | 2 | −59 |
| 20.43 | Fe | 20 | 1 | −58 | 17.18 | Fe | 20 | 3 | −59 |
| 25.89 | Fe | 20 | 1 | −57 | 21.42 | Ti | 14 | 1 | −57 |
| 27.82 | Fe | 45 | 1 | −60 | 24.53 | Ti | 13 | 5 | −58 |
| 28.56 | V | 9 | 1 | −56 | 40.88 | Fe | 20 | 5 | −62 |
| 31.69 | Ni | 31 | Tr | −61 | 44.01 | Al | 1 | 2 | −57 |
| 32.30 | Mg | 3 | Tr | −63 | 47.77 | Ti | 14 | 4 | −60 |
| 34.22 | Fe | 20 | 1.3 | −56 | 48.67 | Ti | 13 | 6 | −59 |
| 36.05 | V | 44 | 1.5 | −60 | 56.34 | Ti | 13 | 5 | −59 |
| 38.29 | Mg | 3 | Tr | −59 | 58.21 | Ti | 13 | 6 | −59 |
| 39.00 | V | 44 | 1 | −56 | 61.52 | Al | 1 | 2 | −56 |
| 40.44 | Fe | 20 | 2 | −62 | 62.85 | Ti | 12 | 3 | −58 |
| 41.05 | Fe | 45 | Tr | −58 | 64.27 | Ti | 12 | 3 | −60 |
| 42.05 | Co | 33 | Tr | −61 | 66.07 | Fe | 45 | 2 | −59 |
| 45.47 | Co | 34 | 2 | −61 | 72.17 | Ni | 29 | B1 | |
| 49.77 | Fe | 20 | 3 | −60 | 73.56 | Ni | 31 | B1 | |
| 50.82 | Fe | 22 | 3? | (−65) | 81.76 | Ti | 12 | 5 | −57 |
| 58.30 | Ni | 32 | 2 | −61 | 82.48 | Ti | 11 | 3 | −58 |
| 64.86 | V | 7 | 2 | −61 | 89.76 | Ti | 12 | 4 | −58 |
| 65.53 | Fe | 20 | 4 | −60 | 98.64 | Ti | 12 | 5 | −58 |
| 72.50 | Fe | 20 | 2 | −57 | | | | | |
| 73.12 | Co | 18 | 1.5 | −60 | Mean | ..... | .. | ..... | −58.8 |

* All lines are from neutral atoms.

TABLE 3

MEAN VALUES OF DIFFERENCES IN DISPLACEMENTS
(Pc 1855 *minus* Pc 2248)

| | | km/sec |
|---|---|---|
| Absorption lines | shortward components | −3.6 |
| | maxima | −2.1 |
| | longward components | +1.4 |
| | measured as single | +0.1 |
| Emission lines | | −1.4 |

of course, be less than this. The centers of the lines yield approximately the radial velocity of the star as a whole.

B. *Chromosphere.*—An emitting zone, presumably somewhat above the reversing layer, is either stationary with respect to the reversing layer or has a small outward motion. Lines from this zone appear either as separate bright lines (Table 2) or as narrow maxima within the wider dark lines from the reversing layer. The narrowness of the lines shows that turbulence is less than in the reversing layer.

C. *Expanding shell.*—Absorption lines from the upper atmosphere are relatively narrow and are shifted about 20 km/sec shortward from the centers of lines formed in the reversing layer.

These three zones contribute in widely differing proportions to various spectrum lines. Many lines appear to be formed of an absorption line from the reversing layer, A, with a narrow, nearly central, emission core from zone B. This central emission varies greatly in intensity from line to line; it may be so strong as to divide the absorption line into two parts which, at first inspection, appear to be separate lines, or it may be so weak, especially longward from 5000 A, as to have little apparent effect on the absorption line. The relatively narrow shortward-displaced absorption line from zone C makes predominant contributions to the great resonance lines of Ca I, Cr I, Mn I, and Sr II (Fig. 1) and lesser contributions to other lines.

In the complex lines listed in Table 1, what is called the "longward component" is that part (about half) of the reversing-layer line lying longward of the narrow superposed central emission. The "shortward component," similarly, is the shortward half of the reversing-layer line, reinforced in some lines by a contribution from the outer shell. The measured displacements of these components are recorded to help give an idea of line structures; they probably do not correspond in any simple way to radial velocities of two separate absorbing zones. This explanation of the complex lines is suggested by the fact that the narrow maxima within wide absorption lines (Table 1) have the same displacements as the well-marked emission lines accompanied by little or no absorption (Table 2).

The profiles of the stronger complex lines support this view. If they were formed merely by the partial overlapping of two absorption components, we would expect the inner overlapping edges to be less steep than the outer free edges. In fact, the inner edges are steeper than the outer ones, as would be true if a sharp emission line were superposed; this is well shown by the shortward absorption component of Ca I 4227 A (Fig. 1).

Other details point in the same direction. On the second spectrogram, on which most emission lines are weaker than on the first one, maxima in the double absorption lines also are weaker. The slight differences in displacements between the two plates (Table 3) are the same, within errors of measurement, for maxima as for emission lines. Moreover, the opposite changes in the displacements of the two absorption components find a plausible explanation in the weakening, on the later plate, of the superposed emission which separates them. Certain curious facts concerning the occurrence and intensities of separate emission lines (Table 2) may be summarized as follows:

1. Emission lines appear conspicuous only at wave lengths less than $\lambda$ 4000 A.

2. Ground-level lines of Ti I are conspicuous in emission, whereas ground-level lines of Fe I are partly or wholly suppressed.

3. Within a given multiplet, lines normally weak may be as intense as those normally strong.

It seems probable that these apparent anomalies will find explanation not in peculiar circumstances of emission but rather in heavy absorption of the stellar atmosphere, especially of those strata that lie above the effective zone of emission. Differential absorption, if sufficiently intense, might tend to equalize strong and weak emission or even to suppress some of the strongest lines. Thus the remarkable weakness of the ultimate

lines of Fe I in emission may possibly be explained by the fact that iron atoms are 100 or so times as abundant as those of other metals whose emission lines are present and that most of them are in the ground state. These emission lines, although originally intense, would thus be subjected to much greater absorption than ultimate lines of other metals or than Fe I lines of higher excitation potentials.

It is not obvious why the strong emission lines are restricted to the wave-length region below 4000 A. Perhaps the background spectrum is so much weaker here than at longer wave lengths that the emission lines simply stand out with more contrast. The star is very red; the distribution of energy in the continuous spectrum may correspond to an unexpectedly low temperature. Perhaps in the shorter wave lengths, overlapping of strong absorption lines contributes to the weakening of the background. A test of these suggestions will be found in longer exposures to show more clearly the behavior of the spectrum shortward from 3700 A.

RW Cephei presents in extreme form phenomena that are probably characteristic of supergiant M-type stars. An outward-moving absorbing shell was, in fact, long ago suggested to account for the well-known spectroscopic peculiarities of the supergiant M-type star, $\alpha$ Orionis (Adams and MacCormack 1935; Spitzer 1939; Adams 1956). A comparison of line profiles in RW Cephei and in $\alpha$ Orionis is shown in Figure 1. We are indebted to W. S. Adams for permission to reproduce a tracing of his spectrogram of $\alpha$ Orionis.

In $\alpha$ Orionis the emission is weak or absent, and the narrow dark cores probably correspond more nearly to the maxima in the complex lines of RW Cephei than to the shortward absorption components. In any event, motions both of turbulence in the reversing layers and of expansion of the outer shell appear to be slower in $\alpha$ Orionis than in RW Cephei.

Somewhat the same stellar model with still slower velocities may account for the (algebraic) increase of displacement with excitation potential shown by lines in spectra of giant stars of advanced M and S types. The effect is shown by extensive measurements in the spectra of $o$ Ceti and other Me variables (Joy 1954). A similar effect is clearly present in the spectrum of R Andromedae, type Se (Merrill and Greenstein 1956).

If the radial velocity of RW Cephei, about $-54$ km/sec, is due to differential galactic rotation, the star must be about 4000 parsecs away, with a distance modulus of $-13$ mag. Even without allowance for obscuration, the absolute magnitude would be $-5$.

## REFERENCES

Adams, Walter S. 1956, *Ap. J.*, **123**, 189.
Adams, W. S., and MacCormack, E. 1935, *Ap. J.*, **81**, 119.
Joy, Alfred H. 1954, *Ap. J. Suppl.*, **1**, 39.
Keenan, P. C. 1942, *Ap. J.*, **95**, 461.
Merrill, Paul W., and Greenstein, Jesse L. 1956, *Ap. J. Suppl.*, **2**, 225.
Spitzer, Lyman, Jr. 1939, *Ap. J.*, **90**, 494.

# THE RADIAL VELOCITY OF DQ CEPHEI = HD 199908

J. SAHADE,* O. STRUVE, O. C. WILSON, AND V. ZEBERGS
Berkeley Astronomical Department, University of California, and
Mount Wilson and Palomar Observatories
*Received November 25, 1955*

ABSTRACT

The radial velocities measured on 215 spectrograms taken on sixteen nights confirm Walker's photoelectric period of 0.0788650 day. The mean velocity of the star is −21.9 km/sec. There is a beat period of 0.3751 day. The total range of the principal oscillation is 9.2 km/sec; that of the interfering oscillation is 2.6 km/sec. The period of the interfering oscillation is 0.06516 or 0.09986 day. The spectrum is approximately F1 IV–V. The maximum brightness occurs halfway on the descending branch of the velocity-curve. Near minimum radial velocity a narrow space of continuous spectrum is visible between Ca H and H$\epsilon$. This feature is absent at other phases.

The variability of HD 199908 was discovered by Merle Walker (1952, 1953). He found that the brightness varies in a period of 0.07886 day and that the star is bluer at maximum brightness than at minimum. The range in brightness varied between 0.078 and 0.041 mag. during the course of observations made in 1952. The material was insufficient to determine the character of the variation in range, but there appeared to be a

TABLE 1

LIST OF STAR LINES

| Wave Length | Element | Wave Length | Element |
|---|---|---|---|
| 3878.39* | Fe I, Fe I | 4215.60 | Sr II, Cr II, Fe I |
| 3903.15* | Fe I, V II | 4233.31 | Fe II, Fe I |
| 4030.65 | Mn I, Fe I, Ti I | 4250.51 | Fe I |
| 4045.80 | Fe I | 4289.97 | Cr I, Ti II |
| 4077.49 | Sr II | 4325.58 | Sc II, Fe I |
| 4181.76 | Fe I, Cr II | 4415.14 | Fe I |
| 4198.66 | Fe I, Fe I | 4481.29† | Mg II, Mg II |

* Not measured on γ plates.
† Not measured on Mount Palomar plates.

sudden change in amplitude of the light-curve between the nights of August 16 and 17, 1952, which led Walker to suggest that "the possibility should be kept in mind that the length of the beat period may be a very small multiple of the short period, as in AI Velorum."

During the four nights of September 17–20, 1954, HD 199908 was observed at Palomar Observatory by Walker with a photoelectric photometer attached to the 20-inch telescope and by O. C. Wilson with the coudé spectrograph of the 200-inch telescope. The photometric observations will be discussed by Walker elsewhere. The spectrograms (48) having a dispersion of 17.8 A/mm were turned over to the Berkeley astronomers for measurement. The Palomar spectrograms are indicated by the letters "Pd" in Table 2. The results of these measurements immediately indicated a periodic change in radial velocity in the same period as that found by Walker at the Lick Observatory. Additional spectrograms (167) were therefore secured by Sahade with the 60-inch telescope of the

* Inter-American John Simon Guggenheim Fellow.

TABLE 2

RADIAL VELOCITIES

| JD 2435000+ | Radial Velocity | JD 2435000+ | Radial Velocity | JD 2435000+ | Radial Velocity |
|---|---|---|---|---|---|
| 002.637 | −20.5 Pd* | 236.846 | −22.6 γ | 300.825 | −28.5 |
| .648 | −21.9 | .862 | −22.5 | .842 | −31.0 |
| .679 | −21.3 | .878 | −21.6 | .863 | −28.9 |
| .691 | −23.1 | .894 | −14.1 | .879 | −30.1 |
| .703 | −23.3 | .910 | −25.7 | .896 | −30.0 |
| .714 | −22.3 | .926 | −20.5 | .912 | −23.3 |
| .726 | −21.1 | .942 | −17.9 | .930 | −24.9 |
| .806 | −17.4 | .958 | −11.0 | .947 | −27.3 |
| .818 | −17.1 | .974 | −12.2 | .965 | −26.1 |
| .829 | −24.3 | .989 | −22.5 | .981 | −22.7 |
| .841 | −23.8 | 237.004 | −25.2 | .997 | −22.7 |
| .854 | −23.9 | 265.862 | −20.5 Xd* | 301.704 | − 9.7 Xd |
| .868 | −21.3 | .894 | −17.9 | .721 | −16.7 |
| .882 | −19.3 | .924 | −21.3 | .738 | −18.7 |
| 003.630 | −26.0 Pd | .943 | −24.8 | .770 | −23.8 |
| .640 | −25.0 | .965 | −23.0 | .786 | −15.5 |
| .652 | −20.4 | .985 | −20.6 | .803 | −29.0 |
| .667 | −17.3 | 266.826 | −22.2 Xd | .819 | −29.5 |
| .681 | −16.2 | .845 | −20.1 | .835 | −27.7 |
| .696 | −19.5 | .864 | −21.8 | .856 | −25.2 |
| .708 | −21.6 | .883 | −24.5 | .871 | −20.1 |
| .720 | −23.9 | .903 | −28.1 | .888 | −29.4 |
| .733 | −24.3 | .923 | −18.4 | .903 | −31.7 |
| .747 | −18.5 | .942 | −25.1 | .922 | −31.5 |
| .760 | −15.6 | .960 | −27.4 | .938 | −19.5 |
| .772 | −17.2 | .978 | −19.7 | .954 | −21.6 |
| .785 | −16.8 | .996 | −30.1 | .970 | −23.2 |
| .800 | −20.6 | 267.760 | −25.1 Xd | .986 | −29.7 |
| 004.632 | −18.5 Pd | .779 | −17.0 | 353.743 | −25.3 Xd |
| .646 | −20.6 | .819 | −23.8 | .761 | −24.5 |
| .658 | −22.6 | .838 | −19.5 | .777 | −26.9 |
| .671 | −24.3 | .857 | −25.3 | .794 | −21.1 |
| .685 | −19.6 | .876 | −19.8 | .827 | −25.5 |
| .699 | −16.6 | .897 | −22.5 | .843 | −20.8 |
| .715 | −17.3 | .916 | −23.9 | .860 | −23.4 |
| .733 | −24.5 | .935 | −19.7 | .893 | −21.9 |
| .750 | −24.2 | .954 | −18.0 | .910 | −18.3 |
| .764 | −21.2 | .971 | −21.1 | .926 | −18.7 |
| 005.624 | −21.3 Pd | .992 | −25.3 | .946 | −27.3 |
| .637 | −21.5 | 268.762 | −26.9 Xd | .964 | −19.8 |
| .650 | −18.4 | .782 | −21.2 | .981 | −15.7 |
| .665 | −19.9 | .801 | −21.8 | 354.633 | −16.5 Xd |
| .678 | −23.5 | .819 | −17.5 | .649 | −22.9 |
| .693 | −23.6 | .838 | −19.1 | .665 | −26.1 |
| .707 | −23.5 | .857 | −25.0 | .697 | −19.0 |
| .719 | −16.4 | .881 | −20.5 | .713 | −15.9 |
| .732 | −14.6 | .899 | − 8.2 | .731 | −25.5 |
| .744 | −17.5 | .917 | −18.2 | .747 | −30.1 |
| 232.865 | −14.0 γ* | .935 | −25.2 | .763 | −23.5 |
| .882 | −30.0 | .953 | −21.3 | .780 | −23.8 |
| .899 | −25.5 | .971 | −11.8 | .812 | −25.0 |
| .914 | −20.7 | .988 | −23.1 | .828 | −19.7 |
| .929 | −20.9 | 300.703 | −25.7 Xd | .846 | −22.7 |
| .945 | −18.4 | .739 | −23.7 | .863 | −26.0 |
| .961 | −15.9 | .757 | −17.8 | .881 | −21.5 |
| .978 | −23.9 | .774 | −16.1 | .897 | −23.4 |
| .992 | −22.8 | .790 | −22.2 | .914 | −23.3 |
| 233.008 | −17.8 | .808 | −32.8 | .931 | −21.2 |

* See the text for explanation of the symbols.

TABLE 2—*Continued*

| JD 2435000+ | Radial Velocity | JD 2435000+ | Radial Velocity | JD 2435000+ | Radial Velocity |
|---|---|---|---|---|---|
| 354.949 | −19.4 | 355.818 | −14.9 | 356.746 | −23.6 |
| .967 | −15.3 | .835 | −25.7 | .762 | −18.4 |
| .984 | − 9.7 | .869 | −22.5 | .778 | −25.4 |
| 355.634 | −23.2 Xd | .888 | −15.8 | .794 | −29.9 |
| .650 | −17.7 | .904 | −17.3 | .810 | −24.7 |
| .667 | −19.4 | .921 | −19.6 | .826 | −21.7 |
| .683 | −28.3 | .954 | −16.0 | .843 | −20.5 |
| .701 | −28.9 | .972 | − 9.3 | .859 | −24.4 |
| .717 | −22.4 | 356.644 | −19.0 Xd | .876 | −21.6 |
| .734 | −16.0 | .661 | −14.9 | .892 | −19.0 |
| .750 | −22.3 | .678 | −23.6 | .909 | −18.3 |
| .767 | −28.9 | .696 | −24.3 | .927 | −16.3 |
| .783 | −24.7 | .712 | −26.1 | .961 | −22.8 |
| .801 | −21.0 | .729 | −20.5 | | |

Mount Wilson Observatory and with two Cassegrain spectrographs. Those of May, 1955, were made with the old prism spectrograph at the Cassegrain focus. They have a dispersion of 31.2 A/mm at λ 4200. They are labeled "γ" in Tables 1 and 2. All the remaining spectrograms were obtained by Sahade with the new grating spectrograph at the Cassegrain focus, having a dispersion of 20.8 A/mm; they are labeled "Xd" in Table 2. Most of the measurements were made by Mrs. Zebergs; those on May 9, 1955, were made by Sahade.

The spectral type is approximately F1 IV–V, according to Stableford. W. P. Bidelman remarks that the spectrum resembles that of β Cassiopeiae, a F2 IV star, the absolute magnitude of which is approximately +1.

Table 1 lists the star lines used for the determination of the radial velocities. Table 2 gives the mean values for all 215 spectrograms. Table 3 lists the observed epochs of maximum and minimum radial velocity. The best period obtained from these data is $P_1 = 0.0788650$ day, which agrees closely with one of the improved values of Walker (1953). Using this principal period, we have computed in the third and sixth columns of Table 3 the epochs of maximum and minimum velocity. The residuals in the fourth and seventh columns of Table 3 show only small systematic departures that may well be due to the effect of an interfering periodicity of small amplitude. The last column of the table lists the mean velocities of each cycle. Although the range is between −17 and −27 km/sec, we are not certain that there is a real systematic variation in γ. We have not been able to find any periodicity in these values.

The individual plate velocities have been plotted in Figures 1*a*, 1*b*, and 1*c*. The computed epochs of maximum radial velocity are indicated by the downward arrows; the computed epochs of minimum velocity are shown by the upward arrows. The scatter is large because of the small amplitude of the velocity-curve and the small dispersion of the spectrograms. Nevertheless, there is general agreement between the observed epochs and the computed ones. Figure 2 shows the average velocity-curve computed with the period of 0.0788650 day. Phase 0.00 corresponds to the value of $T_0$ = JD 2435003.759 of Table 3. The total range of the mean velocity-curve is 6 km/sec, and there is a suggestion that the curve may be unsymmetrical.

The individual cycles strongly suggest that the amplitude of the velocity-curve is variable. The best value of the beat period is 0.3751 day, which is about 4.8 times the principal period, $P_1$. Figure 3 shows the values of $2K$ (total amplitudes) plotted against the period $P = 0.3751$ day. Although the scatter is very large, there is an unmistakable

TABLE 3

OBSERVED AND COMPUTED MAXIMA AND MINIMA, $\gamma$
($P$ = 0.0788650 Day)

| DATE | MAXIMA $T_0$=JD 2435003.759 | | | MINIMA $T_0$=JD 2435003.721 | | | $\gamma$ |
|---|---|---|---|---|---|---|---|
| | Observed Epoch | Computed Epoch | O−C | Observed Epoch | Computed Epoch | O−C | |
| 1954 | JD 2435000+ | JD 2435000+ | | JD 2435000+ | JD 2435000+ | | |
| Sept. 17... | | | | 002.700 | 002.696 | + 4 | |
| | 002.812 | 002.813 | − 1 | .844 | .853 | − 9 | −20.8 |
| Sept. 18... | 003.680 | 003.680 | 0 | 003.731 | 003.721 | +10 | −20.2 |
| | .765 | .759 | + 6 | | | | −20.2 |
| Sept. 19... | | | | 004.671 | 004.667 | + 4 | −20.4 |
| | 004.705 | 004.705 | 0 | .741 | .746 | − 5 | −20.8 |
| Sept. 20... | 005.650 | 005.652 | − 2 | 005.692 | 005.693 | − 1 | −21.4 |
| | .732 | .731 | + 1 | | | | −19.3 |
| 1955 | | | | | | | |
| May 5... | | | | 232.885 | 232.903 | −18 | −22.8 |
| | 232.960 | 232.941 | +19 | .983 | .982 | + 1 | −19.6 |
| May 9... | 236.893 | 236.884 | + 9 | 236.910 | 236.925 | −15 | −19.8 |
| | .962 | .963 | − 1 | | | | −18.8 |
| June 7... | 265.894 | 265.906 | −12 | 265.943 | 265.947 | − 4 | −21.4 |
| June 8... | 266.847 | 266.853 | − 6 | 266.903 | 266.894 | + 9 | −24.1 |
| | .922 | .932 | −10 | .957 | .972 | −15 | −23.0 |
| | .983 | 267.010 | −27 | | | | −23.5 |
| June 9... | 267.951 | 267.957 | − 6 | 267.913 | 267.919 | − 6 | −21.0 |
| June 10... | 268.822 | 268.828 | − 6 | 268.852 | 268.865 | −13 | −21.2 |
| | .899 | .903 | − 4 | .937 | .944 | − 7 | −16.8 |
| | .972 | .982 | −10 | | | | −18.1 |
| July 12... | 300.770 | 300.765 | + 5 | 300.808 | 300.805 | + 3 | −24.4 |
| | | | | .888 | .884 | + 4 | −27.0 |
| | .908 | .922 | −14 | .951 | .963 | −12 | −25.6 |
| | .988 | 301.001 | −13 | | | | −25.0 |
| July 13... | 301.790 | 301.790 | 0 | 301.812 | 301.831 | −19 | −22.7 |
| | .875 | .869 | + 6 | .910 | .910 | 0 | −26.0 |
| | .945 | .948 | − 3 | | | | −25.6 |
| Sept. 3... | 353.845 | 353.841 | + 4 | 353.880 | 353.882 | − 2 | −23.1 |
| | .917 | .920 | − 3 | .948 | .960 | −12 | −22.5 |
| Sept. 4... | | | | 354.670 | 354.670 | 0 | −21.1 |
| | 354.713 | 354.708 | + 5 | .747 | .749 | − 2 | −23.5 |
| Sept. 5... | 355.655 | 355.654 | + 1 | 355.695 | 355.695 | 0 | −23.6 |
| | .737 | .733 | + 4 | .768 | .774 | − 6 | −22.3 |
| | .820 | .812 | + 8 | .845 | .853 | − 8 | −20.5 |
| | .892 | .891 | + 1 | .937 | .932 | + 5 | −18.5 |
| Sept. 6... | 356.663 | 356.680 | −17 | 356.712 | 356.721 | − 9 | −20.5 |
| | | | | .794 | .800 | − 6 | −25.1 |
| | .843 | .838 | + 5 | .861 | .878 | −17 | −22.5 |
| | .926 | .916 | +10 | | | | −20.4 |

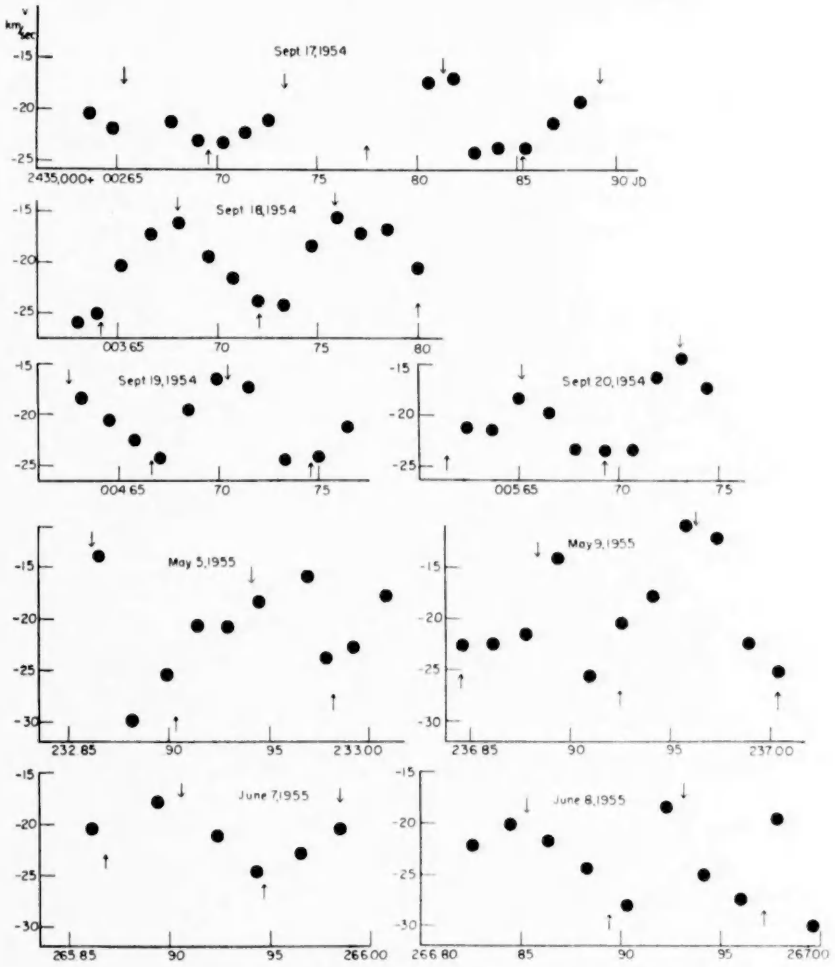


FIG. 1*a*.—Velocity-curves of HD 199908

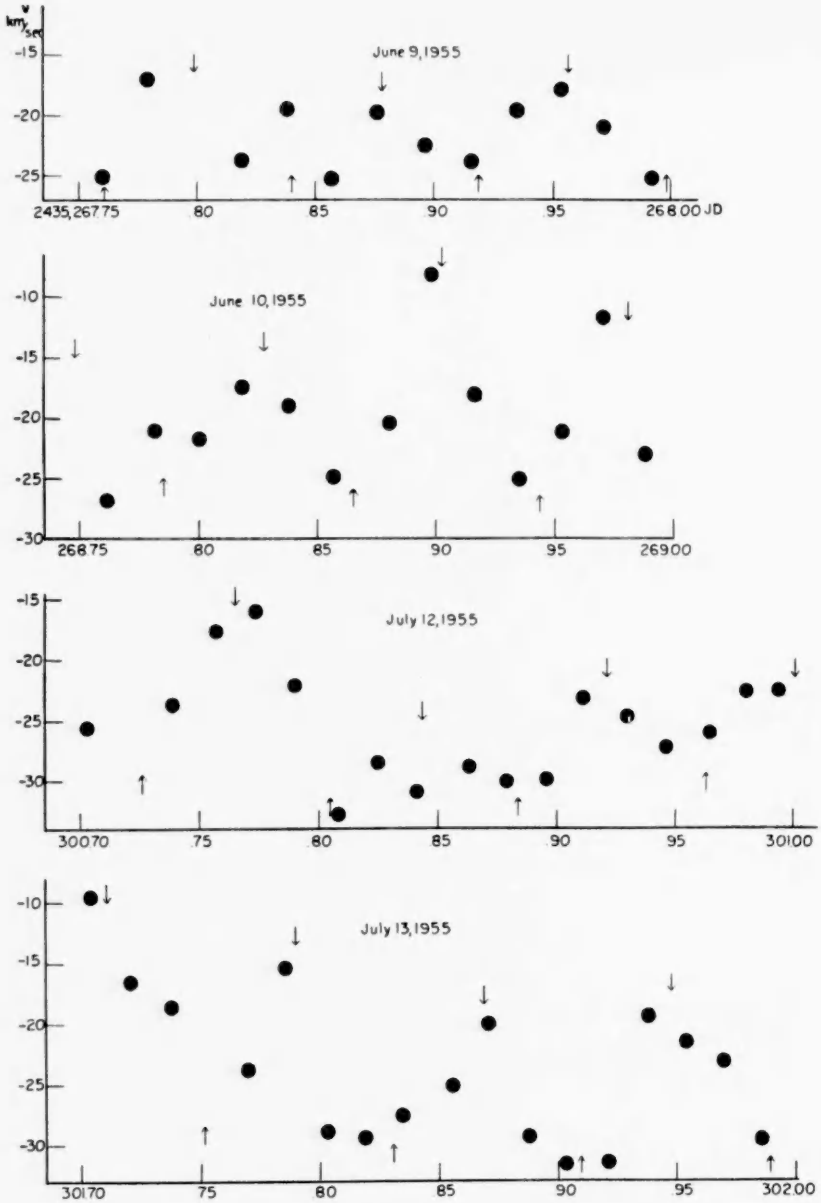


FIG. 1*b*.—Velocity-curves of HD 199908

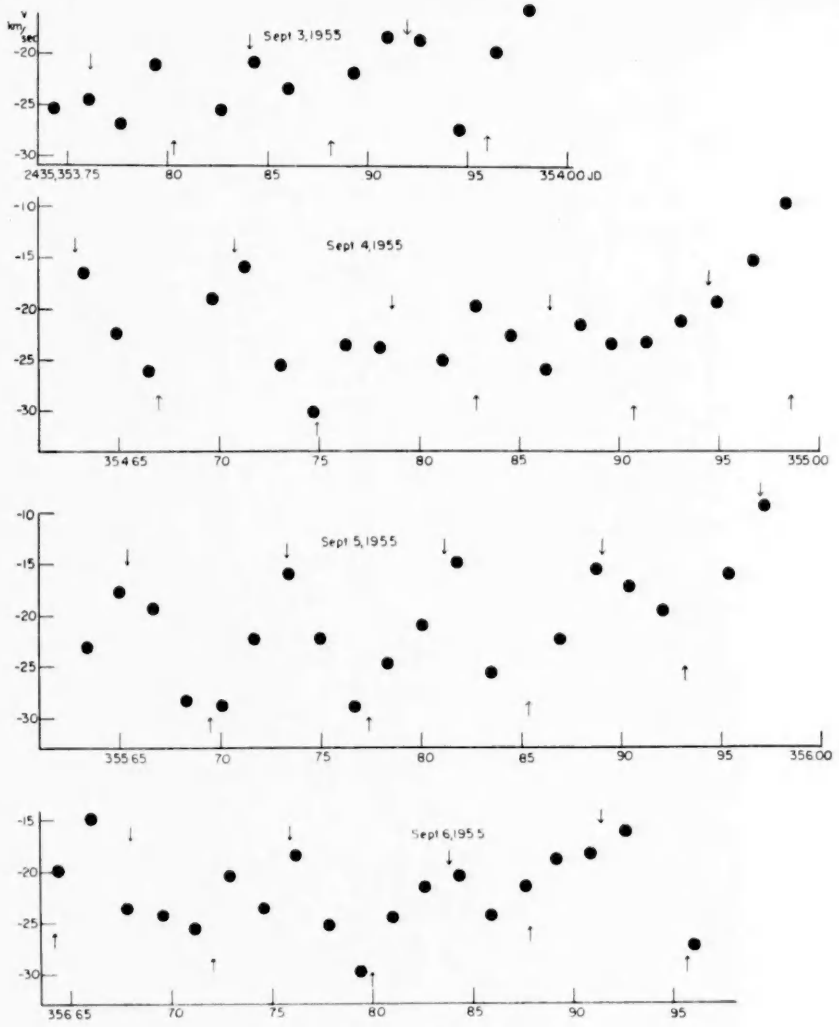


FIG. 1*c*.—Velocity-curves of HD 199908

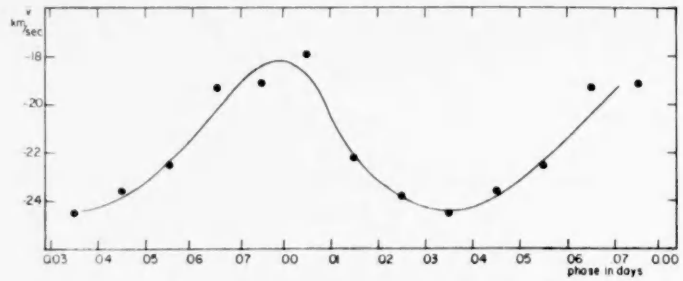


FIG. 2.—Mean velocity-curve of HD 199908

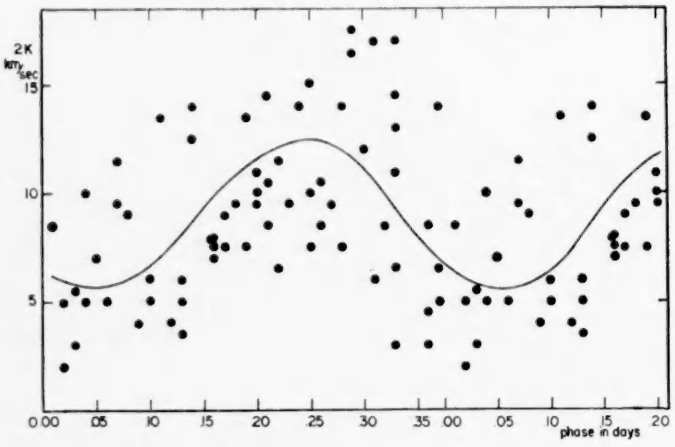


FIG. 3.—Plot of values of $2K$ against the beat period of 0.3751 day

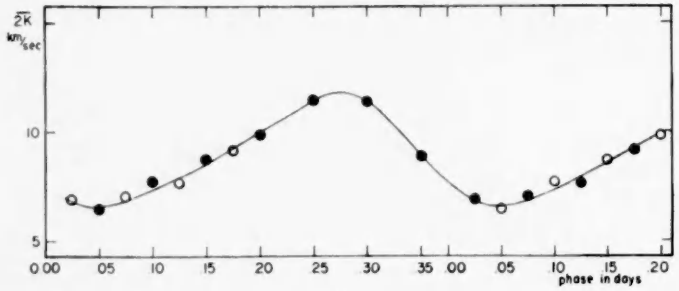


FIG. 4.—Smoothed plot of values of $2K$ against the beat period of 0.3751 day

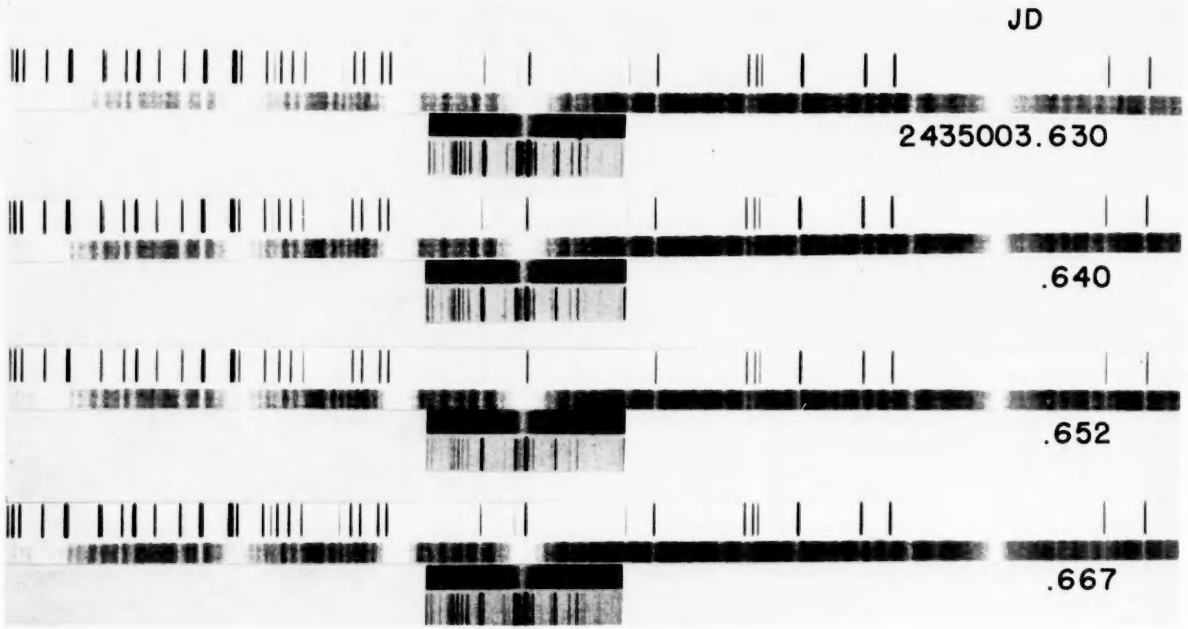


FIG. 5.—Spectra of HD 199908

maximum at phase 0.25 day and a minimum at phase 0.05 day. The phase 0.00 corresponds to JD 2435005.640. Figure 4 shows a plot of the smoothed values of $2K$, each dot representing the mean value between 0.00 and 0.10, between 0.05 and 0.15, etc. The curves in Figures 3 and 4 have been drawn arbitrarily to represent the points; they have not been computed from the theory of beats. We conclude that the maximum value of $2K$ = 11.8 km/sec and the minimum value is $2K$ = 6.5 km/sec. Consequently, the total range of the principal oscillation is 9.2 km/sec, and the total range of the interfering oscillation is 2.6 km/sec. These values are not entirely consistent with the range of the mean curve in Figure 2, but this is probably due to the intrinsic uncertainties in the smoothing processes adopted for the two curves of Figures 2 and 4. We cannot distinguish between two values of the interfering period. They are $P_2 = 0.06516$ day or $P_2 = 0.09986$ day.

According to the preliminary light-curves of Walker in September, 1954, the epoch of maximum brightness occurs about halfway on the descending branch of the velocity-curve and minimum light about halfway on the ascending branch of the velocity-curve. This is the same phase relation that has been observed in the $\beta$ Canis Majoris stars.

A remarkable spectroscopic phenomenon has been observed on the Palomar spectrograms which are the only ones that have a sufficiently large resolving power to show it. Approximately at minimum radial velocity a narrow bright feature appears between the lines Ca H and H$\epsilon$. This feature often looks like a fairly narrow emission line, but it is probably a strip of continuous spectrum between the two strong absorption lines. Figure 5 illustrates this effect. At phase JD 2435003.630 this feature is clearly visible. It corresponds to the first minimum on September 18, 1954, in Figure 1*a*. The other spectrograms that were equally exposed do not show this feature. Although it is visible on all good spectrograms of the Palomar series near minimum radial velocity, its intensity seems to be variable. The material is not sufficient to connect this variation either with the beat period or with any other property of the star. It may be caused by a change in the spectral type of HD 199908, although from the color observations we should have expected such a change in spectral type to be most pronounced when we compare spectrograms taken at the epochs of maximum and minimum brightness rather than at the epochs of maximum and minimum radial velocity.

HD 199908 is undoubtedly a member of the group of pulsating variables of the AI Velorum type (Gratton 1953 *a* and *b;* Walraven 1955). It also resembles $\delta$ Scuti (Paddock and Struve 1954). There are a number of other F-type stars of the same character, some of which have been recently discussed by Smith (1954).

## REFERENCES

Gratton, Livio. 1953a, *B.A.N.*, No. 444.
———. 1953b, *Zs. f. Ap.*, **32**, 69.
Paddock, G. F., and Struve, Otto. 1954, *Ap. J.*, **119**, 309.
Smith, H. J. 1954, unpublished; see *Sky and Telescope*, **14**, 461, 1955.
Walker, Merle F., 1952, *Pub. A.S.P.*, **64**, 192.
———. 1953, *ibid.*, **65**, 39.
Walraven, T. 1955, *B.A.N.*, No. 459.

# ON THE LUMINOSITIES, MOTIONS, AND SPACE DISTRIBUTION OF THE NEARER NORTHERN O–B5 STARS

A. BLAAUW
Yerkes Observatory
*Received January 24, 1956*

## ABSTRACT

The luminosities, motions, and space distribution of the O–B5 stars within 600 pc and north of declination $-20°$ have been studied, with emphasis on the problem of the calibration of the MK luminosity classifications for the subclasses B1 V, B2 IV, B2 V, and B3 V. Analysis of the apparent distribution of the stars in different distance groups and of their proper motions reveals the existence of a loose group of stars in the constellations Cassiopeia to Taurus, with very small internal velocity dispersion and probably of related origin. This Cassiopeia-Taurus group is identical with the extended Perseus stream recognized by earlier investigators but subjected to doubt more recently. Solutions for the elements of the motions of these stars with respect to the sun are discussed in detail. The conventional procedure of applying corrections for differential galactic rotation does not appear to be justified in the present case, since the principal feature of the relative motions within the group is that of a general expansion and not of differential motions according to different circular galactic orbits. A solution based on the assumption of approximately linear expansion leads to satisfactory elements of motion and an "expansion age" of at least 50 million years. This seems compatible with the H-R diagram of the group, which contains no stars of types earlier than B0 and no absolute magnitudes brighter than $-4.7$. The average peculiar motions are found to be 2 km/sec in the $\tau$ components and 3 km/sec in the radial components. Individual parallaxes and absolute magnitudes are derived for the members of this group.

Other information on absolute magnitudes used for the calibration is derived from the field stars in the region between galactic longitudes 340° and 50°, where the motions are random except for a common solar motion and where they are undisturbed by local streamings or associations. The data thus derived on the luminosities of the northern stars are supplemented with absolute magnitudes in the Scorpio-Centaurus association borrowed from a recent investigation by Bertiau, particulars of which will be published separately. We thus arrive at the following mean visual absolute magnitudes in the $U-B-V$ system: $-3.8$ for B1 V, $-2.7$ for B2 IV, $-2.4$ for B2 V, and $-1.5$ for B3 V. These apply to stars selected per volume of space and not per apparent magnitude, as were the preliminary values tabulated by Morgan and Keenan. The average deviations from these means are $\pm 0.6$ mag. for the three subclasses V and $\pm 0.3$ for B2 IV.

The moving cluster around $\alpha$ Persei is shown to belong to the Cassiopeia-Taurus group, which leads to a determination of its distance (127 pc) and of the absolute magnitudes of its members. Mean values for luminosity class V are $-0.5$ for B3–B5 and $+1.6$ for B9–A1, suggesting that the main sequence around B3 in the extended group lies somewhat higher than in the cluster.

A few stars of very high space velocity occur in the region of space studied. Of particular interest are 53 Arietis (B2 V) and 68 Cygni (O8). 53 Arietis appears to have originated in the Orion association about 4.8 million years ago and is moving away from it with a speed of 73 km/sec. It is thus the third star known to move with very high velocity from this origin. 68 Cygni very probably originated in the association I Cephei 5.1 million years ago and has a space velocity of 45 km/sec.

## I. INTRODUCTION

The present paper describes a study of the space distribution, the motions, and the luminosities of the nearer northern early B-type stars. It is based on the extensive material of spectral and luminosity classifications made by W. W. Morgan on the MK system, and special attention is given to the problem of the calibration of these luminosity classifications. The investigation is limited to the stars within about 600 pc and north of $-20°$ declination. The absolute magnitudes are derived exclusively from the proper motions. Only a few stars of high luminosity occur within the region studied, and the results for the calibration therefore refer mainly to the low-luminosity classes, particularly for B2 and B3. Additional information on the absolute magnitudes of the low-luminosity classes, included in the present discussion, is borrowed from a recent investi-

gation of the Scorpio-Centaurus cluster by Bertiau. The detailed results of Bertiau's work will soon be published separately.

The results of the present paper represent a fundamental step in the process of the calibration of the MK classifications, inasmuch as they determine the zero point of the scale of the absolute magnitudes. They will later be supplemented by the information derived from the associations of early B stars; these will add data particularly on the relative luminosities of the high- and low-luminosity classes. No distances will be derived from the effect of differential galactic rotation, so that this, and particularly the value of the constant $A$, can later be investigated independently.

Numerous investigations of the motions of the bright B stars have been published during the last twenty-five years. A summary of these has been given by Torondjadze (1953), and we will therefore only occasionally refer to earlier work. It appeared desirable to reinvestigate the kinematical properties of the nearer B-type stars in order to arrive at the most reliable use of the proper motions as a measure of distance. As a result, the data on the calibration obtained in the present paper are based mainly on the following stars:

1. The nearer stars in the region from Cassiopeia to Taurus. These stars seem to form a loose association. The small internal velocities in this group allow an estimate of the individual absolute magnitudes.

2. The stars in the region between galactic longitudes 340° and 50°. Here the proper motions can be interpreted on the basis of solar motion and random peculiar motions without complications by associations.

The region occupied by the stars studied in this paper contains several associations—Orion, Lacerta, II ($\zeta$) Persei—the $\alpha$ Persei cluster, the loose group just mentioned, and a fairly uniformly distributed population of "field" stars in the lower longitude section. It may well be considered as a representative sample of a spiral-arm population of early-type stars.

## II. BASIC OBSERVATIONAL DATA

Morgan's observations have covered most of the *Henry Draper* O to B3 stars north of declination $-20°$ and many south of this limit. The *HD* B5 stars were completely observed to apparent magnitude 6.5, whereas the fainter ones are as yet very incompletely observed.

Accordingly the basic list of stars in the present investigation was chosen as follows: (*a*) all the stars north of declination $-20°$ and brighter than visual magnitude 8.5, classified by W. W. Morgan as O–B5 in the MK system; and (*b*) the remaining *HD* O–B3 stars within the same limits of declination and magnitudes. These stars were included in the first stage of the investigation in order to obtain an estimate of the completeness of the data for O–B3 in the various distance groups discussed later.

The basic list may thus be assumed to be fairly complete for the MK types O–B3 (classified *plus* still unclassified), but it contains only the brightest of the MK B5 stars. Some aspects of the completeness of the basic list will be considered in the next section.

In correcting the visual magnitudes for interstellar absorption, we have used the observed colors by Stebbins, Huffer, and Whitford (1940) and the intrinsic colors and the relation $A_{vis} = 6.1E_1$ as given by Morgan, Harris, and Johnson (1953). For a small number of stars, $B - V$ colors and $V$ magnitudes have been used (see Sec. V, *d*).

The proper motions were taken from the Albany *General Catalogue* (Boss 1937) and combined with new values derived by Dr. H. R. Morgan from recent meridian observations. Part of these have been published in the "N30" catalogue (H. R. Morgan 1952). For the fundamental system we adopted the average of FK3 and N30. The difference between the two systems is generally small for the region of the sky with which we are concerned here. Precessional corrections were applied as recommended by Morgan and Oort (1951). The radial velocities were taken from Wilson's (1953) catalogue.

### III. DISTANCE GROUPS; COMPLETENESS

The stars in the basic list were first divided into distance groups according to provisional distance moduli, computed with the provisional mean visual absolute magnitudes for stars of a given apparent magnitude, tabulated by Keenan and Morgan (1951). For the main-sequence subclasses these values were based partly on a preliminary analysis by the author (Blaauw 1952*a*). Only the stars in three distance groups within 600 pc were retained for the present discussion. Particulars about these three groups are given in Table 1. The distribution on the sky for the stars between galactic latitudes $-50°$ and $+40°$ in these three modulus groups is shown in Figures 1*a* and 1*b*, 2*a* and 2*b*, and 3*a* and 3*b*. Stars of MK types O–B3 are represented by dots; types B5 by open circles.

The stars in the three associations within 600 pc were all plotted in the modulus group corresponding to the distance of the association, although a good many of them would have been assigned to other modulus groups on the basis of individual values of $m_0 - M$. In the case of the Orion association with $m_0 - M = 8.5$ (Sharpless 1952), all stars within the region R.A. = $5^h12^m$ to $5^h44^m$, Decl. = $+5°$ to $-8°$ were assigned to modulus group C. All stars in the II ($\zeta$) Persei association, for which $m_0 - M = 7.4$ (Blaauw 1952*b*), were placed in group B, and those in the Lacerta association, with $m_0 - M = 8.3$ (Blaauw and Morgan 1953), in group C.

TABLE 1

DISTANCE GROUPS AND NUMBERS OF STARS

| | Group A | Group B | Group C |
|---|---|---|---|
| Provisional distance moduli | <6.6 | 6.6–7.9 | 8.0–8.9 |
| Provisional distances (pc) | 0–200 | 200–400 | 400–600 |
| No. MK O–B3 stars outside associations and clusters in basic list | 24 | 83 | 128 |
| No. MK B5 stars outside associations and clusters in basic list | 19 | 31 | 7 |

To those stars in the basic list which have no MK classification (*HD* types B3 and earlier) but for which the color is known, we have tentatively assigned a distance modulus according to the *HD* spectral type and luminosity class V. None of these stars then falls into group A or B and 10 into group C. For 35 stars no color or MK type is available. All these are fainter than visual magnitude 7.5, three are of *HD* type B2 and the remainder of type B3. These 35 stars and the 10 mentioned before are plotted as plus signs in Figures 3*a* and 3*b*. Very likely a considerable fraction of these will eventually prove to be beyond the distance limit of 600 pc of group C, and few or none in group A or B. Further, there are 10 stars in the region studied without MK classification and classified as B without subclass in the *Henry Draper Catalogue*. All these are fainter than visual magnitude 8.0. Judging by the MK classifications of other stars in this category, we can safely assume that they will all turn out to be OB stars beyond 600 pc. We conclude that within the distance of 600 pc we have MK classifications for nearly all the stars classified as B3 or earlier in the *Henry Draper Catalogue*.

Part of the stars belonging to MK types B2 and B3 occur as later-type B stars in the *Henry Draper Catalogue*. Therefore, the incompleteness of the observations of the *HD* B5 stars fainter than magnitude 6.5 also causes incompleteness in the MK types B3 and earlier. The same holds for the *HD* types B8 and later, but these will contribute less to the MK types B3 and earlier. The numbers of stars of MK types B3 and earlier which would be added by a complete classification of the *HD* type B5 and later are hard to estimate, as the relation between the two systems of classification appears to vary over

the sky and the MK classifications for the fainter *HD* stars are not yet numerous enough. A rough estimate indicates that probably very few stars of MK types B3 and earlier are lacking from the modulus groups A and B but that some 20 or 30 B2 and B3 main-sequence stars are still missing in modulus group C.

## IV. PROPER MOTIONS AND APPARENT DISTRIBUTION ON THE SKY

The proper motions are quite accurate for the brightest and nearest stars. For the stars in modulus group C they are generally poor. With increasing distance of the stars, the sizes of the proper motions diminish, whereas their probable errors increase, the stars becoming fainter and having less meridian observations; hence the proportions between the errors and the sizes of the proper motions increase rapidly from modulus group A to group C. For our present purpose proper motions with probable errors in excess of $\pm 0''.006$ are of little use, and only the more accurate ones have been plotted in Figures 1–3; those with probable errors below $\pm 0''.004$ as full lines, the remaining ones as dashed lines. The scale is indicated in the lower-left-hand corner of Figures 1*a*, 2*a*, and 3*a*. No individual proper motions are plotted for the stars in the three associations (II [$\chi$] Persei, Orion, and Lacerta) and in the $\alpha$ Persei moving cluster. For the Perseus and Lacerta associations and the $\alpha$ Persei cluster the mean values are plotted at their centers. Stars for which no proper motions were plotted are represented by somewhat smaller symbols.

The six diagrams reveal some interesting properties of the space distribution and motions:

1. In modulus group A, Figures 1*a* and 1*b* ( stars within 200 pc), the stars are somewhat more numerous between longitudes 80° and 200° than between 340° and 80°, even if we do not count those in the $\alpha$ Persei cluster, which is located at $l = 115°$, $b = -5°$. Nearly all stars in Figure 1*a* are at negative galactic latitudes, whereas those in Figure 1*b* are distributed symmetrically with respect to the galactic circle. The Gould belt is very clearly marked by the location of these nearest stars.

The proper motions in Figure 1*a* are remarkably parallel and generally of the same size. Those in Figure 1*b* are smaller. This does not seem to be due only to the fact that these latter stars are located around the solar apex, the standard co-ordinates of which are $l = 24°$, $b = +22°$, for we notice that the large motions in Figure 1*a* persist up to about 30° from the standard antapex ($l = 204°$, $b = -22°$). Figures 1*a* and 1*b* suggest strongly that between longitudes 80° and 170° there is a group of stars within 200 pc from the sun whose relative velocities are very small compared to their systematic motion with respect to the sun. We shall call this group the "Cassiopeia-Taurus group."

2. The distribution of the stars in Figure 2*a* (modulus group B, 200–400 pc) lends support to the assumption that the nearest Cassiopeia-Taurus stars form a more or less isolated group, for there are very few more distant stars in modulus group B between galactic longitudes 90° and 140°. Near the center of this region is the II Persei association, and the region immediately around it is remarkably devoid of stars. It is unlikely that this is due to interstellar absorption, which might have eliminated these stars from our basic list, for the heavy absorption takes place mainly in the Taurus clouds and in the immediate vicinity of the II Persei association. The Taurus clouds are represented by the shaded area around $l = 140°$, $b = -10°$ in Figure 1*a*; the contour lines correspond to photographic absorptions of 1, 2, and 3 mag., according to McCuskey's (1941) analysis of star counts. The distance of the Taurus clouds is estimated at about 145 pc (see, e.g., Greenstein 1937).

The proper motions in Figure 2*a* are generally smaller than those in Figure 1*a*, as one would expect from the difference in the mean distances, but a number of them have the same size and direction as those in modulus group A. They may actually be stars at the smaller distances of group A, but with lower-than-average luminosities, which place

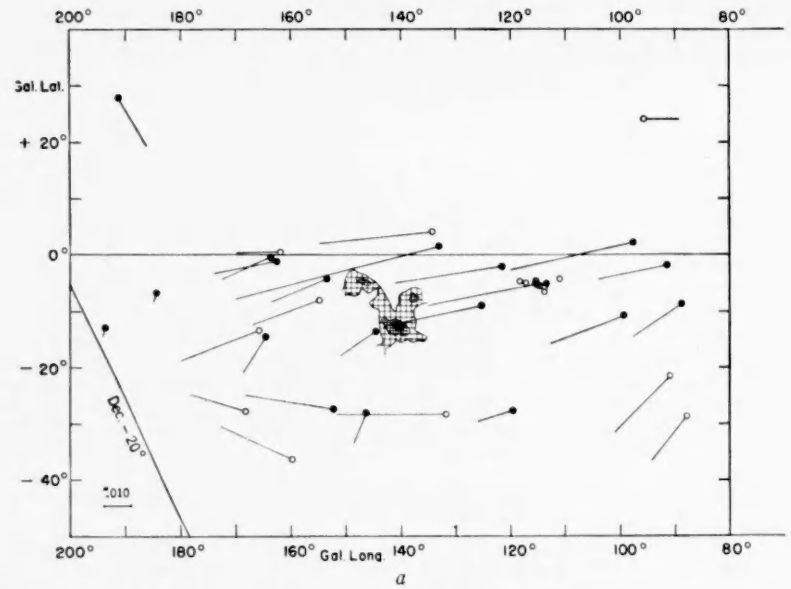


*a*

FIG. 1, *a* and *b*.—Apparent distribution and proper motions of the stars in modulus group A (corresponding to distances within 200 pc). *Dots:* MK types B3 and earlier. *Open circles:* MK type B5. Lines drawn from the dots and circles represent proper motions with probable errors below ".0040; dashed lines represent those with probable errors between ".0040 and ".0060. The scale of the proper motions is given in the lower left corner. The hatched region represents the Taurus dark cloud complex. At $l = 115°$, $b = -4°$ is the α Persei cluster.

them in modulus group B. There is a striking difference in the character of the proper motions of the stars above and below galactic longitude 160°. This longitude appears to mark the boundary of the Cassiopeia-Taurus group. On the whole, the space distribution of the stars in group B at longitudes higher than 90° is rather spotty, and it clearly follows the Gould belt.

In Figure 2*b* we find almost ten times as many B3 and earlier-type stars as in Figure 1*b*, whereas, on the basis of the distance limits, one would expect only three or four times as many (we do not count the B5 stars which are already incomplete in modulus group B). The distribution of the stars is fairly uniform, with a majority of them north of the galactic plane. There is a chain of stars at high negative latitudes around longitude 45°. This region is not known to contain heavily obscuring near-by clouds (Bok 1937), but it is of some interest to notice that it shows large deficiencies in Hubble's (1934) counts of extragalactic nebulae. These high-latitude stars may perhaps be associated with a cloud complex at a great distance from the galactic plane. The Lacerta association (at $l = 65°$, $b = -15°$ in Fig. 3*b*) may also be associated with this "flare" of interstellar gas. From Figures 2*b* and 1*b*, it looks as if a uniformly distributed population of early B stars sets in at a distance of about 200 pc. The peculiar motions of these stars are appreciably larger than those in the Cassiopeia-Taurus group (see also Sec. VII).

3. In Figure 3*a* (modulus group C, 400–600 pc) the small number of stars between longitudes 100° and 150° indicates that the emptiness at these longitudes, noted in Figure 2*a*, extends to at least 600 pc. The scarcity of early B-type stars in these directions has

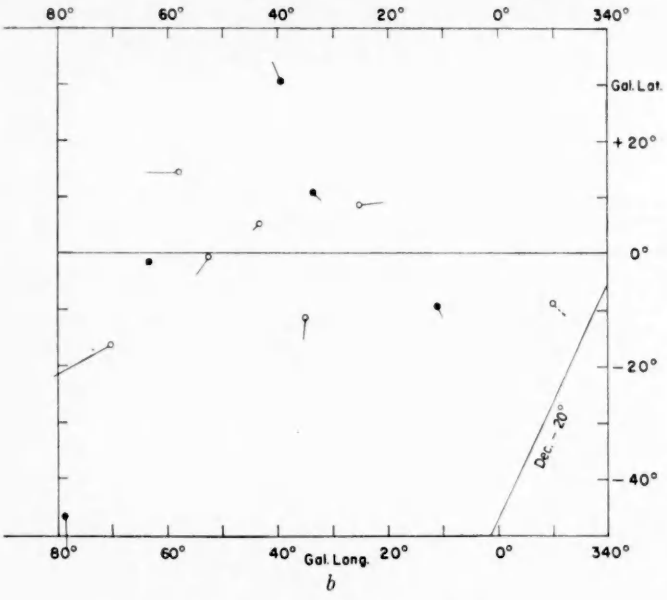


FIG. 1*b*.—See legend under Figure 1*a*

been pointed out earlier by Weaver (1953) on the basis of a study of the space distribution of the OB stars. The local arm, according to Weaver, shows a break in the directions $l = 110°$–$145°$. The population according to Figure 3*a* is dense at higher longitudes, where the Orion association is located. At longitudes below 90° the population is more or less uniform, as in group B, but in addition it contains the Lacerta association. The Orion association still lies in Gould's belt, which is, however, no longer perceptible below longitudes 150°. Only a few stars in modulus group C have accurate proper motions. Some of them, according to the size and direction of the proper motion, seem to belong to the near group of Figure 1*a*.

In Figure 3*b* the motions are rather irregular. Between longitudes 50° and 80° they are complicated by the fact that part of the stars may be associated with the association I Cephei, around $l = 69°$, $b = +4°$, which is located at a distance of 720 pc just beyond group C (Morgan, Whitford, and Code 1953). There appears to be considerable internal motion and probably expansion in this association (see also Markarian 1953; Artiukhina 1954), and some stars outside the association may be connected with it. An example is the O8 star HD 203064 (68 Cygni) at $l = 55\overset{\circ}{.}4$, $b = -4\overset{\circ}{.}4$ (see also Sec. X for more particulars about this star). A few stars may be associated with the Lacerta association, like those at $l = 44\overset{\circ}{.}4$, $b = -5\overset{\circ}{.}5$ (HD 197419) and at $l = 52\overset{\circ}{.}5$, $b = -5\overset{\circ}{.}4$ (HD 201910) (see also Blaauw and Morgan 1953).

For the calibration of the luminosity classifications it is important that those stars be used for which the interpretation of the proper motions in terms of distances is most reliable. We have, therefore, decided to confine the further analysis to two selections: the Cassiopeia-Taurus group, with its small internal velocities, and the region around the solar apex, where the proper motions can be interpreted on the basis of a common

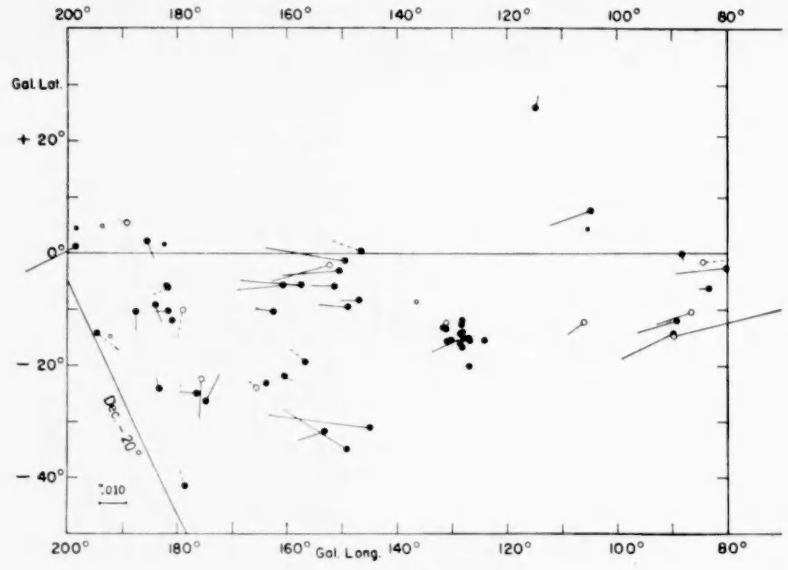


*a*

FIG. 2, *a* and *b*.—Apparent distribution and proper motions for modulus group B (200 to 400 pc). The meaning of the symbols is the same as in Fig. 1. At $l = 128°$, $b = -15°$ is the II ($\zeta$) Persei association.

solar motion combined with random peculiar motions. For the latter, we chose the region between galactic longitudes 340° and 50°, thus avoiding the complicated motions between $l = 50°$ and $l = 80°$.

## V. THE CASSIOPEIA-TAURUS GROUP

### *a) Solutions for Convergent Point and Stream Velocity*

The speed and direction of the motion of this group with respect to the sun have been determined from the directions of the proper motions and from the radial velocities. The sizes of the proper motions were not used. This could have been done, with an assumption concerning the relative distances of the stars based on their provisional distance moduli. The method would have remained somewhat uncertain, however, because of the fairly large range in absolute magnitudes within the principal luminosity classes (see Secs. V, *f*, and VIII). Since the directions alone gave a sufficiently accurate convergent point for our present purpose, the sizes of the proper motions were used only in the determination of the distances.

Usually, in the determination of the elements of the solar motion from stars distributed over a large region of space, one applies corrections for differential galactic rotation to the observed proper motions and radial velocities. This is done on the assumption that different parts of the assembly of stars studied have relative motions which are approximately the same as the relative motions in circular orbits around the galactic center. By applying corrections for differential galactic rotation, one eliminates these relative motions. What is left, then, are the motions of the stars with respect to the local circular velocities plus a common solar motion.

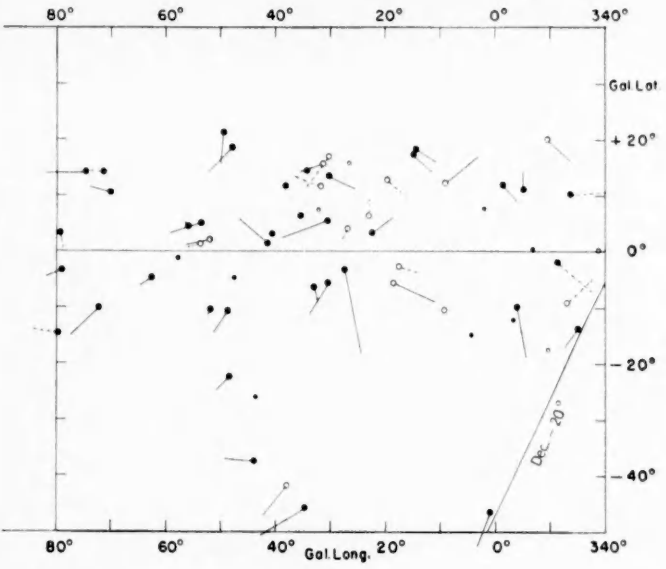


FIG. 2*b*.—See legend under Figure 2*a*

It is questionable whether this procedure should be applied to the Cassiopeia-Taurus group. Both the observation that the group is confined within a region of a few hundred parsecs and the fact that the internal velocity dispersion is small suggest that we are dealing with stars of related origin. If that is the case, the relative motions in different parts may be entirely different from those corresponding to circular motions around the galactic center. We might, for instance, suppose that the stars originated more or less simultaneously in a small volume of space; the question then is whether, after a reasonable lapse of time, the relative motions still display as a principal feature the motions away from this origin or whether they approximate the differential galactic rotation just described.

In order to see how much the corrections for differential galactic rotation affect the solution, we have analyzed the proper motions and radial velocities with and without these corrections. The corrections were based on the values of the constants $A$ and $B$ of rotation as recommended by Morgan and Oort (1950). We shall distinguish between solution I, without corrections, and solution II, with corrections applied. After the convergent point had been determined from the proper motions, the stream velocity toward this convergent and a $K$ term were derived from the radial velocities. The procedure was formally the same in both solutions. Their interpretations are, however, quite different. They will be discussed in the next subsections.

We have used the following stars in determining the convergent point:

1. Those in Figure 1*a*, below galactic longitude 180° and between the latitudes of −40° and +10° but excluding the α Persei cluster, which will be discussed separately in Section IX, and the star λ Tauri at $l = 146°$, $b = -28°$. The exclusion of the latter is somewhat arbitrary. The deviation of its motion from the general pattern is well estab-

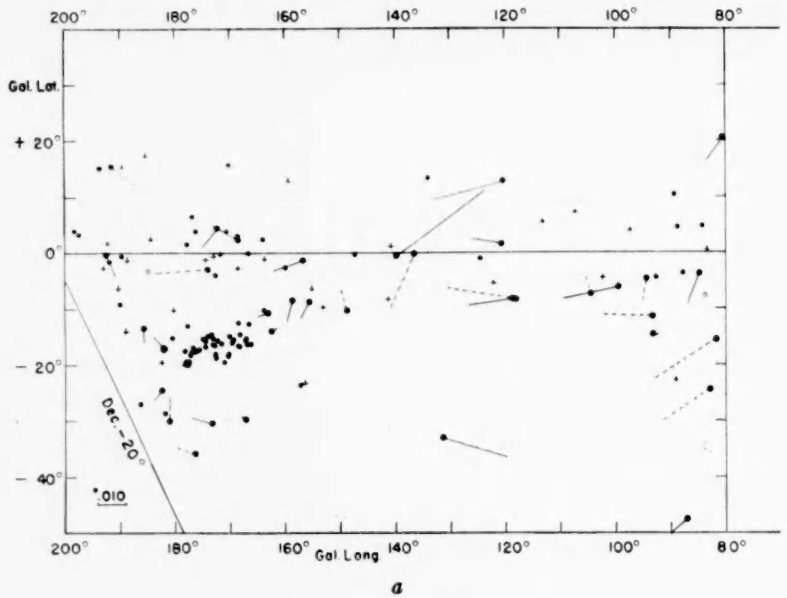


*a*

FIG. 3, *a* and *b*.—Apparent distribution and proper motions for modulus group C (400 to 600 pc). Plus signs represent stars without MK classification which may lie in the modulus group. The meaning of the other symbols is the same as in Fig. 1. At $l = 170°$, $b = -17°$ is the Orion association and at $l = 67°$, $b = -16°$ the Lacerta association.

lished; on the other hand, the other stars also show certain, though smaller, mutua differences in motion.

2. Of the stars in Figure 2*a*, the group around $l = 150°$, $b = -5°$; the three stars around $l = 150°$, $b = -30°$; the four with proper motions of about 0".015 around $l = 85°$, $b = -10°$; and the star at $l = 105°$, $b = +8°$.

The star at $l = -70°$, $b = -16°$ in Figure 1*b* was also included in the first steps but does not contribute to the final determination (see below).

The stars were divided into subgroups according to their position in the sky. Table 2 gives their mean co-ordinates, the numbers of stars, the mean proper motions in galactic longitude and latitude, and the mean radial velocities, all without corrections for differential galactic rotation. The mean proper motions and the numbers of the subgroups are also shown in Figure 4. Almost all the stars used occur in Table 5, where the number in the fourth column refers to the subgroup in which the star was used.

Some explanation is required for the treatment of the stars around $l = 150°$, $b = -5°$. One notices in Figures 1*a* and 2*a* a curious difference between the direction of the motions in that part of the sky for the two modulus groups. Those in group B (Fig. 2*a*) are approximately parallel to the galactic equator, whereas those in group A (Fig. 1*a*) are directed away from it. At first sight, the stars in the two groups seem to have a relative motion perpendicular to the galactic plane. There are, however, reasons to doubt whether this is real. There is probably considerable overlap in the true distances of the stars in the two groups. This follows both from the fact that the range of the true absolute magnitudes within the subclasses B2 V and B3 V, to which most of these stars

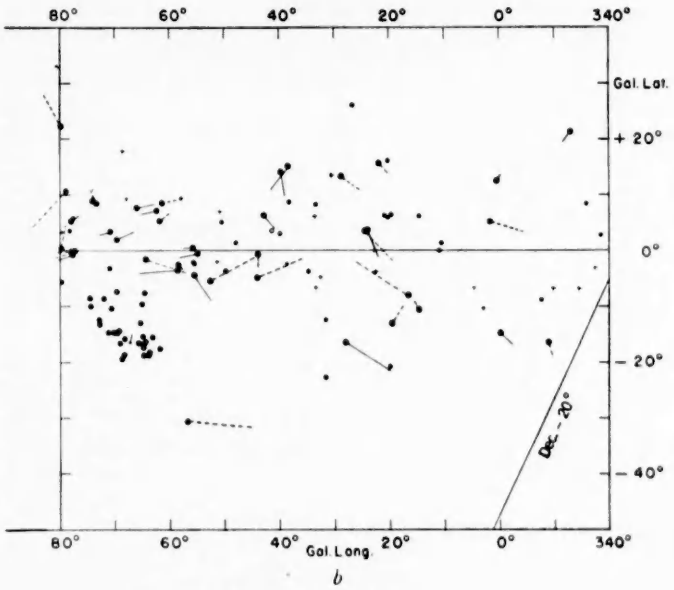


FIG. 3*b*.—See legend under Figure 3*a*

belong, is considerable, so that the true distance moduli of groups A and B are not sharply separated, and from the fact that the sizes of the proper motions in the two modulus groups overlap. We would then be dealing with two kinematically different, but intermingled, groups, and it is hard to see how our division into modulus groups could so nicely have separated them. No quite satisfactory explanation can be offered, and only a suggestion will be made. The differences in the proper motions in latitude are approximately differences in the motions in right ascension. The stars in modulus group

TABLE 2

SUBGROUPS IN THE CASSIOPEIA-TAURUS REGION
(Observed Quantities Not Corrected for Differential Galactic Rotation)

| No. of Subgroup | No. of Stars | Mean Co-ordinates | | Mean Proper Motion (0".0001) | | Mean Radial Velocity ± P.E. (km/sec) | Residuals in Radial Velocity (km/sec) | |
|---|---|---|---|---|---|---|---|---|
| | | $l$ | $b$ | $\mu_l \cos b$ | $\mu_b$ | | Solution I | Solution II |
| 1 | 3 | 83°0 | −22°2 | +180 | −157 | − 9.7±10 | ..... | ..... |
| 2 | 9 | 92.0 | − 5.6 | +207 | − 57 | − 3.4± 2.3 | +1.4 | +0.7 |
| 3 | 2 | 125.7 | −28.2 | +265 | − 20 | +16.5± 2.2 | +6.6 | +6.6 |
| 4 | 4 | 128.4 | − 1.3 | +470 | − 90 | + 4.0± 1.3 | −5.2 | −5.2 |
| 5 | 6 | 154.7 | −31.6 | +245 | + 67 | +14.9± 1.3 | −3.6 | −4.1 |
| 6 | 8 | 155.8 | − 4.9 | +245 | − 41 | +20.5± 0.9 | +2.2 | +1.6 |
| 7 | 9 | 154.4 | − 6.4 | +122 | − 29 | +21.3± 1.4 | +1.8 | +1.2 |

A have apparent magnitudes 1.7–5.3; those in group B from 4.9 to 6.1 (the mean magnitudes are 4.0 and 5.4, respectively). A magnitude error in the proper motions in right ascension of 0".007 (0$^s$.0005) would account for the difference. So large an error for bright stars seems unlikely, but, on the other hand, regional magnitude errors amounting to as much as 0$^s$.0010 have been shown to exist for stars fainter than magnitude 6.0 (Delhaye 1955). We have assumed that the difference in the latitude motion is not real and,

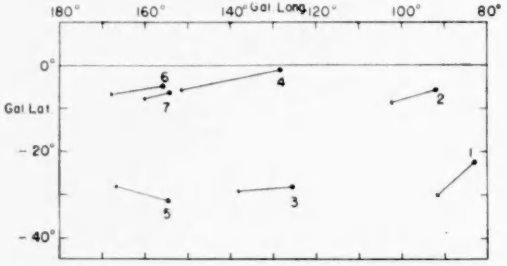


FIG. 4.—Mean positions and mean proper motions of the subgroups in the Cassiopeia-Taurus region. Numbers refer to the numbering of the subgroups.

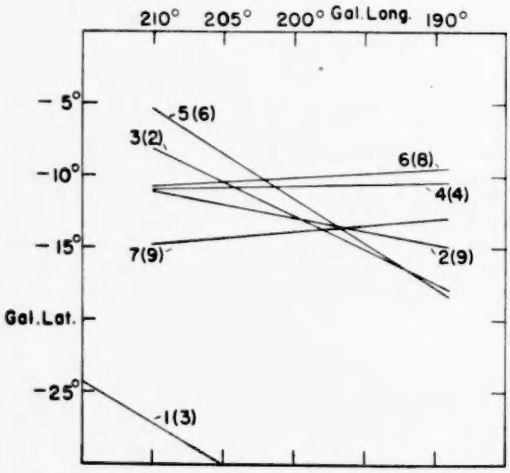


FIG. 5.—Sections of the great circles defined by the mean proper motions, determining the convergent point of the Cassiopeia-Taurus group. Numbers of stars in the various subgroups are in parentheses.

for further analysis, have subdivided the stars in this region into one subgroup (No. 6) with large and one (No. 7) with small proper motions. This selection avoids most of the possible magnitude effect.

Figure 5 shows, for solution I (no corrections for differential galactic rotation), the sections of the great circles defined by the directions of the mean proper motions in the vicinity of the convergent point. The numbers refer to the numbers of the subgroup with the numbers of stars in parentheses. Except for subgroup 1, the great circles define the

convergent point reasonably well. The three stars in subgroup 1, all of type B5, deviate systematically. They are excluded from further discussion. The position of the convergent point was determined by computing the latitudes at which the circles intersect the galactic meridian circles between $l = 195°$ and $l = 205°$ and by defining the longitude of the convergent point, $L_0$, as the value for which the scatter in these latitudes is a minimum. The mean latitude at this point was taken as the latitude of the convergent point, $B_0$. The various subgroups were weighted according to the numbers of stars. The

TABLE 3

SOLUTIONS FOR SOLAR MOTION AND $K$ TERM

| | Solution I (No Corrections for Differential Galactic Rotation) | Solution II (Differential Galactic Rotation Eliminated) |
|---|---|---|
| Longitude of convergent point ($L_0$) | $201° \pm 3°$ (p.e.) | $198° \pm 3°$ (p.e.) |
| Latitude of convergent point ($B_0$) | $-12°.0 \pm 0°.5$ | $-11°.9 \pm 0°.5$ |
| R.A. of convergent point | 99° | 97° |
| Decl. of convergent point | $-24°$ | $-21°$ |
| Stream velocity, $S$ (km/sec) | $24.1 \pm 2.1$ | $19.8 \pm 2.2$ |
| $K$ term (km/sec) | $+2.2 \pm 1.0$ | $+5.1 \pm 1.1$ |

results for solutions I and II are in the first lines of Table 3. The difference between the two solutions is small.

The radial velocities were analyzed with the formula

$$\rho = S \cos \lambda + K \,, \tag{1}$$

where $\rho$ is the observed radial velocity of a star and $\lambda$ its angular distance from the convergent point. $S$ and $K$ will provisionally be called the "stream velocity" and the "$K$ term," but we shall see later that their interpretation is different for solutions I and II. The results are in Table 3. We notice that solution II, with corrections for differential galactic rotation applied, differs from solution I by a larger $K$ term and smaller stream velocity. Residuals O − C for the two solutions are in the last two columns of Table 2. They are similar.

*b) Interpretation of Solutions I and II*

Let us first consider a group of stars in a state of strictly linear expansion, i.e., with velocities directed outward from the center and proportional to the distance from it. The rate of expansion is $k$ km/sec/pc. The motions of these stars are observed from the sun, which has a certain velocity with respect to the center of the group. How are this velocity and the expansion effect shown in the proper motions and radial velocities?

The rate of expansion of the group is the same, irrespective of the star in the group from which it is observed. Hence the state of motion of the members of the group with respect to the sun can be described by the motion of any of its members and an expansion at the rate $k$ with respect to this star. Consider an imaginary star N, belonging to the group and at the time of observation coinciding with the sun, but with a relative velocity $S'$ with respect to the sun. As seen from the sun, all the stars will have the velocity $S'$ and, superimposed on this, the linear expansion $k$ with respect to the sun. From this the following conclusions may be drawn:

1. The proper motions cannot reveal the expansion of the group, as this is observable only in the line of sight; they all converge toward one convergent point just as in the case of parallel motions of the members. However, the direction of the convergent is the

direction of the motion of star N with respect to the sun, not the direction of the motion of the group's center with respect to the sun.

2. The radial velocities will contain two terms: one is due to the motion $S'$ and equal to $S' \cos \lambda$; the other is $rk$, where $r$ is the distance of the star from the sun:

$$\rho = S' \cos \lambda + r k \ . \tag{2}$$

If the distance of the center of the group from the sun is $r_0$, then the motion of this center with respect to the sun is the vector sum of $S'$ and $r_0 k$.

Before discussing the applicability of relations (1) and (2), let us now investigate how far we are justified in assuming that an association in a state of disintegration resembles the case of strictly linear expansion, as described previously. The evolution of expanding

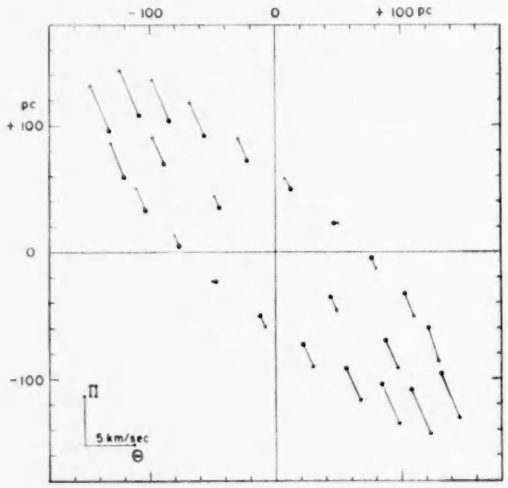


FIG. 6.—Pattern of velocities parallel to the galactic plane for the stars in an expanding association in the neighborhood of the sun at an age of 70 million years and with initial velocities of 1 km/sec or less. Direction of components Π (toward anticenter) and Θ (of galactic rotation) are indicated in the lower-left-hand corner, showing also the scale of velocities.

associations has been considered in an earlier paper, with special application to the Scorpio-Centaurus association (Blaauw 1952*c*). As an illustration, we reproduce here in somewhat modified form the case in which the initial velocities of expansion from the origin are 1 km/sec or less and the age of the association $70 \times 10^6$ years. The initial velocities are supposed to be in the galactic plane and isotropic. Figure 6 shows the configuration in the galactic plane after $70 \times 10^6$ years. The outer ellipse corresponds to the stars with initial velocities $s_0 = 1$ km/sec. The shape of this configuration depends only on the time elapsed since the beginning of the expansion; its dimensions depend on $s_0$. Stars with velocities $s_0$ smaller than 1 km/sec will be located on a configuration of the same shape as that for $s_0 = 1$ but of proportionally smaller dimensions. A few of the stars with $s_0 < 1$ km/sec are shown in the drawing.

The arrows represent the velocities of the stars with respect to the origin of the group. The components Θ are in the direction of galactic rotation, the components Π in the direction of the anticenter of the Galaxy. The pattern of velocities is slightly different from that given in Figure 5*b* of the earlier paper, as the motions there were counted in

the specially selected rotating co-ordinate system $\xi$, $\eta$. For the comparison with actually observed quantities it is better to consider them in the II, $\Theta$ system. The scale of velocities is given in the lower-left-hand corner of Figure 6.

We compare this velocity pattern with the patterns for differential galactic rotation and for linear expansion. The latter can easily be visualized. The pattern for differential galactic rotation is rather complicated; its radial components with respect to the origin are inward in the upper-right and lower-left quadrants of Figure 6 and outward in the other two. The tangential component shows the well-known double sine wave in galactic latitude combined with the constant term connected with the constant $B$.

If a detailed comparison is made with these two cases, it is found that the pattern of Figure 6, although it is definitely different from both, shows more resemblance to the case of linear expansion than to that of differential galactic rotation. The quality of the observational data does not justify a more refined consideration of the velocity pattern of a dispersing group. We shall therefore assume that the case of linear expansion is a suitable approximation of its state of motion and shall ask whether the motions in the Cassiopeia-Taurus group are better represented by this or by the differential galactic rotation exhibited by a sample of field stars.

Solution II applies to the latter case. Since corrections for differential galactic rotation were applied to the observational quantities, we would expect to find an approximately normal solar motion, but no $K$ term. The solar motion has indeed its usual value, but the $K$ term, even after subtraction of a gravitational red shift of $+1$ km/sec, is much higher than can be accounted for by observational errors in the radial velocities. We conclude that the motions in the Cassiopeia-Taurus group are distinctly different from those in a sample of field stars.

In the case of linear expansion, no corrections should be applied for differential galactic rotation. Solution I is therefore applicable to this case, except that the solution should have been made with equation (2) instead of equation (1). We may, however, with sufficient approximation put $\langle r \rangle k = K$, where $\langle r \rangle$ is the mean distance of the stars in the Cassiopeia-Taurus group, because the mean provisional distances in the six subgroups 2–7 are approximately the same. They are all between 170 (for subgroup 5) and 200 pc (for the mean of subgroups 6 and 7) except for group 4, 110 pc; but this group has only four stars. It would, therefore, have made little difference if a solution had been made with equation (2) and the provisional individual distances $r$ instead of equation (1). Using the mean provisional distance, 180 pc, we have $180k = K$. We subtract from $K$ a gravitational red shift of $+1.0$ km/sec and hence have $180k = +1.2$ km/sec $\pm$ 1.0 (p.e.), and $k = 0.007 \pm 0.006$ km/sec/pc.

Apparently the rate of expansion may have any value between 0 and 2 km/sec per 100 pc. On the assumption of linear expansion, this corresponds to an age of more than $50 \times 10^6$ years. It can easily be shown that this age, derived for the case of strictly linear expansion, also applies if we have only the approximate linear expansion shown in Figure 6, which is a result of the galactic orbits of the stars with respect to their origin. The mean outward velocity along the major axis of the elliptical configuration in Figure 6 increases linearly and amounts to 2.4 km/sec at a distance of 170 pc from the center. This corresponds to an expansion rate of 0.014 km/sec/pc. The linear expansion derived from the assumed initial velocity $s_0 = 1$ km/sec and the age of $70 \times 10^6$ years would give a rate of expansion of 1 km/sec per 70 pc or 0.015 km/sec/pc. Hence we see that the expansion age derived from the observed state of motion on the assumption of strictly linear expansion is a good approximation of the true age. An age of $50 \times 10^6$ years or more seems quite reasonable for the Cassiopeia-Taurus group, in view of the fact that the group contains no stars of absolute magnitudes brighter than $-4.7$ and no types earlier than B0.

The foregoing considerations are, of course, of a very simplified nature in several respects. No attention has been paid to the motions in the direction perpendicular to the

galactic plane. If the initial velocities were less than 1 km/sec on the average, the velocities perpendicular to the galactic plane probably would not have significantly changed the thickness of the group in this direction, which is compatible with the fact that it is still confined within the Gould belt.

We conclude that solution I leads to a plausible interpretation, whereas solution II does not. Solution I will, therefore, be preferred for the further treatment in this paper. It seems quite natural to assume the stars of the Cassiopeia-Taurus group to have a more or less related origin. On the other hand, the foregoing considerations should not be taken as an attempt to demonstrate that these stars have really been formed simultaneously in one association. We would prefer the more general statement that they may have originated within a much smaller volume than that occupied by the group at present and that their average age is of the order of 50 million years or more.

The elements of the solar motion with respect to the center of the group can now be found, adopting for $S'$ the value of $S$ in Table 3, solution I, and combining this, as previously described, with the velocity $r_0 k$, where $r_0 = 150$ pc, taken from Table 4 (see also Sec. V, *g*). The galactic longitude of the center of the group is 124°. We thus find the elements of motion in Table 4.

TABLE 4

MEAN POSITION AND MOTION OF CASSIOPEIA-TAURUS GROUP

| | |
|---|---|
| *Mean position:* | |
| $l=124°$, $b=-11°$, distance, $r_0=150$ pc | |
| *Mean motion with respect to the sun:* | |
| Component $X$ (toward $l=0°$, $b=0°$) | $-22.6$ km/sec |
| Component $Y$ (toward $l=90°$, $b=0°$) | $-7.6$ km/sec |
| Component $Z$ (toward $b=90°$) | $-5.0$ km/sec |
| *Mean motion corrected for standard solar motion:* | |
| Component $X$ | $-5.6$ km/sec |
| Component $Y$ | $-0.2$ km/sec |
| Component $Z$ | $+2.3$ km/sec |
| Total velocity, 6.1 km/sec toward $l=182°$, $b=+22°$ | |

The latitude of the convergent point is lower than that found from the bright stars of later types for which an average value of $-20°$ might be taken (Delhaye 1951), whereas somewhat better agreement exists with the results derived from tenth- and eleventh-magnitude A–K stars (Vyssotsky and Williams 1948). The Cassiopeia-Taurus group appears to have a motion perpendicular to the galactic plane with respect to the A–K stars in the vicinity of the sun of about +3 km/sec.

A different interpretation of the large positive $K$ term which results from solutions similar to solution II has recently been proposed by Torondjadze (1953). This author considers the state of motion which would have existed for the B-type stars if these had originated simultaneously in expanding associations arranged along a spiral arm. It appears that the motions observed at present from the location of the sun should then show a $K$ term which might well be of the order of that observed for the bright B stars. In this manner, Torondjadze relates the observed dynamical properties of these stars—which are in several respects different from those of later types—to their young age and their initial velocities in the association.

Although this theory has some attractive features, it is doubtful whether it is really applicable to the bright B stars. The Cassiopeia-Taurus group and the Scorpio-Centaurus association are together almost fully responsible for the large $K$ term in the classical radial-velocity solutions, but the limited dimensions and the very small internal velocity dispersion of both the Cassiopeia-Taurus group (see the next paragraph) and

the Scorpio-Centaurus association (Blaauw 1946; Bertiau, unpublished) indicate strongly that these groups consist of stars of common origin and are not assemblies of stars at present occupying the same region in space but having originated in different associations. Furthermore, as was shown by Markowitz (1948) in a study of the clustering and the $K$ term of the bright B stars, the stars outside the clusterings give a negligible $K$ term. One would expect Torondjadze's theory to be especially applicable to these stars.

*c) Peculiar Motions*

With the elements derived from solution I we have computed $v$ components in the direction of the convergent point and $\tau$ components perpendicular to it for all stars in the Cassiopeia-Taurus group. The peculiar motions can be studied by means of the $\tau$ components and the radial velocities.

For the analysis of the $\tau$ components we have selected the stars which, according to Table 5 (explained in Sec. V, *e*), have individual parallaxes larger than $p = 0''.0025$ and probable errors of the proper motions below $0''.0030$. These include not only stars used in the preceding calculations but also some more which may belong to the Cassiopeia-Taurus group according to Section V, *e*. We consider separately the stars with parallaxes larger than $0''.0050$ (24 stars) and those with smaller ones (14 stars). After correcting the mean absolute values of the $\tau$ components for the influence of accidental errors in the proper motions, we get $\langle |\tau| \rangle = 0''.0029$ and $0''.0022$, respectively. Converting these values into linear velocities by means of the parallaxes of Table 5, we find 1.8 and 2.8 km/sec, respectively. The latter value is less reliable, because in that group the true $\tau$ components are of the order of the accidental errors in the proper motions. We conclude that

$$t = \pm 2.0 \text{ km/sec}$$

is the most probable value of the mean peculiar velocity in the $\tau$ direction.

The radial velocities have been used for the 26 stars in the quality classes *a* and *b* in Wilson's (1953) catalogue. These have probable errors below 2.0 km/sec. Residuals were computed by means of formula (1) and solution I of Table 3. We get, after a correction for the influence of accidental errors, $\pm 3.4$ km/sec for the mean residual in the radial velocity. This is an upper limit rather than the most probable value of the peculiar motions in the radial direction, since the true probable errors may be somewhat larger than the adopted values and the distance dependence, as expressed by formula (2), has not been taken into account. However, the difference is probably not more than 0.5 km/sec, and we adopt, for the mean residual radial velocity,

$$u = \pm 3.0 \text{ km/sec}.$$

The star HD 21448 appeared to have a well-determined large residual ($-18$ km/sec) and will therefore not be regarded as belonging to the group.

Most of the $\tau$ components are directed approximately perpendicular to the galactic plane, whereas those in the line of sight are mostly in this plane. The difference between the values of $t$ and $u$ may well represent a true difference between the peculiar motions in these two directions. One would indeed expect such a difference if the expansion hypothesis is correct.

*d) Individual Parallaxes and Absolute Magnitudes*

The small amount of the peculiar motions as compared with the solar motion allows the determination of fairly accurate individual parallaxes from the $v$ components. Such parallaxes were computed with the elements of the solar motion as given in Table 3,

solution I. From the interpretation of this solution given in Section V, *b*, it is clear that one can derive individual parallaxes according to the usual formula,

$$p = \frac{4.74v}{S \sin \lambda}, \tag{3}$$

where $p$ is the parallax, and the $v$ component is computed without the application of corrections for differential galactic rotation.

The sources of accidental errors in the determination of these individual parallaxes are the observational errors of the proper motions and the peculiar motions. Denoting the corresponding probable errors by $\epsilon_0''$ and $\epsilon_c$ km/sec, respectively, we have

$$f = \frac{\text{p.e. of parallax}}{\text{parallax}} = \sqrt{\left[\left(\frac{\epsilon_0}{v}\right)^2 + \left(\frac{\epsilon_c}{S \sin \lambda}\right)^2\right]}.$$

For $\epsilon_c$ we adopted $0.85u = 2.5$ km/sec. The individual parallaxes, $p$, and the values of $f$ are given in Table 5. The table also gives the corresponding visual absolute magnitudes, $M_v$, derived by means of these parallaxes. These are either in the system of the *Revised Harvard Photometry* or in the $U - B - V$ system when $B$ and $V$ measures were available. Most of the latter were kindly provided by Dr. W. A. Hiltner in advance of publication. Absolute magnitudes in the $V$ system are printed in italics. For the stars considered, it was found that there is no systematic difference between the absolute magnitudes in the two systems. The probable errors of the absolute magnitudes given in Table 5 were derived from the probable errors of the parallaxes.

### *e) Stars Listed in Table 5*

Apart from the stars used in subgroups 2–7 discussed before, the following, with their individual parallaxes and visual absolute magnitudes derived from the $v$ components, are listed in Table 5.

1. Stars in modulus group C and probably belonging to the Cassiopeia-Taurus group. We noticed in Section IV that a number of the stars in Figure 3*a* show proper motions similar to those in Figures 1*a* and 2*a*. They were included in the discussion after it had become apparent that there is appreciable scatter in the absolute magnitudes within the luminosity classes B2 V and B3 V. These stars in modulus group C might be the ones with lower-than-average luminosities, and their omission might, therefore, systematically affect the determination of the mean luminosities.

It is hard to decide which of these stars really belong to the Cassiopeia-Taurus group. The nine stars marked "C" in the fourth column of Table 5 are probably members; their proper motions fit the convergent point somewhat better than the standard antapex. It is somewhat doubtful whether they represent all members in modulus group C, and there are dubious cases, like HD 829 at $l = 82°.9$, $b = -24°.4$, which may be related to the Lacerta association. The star HD 21448 at $l = 117°.9$, $b = -8°.4$ has already been excluded because of its strongly deviating radial velocity. The radial velocities of the remaining stars agree very well with those predicted by means of formula (1) and solution I.

2. The two high-latitude stars, $\delta$ Ceti (HD 16582) and $\eta$ Ursa Majoris (HD 120315). In both cases there is little doubt that the star belongs to the Cassiopeia-Taurus group. The directions of the proper motions are in agreement with this hypothesis. $\delta$ Ceti is in the general region near subgroup 5. $\eta$ Ursa Majoris is at lower longitude than the other members of the group, but its position in space, close to the sun, is certainly within the boundaries of the group. For none of the other stars outside the latitudes of Figures 1–3 does membership of the Cassiopeia-Taurus group seem likely.

3. The star $\alpha$ Arae (HD 158427). No systematic search for members of the Cassiopeia-

Taurus group south of declination $-20°$ has been made, and so far only a few of the brighter stars, with large proper motions, have been investigated. In the case of α Arae, the proper motion as well as the radial velocity indicate membership. This star is probably also the nearest of the bright southern stars considered.

*f) Distribution and Mean Values of Absolute Magnitudes*

The Cassiopeia-Taurus group, according to Table 5, contains only two stars of types earlier than B2, namely, γ Cas (B0 IV: e) and ε Per (B0.5 V), and, except for ζ Tau (B2 III: p), all stars are of luminosity classes IV or V. Most numerous are the subclasses B2 V (12 stars) and B3 V (15 stars). In the H-R diagram in Figure 7, absolute magnitudes with p.e. $< 0.55$ mag. are represented by dots, the more uncertain ones by open circles.

The large range in absolute magnitudes within the two subclasses, B2 V and B3 V, is partly real and partly due to the accidental errors of $M_v$. For the determination of the

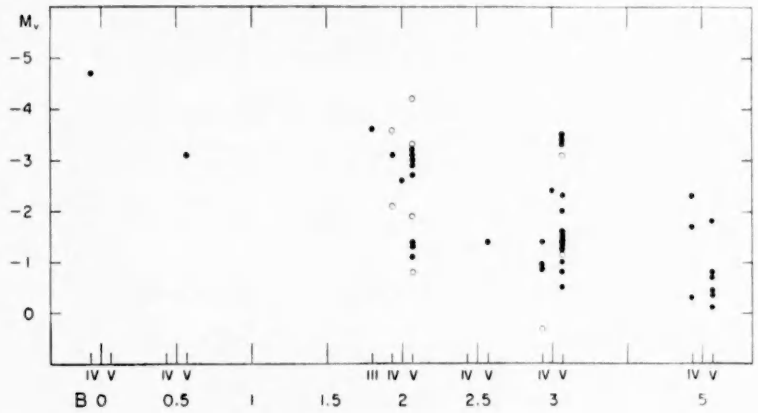


FIG. 7.—Luminosity–spectral-type diagram for stars in the Cassiopeia-Taurus group. *Circles:* stars for which (p.e. of $p$)/$p$ is larger than 0.25; *abscissae:* MK subclasses; *ordinates:* visual absolute magnitudes.

mean absolute magnitudes and of the true value of the scatter in the absolute magnitudes we shall rely mainly on the most accurately determined parallaxes. For this purpose it is useful first to consider Table 6. This shows the distribution of the parallaxes for the different classes of accuracy given in the heading of the second to fourth columns. The stars in the fourth column are the ones with p.e. of $M_v > 0.55$ mag.; they are represented by open circles in Figure 7. One notices that the large values of (p.e. of $p$)/$p$, in the last column, occur at the small values of $p$. This is due to two causes:

1. The smaller parallaxes are those of the apparently fainter stars with the less accurate proper motions. The mean apparent magnitudes for the three classes of (p.e. of $p$)/$p$ in the table are 3.7, 5.0, and 6.0, respectively.

2. If the accidental error of the proper motion happens to decrease the $v$ component, it will cause $p$ to be smaller than the true parallax and increase the ratio (p.e. of $p$)/$p$. Thus we must expect the parallaxes in the last category in Table 6 to be systematically too small.

The latter effect also influences the absolute magnitudes derived from the parallaxes. It works in the sense that the stars in the last category will come out too bright, whereas those in the first category will be too faint. However, as the ratios (p.e. of $p$)/$p$ are so

TABLE 5

STARS IN THE CASSIOPEIA-TAURUS GROUP

| Name | HD No. | GC No. | g* | l | b | m | v† | r† | p.e.† ± | p† | f‡ ± | Rad. Vel. (km/sec) | q§ | $A_v$ (0.01 mag.) | MK | $M_v$ | p.e. ± |
|---|---|---|---|---|---|---|---|---|---|---|---|---|---|---|---|---|---|
| AR Cas | 221253 | 32683 | 2 | 80°2 | − 2°6 | 4.9 | 178 | + 29 | 12 | 40 | 0.17 | −15.9 | a | 24 | B3 V: | −2.3 | 0.4 |
| | 224559 | 33252 | C | 81.7 | −15.4 | 6.46 | 256 | − 53 | 40 | 55 | .21 | − 1.1 | b | 24 | B3 IV | −0.9 | .5 |
| | 829 | 228 | C | 82.9 | −24.4 | 6.57 | 200 | − 33 | 50 | 42 | .29 | − 9.0 | b | 48 | B2 V | −0.8 | .6 |
| | 1976 | 476 | 2 | 86.7 | −10.4 | 5.36 | 136 | 0 | 25 | 29 | .23 | −12 | c | 15 | B5 IV | *−2.3* | .5 |
| ζ 17 Cas | 3360 | 727 | 2 | 88.7 | − 8.6 | 3.72 | 206 | − 65 | 9 | 43 | .15 | + 2.1 | a | 8 | B2 V | *−3.2* | .3 |
| ξ 19 Cas | 3901 | 828 | 2 | 89.4 | −12.0 | 4.85 | 146 | + 3 | 20 | 30 | .24 | − 8 | c | 32 | B2 V | *−3.1* | .5 |
| o 22 Cas | 4180 | 882 | 2 | 89.9 | −14.3 | 4.70 | 208 | − 29 | 10 | 43 | .15 | − 8 | c | 52 | B2 V | *−2.7* | .3 |
| γ 27 Cas | 5394 | 1117 | 2 | 91.3 | − 1.8 | 2.25 | 255 | + 10 | 7 | 53 | .14 | − 6.8 | a | 90: | B0 IV:e | *−4.7* | .3 |
| | 6300 | 1293 | C | 93.1 | −11.4 | 6.50 | 170 | + 59 | 40 | 35 | .27 | − 5.4 | b | 36 | B3 V | −1.2 | .6 |
| φ Per | 10516 | 2102 | 2 | 99.3 | −10.8 | 4.19 | 287 | − 31 | 9 | 57 | .13 | + 0.8 | a | 60 | B2 pe | −2.6 | .3 |
| 1 Per | 11241 | 2241 | C | 99.4 | − 6.2 | 5.49 | 203 | + 7 | 20 | 41 | .16 | − 3 | c | 00 | B2 V | −1.4 | .4 |
| ε 45 Cas | 11415 | 2289 | 2 | 97.5 | + 2.2 | 3.44 | 383 | − 22 | 7 | 77 | .13 | − 8.1 | a | 16 | B3 p | *−2.4* | .3 |
| δ 82 Cet | 16582 | 3192 | ... | 139.4 | −50.9 | 4.04 | 183 | + 25 | 7 | 40 | .16 | +13.0 | a | 12 | B2 IV | *−3.1* | .4 |
| 35 Ari | 16908 | 3273 | 3 | 119.6 | −27.9 | 4.58 | 134 | − 25 | 11 | 27 | .15 | +19 | c | 17 | B3 V | *−3.3* | .3 |
| | 20336 | 3947 | 2 | 105.0 | + 7.7 | 4.76 | 157 | − 20 | 17 | 31 | .17 | +20 | c | 18 | B2 Ve | −2.9 | .4 |
| τ 61 Ari | 20756 | 4007 | 3 | 131.9 | −28.4 | 5.17 | 400 | + 8 | 9 | 86 | .14 | +14 | c | 32 | B5 Vp: | *−0.4* | .3 |
| | 21803 | 4217 | C | 118.5 | − 8.2 | 6.33 | 161 | + 11 | 35 | 32 | .26 | + 3.7 | b | 90 | B2 IV | −2.1 | .6 |
| 29 Tau | 23466 | 4505 | 5 | 149.3 | −35.0 | 5.36 | 257 | + 95 | 17 | 64 | .17 | +13 | c | 36 | B3 V | −1.0 | .4 |
| 30 Tau | 23793 | 4568 | 5 | 145.2 | −31.2 | 5.03 | 363 | + 4 | 19 | 87 | .17 | +18.9 | b | 27 | B3 V | *−0.5* | .4 |
| ε 45 Per | 24760 | 4759 | 4 | 125.2 | − 9.0 | 2.96 | 347 | − 10 | 8 | 71 | .13 | − 1 | c | 29 | B0.5V | *−3.1* | .3 |
| 35 Eri | 25340 | 4828 | 5 | 159.7 | −36.3 | 5.25 | 286 | + 11 | 15 | 81 | .20 | +16 | c | 18 | B5 V | −0.4 | .4 |
| 40 Tau | 25558 | 4876 | 5 | 153.3 | −31.9 | 5.33 | 90 | − 52 | 21 | 24 | .29 | +12.1 | b | 38 | B3 V | *−3.1* | .6 |
| 48 Per | 25940 | 4967 | 4 | 121.4 | − 2.0 | 4.03 | 394 | + 21 | 8 | 79 | .13 | + 3.0 | b | 52 | B3 Vp | *−2.0* | .3 |
| μ 49 Tau | 26912 | 5134 | 5 | 152.1 | −27.4 | 4.32 | 323 | + 4 | 13 | 85 | .17 | +18.2 | b | 46 | B3 V | *−1.4* | .4 |
| | 27192 | 5207 | C | 120.5 | + 1.6 | 5.54 | 103 | + 44 | 30 | 20 | 0.32 | −18 | d | 66 | B2 IV | −3.6 | 0.7 |

* g = number of subgroup. † unit (0.0001). ‡ f = (p.e. of p)/p. § q = quality of radial-velocity determination.

TABLE 5—*Continued*

| Name | HD No. | GC No. | g* | l | b | m | v† | r† | p.e.† ± | p† | f‡ ± | Rad. Vel. (km/sec) | q§ | $A_v$ (0.01 mag.) | MK | $M_v$ | p.e. ± |
|---|---|---|---|---|---|---|---|---|---|---|---|---|---|---|---|---|---|
| τ 94 Tau | 29763 | 5716 | 7 | 144°.5 | −13°.7 | 4.33 | 137 | − 78 | 6 | .33 | 0.16 | +14.6 | b | 36 | B3 V | −3.4 | 0.4 |
| μ 57 Eri | 30211 | 5796 | 5 | 168.2 | −27.9 | 4.18 | 209 | − 15 | 8 | .72 | .23 | + 7 | d | 6 | B5 IV | *−1.7* | 0.5 |
| η 10 Aur | 32630 | 6226 | 4 | 133.0 | + 1.5 | 3.28 | 765 | − 9 | 8 | 162 | .14 | + 7.4 | b | 10 | B3 V | *−0.8* | 0.3 |
| 103 Tau | 32990 | 6267 | 7 | 147.0 | − 8.2 | 5.50 | 69 | + 11 | 15 | 17 | .27 | +16.2 | a | 90 | B2 V | −4.2 | 0.6 |
| 105 Tau | 32991 | 6263 | 7 | 149.1 | − 9.7 | 5.95 | 108 | + 24 | 17 | 27 | .23 | +25 | c | 114 | B2 Vp | −3.0 | 0.5 |
| 15 Cam | 34233 | 6478 | C | 120.2 | +12.8 | 6.23 | 257 | + 2 | 25 | 51 | .16 | − 3 | c | 60 | B3 IV | −0.9 | 0.4 |
| ρ 20 Aur | 34759 | 6556 | 4 | 134.2 | + 4.2 | 5.12 | 407 | + 65 | 23 | 86 | .15 | + 5 | c | 7 | B5 V | *−0.1* | 0.3 |
| 115 Tau | 35671 | 6714 | 6 | 154.8 | − 8.0 | 5.31 | 251 | − 52 | 13 | 70 | .19 | +19 | c | 30 | B5 V | −0.8 | 0.4 |
| 114 Tau | 35708 | 6723 | 7 | 151.5 | − 5.8 | 4.83 | 89 | + 17 | 15 | 23 | .24 | +14.4 | b | 18 | B3 V | −3.5 | 0.5 |
| 32 Ori | 36267 | 6813 | 6 | 165.7 | −13.5 | 4.32 | 361 | −102 | 29 | 126 | .24 | +21 | c | 12 | B5 IV | −0.3 | 0.5 |
| 121 Tau | 36819 | 6916 | 6 | 150.7 | − 3.1 | 5.28 | 207 | + 38 | 20 | 53 | .20 | +22.6 | b | 36 | B3 V | *−1.4* | 0.4 |
| ζ 123 Tau | 37202 | 6985 | 6 | 153.4 | − 4.2 | 3.00 | 212 | − 34 | 7 | 56 | .17 | +24.3 | b | 33: | B2 III:p | *−3.6:* | 0.4 |
| 125 Tau | 37367 | 7026 | 7 | 146.8 | + 0.4 | 6.00 | 96 | + 67 | 40 | 23 | .45 | +30 | d | 108 | B2 V | −3.3 | 1.1 |
| 126 Tau | 37438 | 7047 | 6 | 149.6 | − 1.3 | 5.00 | 267 | +121 | 17 | 67 | .18 | +14.8 | a | 18 | B2 V | −1.1 | 0.4 |
| | 37711 | 7094 | 6 | 157.8 | − 5.8 | 4.87 | 213 | + 53 | 20 | 62 | .21 | +21 | c | 24 | B3 IV | *−1.4* | 0.5 |
| 133 Tau | 37967 | 7148 | 6 | 152.3 | − 2.0 | 6.06 | 218 | − 7 | 30 | 56 | .22 | +19.1 | b | 42 | B5 Vp | −0.7 | 0.5 |
| 57 Ori | 38622 | 7249 | 7 | 160.9 | − 5.9 | 5.20 | 169 | + 24 | 17 | 52 | .22 | +28.3 | b | 12 | B2 V | −1.3 | 0.5 |
| ν 67 Ori | 39698 | 7436 | C | 156.7 | − 1.4 | 5.89 | 114 | + 1 | 20 | 32 | .25 | + 7.2 | b | 30 | B2 V | −1.9 | 0.5 |
| 69 Ori | 41753 | 7772 | 6 | 162.5 | − 1.2 | 4.40 | 231 | + 31 | 7 | 71 | .20 | +22.1 | a | 11 | B3 V | *−1.4* | 0.4 |
| ξ 70 Ori | 42545 | 7891 | 7 | 161.8 | + 0.3 | 4.92 | 152 | + 51 | 20 | 46 | .24 | +22 | c | 8 | B5 V | *−1.8* | 0.5 |
| | 42560 | 7889 | 7 | 163.5 | − 0.6 | 4.35 | 196 | − 19 | 16 | 62 | .22 | +24 | d | 11 | B3 V | *−1.6* | 0.5 |
| η 85 UMa | 44700 | 8227 | C | 174.0 | − 3.0 | 6.25 | 182 | + 57 | 40 | 76 | .36 | +29 | c | 30 | B3 IV | +0.3 | 0.8 |
| α Ara | 120315 | 18643 | ... | 65.2 | +65.0 | 1.91 | 1196 | + 35 | 5 | 269 | .15 | −10.9 | b | 00 | B3 V | *−1.4* | 0.3 |
| | 158427 | 23708 | ... | 308.3 | −10.0 | 2.97 | 714 | − 81 | 18 | 145 | 0.13 | − 2 | c | 12 | B2.5V | −1.4 | 0.3 |

much smaller in the first one, this effect is much weaker in the first category than in the third.

Therefore, we have decided to determine the mean absolute magnitudes and the scatter with respect to these means exclusively from the stars with (p.e. of $p$)/$p$ < 0.25. The probable errors of $M_v$ for these stars range from 0.28 to 0.53 mag., and the average p.e. is ±0.40 mag. The mean value of $M_v$ for B3 V has been corrected by +0.2, to account for incompleteness at the low luminosities, as will be explained later. The final values and their probable errors are in the second column of Table 8. The probable errors of the mean absolute magnitudes represent the uncertainty due to three causes:

1. The uncertainty due to the scatter in the individual absolute magnitudes within each subclass. This amounts to a p.e. of ±0.26 mag. for class B2 V and of ±0.20 mag. for class B3 V.

2. The common error due to errors in the stream elements of solution I. The principal source of uncertainty is in the stream velocity $S$. Its p.e. amounts to 9 per cent of $S$ itself, which corresponds to a probable error of ±0.19 mag. in the zero point of all absolute magnitudes in Table 5 and Figure 7.

TABLE 6

DISTRIBUTION OF PARALLAXES AND THEIR PROBABLE ERRORS

| $p$ (0".0001) | (P.E. OF $p$)/$p$ | | | $p$ (0".0001) | (P.E. OF $p$)/$p$ | | |
|---|---|---|---|---|---|---|---|
| | ≤0.15 | 0.16–0.24 | ≥0.25 | | ≤0.15 | 0.16–0.24 | ≥0.25 |
| 15–19 | | | 1 | 55–59 | 1 | 3 | |
| 20–24 | | 1 | 3 | 60–64 | | 3 | |
| 25–29 | 1 | 2 | | 65–69 | | 1 | |
| 30–34 | | 3 | 2 | 70–74 | 1 | 3 | |
| 35–39 | | | 1 | 75–79 | 2 | | 1 |
| 40–44 | 2 | 3 | 1 | 80–84 | | 1 | |
| 45–49 | | 1 | | 85–89 | 2 | 2 | |
| 50–54 | 1 | 3 | | 90 | 3 | 1 | |

3. The correction for the possible omission of the intrinsically faintest stars in the compilation of Table 5. We have estimated its effect as follows: We assume that the group does not extend beyond about 330 pc. This is based on the remarks in Section IV and is not incompatible with the distribution of parallaxes in Table 6. The few values of $p$ below 0".0030 in that table can be explained by the accidental errors in the parallaxes. A distance of 330 pc corresponds to $m_0 - M = 7.6$. Stars with $M_v = -1$ at this distance limit have $m_0 = 6.6$ and, with the generally small visual absorption, $m = 7$. Our data are probably not quite complete between $m = 6$ and $m = 7$, and this incompleteness will affect especially the subclass B3 V. Assuming that two or three stars are missing in the interval between $M_v = 0$ and $M_v = -1$, we estimate the correction to the mean value for B3 V derived from Table 5 to be +0.2 mag. The uncertainty of this estimate is represented by an additional probable error of ±0.1 mag.

Thus we arrive at the total probable error of about ±0.3 mag. of the mean values for both B2 V and B3 V. These mean absolute magnitudes apply to the stars selected per volume of space. In general, mean absolute magnitudes can be defined, either in this way or per apparent magnitude. The latter are brighter because they include the intrinsically luminous stars within a larger volume of space than the faint ones. We present mean values per volume of space, as these have more fundamental significance and because they are more naturally determined from the Cassiopeia-Taurus group and from the Scorpio-Centaurus association.

The mean deviations of the individual absolute magnitudes from the average values for B2 V and B3 V have been determined from the same stars as those used for the mean absolute magnitudes. Corrections for the accidental errors of $M_v$ were applied. The results are also in Table 8. The mean deviations, 0.6 mag. for both B2 V and B3 V, are somewhat larger than might have been expected. They are, however, confirmed by the study of the Scorpio-Centaurus association reported in Section VI.

Part of the scatter of the absolute magnitudes must be due to the fact that we have not corrected them for the duplicity of some of the stars. Such corrections would have reduced somewhat the average deviations and also changed the mean absolute magnitudes in Table 8 by about +0.1 mag. However, in the present paper we are primarily interested in obtaining the information on the distribution of absolute magnitudes which can later serve for the distance determinations of faint associations. For these, no information on the duplicity of the main-sequence stars will be available. The duplicity and multiplicity properties of the stars in the Cassiopeia-Taurus group and their relation to the kinematical properties will be discussed in a later paper.

We have made a provisional investigation of the possibility of improving the estimation of individual absolute magnitudes by means of $H\gamma$-line intensity measurements. These were available for part of the stars in Table 5, mostly from unpublished measurements kindly communicated by Dr. R. M. Petrie and by Dr. J. Stock. We find that the data for most stars fit a mean relation with an average deviation of about $\pm 0.5$ in the absolute magnitude. There are, however, some striking deviations: namely, the stars HD 16908 and HD 29763, both of type B3 V and about 2 mag. too bright, and some stars in the $\alpha$ Persei cluster discussed in Section IX, which are of lower than expected luminosity. A more complete discussion of the relation between $H\gamma$ intensities and absolute magnitudes is postponed until the calibration of the high-luminosity classes is completed.

### *g) Space Distribution of Members of Group and of Field Stars*

The space distribution of the stars in Table 5 projected on the galactic plane is shown by the dots in Figure 8. The distances plotted were based on the individual parallaxes of Table 5 and on values derived from the mean absolute magnitudes per subclass given in Table 9. These latter are not quite independent of the first, as the mean absolute magnitudes were based partly on the data of Table 5, but the photometric data can in this way contribute to the determination of relative distances within the group. Weighted means of the two distances were used. Dots in parentheses represent the stars with (p.e. of $p$)/$p \geq 0.25$; their distances are more uncertain than those of the other members of the group and may be systematically too large. The mean position of the Cassiopeia-Taurus group, derived from the more reliable distances, is given in the upper part of Table 4.

The diagram covers the region within a distance of 400 pc and between galactic longitudes 340° and 200°. Field stars are represented by plus signs if they are at positive galactic latitude and by minus signs if at negative latitude. Their distances are based on the mean absolute magnitudes per subclass, with allowance for the fact that these stars were selected on the basis of apparent magnitude. The distribution shown here is probably only a rough approximation of the true distribution and is intended only to give some idea of the relative population of field stars around the Cassiopeia-Taurus group. We notice that this group, as well as the II Persei association, lies in a region which is almost unpopulated by the field stars, a feature which we had already observed in Section IV. It seems that in the section of our spiral arm between galactic longitudes 90° and 160° formation of the early-type stars started at a more recent date than in the adjacent regions. It is interesting to notice that the population of these field stars contains no star of type B0 or earlier and no star of luminosity class I or II. The percentages of stars in the various subclasses are as follows: B1 II–III, 1; B1 IV, 0; B1 V, 7; B2 III, 4; B2 IV,

5; B2 V, 24; B3 III, 1; B3 IV, 7; B3 V, 46; B2–B3, no subclass, 4. O-type stars and stars of luminosity classes I and II occur only in the associations.

The positions of the three associations within 600 pc in the northern sky and of the Scorpio-Centaurus association are also shown. The distances for the first three were taken from the sources referred to in Section III, although these may have to be revised when the calibration for all MK luminosity classes has been completed. The location of the Scorpio-Centaurus association was copied from earlier work by the author (Blaauw 1946).

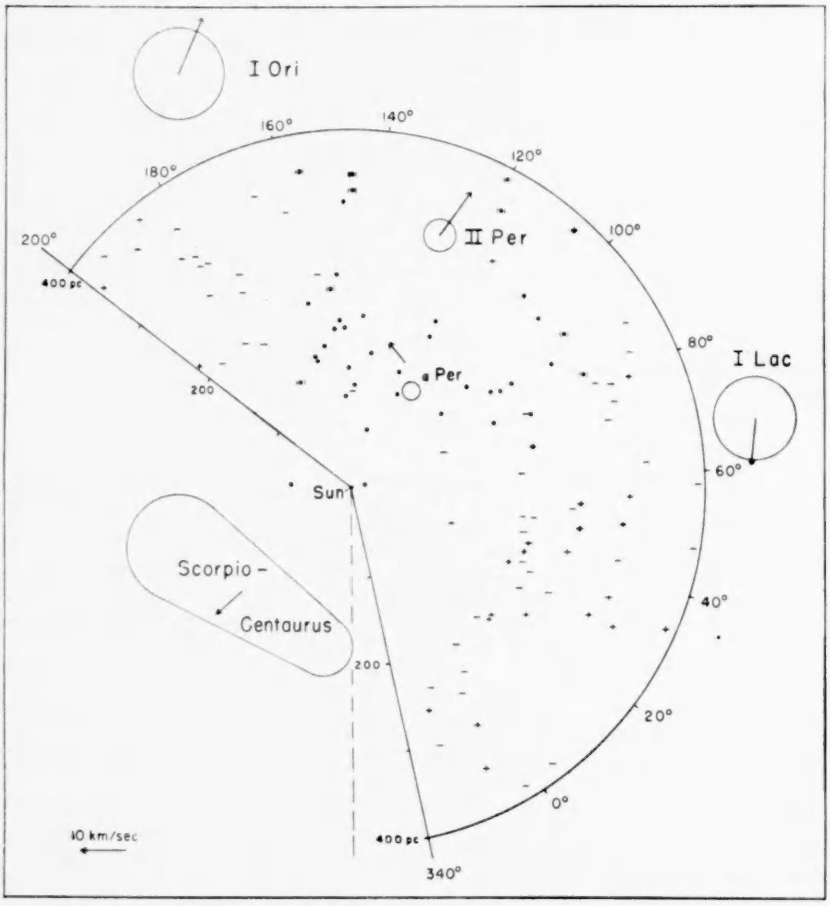


FIG. 8.—Distribution of stars B3 and earlier within 400 pc and between galactic longitudes 340° and 200°, projected on the galactic plane. *Dots:* stars in the Cassiopeia-Taurus group (dots in parentheses have the most uncertain distances from the sun); *plus signs:* field stars at positive galactic latitudes; *minus signs:* field stars at negative latitudes. "α Per" marks the position of the α Persei cluster. The locations of the nearest associations are represented by the large circles. The dashed line is in the direction toward the galactic center.

The arrows represent the projected mean space velocities for the stars in the four associations and in the Cassiopeia-Taurus group, corrected for the standard solar motion (20 km/sec toward R.A. = 270°, Decl. = +30°), but not for differential galactic rotation. For all five objects the velocity perpendicular to the galactic plane is smaller than 4 km/sec. The scale of velocities is shown in the lower-left-hand corner of the diagram.

## VI. THE SCORPIO-CENTAURUS ASSOCIATION

The principal data derived from Bertiau's study are in Table 8. Full particulars about this study will soon be published. The study is based on better proper motions, radial velocities, and photometry than were available at the time of a previous investigation by the author (Blaauw 1946). It is the most precise one of the contributions to the calibration of the MK luminosity classifications discussed in the present paper. The small internal motions in this association, its short distance from the sun, and the high accuracy of the proper motions allow a very accurate determination of the distances and absolute magnitudes.

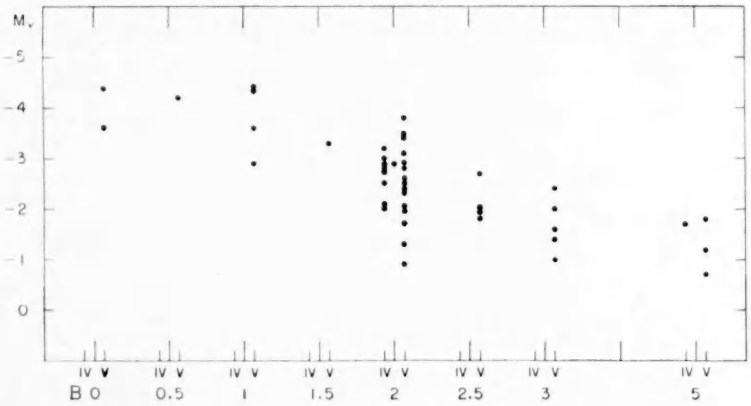


FIG. 9.—Luminosity–spectral-type diagram for the Scorpio-Centaurus association according to Bertiau.

The H-R diagram is shown in Figure 9. This is probably complete for types B2 and earlier but somewhat incomplete for B3 and very incomplete for B5. The third column of Table 8 gives the mean visual absolute magnitudes in the $U - B - V$ system and the average deviations from the means for B1 V, B2 IV, B2 V, and B3 V. The probable errors of the mean absolute magnitudes include the uncertainty in the zero point due to the possible errors in the elements of the stream motion; the probable error in the zero point is ±0.10 mag.

## VII. THE REGION BETWEEN LONGITUDES 340° AND 50°

The fairly uniform distribution of the stars and the absence of local stream motions in this region justify the assumption that the proper motions can be interpreted as due to random peculiar motions superimposed on a common motion with respect to the sun. Mean parallaxes have been derived from the $v$ and from the $\tau$ components and, from these, the mean luminosities for the subclasses B2 IV and V and B3 IV and V. The stars used are those with probable errors of the proper motions smaller than 0″.005 and with provisional distance moduli smaller than 8.4.

It was assumed that in the present case the mean motions of the stars show the effect of differential galactic rotation, and this was therefore eliminated from the proper motions and radial velocities, using the provisional distance moduli and the values of the constants $A$ and $B$ referred to in Section V, *a*. For the apex of the solar motion, we used the standard co-ordinates $l = 24°$, $b = +22°$ after we had checked these by means of mean proper motions for ten small subdivisions of the whole area. These mean proper motions gave $l = 20°$, $b = +22°$ for the apex, with an uncertainty of about $\pm 4°$. This checking on the apex was based on 62 stars, including some B5 stars and some earlier than B2.

TABLE 7

RESULTS FOR REGION BETWEEN LONGITUDES 340° AND 50°
(Numbers of Stars in Parentheses)

| | PROVISIONAL $m_0 - M$ | | | | | |
|---|---|---|---|---|---|---|
| | ≤7.2 | | 7.3–8.4 | | All ≤ 8.4 | |
| *From radial velocities:* | | | | | | |
| Solar motion, $S$ (km/sec) | 20.7±1.0 (p.e.) | (29) | 24.7±1.3 (p.e.) | (37) | 22.3 ±0.8 (p.e.) | (66) |
| Mean residual $\langle \lvert \Delta\rho \rvert \rangle$ | 5.5±0.5 | | 6.4±0.5 | | 6.3 ±0.4 | |
| *From v components:* | | | | | | |
| $\langle p \rangle S/4.74$ (0".0001) | 186±23 | (18) | 87±26 | (15) | ..... | |
| $\langle p \rangle$ (0".0001) | 43±5 | | 17± 5 | | ..... | |
| Mean $m_0 - M_v$ | 6.85±0.25 | | 8.9±0.65 | | ..... | |
| Mean $M_v$ per apparent magnitude | −2.44±0.25 | | ..... | | ..... | |
| *From τ components:* | | | | | | |
| $\langle \lvert \tau \rvert \rangle$ (0".0001) | ..... | | ..... | | 52±5 | (33) |
| $\langle p \rangle$ (0".0001) | ..... | | ..... | | 39±4 | |
| Mean $m_0 - M_v$ | ..... | | ..... | | 7.0±0.25 | |
| Mean $M_v$ per apparent magnitude | ..... | | ..... | | −2.10±0.25 | |
| *Means from τ and v components:* | | | | | | |
| Mean $M_v$ for B2 and B3, IV and V | ..... | | ..... | | −2.27±0.18 | (33) |
| Mean $M_v$ for B2, IV, V | ..... | | ..... | | −2.82±0.30 | (13) |
| Mean $M_v$ for B3, IV, V | ..... | | ..... | | −1.92±0.25 | (20) |

The results obtained in this section are summarized in Table 7. For the analysis of the $v$ components, we first subdivided the stars into the modulus groups $m_0 - M \leq 7.2$ and 7.3–8.4. The solar velocity, $S$, was determined separately for these two groups and for the two combined. Stars with inaccurate proper motions but good radial velocities were also used in this determination. The radial velocities had been corrected for a gravitational red shift of 1.0 km/sec. No $K$ term was introduced into the solution; this would have been indeterminate, as the region considered lies around the apex. The results for $S$ are in the first division of Table 7, where also is given the mean residual radial velocity $\langle \lvert \Delta\rho \rvert \rangle$ for the three solutions.

The next division gives, first, the quantity $\langle p \rangle S/4.74$ derived from the $v$ components by means of the formula

$$\frac{\langle p \rangle S}{4.74} = \frac{\langle v \sin \lambda \rangle}{\langle \sin^2 \lambda \rangle},$$

and next the mean parallax $\langle p \rangle$ derived with the value of $S$ for the corresponding distance group and the mean distance modulus.

The result for the second modulus group is quite uncertain. The probable error of the mean distance modulus is large, and, moreover, this value can easily be affected by a systematic error in the proper motions, as the mean $v$ component is only 0".004. Therefore, we have discarded this modulus group as far as the $v$ components are concerned. The mean visual absolute magnitude for the first modulus group is in the fourth line of this division of Table 7.

For the $\tau$ components, there is no reason to reject the second modulus group, as the mean value of $|\tau|$ will not be much affected by a systematic error in the proper motions. The two modulus groups were combined, and the results are in the third section of Table 7. With the observed value of $\langle|\tau|\rangle$ and $\langle|\Delta\rho|\rangle = 6.3$ km/sec, one finds the mean parallax according to $\langle p\rangle = 4.74\langle|\tau|\rangle/\langle|\Delta\rho|\rangle$ and the mean distance modulus and mean absolute magnitude in the fourth line of this section of the table.

TABLE 8

MEAN VISUAL ABSOLUTE MAGNITUDES PER VOLUME OF SPACE FROM THREE INDEPENDENT SOURCES
(Numbers of Stars in Parenthesis)

| | Cassiopeia-Taurus Group | Scorpio-Centaurus Association | Stars between $l=340°$ and $l=50°$ |
|---|---|---|---|
| *Mean visual absolute magnitudes:* | | | |
| B1 V | | $-3.8 \pm 0.29$ (p.e.) (4) | |
| B2 IV | $-3.1 \pm 0.4$ (p.e.) (1) | $-2.73 \pm 0.14$ (7) | $-2.30 \pm 0.30$ (p.e.) (1) |
| B2 V | $-2.34 \pm 0.31$ (8) | $-2.48 \pm 0.17$ (15) | (12) |
| B3 V | $-1.65 \pm 0.29$ (16*) | $-1.40 \pm 0.25$ (6†) | $-1.40 \pm 0.25$ (20‡) |
| *Average deviations:* | | | |
| B1 V | | 0.6 ±0.17 (4) | |
| B2 IV | | 0.31 ±0.06 (7) | |
| B2 V | 0.6 ±0.11 (8) | 0.65 ±0.09 (15) | |
| B3 V | 0.6 ±0.08 (16*) | 0.6 ±0.15 (6†) | |

* Includes three hypothetical stars with $M_v = -0.5$.
† Includes two hypothetical stars with $M_v = -0.5$.
‡ Includes four stars of type B3 IV.

The mean absolute magnitudes obtained from the two components are averaged in the first line of the bottom section of the table. This average applies, altogether, to sixteen B3 V; four B3 IV; twelve B3 V; and one B2 IV stars. Only part of these were used in the treatment of the $v$ components, but the subclasses occur in about the same proportions for the $v$ and the $\tau$ components. We have derived from this average one mean value for B3 IV and V and one for B2 IV and V, assuming the difference between these two to be 0.9 mag., as suggested by the second and third columns of Table 8. This leads to the mean values for B2 IV and V and B3 IV and V in the last lines of Table 7.

The mean absolute magnitudes thus obtained apply to stars selected according to a certain apparent magnitude and not per volume of space. The latter are fainter by an amount of

$$\Delta M = \frac{\sigma^2}{0.434} \frac{d \log A(m)}{dm}, \tag{4}$$

where $\sigma$ is the dispersion of the absolute magnitudes and $A(m)$ is the number of stars per unit area as a function of the apparent magnitude (Malmquist 1920). We have adopted $\Delta M = +0.52$ mag., using the value of 0.6 mag. for the average deviation in $M_v$, as suggested by the data on the Cassiopeia-Taurus and the Scorpio-Centaurus associations in Table 8, and $d \log A(m)/dm = 0.4$. The latter value corresponds to an increase

in the number of stars with the square of the distance, as seems most plausible in view of the strong galactic concentration of the stars considered here. We thus obtain the mean absolute magnitudes per volume of space in the last column of Table 8.

## VIII. ADOPTED MEAN ABSOLUTE MAGNITUDES PER VOLUME OF SPACE

Weighted means of the visual absolute magnitudes derived in the preceding sections for B1 V, B2 IV, B2 V, and B3 V, together with their probable errors, are given in the second column of Table 9. The few data which the Cassiopeia-Taurus group and the Scorpio-Centaurus association provide for the other subclasses will be incorporated later in more extensive discussions of these classes. The third column gives the average deviations from the mean absolute magnitudes per subclass, together with their probable errors.

The next columns give the provisional standard absolute magnitudes of Keenan and Morgan (1951) and the differences between these and our adopted values. Our new results apply to the stars per volume of space, whereas the tabulation by Keenan and Morgan refers to the stars selected per apparent magnitude. The difference, $\Delta M$, between the two kinds of mean absolute magnitudes depends on the dispersion of the absolute

TABLE 9

ADOPTED MEAN ABSOLUTE MAGNITUDES PER VOLUME OF SPACE

| Subclass | Adopted Mean Visual Absolute Magnitude per Volume of Space $\langle M_v \rangle$ | Average Deviation from $\langle M_v \rangle$ | Provisional Standard Absolute Magnitudes | Adopted $\langle M_v \rangle$ *minus* Standard Values |
|---|---|---|---|---|
| B1 V..... | $-3.8 \pm 0.29$ (p.e.) | $0.6 \pm 0.2$ (p.e.) | $-3.2$ | $-0.6$ |
| B2 IV..... | $-2.7 \pm .13$ | $.3 \pm .06$ | $-3.3$ | $+.6$ |
| B2 V..... | $-2.4 \pm .13$ | $.6 \pm .08$ | $-2.6$ | $+.2$ |
| B3 V..... | $-1.5 \pm 0.15$ | $0.6 \pm 0.07$ | $-2.0$ | $+0.5$ |

magnitudes within the subclass and on the space distribution of the stars as described in Section VII (eq. [4]). In the case of the general population of field stars discussed in Section VII, we estimated $\Delta M$ to be about $+0.5$ mag. for B2 V and B3 V. For most applications the differences will be between this value and zero. The latter value holds, for instance, if we are dealing with an isolated group of stars in which the observations cover the complete range in luminosities for the subclass.

The differences for B2 V and B3 V in the last column of Table 9 are thus of the order of magnitude to be expected and show that the provisional standard absolute magnitudes per apparent magnitude were approximately correct. For B2 IV our results indicate a smaller difference with respect to B2 V than that in the Keenan-Morgan table. The value for this subclass is based mainly on the contribution from the Scorpio-Centaurus group; it suggests that subclass B2 IV is a well-defined group with a narrow range in absolute magnitude, which may make it particularly useful for distance determinations.

The mean absolute magnitude for B1 V is considerably brighter than that in the Keenan-Morgan table but also much more uncertain than that for the other three subclasses. It is based entirely on the Scorpio-Centaurus association and requires further confirmation.

Although there is good agreement between the three sources from which the mean absolute magnitudes have been obtained, these should be adopted with some reservation. In all three classes we were dealing with assemblies of stars which are not of recent

formation, judging from the absence of O-type stars and of stars of high luminosity, as well as from the kinematics and space distribution. We must expect that for these stars evolutionary changes have already caused the main-sequence absolute magnitudes to be somewhat different from those for stars of more recent origin. For the latter we would expect the luminosities to be lower, especially for the earliest types. See, for instance, Tayler's (1954) computation of the evolutionary path of a star of 10 solar masses (original type around B2) in the course of 50 million years, which shows that a differential effect of at least several tenths of a magnitude must be expected.

## IX. THE α PERSEI MOVING CLUSTER

The α Persei cluster is represented in Figure 1*a* by two B3 and eight B5 stars around the mean position $l = 115°$, $b = -5°$. It also contains later-type stars, one of which is α Persei of type F5 Ib, the brightest of its members, after which we shall name it. The cluster has sometimes also been named after Boss, Eddington, or Kapteyn, who detected it independently.

The mean proper motion derived from the ten stars with probable errors of the proper motions smaller than 0".0040 is shown in Figure 1*a*. Its equatorial and galactic components are

$$\mu_\alpha \cos\delta = +0''.0286\,, \qquad \mu_\delta = -0''.0280\,,$$

$$\mu_l \cos b = +0''.0394\,, \qquad \mu_b = -0''.0069\,,$$

with a probable error of ±0".0009 as determined from the scatter of the individual values around the mean.

The cluster was not included in the discussion of the Cassiopeia-Taurus group in Section V, but there are strong reasons to believe that it belongs to this group. Earlier studies like, for instance, the one by Rasmuson (1921), have revealed the probable existence of an extended stream of stars around the cluster, sharing its motion. The evidence for such an extended stream was criticized by Smart and Ali (1940) mainly on the basis of the large internal motions. The existence of extended streams with large internal velocities and in a state of disintegration is, however, quite compatible with modern ideas on stellar evolution, and the significance of the stream around the Perseus moving cluster as described by Rasmuson cannot be doubted. In fact, his Figure VI, displaying the proper motions of the bright stars of the extended stream, bears close resemblance to our Figure 1*a*. The cluster deserves special attention because the assumption of its membership in the Cassiopeia-Taurus group leads to a geometrical determination of the luminosities of its members, and these luminosities are found to be considerably fainter than the values for the field stars of the corresponding MK spectral types.

The mean proper motion is almost exactly in the direction of the convergent point given in Table 3. This is apparent from Figure 1*a*, where its direction agrees very well with that of the proper motions of the surrounding stars. It is shown more precisely by the values of the $v$ and $\tau$ components computed with the elements of solution I, for which we have

$$v = 0''.0400\,, \qquad \tau = +0''.0012\,, \qquad \text{p.e.} = \pm 0''.0009\,.$$

The direction of the mean proper motion differs by only 1°.7 from that toward the convergent, which is well within the observational uncertainties, whereas it differs about 10° from the direction toward the standard solar antapex.

The radial velocity also fits the elements of solution I quite well. The predicted value is +2.8 km/sec, which includes the term $rk = +0.8$ km/sec based on the distance of 127 pc derived below. The mean observed value for eight B3 and B5 stars, corrected for gravitational red shift, is +3.2 km/sec, whereas for α Persei it is −2.4 km/sec. These

results leave little doubt that the cluster does indeed belong to the Cassiopeia-Taurus group. Computing the parallax from the $v$ component and solution I, we get $p = 0''.0079 \pm 0''.0007$ (p.e.) with the corresponding distance and distance modulus: $r = 127$ pc $\pm$ 11 (p.e.); $m_0 - M = 5.5 \pm 0.2$ (p.e.). The uncertainty in these values is due mainly to that in the stream velocity, $S$. The elements of the space motion of the cluster with respect to the sun can, for all practical purposes, be taken to be the same as those for the Cassiopeia-Taurus group given in Table 4.

With the foregoing distance modulus we have computed the visual absolute magnitudes for the ten B3 and B5 stars, for $\alpha$ Persei, and for the remaining stars of types A2 and earlier which were considered to be members by Roman and Morgan (1950). These authors' corrections for interstellar absorption for the stars for which no direct observations are available were slightly reduced in accordance with the somewhat smaller ratio between total absorption and color excess used for the B-type stars in the present paper.

For $\alpha$ Persei we find $M_v = -4.1$. Most of the other stars belong to luminosity class V, and, for these, Table 10 gives the mean absolute magnitudes per spectral subclass. The table also gives, in the last column, the amount by which these mean absolute magnitudes are fainter than the standard values tabulated by Keenan and Morgan (1951). The mean difference is $+1.06 \pm 0.20$ (p.e.) mag. The probable error consists mainly of the zero-point error, which is common to all values of $M_v$ in Table 10.

TABLE 10

VISUAL ABSOLUTE MAGNITUDES FOR LUMINOSITY CLASS V IN $\alpha$ PERSEI CLUSTER

| Spectral Class | No. of Stars | Mean $M_v$ | Mean $M_v$ *minus* Prov. Standard | Spectral Class | No. of Stars | Mean $M_v$ | Mean $M_v$ *minus* Prov. Standard |
|---|---|---|---|---|---|---|---|
| B3 V | 2 | −1.0 | +1.0 | B9 V | 4 | +1.2 | +1.2 |
| B5 V | 3 | −0.2 | +1.1 | A0 V | 4 | +1.7 | +1.2 |
| B6 V | 1 | −0.4 | +0.7 | A1 V | 3 | +1.8 | +0.9 |
| B8 V | 2 | +0.8 | +1.3 | A2 V | 1 | +1.5 | +0.3 |

We do not conclude that this mean difference represents a correction to be applied to the provisional standard absolute magnitudes of Keenan and Morgan. A small but uncertain fraction of it is due to the fact that the Keenan-Morgan values apply to stars selected per apparent magnitudes, whereas the proper comparison would be with values per volume of space. The remaining difference is similar to that between the A-type stars in the Pleiades and the near-by stars, noticed by Johnson and Knuckles (1951) and interpreted by these authors as an age effect, the near-by stars in general being older and more luminous than those in the Pleiades.

We further notice that, around spectral class B3 V, Tables 8 and 9 indicate a smaller difference in the sense Cassiopeia-Taurus group *minus* standard values than the difference $\alpha$ Persei cluster *minus* standard values just described. This suggests a small difference between the Cassiopeia-Taurus group and the $\alpha$ Persei cluster, the class V stars of the group being a few tenths of a magnitude brighter than the main sequence of the cluster. Since the zero point of the luminosities of the group and of the cluster are affected in the same way by a possible error in the stream velocity $S$, the probable error of this difference in the luminosities is only between 0.1 and 0.2 mag.

If this difference between group and cluster is also interpreted in terms of a different age, it means that the $\alpha$ Persei cluster is of more recent origin than the Cassiopeia-Taurus group as a whole. For the latter we found a minimum age of $50 \times 10^6$ years. An indication of expansion of the cluster derived from the proper motions of fainter stars and corresponding to an expansion age of $8 \pm 3$ (p.e.) million years has been announced by

Dieckvoss (1953). An accurate study of the color-magnitude diagram, including the faint cluster stars found by Dieckvoss, Heckmann, and Kox (1954) and additional measures of the proper motions, will be of great interest.

### X. STARS WITH HIGH SPACE VELOCITIES; MOTIONS AND ORIGINS

The region $l = 340°$–$200°$ contains several stars whose motions deviate considerably from the general pattern. Some of these stars have high space velocities. We shall consider the most conspicuous cases, beginning with those in which the origin and age of the star can be determined. A more complete study of the space motions and physical properties of these stars, will be published later.

1. HD 34078 = AE Aurigae, $l = 139°.8$, $b = 0°.9$, O9.5 V (see Fig. 3*a*). This star and HD 38666 ($\mu$ Columbae), which lies just outside the region considered, are known to have originated in the Orion association (Blaauw and Morgan 1954*a*, *b*).

2. HD 19374 = 53 Arietis, $l = 131°.3$, $b = -33°.0$, B2 V (see Fig. 3*a*). The direction of the proper motion suggests that this star also originated in the Orion association, and this is confirmed by closer study. Some data on the star are assembled in Table 11. The

TABLE 11

OBSERVED AND DERIVED QUANTITIES FOR 53 ARIETIS (HD 19374, GC 3728)*

| | | | |
|---|---|---|---|
| Adopted visual absolute magnitude | − 2.5 | − 2.9 | − 3.5 |
| Parallax (0".0001) | 26.3 | 21.9 | 16.6 |
| Distance (pc) | 380 | 456 | 603 |
| $\mu_\alpha \cos\delta$ / $\mu_\delta$ corrected for standard solar motion (0".0001) | −304 / +156 | −292 / +144 | −278 / +133 |
| Declination of intersection with R.A. $5^h30^m$ | − 4°.9 | − 3°.4 | − 2°.4 |
| Tangential velocity (km/sec) | 61.6 | 70.6 | |
| Predicted radial velocity if origin in Orion association (solar motion not included) (km/sec) | +1.8 | + 18.1 | |

| | |
|---|---|
| Observed radial velocity corrected for standard solar motion and red shift | +18.0±3.4 (p.e.) |
| Total space velocity (km/sec) | 73 |
| Age (years) | $4.8\times10^6$ |

* R.A. = $3^h1^m.8$; Decl. = +17°30′ (1900); $l = 131°.3$, $b = -33°.3$; Sp. MK B2 V. $\mu_\alpha \cos\delta = -0".0233$; $\mu_\delta = +0".0085$; p.e. = ±0".0020; Rad. Vel. = +27.8 km/sec± 3.4 (p.e.).

proper motion was first corrected for the standard solar motion. This correction depends on the star's distance and is given for three assumed values of the absolute magnitude: −2.5, −2.9, and −3.5.

In order to show how well the direction of the corrected proper motion fits the hypothesis that the star originated in the Orion association, we give in Table 11 the declination of the point of intersection of the great circle defined by this proper motion with the meridian at R.A. $5^h30^m$. This is the R.A. of the Trapezium stars, whose declination is −5°.5. For each of the three cases the coincidence with this declination is quite close, and the great circle always passes through the Orion Nebula. The probable error of the declination of intersection corresponding to the probable error in the proper motion is about 2°.5.

We next test how well the radial velocity fits the hypothesis of the star's origin in the region of the Orion Nebula. The radial velocity can be predicted from the geometry of the triangle Orion-star-sun and from the tangential velocity. The latter was derived from the proper motion for the different values of $M_v$. The distance of the Orion Nebula was assumed to be 500 pc, as in the work on AE Aurigae and $\mu$ Columbae, although this may have to be revised when the calibration is complete. The table shows that exact

agreement of observed and predicted radial velocity is obtained for $M_v = -2.9$. This is within the range of possible values for B2 V, according to Table 9.

The evidence that the star originated in the Orion association thus appears quite strong, and we have computed the space velocity and the age, assuming $M_v = -2.9$. We find 73 km/sec and $4.8 \times 10^6$ years, respectively. For AE Aurigae and $\mu$ Columbae we found an age of $2.6 \times 10^6$ years. The difference between these two ages being considerably larger than its probable error, we conclude that star formation in the central region of the Orion association took place over a period of at least 2 million years.

The fact that AE Aurigae and $\mu$ Columbae form the remarkable pair, with equal and opposite velocities with respect to the region around the Trapezium stars, was reason to

TABLE 12

PRINCIPAL DATA ON 68 CYGNI (HD 203064)

| | |
|---|---|
| Observed proper motion | $\mu_l \cos b = -0''.006$, $\mu_b = -0''.009$ |
| Corrected for standard solar motion | $\mu_l \cos b = -0''.0085$, $\mu_b = -0''.0065$ |
| Total corrected proper motion | $\mu = 0''.011 \pm 0''.002$ (p.e.) |
| Observed radial velocity | +1 km/sec |
| Best-fitting distance | 780 pc |
| Visual absolute magnitude | −5.1 |
| Space velocity | 45 km/sec |
| Age | $5.1 \times 10^6$ years |

TABLE 13

STARS WITH WELL-ESTABLISHED STRONGLY DEVIATING MOTIONS

| | HD 4142 | HD 26356 | HD 214930 |
|---|---|---|---|
| Adopted visual absolute magnitude | −0.7 | −0.7 | −1.5 |
| Distance (pc) | 170 | 140 | 440 |
| *Observed quantities:* | | | |
| $\mu_l \cos b$ and p.e. (0".0001) | −360 ± 34 | −141 ± 16 | −230 ± 50 |
| $\mu_b$ and p.e. (0".0001) | +100 ± 34 | − 5 ± 16 | − 20 ± 50 |
| Radial velocity (km/sec) and quality class | − 60 (*c*) | − 7 (*c*) | − 53 (*b*) |
| *Space-velocity components corrected for standard solar motion:* | | | |
| $X$ (toward $l=0°$, $b=0°$) (km/sec) | + 46 | + 27 | + 31 |
| $Y$ (toward $l=90°$, $b=0°$) (km/sec) | − 49 | + 2 | − 58 |
| $Z$ (toward $b=90°$) (km/sec) | + 31 | + 4 | + 31 |
| Total space velocity (km/sec) | 74 | 28 | 73 |

look for the same phenomenon in connection with 53 Arietis. There are a few stars which may match 53 Arietis in this respect, the most likely candidate being HD 54224 ($m = 6.38$, *HD* spectral class B3). However, the proper motions of these stars are poor, no radial velocities are known, and the stars have not yet been classified in the MK system. A satisfactory answer to this question also requires a careful study of the motions of the early-type stars in the Canis Major region in general.

3. HD 203064 = 68 Cygni, $l = 55°.4$, $b = -4°.4$, O8 (see Fig. 3*b*). When the proper motion of this star is corrected for the standard solar motion, we find it to point exactly away from the center of the association I Cephei. This is located around $l = 69°$, $b = +4°$, at a distance of about 720 pc (Morgan, Whitford, and Code 1953; Markarian 1953). We can, as in the case of 53 Arietis, specify the absolute magnitude for which the photometric distance of the star is such that its radial velocity and proper motion fit the same

value of the space velocity away from the association. Table 12 summarizes the observational data and the results. The probable error of the last two quantities is of the order of 20 per cent. The age found, $5.1 \times 10^6$ years, agrees well with that of $4.5 \times 10^6$ years found by Markarian for the association I Cephei as a whole.

4. HD 197419, $l = 44°.4$, $b = -5°.5$, B2 Ve; and HD 201910, $l = 52°.5$, $b = -5°.4$, B5 V. These two stars may be moving from the Lacerta association. The proper motions are rather uncertain. They lead to an average estimated space velocity of 35 km/sec and an age of $5 \times 10^6$ years for the two stars, with an uncertainty of about 25 per cent.

5. HD 4142, $l = 89°.8$, $b = -14°.7$, B5 V; HD 26356, $l = 95°.5$, $b = +23°.9$, B5 V; and HD 214930, $l = 56°.8$, $b = -30°.7$, B3 V. For these three stars we have computed the space-velocity components corrected for the normal solar motions, using the visual absolute magnitude given in Table 13. This table summarizes the observed quantities and the resulting space velocities. We have checked whether HD 4142 may have originated from the II ($\zeta$) Persei association, but this seems to be out of the question.

It is a great pleasure to acknowledge the stimulating discussions with Dr. W. W. Morgan on the problems connected with the calibration of his luminosity classifications and to express my indebtedness to Dr. H. R. Morgan for his generous collaboration in providing me with improved proper motions at various stages of this investigation.

## REFERENCES

Artiukhina, N. M. 1954, *Astr. J., U.S.S.R.*, **31**, 264.
Blaauw, A. 1946, *Pub. Kapteyn. Astr. Lab. Groningen*, No. 52.
———. 1952*a*, *Trans. I.A.U.*, **8**, 505.
———. 1952*b*, *B.A.N.*, **11**, 405.
———. 1952*c*, *ibid.*, p. 414.
Blaauw, A., and Morgan, W. W. 1953, *Ap. J.*, **117**, 256.
———. 1954*a*, *B.A.N.*, **12**, 76.
———. 1954*b*, *Ap. J.*, **119**, 625.
Bok, B. J. 1937, *The Distribution of the Stars in Space* (Chicago: University of Chicago Press).
Boss, B. 1937, *General Catalogue* (Washington, D.C.: Carnegie Institution of Washington).
Delhaye, J. 1951, *Bull Astr.*, **16**, 1.
———. 1955, *ibid.*, **18**, 309.
Dieckvoss, W. 1953, *Naturwiss.*, **40**, 505.
Dieckvoss, W., Heckmann, O., and Kox, H. 1954, *Mitt. Astr. Gesellschaft 1953*, p. 21.
Greenstein, J. L. 1937, *Harvard Ann.*, **105**, 359.
Hubble, E. P. 1934, *Ap. J.*, **79**, 8.
Johnson, H. L., and Knuckles, C. F. 1955, *Ap. J.*, **122**, 209
Keenan, P. C., and Morgan, W. W. 1951, *Astrophysics*, ed. J. A. Hynek (New York: McGraw-Hill Book Co.), p. 23.
McCuskey, S. W. 1941, *Ap. J.*, **94**, 468.
Malmquist, K. G. 1920, *Lund Medd.*, Ser. II, No. 22.
Markarian, B. E. 1953, *Contr. Bjurakan Obs.*, No. 11.
Markowitz, W. 1948, *A.J.*, **53**, 217.
Morgan, H. R. 1952, *Astronomical Papers Prepared for the Use of the American Ephemeris and Nautical Almanac*, Vol. **13**, Part III.
Morgan, H. R., and Oort, J. H. 1951, *B.A.N.*, **11**, 379.
Morgan, W. W., Harris, D. L., and Johnson, H. L. 1953, *Ap. J.*, **118**, 92.
Morgan, W. W., Whitford, A. E., and Code, A. D. 1953, *Ap. J.*, **118**, 318.
Rasmuson, N. H. 1921, *Lund Medd.*, Ser. II, No. 26.
Roman, N. G., and Morgan, W. W. 1950, *Ap. J.*, **111**, 426.
Sharpless, S. 1952, *Ap. J.*, **116**, 251.
Smart, W. M., and Ali, A. 1940, *M.N.*, **100**, 560.
Stebbins, J., Huffer, C. M., and Whitford, A. E. 1940, *Ap. J.*, **91**, 20.
Tayler, R. J. 1954, *Ap. J.*, **120**, 332.
Torondjadze, A. F. 1953, *Bull. Abastumani Obs.*, **15**, 115.
Vyssotsky, A. N., and Williams, E. T. R. 1948, *A.J.*, **53**, 85.
Weaver, H. F. 1953, *A.J.*, **58**, 177.
Wilson, R. E. 1953, *General Catalogue of Radial Velocities* ("Carnegie Institution of Washington Publication," No. 601 [Washington, D.C.: Carnegie Institution of Washington]).

# SIX-COLOR PHOTOMETRY OF STARS. VIII. THE COLORS OF 409 STARS OF DIFFERENT SPECTRAL TYPES*

JOEL STEBBINS AND GERALD E. KRON
Lick Observatory, University of California
*Received January 10, 1956*

## ABSTRACT

Photoelectric measures in six colors have been obtained for 171 stars in addition to the previous list of 238, making a total of 409 stars. Also the colors of 35 stars from the earlier list have been revised. The new colors determined with the Crossley reflector at the Lick Observatory have been reduced to the system of those with the reflectors at Mount Wilson. The mean colors for the different spectral types have been compared with those of the O stars as nearest to black-body standards. The Paschen and Balmer depressions in the continuum are measures of the hydrogen absorption, most conspicuous in A stars. Our observed Paschen effect agrees with that shown by Hall and Williams, and our Balmer effect is well correlated quantitatively with the measures of Barbier and Chalonge. Deviations from the law of interstellar absorption, previously noted in the case of $\theta^1$ Orionis, are shown to be complicated by the possible presence of unseen companions of later spectral type.

## INTRODUCTION

The present work on multicolor photometry of stars with a photoelectric cell is a continuation of that carried on by Stebbins and Whitford (1945) at Mount Wilson from 1940 to 1944. The new results include those obtained in 1945 and 1946 with the 60-inch reflector and from 1949 to 1954 with the Crossley reflector at the Lick Observatory with

TABLE 1

SYSTEMATIC CORRECTIONS TO LICK COLORS, 1949–1954

| V−I | U | V | B | G | R | I |
|---|---|---|---|---|---|---|
| −2.5 | +0.08 | +0.08 | −0.02 | +0.01 | +0.01 | +0.03 |
| −2.0 | + .04 | + .04 | − .01 | + .005 | + .005 | + .02 |
| −1.0 | − .03 | − .03 | + .01 | − .01 | .00 | − .01 |
| 0.0 | − .08 | − .08 | + .04 | − .03 | − .01 | − .05 |
| +1.0 | −0.13 | − .13 | + .07 | − .04 | − .03 | − .10 |
| +2.0 | ..... | − .19 | + .09 | − .05 | − .04 | − .13 |
| +3.0 | ..... | −0.24 | +0.10 | −0.06 | −0.04 | −0.14 |

a new photometer developed and constructed by Kron. Although the original photocell and set of filters were available at Lick, a slightly better cell of the same type, Western Electric D97087, was used, and the substitution of a quartz-fluorite Fabry lens for the previous glass one at the primary focus gave about double the relative sensitivity in the ultraviolet region. With the addition of a feedback circuit that eliminates drift of the zero reading, the change from a galvanometer to a Brown recorder made it possible to obtain a double run over the six colors in about 5 minutes instead of 8 minutes for a star. Otherwise the methods of observation and reduction remained the same.

The limit of seventh or eighth magnitude attainable with the new installation on the 36-inch Crossley is not very different from that previously found for the 60-inch, but for sixth magnitude and brighter the limit of accuracy for either telescope is set by

* *Contributions from the Lick Observatory, University of California*, Ser. II, No. 59. This work has been supported in part by the Office of Naval Research under a contract with the University of California.

TABLE 2

LIST OF STARS OBSERVED

| HD | V, W | Y | R.A. (1900) h m | Dec. ° ′ | HD | V, W | Y | R.A. (1900) h m | Dec. ° ′ |
|---|---|---|---|---|---|---|---|---|---|
| 358n | A0 | B9p | 0 3.2 | +28 32 | 26356n | B5 | B5 V | 4 5.0 | +83 34 |
| 432r | dF2 | F2 IV | 0 3.8 | +58 36 | 26659n | gG4 | ..... | 4 8.0 | +83 6 |
| 571 | cF2 | F2 II | 0 5.1 | +45 31 | 27697n | gG8 | K0 III | 4 17.2 | +17 18 |
| 886n | B2 | B2 IV | 0 8.1 | +14 38 | 28305n | gG7 | K0 III | 4 22.8 | +18 58 |
| 1064 | B9 | ..... | 0 9.8 | -10 7 | 29139 | gK5 | K5 III | 4 30.2 | +16 18 |
| 1337r | O8 | O9 III | 0 12.5 | +50 53 | 29248n | B2 | B2 III | 4 31.3 | - 3 33 |
| 2905 | B0 | B1 Ia | 0 27.3 | +62 23 | 30211n | B5 | B5 IV | 4 40.5 | - 3 26 |
| 3627n | gK4 | K3 III | 0 34.0 | +30 19 | 31398n | gK3 | K3 II | 4 50.5 | +33 0 |
| 3651 | dK1 | K0 V | 0 34.2 | +20 43 | 31964r | cF2 | F0 Iap | 4 54.8 | +43 41 |
| 3712n | gG7 | K0 II-III | 0 34.8 | +55 59 | 32068n | cK4 | K5 II+B | 4 55.5 | +40 56 |
| 3765 | dK5 | K2 V | 0 35.3 | +39 39 | 32630n | B4 | B3 V | 4 59.5 | +41 6 |
| 4406 | dG3 | ..... | 0 41.3 | +45 49 | 34029n | gG1 | G8 III+F | 5 9.3 | +45 54 |
| 4727 | B5 | B5 V | 0 44.3 | +40 32 | 34085 | B8 | B8 Ia | 5 9.7 | - 8 19 |
| 5394r | B0 | B0 IV:pe | 0 50.7 | +60 11 | 34411n | dG0 | G0 V | 5 12.1 | +40 1 |
| 5848n | gK2 | K2 III | 0 55.0 | +85 43 | 34759 | B5 | B5 V | 5 14.7 | +41 43 |
| 5914r | A5 | ..... | 0 55.6 | +88 29 | 35411n | B0 | B1 V | 5 19.4 | - 2 29 |
| 6860n | gM0 | M0 III | 1 4.1 | +35 5 | 35439n | B3ne | B1 V | 5 19.6 | + 1 45 |
| 6920 | dF7 | F8 V | 1 4.6 | +41 33 | 35468n | B2s | B2 III | 5 19.8 | + 6 16 |
| 8538n | A3 | A5 V | 1 19.3 | +59 43 | 35497n | B8 | B7 III | 5 20.0 | +28 31 |
| 8890r | cF7 | F8 Ib | 1 22.6 | +88 46 | 35715n | B2 | B2 IV | 5 21.6 | + 3 0 |
| 9270 | gG3 | G8 III | 1 26.1 | +14 50 | 36395n | dM3 | ..... | 5 26.4 | - 3 42 |
| 10204 | A9 | ..... | 1 34.7 | +42 47 | 36486r | B0 | O9.5 II | 5 26.9 | - 0 22 |
| 10307r | dG0 | G2 V | 1 35.7 | +42 7 | 36695n | B2 | B1 V | 5 28.5 | - 1 14 |
| 10516 | B0 | B1pe (III, V) | 1 37.4 | +50 11 | 36822n | B0 | B0 IV | 5 29.3 | + 9 25 |
| 11443n | dF2 | F6 IV | 1 47.4 | +29 6 | 36861n | O8 | O8 | 5 29.6 | + 9 52 |
| 12533n | gK3 | K3 II | 1 57.8 | +41 51 | 37018n | B2 | B2 III | 5 30.4 | - 4 54 |
| 12929n | gK1 | K2 III | 2 1.5 | +22 59 | 37022 | B0 | O6p | 5 30.4 | - 5 27 |
| 14622 | dF2 | ..... | 2 16.6 | +40 57 | 37041n | O9 | O9.5 Vp | 5 30.5 | - 5 29 |
| 14633 | O8 | O8 | 2 16.7 | +41 2 | 37043n | O8 | O9 III | 5 30.5 | - 5 59 |
| 14662 | cF8 | F7 Ib | 2 16.9 | +54 55 | 37128r | B0 | B0 Ia | 5 31.1 | - 1 16 |
| 15830 | dG5 | ..... | 2 27.7 | +42 21 | 37468n | B0 | O9.5 V | 5 33.7 | - 2 39 |
| 16397 | dG0 | ..... | 2 32.6 | +30 24 | 37742r | B0 | O9.5 Ib | 5 35.7 | - 2 0 |
| 16901 | cG0 | G0 Ib | 2 37.6 | +43 52 | 38771n | B0 | B0.5 Ia | 5 43.0 | - 9 42 |
| 18411n | A2 | A2 V | 2 52.1 | +39 16 | 39587n | dF9 | G0 V | 5 48.5 | +20 15 |
| 18884n | gM2 | M2 III | 2 57.1 | + 3 42 | 39801 | gM2 | M2 Iab | 5 49.8 | + 7 23 |
| 18925n | cF7 | G8 III:+A3 | 2 57.6 | +53 7 | 40035n | gG6 | K0 III | 5 51.3 | +54 17 |
| 19356r | B9 | B8 V | 3 1.7 | +40 34 | 40111n | B0 | B1 Ib | 5 51.8 | +25 57 |
| 19373n | dG1 | G0 V | 3 1.8 | +49 14 | 40183n | A2 | A2 V | 5 52.2 | +44 56 |
| 20123 | cG2 | G5 II | 3 9.1 | +50 34 | 40312n | A1 | B9.5pv | 5 52.9 | +37 12 |
| 20677n | A0 | A3 V | 3 14.7 | +42 58 | 41074 | A8 | ..... | 5 57.9 | +42 59 |
| 20902r | cF4 | F5 Ib | 3 17.2 | +49 30 | 42995n | gM3 | ..... | 6 8.8 | +22 32 |
| 22928n | B8 | B5 III | 3 35.8 | +47 28 | 44478n | gM3 | ..... | 6 16.9 | +22 34 |
| 23230n | cF4 | F5 II | 3 38.4 | +42 16 | 44743n | B1 | B1 II-III | 6 18.3 | -17 54 |
| 23249n | dK0 | ..... | 3 38.5 | -10 6 | 46136An | dF6 | ..... | 6 26.5 | +17 51 |
| 23288 | B7 | B7 IV | 3 38.9 | +23 59 | 46136Bn | dF6 | ..... | 6 26.5 | +17 51 |
| 23302 | B7 | B6 III | 3 39.0 | +23 48 | 46300n | A0 | A0 Ib | 6 27.5 | + 7 24 |
| 23324 | B8 | B8 V | 3 39.2 | +24 32 | 47105n | A3 | A0 IV | 6 31.9 | +16 29 |
| 23338 | B7 | B6 V | 3 39.3 | +24 10 | 47138n | gG4 | ..... | 6 32.0 | -18 35 |
| 23408 | B9 | B7 III | 3 39.9 | +24 4 | 47205n | gK1 | K1 IV | 6 32.3 | -19 10 |
| 23432 | B8 | B8 V | 3 40.0 | +24 15 | 47442n | gK1 | K1 II-III | 6 33.5 | -18 9 |
| 23441 | B9 | B9 V | 3 40.1 | +24 13 | 47561n | A0 | ..... | 6 34.1 | -16 47 |
| 23480 | B6 | B6 IV | 3 40.4 | +23 39 | 47667n | gK5 | K3 III | 6 34.7 | -14 3 |
| 23630 | B7 | B7 III | 3 41.5 | +23 48 | 47839n | O7 | O7 | 6 35.5 | + 9 59 |
| 23753 | B8 | B8 V | 3 42.5 | +23 8 | 48329n | cG8 | G8 Ib | 6 37.8 | +25 14 |
| 23850 | B8 | B8 III | 3 43.2 | +23 45 | 48737n | dF3 | F5 IV | 6 39.7 | +13 0 |
| 23862 | B8 | B8p | 3 43.3 | +23 51 | 48915n | A2 | A1 V | 6 40.7 | -16 35 |
| 24398r | B1 | B1 Ib | 3 47.8 | +31 35 | 49048n | A2 | ..... | 6 41.4 | -14 41 |
| 24504 | B7 | B6 V | 3 48.8 | +47 35 | 49229n | B8 | ..... | 6 42.3 | -14 19 |
| 24760r | B2 | B0.5 V | 3 51.1 | +39 43 | 51309n | B5 | B3 II | 6 51.7 | -16 55 |
| 24912r | O7 | O7 | 3 52.5 | +35 30 | 51802r | gM0 | ..... | 6 53.7 | +87 12 |

TABLE 2 (Cont'd)

| HD | V, W | Y | R.A. (1900) h m | Dec. ° ' | HD | V, W | Y | R.A. (1900) h m | Dec. ° ' |
|---|---|---|---|---|---|---|---|---|---|
| 58207n | gG7 | K0 III | 7 19.5 | +28 0 | 128998 | A0 | ..... | 14 35.1 | +54 27 |
| 60179n | A2 | A1 V | 7 28.2 | +32 6 | 131873n | gK5 | K4 III | 14 51.0 | +74 34 |
| 60179Cn | dM1 | ..... | 7 28.2 | +32 6 | 132813 | gM5 | ..... | 14 56.0 | +66 20 |
| 61421n | dF3 | F5 IV-V | 7 34.1 | + 5 29 | 133208 | gG5 | G8 III | 14 58.2 | +40 47 |
| 62345n | gG7 | G8 III | 7 38.4 | +24 38 | 135722 | gG4 | G8 III | 15 11.5 | +33 41 |
| 62509n | gG8 | K0 III | 7 39.2 | +28 16 | 136064r | dF9 | F8 V | 15 13.5 | +67 44 |
| 66368 | A3 | ..... | 7 58.0 | +88 56 | 137422 | A1 | A3 II-III | 15 20.9 | +72 11 |
| 71369n | gG1 | G5 III | 8 22.0 | +61 3 | 139006n | A1 | A0 V | 15 30.5 | +27 3 |
| 72905n | dG0 | ..... | 8 30.3 | +65 22 | 140436n | A0 | A0 IV | 15 38.6 | +26 37 |
| 73108n | gK2 | K2 III | 8 31.5 | +64 41 | 140573n | gK2 | K2 III | 15 39.3 | + 6 44 |
| 76294n | gG5 | K0 II-III | 8 50.1 | + 6 20 | 141004n | dG0 | G0 V | 15 41.6 | + 7 40 |
| 81797n | gK5 | K4 III | 9 22.7 | - 8 14 | 142143 | gM7 | ..... | 15 47.8 | +48 47 |
| 82210n | dG | G2 IV | 9 25.6 | +70 16 | 142267n | dF9 | ..... | 15 48.5 | +13 31 |
| 82328n | dF4 | F6 IV | 9 26.2 | +52 8 | 142373r | dF7 | F9 V | 15 49.2 | +42 44 |
| 84441n | cG3 | G0 II | 9 40.2 | +24 14 | 143807 | A1 | A0 III | 15 57.4 | +30 7 |
| 84737n | dG0 | G1 V | 9 42.1 | +46 29 | 144205 | gM6 | ..... | 15 59.6 | +47 31 |
| 87901n | B6 | B7 V | 10 3.0 | +12 27 | 144206 | B8 | B9p | 15 59.6 | +46 19 |
| 89025n | gF0 | F0 III | 10 11.1 | +23 55 | 145328 | gK1 | K0 III | 16 5.3 | +36 45 |
| 90839n | dF8 | F8 V | 10 24.2 | +56 30 | 146791n | gG7 | G9 III | 16 13.0 | - 4 27 |
| 95128n | dG0 | G0 V | 10 53.9 | +40 58 | 147365 | A9 | ..... | 16 16.5 | +39 57 |
| 95418n | A2 | A1 V | 10 55.8 | +56 55 | 147379 | dM0 | M0 V | 16 16.5 | +67 29 |
| 95689n | gG7 | K0 III | 10 57.6 | +62 17 | 147394 | B7 | B5 IV | 16 16.7 | +46 33 |
| 97603n | A2 | A4 V | 11 8.8 | +21 4 | 148387n | gG6 | G8 III | 16 22.6 | +61 44 |
| 102212n | gM1 | M1 III | 11 40.7 | + 7 5 | 148478 | gM1 | M1 Ib+B | 16 23.3 | -26 13 |
| 102647n | A4 | A3 V | 11 44.0 | +15 8 | 148783 | gM6 | ..... | 16 25.4 | +42 6 |
| 102870n | dF8 | F8 V | 11 45.5 | + 2 20 | 148856n | gG5 | G8 III | 16 25.9 | +21 42 |
| 103095n | dG5 | G8 Vp | 11 47.2 | +38 26 | 149757n | B0 | O9.5 V | 16 31.7 | -10 22 |
| 103287n | A0 | A0 V | 11 48.6 | +54 15 | 150680n | dG0 | G0 IV | 16 37.5 | +31 47 |
| 103483 | A0 | ..... | 11 49.9 | +47 2 | 150997n | gG4 | G7 III-IV | 16 39.5 | +39 7 |
| 106591n | A0 | A3 V | 12 10.5 | +57 35 | 151288 | dM0 | K7 V | 16 41.4 | +33 41 |
| 107113r | dF4 | ..... | 12 13.9 | +86 59 | 152391 | dG9 | G8 V | 16 48.0 | + 0 11 |
| 107192r | dF2 | ..... | 12 14.4 | +88 15 | 152601 | gK3 | K2 III | 16 49.2 | - 5 59 |
| 109358r | dG0 | G0 V | 12 29.0 | +41 54 | 153344 | dG4 | ..... | 16 53.8 | +62 16 |
| 110897n | dF8 | ..... | 12 40.3 | +39 50 | 153751n | gG1 | G5 III | 16 56.2 | +82 12 |
| 111395 | dG6 | G7 V | 12 43.9 | +25 23 | 154345 | dK0 | ..... | 16 59.8 | +47 12 |
| 111812 | dF5 | G0 III | 12 46.8 | +28 5 | 155125n | A2 | A2.5 V | 17 4.6 | -15 36 |
| 112185n | A2 | A0pv | 12 49.6 | +56 30 | 156014n | gM5 | ..... | 17 10.1 | +14 30 |
| 112413 | A1 | B9.5pv | 12 51.4 | +38 52 | 156729 | A0 | A2 V | 17 14.2 | +37 24 |
| 112570 | gK0 | ..... | 12 52.6 | +46 44 | 157056 | B2 | B2 IV | 17 15.9 | -24 54 |
| 113139 | A6 | F2 V | 12 56.5 | +56 55 | 157588n | gK1 | ..... | 17 19.0 | -24 9 |
| 113226n | gG6 | G9 II-III | 12 57.2 | +11 30 | 157779 | B9 | B9.5 III | 17 20.2 | +37 14 |
| 113865 | A3 | ..... | 13 1.5 | +29 34 | 157792n | A9 | ..... | 17 20.3 | -24 5 |
| 114282 | gK2 | ..... | 13 4.5 | +88 11 | 157910 | gG2 | ..... | 17 21.0 | +37 2 |
| 114710 | dG0 | G0 V | 13 7.2 | +28 23 | 158704n | B9 | ..... | 17 25.6 | -26 11 |
| 115383n | dF8 | F8 V | 13 11.8 | + 9 57 | 158996n | gK2 | ..... | 17 27.2 | +80 14 |
| 115735 | A0 | ..... | 13 14.0 | +50 12 | 159181 | cG2 | G2 II | 17 28.2 | +52 23 |
| 116656n | A2 | A2 V | 13 19.9 | +55 27 | 159561n | B9 | A5 III | 17 30.3 | +12 38 |
| 116658n | B2 | B1 V | 13 19.9 | -10 38 | 159881n | gK5 | ..... | 17 31.9 | -27 59 |
| 118216 | dF2 | F2 IV | 13 30.3 | +37 42 | 161096n | gK1 | K2 III | 17 38.5 | + 4 37 |
| 120315r | B3 | B3 V | 13 43.6 | +49 49 | 161797n | dG4 | G5 IV | 17 42.5 | +27 47 |
| 120933 | gM2 | ..... | 13 47.4 | +34 56 | 163506 | cF5 | F2 Ia | 17 51.4 | +26 4 |
| 121370n | dF7 | G0 IV | 13 49.9 | +18 54 | 163770 | cK1 | K1 II | 17 52.8 | +37 16 |
| 121409 | A0 | ..... | 13 50.1 | +54 13 | 163917n | gG9 | G9 III | 17 53.5 | - 9 46 |
| 124294n | gK2 | K3 III | 14 7.6 | - 9 48 | 163993n | gG7 | G9 III | 17 53.9 | +29 16 |
| 124897n | gK0 | K2 IIIp | 14 11.1 | +19 42 | 164058n | gK5 | K5 III | 17 54.3 | +51 30 |
| 125162 | A0 | A0p | 14 12.6 | +46 33 | 164514 | A6 | A5 Ia | 17 56.4 | -22 54 |
| 125351 | gK1 | K0 III | 14 13.8 | +35 58 | 165401n | dF7 | ..... | 18 0.7 | + 4 39 |
| 126327 | gM7 | ..... | 14 19.7 | +26 11 | 166182 | B2 | B2 V | 18 4.4 | +20 48 |
| 127762 | A5 | A7 III | 14 28.1 | +38 45 | 166205 | A2 | ..... | 18 4.5 | +86 37 |
| 128165 | dK5 | K3 V | 14 30.2 | +53 20 | 166620 | dK2 | K2 V | 18 6.3 | +38 27 |

TABLE 2 (Cont'd)

| HD | V, W | Y | R.A. (1900) h m | Dec. ° ' |
|---|---|---|---|---|
| 166734 | B0 | O9 If | 18 6.9 | -10 46 |
| 166926 | A3 | ..... | 18 7.8 | +87 0 |
| 168723n | gG8 | K0 III-IV | 18 16.1 | - 2 55 |
| 169034 | B0 | B5 Ia | 18 17.6 | -13 39 |
| 169454 | B1 | B1 Ia+ | 18 19.6 | -14 2 |
| 170740n | B3 | B2 V | 18 25.9 | -10 52 |
| 171635 | cF8 | F7 Ib | 18 30.8 | +56 58 |
| 171779 | gG5 | ..... | 18 31.7 | +52 16 |
| 171871 | B2 | B2 III-IV | 18 32.0 | +51 2 |
| 172167 | A1 | A0 V | 18 33.6 | +38 41 |
| 173638 | cF4 | F2 Ib-II | 18 41.2 | -10 14 |
| 173648 | A9 | A7 (m) | 18 41.3 | +37 30 |
| 173649 | A3 | F0 IV | 18 41.3 | +37 30 |
| 175588r | gM4 | ..... | 18 51.0 | +36 46 |
| 175865 | gM5 | ..... | 18 52.3 | +43 49 |
| 178770 | gM6 | ..... | 19 4.8 | +39 0 |
| 179406n | B3 | B3 IV | 19 7.3 | - 8 7 |
| 180163 | B5 | B2 IV | 19 10.4 | +38 58 |
| 180711n | gG8 | G9 III | 19 12.5 | +67 29 |
| 182640n | A5 | F0 IV | 19 20.5 | + 2 55 |
| 182917 | gM6 | ..... | 19 21.9 | +50 3 |
| 183030r | gM1 | ..... | 19 22.5 | +88 59 |
| 183124n | gG5 | ..... | 19 22.9 | +44 44 |
| 183204n | A0 | ..... | 19 23.3 | +39 45 |
| 183912 | gK0 | K3 II:+B: | 19 26.7 | +27 45 |
| 183914 | B9 | B8 V | 19 26.7 | +27 45 |
| 184279 | B2 | B0.5 IV | 19 28.6 | + 3 34 |
| 184915 | B0 | B0.5 III | 19 31.5 | - 7 15 |
| 186791n | gK4 | K3 II | 19 41.4 | +10 22 |
| 186882n | A0 | B9.5 III | 19 41.8 | +44 53 |
| 186994 | B0 | B0 III | 19 42.5 | +44 43 |
| 187076 | gM2 | M2 II:+B: | 19 42.9 | +18 17 |
| 187138 | gG9 | ..... | 19 43.3 | +88 41 |
| 187642 | A1 | A7 IV, V | 19 45.9 | + 8 36 |
| 187691n | dF8 | F8 V | 19 46.2 | +10 10 |
| 188209 | O8 | O9.5 III | 19 49.0 | +46 47 |
| 188252 | B2 | B2 III | 19 49.2 | +47 41 |
| 188439 | B2 | B0.5 IIIp | 19 50.1 | +47 34 |
| 188512n | dG8 | G8 IV | 19 50.4 | + 6 9 |
| 188892 | B5 | B6 III | 19 52.3 | +38 13 |
| 189340n | dF8 | ..... | 19 54.4 | -10 13 |
| 190406n | dG1 | ..... | 19 59.6 | +16 48 |
| +35°3955 | B0 | B1 Ib | 20 2.2 | +35 32 |
| 190919 | B1 | B1 Ib | 20 2.2 | +35 24 |
| 191026n | dG3 | ..... | 20 2.6 | +35 42 |
| 191201 | B0 | B0 III | 20 3.6 | +35 26 |
| 192107 | gK5 | ..... | 20 8.1 | - 1 19 |
| 192281 | O5 | O5f | 20 9.0 | +39 58 |
| 192422 | B0 | B0.5 Ib | 20 9.7 | +38 28 |
| 192639 | O7 | O8f | 20 10.8 | +37 3 |
| 192640 | A1 | A2 III | 20 10.8 | +36 30 |
| 192876r | cG5 | G3 Ib | 20 12.1 | -12 49 |
| 192947r | gG8 | G9 III | 20 12.5 | -12 51 |
| 193183 | B2 | B1.5 Ib | 20 13.8 | +37 55 |
| 193237 | B1 | Bp | 20 14.1 | +37 43 |
| 193322 | O8 | O8 | 20 14.6 | +40 25 |
| 193370 | cF5 | F5 Ib | 20 14.8 | +34 40 |
| 193443 | O9 | O9 III | 20 15.2 | +37 57 |
| 193514 | O8 | O7f | 20 15.5 | +38 57 |
| 193536 | B2 | B2 V | 20 15.6 | +46 0 |
| 194093r | cF7 | F8 Ib | 20 18.6 | +39 56 |
| 194279 | B2 | B1.5 Ia | 20 19.7 | +40 26 |
| 194335 | B3 | B2 Vp | 20 20.0 | +37 10 |
| 194839 | B0 | B0.5 Ia | 20 22.8 | +41 3 |
| 195295 | cF4 | F5 II | 20 25.3 | +30 2 |
| 195592 | B0 | O9.5 Ia | 20 27.2 | +43 59 |
| 195593 | cF5 | F5 Iab | 20 27.2 | +36 36 |
| 196321 | gK5 | K4 III | 20 31.5 | - 2 54 |
| 196787n | gG8 | ..... | 20 34.5 | +81 5 |
| 197345 | A2 | A2 Ia | 20 38.0 | +44 55 |
| 197770 | B2 | B2 IV | 20 40.7 | +56 46 |
| 197989n | gK0 | K0 III | 20 42.2 | +33 36 |
| 198084 | dF9 | ..... | 20 42.9 | +57 13 |
| 198149n | dG7 | K0 IV | 20 43.3 | +61 27 |
| 198478 | B2 | B3 Ia | 20 45.5 | +45 45 |
| 198781 | B1 | B0.5 V | 20 47.5 | +63 40 |
| 198802n | dG1 | ..... | 20 47.6 | -11 57 |
| 198846 | O9 | B0 IV | 20 48.1 | +34 17 |
| 199081 | B3 | B5 V | 20 49.7 | +44 0 |
| 199095n | A0 | ..... | 20 49.8 | +82 10 |
| 199216 | B1 | B1 II | 20 50.7 | +49 9 |
| 199437n | gK1 | ..... | 20 52.1 | +80 11 |
| 199478 | B8 | B8 Ia | 20 52.4 | +47 2 |
| 199579 | O6 | O6 | 20 53.1 | +44 33 |
| 199960n | dG1 | ..... | 20 55.3 | - 5 7 |
| 200120 | B3 | B1 IV:e | 20 56.4 | +47 8 |
| 200790n | dF7 | ..... | 21 0.5 | + 5 34 |
| 200857 | B2 | B3 III | 21 1.0 | +54 51 |
| 200905 | cK5 | K5 Ib | 21 1.3 | +43 32 |
| 201091n | dK6 | K5 V | 21 2.4 | +38 15 |
| 201092n | dM0 | K7 V | 21 2.4 | +38 15 |
| 201601 | cF1 | F0pv | 21 5.5 | + 9 44 |
| 201819 | B1 | B1 Vp | 21 7.0 | +35 53 |
| 202109n | gG4 | G8 II | 21 8.7 | +29 49 |
| 202751 | dK6 | ..... | 21 12.9 | - 0 15 |
| 203064 | O8 | O8 | 21 14.8 | +43 31 |
| 203280r | A3 | A7 IV, V | 21 16.2 | +62 10 |
| 203374 | B0 | B0 IVpe | 21 16.7 | +61 25 |
| 203938 | B1 | B0.5 IV | 21 20.2 | +46 44 |
| 204075r | cG4 | G4 Ib p | 21 21.0 | -22 51 |
| 204172 | B0 | B0 Ib | 21 21.7 | +36 14 |
| 204867 | cG1 | G0 Ib | 21 26.3 | - 6 1 |
| 205021r | B1 | B2 III | 21 27.4 | +70 7 |
| 205139 | B1 | B1 II | 21 28.3 | +60 1 |
| 205196 | B0 | B0 Ib | 21 28.6 | +57 4 |
| 206165 | B2 | B2 Ib | 21 35.2 | +61 38 |
| 206773 | B0 | B0 V:pe | 21 39.3 | +57 17 |
| 206778r | cK0 | K2 Ib | 21 39.3 | + 9 25 |
| 206859 | cG3 | G5 Ib | 21 39.8 | +16 53 |
| 206936 | gM2 | M2 Ia | 21 40.4 | +58 19 |
| 207198 | O9 | O9 II | 21 42.2 | +61 59 |
| 207538 | O9 | B0 V | 21 44.6 | +59 14 |
| 209339 | B0 | B0 IV | 21 57.6 | +62 0 |
| 209750 | cG1 | G2 Ib | 22 0.6 | - 0 48 |
| 209772r | gM5 | ..... | 22 0.9 | +62 38 |
| 209975 | O9 | O9.5 Ib | 22 2.1 | +61 48 |
| 210745 | cK5 | K1 Ib | 22 7.4 | +57 42 |
| 210839 | O6 | O6f | 22 8.1 | +58 56 |
| 211336 | A6 | F0 IV | 22 11.4 | +56 33 |
| 212455 | B3 | B5 Iab | 22 19.3 | +54 44 |

TABLE 2 (Cont'd)

| HD | V,W | Y | R.A. (1900) h m | Dec. ° ' | HD | V,W | Y | R.A. (1900) h m | Dec. ° ' |
|---|---|---|---|---|---|---|---|---|---|
| 212710r | B9 | ..... | 22 21.3 | +85 36 | 218342 | B1 | B0 IV | 23 2.1 | +62 41 |
| 213087 | B0 | B0.5 Ib | 22 23.9 | +64 37 | 218356 | cK0 | K0 Ibp | 23 2.2 | +24 56 |
| 213306 | cF4 | ..... | 22 25.4 | +57 54 | 218376 | B1 | B0.5 IV | 23 2.4 | +58 53 |
| 213307n | A0 | ..... | 22 25.4 | +57 54 | 218634 | gM4 | ..... | 23 4.5 | + 8 8 |
| 213310 | gM0 | M0 Iab+B | 22 25.4 | +47 12 | 218639 | A0 | ..... | 23 4.5 | -15 3 |
| 214168 | B3 | B1 (V) e | 22 31.4 | +39 7 | 218753 | A9 | ..... | 23 5.5 | +58 47 |
| 214665r | gM4 | ..... | 22 34.7 | +56 17 | 219615n | gG4 | G7 III | 23 12.0 | + 2 44 |
| 214680r | O9 | O9 V | 22 34.8 | +38 32 | 219659 | A0 | ..... | 23 12.4 | -12 16 |
| 214868 | gK2 | K3 III | 22 36.1 | +43 45 | 219833 | A0 | ..... | 23 13.8 | -12 43 |
| 214993 | B1 | B2 III | 22 37.0 | +37 43 | 220020 | A0 | ..... | 23 15.4 | - 9 28 |
| 214994n | A2 | A1 V | 22 37.0 | +28 48 | 221356n | dF8 | ..... | 23 26.4 | - 4.38 |
| 215182n | gG2 | G8 II:+F | 22 38.3 | +29 42 | 221525 | gF0 | ..... | 23 27.8 | +86 45 |
| 215766 | A0 | ..... | 22 42.4 | -14 35 | 221830n | dG0 | ..... | 23 30.4 | +30 27 |
| 216131n | gG6 | G8 III | 22 45.2 | +24 4 | 222574 | cG1 | G0 II | 23 36.6 | -18 22 |
| 216200n | B3 | B3 IV: | 22 45.8 | +41 26 | 222661 | B9 | B9.5 V | 23 37.5 | -15 6 |
| 216411 | B1 | B1 Ia | 22 47.6 | +58 28 | 222847 | B9 | ..... | 23 39.0 | -18 50 |
| 216446n | gK3 | K3 III | 22 47.9 | +82 37 | 222935 | dK2 | ..... | 23 40.0 | +29 0 |
| 216494 | B9 | ..... | 22 48.2 | -12 9 | 223640 | B9 | B9.5p | 23 46.2 | -19 28 |
| 217014n | dG0 | ..... | 22 52.6 | +20 14 | 224014 | cG0 | F8-Mp | 23 49.4 | +56 57 |
| 217101 | B2 | B2 IV-V | 22 53.1 | +38 48 | 224572 | B2 | B1 V | 23 53.9 | +55 12 |
| 217382n | gK5 | K4 III | 22 55.2 | +83 49 | 224758n | dF5 | ..... | 23 55.3 | +26 22 |
| 217476 | cG3 | G0 Ia | 22 55.9 | +56 5 | 224930n | dG1 | G2 V | 23 56.9 | +26 33 |
| 217906n | gM2 | M2 II-III | 22 58.9 | +27 32 | 225132 | A0 | B9 IV | 23 58.6 | -17 54 |
| 218045n | A0 | B9.5 III | 22 59.8 | +14 40 | 225212 | cK5 | K3 Ib | 23 59.4 | -11 4 |
| 218173 | B9 | ..... | 23 0.7 | - 8 29 | | | | | |

the sky; any undetected general or local variation in the extinction will cause larger errors than those caused by concealed defects of the apparatus. The same tables for the mean extinction have been used at Mount Hamilton as at Mount Wilson; any differences between first-class nights at the two stations seem to be negligible.

The later colors obtained with the 60-inch were on the original system, but, because of the different photocell and the more transparent Fabry lens at Lick, there are systematic changes in the colors along the spectral sequence. Even if the exact differences in effective wave lengths between the two systems were evaluated, the best procedure would seem to be to refer all new results to the first system and then, if necessary, to make the proper small changes in the originally assigned wave lengths. Hence we reobserved several dozen stars of all types, enough to establish the differences along the scale. When the new system is made to agree with the old one for polar standards near spectral type A, or $V - I = -1.50$, the other corrections are as in Table 1. These corrections have already been applied in all printed results in the present paper.

The first list, in what we shall call "Paper III" (Stebbins and Whitford 1945), contained results for 238 stars of different spectral types; the present or second list has new data for 171 stars, for a total of 409 stars; also now included are the colors of 35 stars from the first list that have been revised by additional measures. The combined list of all stars observed is in Table 2. In the first column, the plain HD numbers refer to stars in the first list; those marked "n" and "r" refer to the new and revised colors, respectively. For only these latter colors are the new measures given in Table 3 of the present paper; for the old colors the reader is referred to Paper III. In the second column of Table 2 the spectral types are from the same sources as before, "V" from Victoria, usually for the O to B5 types, "W" from Mount Wilson for the later types. In the third column are the available Yerkes classifications, kindly furnished by Dr. W. W. Morgan.

## THE OBSERVATIONS

In Table 3 are the principal new results of the present paper. As before, the HD numbers in the first column are marked with "n" or "r" for new or revised, respectively; an asterisk indicates a note at the end of the table. The "Z" in the third column refers to Hubble's (1934) zone of avoidance of the nebulae; "i" means in, "o" out, and "?" doubtful. The magnitude "m" is Harvard visual. The spectral types are from the same sources as those in Table 2—Victoria, Mount Wilson, and Yerkes. The visual absolute magnitude, "M," for stars of type F or later, are from Mount Wilson. The six colors from U to I are, as usual, referred in magnitude to the mean of BGR; they are arranged in the order of $V - I$, beginning with the bluest. The figures in the last column refer to the number of nights.

## DISCUSSION

Since the bluest stars are listed first in each type in Table 3, we select the first two or three, in order to minimize interstellar reddening, and compare them with the O stars, which are probably as nearly like black bodies as we can find. In Table 4 the groups are arranged according to the Victoria and Mount Wilson spectral types; those from Yerkes were not available for all the later types. The mean spectral types of the dwarfs and giants were selected, with the stars available, to be as nearly as possible of the same type.

The data of Table 4 are shown graphically in Figure 1, where the scale of ordinates in the left half for the B stars is drawn to ten times the magnitude scale of the right half for the later types. If we exclude for the moment the possibility of space reddening, we see at once that the Balmer depression in the ultraviolet, referred to the O stars, already sets in at B0 and increases with the temperature reddening for the later B's. In fact, this Balmer absorption is not a bad criterion for the spectral classification of the early types, though we have not been able to find enough nonreddened B stars to evaluate a possible effect of absolute magnitude. Corresponding to the Balmer effect in the ultraviolet, there

Table 3

Colors of 210 Stars

| HD | Name | Z | m | V,W | Y | U | V | B | G | R | I | V-I | Obs. |
|---|---|---|---|---|---|---|---|---|---|---|---|---|---|
| | | | | | O | | | | | | | | |
| 47839n | 15 Mon | ? | 4.68 | O7s | O7 | -2.29 | -1.20 | -0.53 | -0.06 | +0.59 | +1.38 | -2.58 | 3 |
| 37043n | ι Ori | i | 2.87 | O8 | O9 III | -2.21 | -1.17 | -0.55 | -0.05 | +0.60 | +1.39 | -2.56 | 2 |
| 14633 * | ..... | o | 7.3 | O8 | ..... | -2.27 | -1.17 | -0.53 | -0.03 | +0.57 | +1.38 | -2.55 | 4 |
| 214680r | 10 Lac | o | 4.91 | O9s | O9 V | -2.25 | -1.16 | -0.52 | -0.05 | +0.57 | +1.32 | -2.48 | 6 |
| 36861n | λ Ori | i | 3.66 | O8 | O8 | -2.16 | -1.12 | -0.51 | -0.04 | +0.55 | +1.26 | -2.38 | 3 |
| 1337r | HR 65 | i | 6.12 | O8n | O9 III | -2.10 | -1.06 | -0.45 | -0.06 | +0.51 | +1.18 | -2.24 | 2 |
| 37041n | $\theta^2$ Ori | i | 5.17 | O9 | O9.5 Vp | -1.97 | -0.98 | -0.41 | -0.02 | +0.43 | +0.92 | -1.90 | 2 |
| 24912r | ξ Per | i | 4.05 | O7n | O7 | -1.85 | -0.90 | -0.36 | -0.04 | +0.40 | +0.89 | -1.79 | 2 |
| | | | | | B0 | | | | | | | | |
| 36486r | δ Ori | ? | 2.48 | B0 | O9.5 II | -2.24 | -1.16 | -0.54 | -0.05 | +0.59 | +1.37 | -2.53 | 6 |
| 37468n* | σ Ori | i | 3.78 | B0 | O9.5 V | -2.18 | -1.15 | -0.53 | -0.06 | +0.59 | +1.38 | -2.53 | 2 |
| 5394r* | γ Cas | i | 2.25 | B0ne | B0 IV:pe | -2.21 | -1.16 | -0.54 | -0.05 | +0.59 | +1.31 | -2.47 | 4 |
| 37742r | ζ Ori | i | 2.05 | B0neα | O9.5 Ib | -2.18 | -1.12 | -0.52 | -0.05 | +0.57 | +1.33 | -2.45 | 4 |
| 35411n | η Ori | ? | 3.44 | B0 | B1 V | -2.05 | -1.10 | -0.52 | -0.05 | +0.57 | +1.30 | -2.40 | 2 |
| 38771n | κ Ori | i | 2.20 | cB0 | B0.5 Ia | -2.12 | -1.10 | -0.50 | -0.05 | +0.55 | +1.29 | -2.39 | 2 |
| 37128r | $\epsilon_1$ Ori | i | 1.75 | cB0eα | B0 Ia | -2.14 | -1.10 | -0.50 | -0.05 | +0.55 | +1.28 | -2.38 | 3 |
| 36822n | $\phi^1$ Ori | i | 4.53 | B0ss | B0 IV | -2.09 | -1.12 | -0.50 | -0.04 | +0.54 | +1.24 | -2.36 | 3 |
| 40111n | 139 Tau | i | 4.90 | B0 | B1 Ib | -1.85 | -0.94 | -0.43 | -0.05 | +0.48 | +1.08 | -2.02 | 2 |
| 149757n | ζ Oph | ? | 2.70 | B0nn | O9.5 V | -1.68 | -0.89 | -0.36 | -0.04 | +0.40 | +0.94 | -1.83 | 2 |
| | | | | | B1 | | | | | | | | |
| 44743n* | β CMa | o | 1.99 | cB1 | B1 II-III | -2.11 | -1.16 | -0.56 | -0.05 | +0.61 | +1.39 | -2.55 | 2 |
| 205021r* | β Cep | i | 3.32 | B1 | B2 III | -2.12 | -1.15 | -0.54 | -0.07 | +0.61 | +1.35 | -2.50 | 5 |
| 24398r | ζ Per | i | 2.91 | cB1 | B1 Ib | -1.60 | -0.79 | -0.32 | -0.05 | +0.37 | +0.79 | -1.58 | 3 |
| | | | | | B2 | | | | | | | | |
| 886n | γ Peg | o | 2.87 | B2ss | B2 IV | -2.00 | -1.14 | -0.54 | -0.06 | +0.60 | +1.39 | -2.53 | 2 |
| 116658n | α Vir | o | 1.21 | B2 | B1 V | -2.08 | -1.17 | -0.53 | -0.06 | +0.59 | +1.34 | -2.51 | 6 |
| 35715n | ψ Ori | o | 4.66 | B2 | B2 IV | -2.06 | -1.14 | -0.54 | -0.04 | +0.58 | +1.36 | -2.50 | 2 |
| 35468n | γ Ori | o | 1.70 | B2s | B2 III | -2.01 | -1.15 | -0.54 | -0.05 | +0.59 | +1.34 | -2.49 | 3 |
| 24760r | ε Per | i | 2.96 | B2 | B0.5 V | -2.11 | -1.15 | -0.52 | -0.07 | +0.59 | +1.31 | -2.46 | 3 |
| 29248n | ν Eri | o | 4.12 | B2s | B2 III | -2.01 | -1.12 | -0.52 | -0.06 | +0.58 | +1.30 | -2.42 | 2 |
| 37018n | 42 Ori | i | 4.65 | B2 | B2 III | -2.06 | -1.12 | -0.52 | -0.05 | +0.57 | +1.27 | -2.39 | 2 |
| 36695n | VV Ori | ? | 5.37 | B2n | B1 V | -2.00 | -1.10 | -0.51 | -0.06 | +0.57 | +1.25 | -2.35 | 2 |

Table 3 (Continued)

| HD | Name | Z | m | V, W | Y | U | V | B | G | R | I | V-I | Obs. |
|---|---|---|---|---|---|---|---|---|---|---|---|---|---|
| | | | | | | | B3 | | | | | | |
| 35439n* | 25 Ori | o | 4.73 | B3ne | B1 V | -2.03 | -1.12 | -0.53 | -0.06 | +0.59 | +1.33 | -2.45 | 2 |
| 120315r | $\eta$ UMa | o | 1.91 | B3n | B3 V | -1.79 | -1.11 | -0.52 | -0.06 | +0.58 | +1.28 | -2.39 | 4 |
| 194335 * | HR 7807 | i | 5.68 | B3ne | B3 V | -2.05 | -1.11 | -0.50 | -0.06 | +0.56 | +1.22 | -2.33 | 2 |
| 32630n | $\eta$ Aur | i | 3.28 | B4 | B3 V | -1.73 | -1.09 | -0.50 | -0.07 | +0.57 | +1.21 | -2.30 | 2 |
| 216200n | 14 Lac | ? | 5.84 | B3 | B3 IV: | -1.35 | -0.80 | -0.33 | -0.04 | +0.37 | +0.70 | -1.50 | 2 |
| 179406n | 20 Aql | i | 5.37 | B3n | B3 IV | -1.17 | -0.74 | -0.31 | -0.03 | +0.34 | +0.68 | -1.42 | 1 |
| 170740n | HR 6946 | i | 5.80 | B3 | B2 V | -1.10 | -0.62 | -0.23 | -0.03 | +0.26 | +0.52 | -1.14 | 3 |
| | | | | | | | B5-B9 | | | | | | |
| 30211n | $\mu$ Eri | o | 4.18 | B5 | B5 IV | -1.60 | -1.04 | -0.50 | -0.04 | +0.54 | +1.19 | -2.23 | 2 |
| 35497n | $\beta$ Tau | i | 1.78 | B8 | B7 III | -1.49 | -1.05 | -0.49 | -0.05 | +0.54 | +1.12 | -2.17 | 2 |
| 22928n | $\delta$ Per | i | 3.10 | B8n | B5 III | -1.50 | -1.04 | -0.47 | -0.06 | +0.53 | +1.12 | -2.16 | 1 |
| 26356n | HR 1289 | o | 5.39 | B5n | B5 V | -1.54 | -1.05 | -0.49 | -0.05 | +0.54 | +1.09 | -2.14 | 1 |
| 87901n | $\alpha$ Leo | o | 1.34 | B6 | B7 V | -1.30 | -1.02 | -0.46 | -0.07 | +0.53 | +1.08 | -2.10 | 3 |
| 51309n | $\iota$ CMa | i | 4.39 | B5 | B3 II | -1.67 | -0.98 | -0.44 | -0.04 | +0.48 | +1.04 | -2.02 | 2 |
| 158704n | HR 6520 | i | 6.01 | B9 | ..... | -1.23 | -0.91 | -0.41 | -0.05 | +0.46 | +1.02 | -1.93 | 1 |
| 19356r* | $\beta$ Per | o | 2.3 | B9n | B8 V | -1.28 | -0.95 | -0.44 | -0.04 | +0.47 | +0.94 | -1.89 | 4 |
| 212710r | NPS 2 | o | 5.38 | B9 | ..... | -0.91 | -0.91 | -0.44 | -0.06 | +0.49 | +0.95 | -1.86 | 4 |
| 49229n | 11 CMa | i | 5.19 | B8 | ..... | -1.01 | -0.90 | -0.38 | -0.06 | +0.44 | +0.90 | -1.80 | 2 |
| 159561n* | $\alpha$ Oph | o | 2.14 | B9.5n | A5 III | -0.52 | -0.69 | -0.32 | -0.04 | +0.36 | +0.70 | -1.39 | 4 |
| | | | | | | | A0 | | | | | | |
| 358n | $\alpha$ And | o | 2.15 | A0.5 | B9p | -1.44 | -1.00 | -0.48 | -0.05 | +0.53 | +1.11 | -2.11 | 2 |
| 218045n | $\alpha$ Peg | o | 2.57 | A0 | B9.5 III | -0.83 | -0.92 | -0.43 | -0.05 | +0.48 | +1.00 | -1.92 | 2 |
| 213307n | $\delta$ Cep B | i | 7.5 | A0 | ..... | -1.20 | -0.94 | -0.40 | -0.05 | +0.45 | +0.93 | -1.87 | 2 |
| 199095n | 76 Dra | o | 5.69 | A0 | ..... | -0.83 | -0.85 | -0.42 | -0.07 | +0.49 | +0.99 | -1.84 | 1 |
| 183204n | ..... | o | 7.22 | A0 | ..... | -0.93 | -0.89 | -0.42 | -0.06 | +0.48 | +0.94 | -1.83 | 1 |
| 186882n | $\delta$ Cyg | o | 2.97 | A0.5n | B9.5 III | -0.86 | -0.90 | -0.43 | -0.04 | +0.47 | +0.92 | -1.82 | 2 |
| 103287n | $\gamma$ UMa | o | 2.54 | A0n | A0 V | -0.76 | -0.88 | -0.42 | -0.05 | +0.47 | +0.94 | -1.82 | 2 |
| 140436n | $\gamma$ CrB | o | 3.93 | A0.5n | A0 IV | -0.75 | -0.85 | -0.41 | -0.05 | +0.46 | +0.95 | -1.80 | 2 |
| 47561n | HR 2448 | ? | 5.93 | A0 | ..... | -0.64 | -0.84 | -0.40 | -0.05 | +0.44 | +0.86 | -1.70 | 1 |
| 20677n | 32 Per | o | 4.98 | A0.5 | A3 V | -0.70 | -0.82 | -0.39 | -0.05 | +0.44 | +0.85 | -1.67 | 6 |
| 46300n | 13 Mon | i | 4.50 | cA0 | A0 Ib | -0.94 | -0.89 | -0.38 | -0.03 | +0.41 | +0.76 | -1.65 | 2 |
| 106591n | $\delta$ UMa | o | 3.44 | A0n | A3 V | -0.65 | -0.79 | -0.38 | -0.05 | +0.43 | +0.83 | -1.62 | 2 |

Table 3 (Continued)

| HD | Name | Z | m | V,W | Y | U | V | B | G | R | I | V-I | Obs. |
|---|---|---|---|---|---|---|---|---|---|---|---|---|---|
| | | | | | A1-A4 | | | | | | | | |
| 40312n | $\theta$ Aur | o | 2.71 | A1sp | B9.5pv | -1.01 | -0.93 | -0.44 | -0.06 | +0.50 | +1.00 | -1.93 | 3 |
| 48915n* | $\alpha$ CMa | i | -1.4 | A2s | A1 V | -0.86 | -0.87 | -0.43 | -0.05 | +0.48 | +1.02 | -1.89 | 7 |
| 95418n | $\beta$ UMa | o | 2.44 | A2s | A1 V | -0.81 | -0.88 | -0.43 | -0.05 | +0.48 | +0.97 | -1.85 | 3 |
| 112185n | $\epsilon$ UMa | o | 1.68 | A2s | A0pv | -0.77 | -0.90 | -0.43 | -0.05 | +0.48 | +0.94 | -1.84 | 3 |
| 139006n | $\alpha$ CrB | o | 2.3 | A1n | A0 V | -0.82 | -0.89 | -0.42 | -0.05 | +0.47 | +0.94 | -1.83 | 5 |
| 214994n | o Peg | o | 4.85 | A2.5s | A1 V | -0.78 | -0.90 | -0.41 | -0.05 | +0.46 | +0.90 | -1.80 | 2 |
| 116656n* | $\zeta$ UMa | o | 2.40 | A2.5s | A2 V | -0.74 | -0.84 | -0.41 | -0.05 | +0.46 | +0.94 | -1.78 | 2 |
| 60179n | $\alpha$ Gem | o | 1.99 | A2.5s | A1 V | -0.77 | -0.84 | -0.41 | -0.04 | +0.45 | +0.92 | -1.76 | 3 |
| 40183n | $\beta$ Aur | o | 2.8† | A2n | A2 V | -0.72 | -0.84 | -0.40 | -0.06 | +0.46 | +0.91 | -1.75 | 5 |
| 47105n | $\gamma$ Gem | ? | 1.93 | A3s | A0 IV | -0.71 | -0.86 | -0.42 | -0.04 | +0.46 | +0.89 | -1.75 | 2 |
| 166205 | NPS 1 | o | 4.44 | A2 | ..... | -0.72 | -0.85 | -0.41 | -0.05 | +0.46 | +0.88 | -1.73 | Stand. |
| 155125n | $\eta$ Oph | i | 3.1† | A2s | A2.5 V | -0.58 | -0.80 | -0.39 | -0.05 | +0.44 | +0.81 | -1.61 | 2 |
| 102647n | $\beta$ Leo | o | 2.23 | A4n | A3 V | -0.61 | -0.76 | -0.36 | -0.06 | +0.42 | +0.84 | -1.60 | 4 |
| 18411n | $\pi$ Per | o | 4.62 | A2 | A2 V | -0.61 | -0.81 | -0.38 | -0.04 | +0.42 | +0.79 | -1.60 | 6 |
| 49048n | HR 2498 | i | 5.30 | A2 | ..... | -0.62 | -0.80 | -0.36 | -0.05 | +0.41 | +0.79 | -1.59 | 2 |
| 97603n | $\delta$ Leo | o | 2.58 | A2n | A4 V | -0.55 | -0.73 | -0.35 | -0.04 | +0.39 | +0.76 | -1.49 | 2 |
| 8538n | $\delta$ Cas | i | 2.80 | A3n | A5 V | -0.51 | -0.70 | -0.34 | -0.04 | +0.38 | +0.74 | -1.44 | 4 |
| 166926 | NPS 4 | o | 5.86 | A3n | ..... | -0.49 | -0.60 | -0.29 | -0.04 | +0.33 | +0.68 | -1.28 | Stand. |
| 203280r | $\alpha$ Cep | i | 2.60 | A3n | A7 IV, V | -0.49 | -0.61 | -0.29 | -0.04 | +0.33 | +0.62 | -1.23 | 6 |
| | | | | | A5-A9 | | | | | | | | |
| 5914r | NPS 5 | o | 6.43 | A5 | ..... | -0.62 | -0.76 | -0.36 | -0.05 | +0.41 | +0.80 | -1.56 | 3 |
| 157792n | 44 Oph | i | 4.28 | A9s | ..... | -0.33 | -0.48 | -0.19 | -0.05 | +0.25 | +0.59 | -1.07 | 1 |
| 182640n | $\delta$ Aql | i | 3.44 | A5n | F0 IV | -0.48 | -0.49 | -0.20 | -0.03 | +0.23 | +0.48 | -0.97 | 13 |
| | | | | | F Dwarfs | | | | | | | | |
| HD | Name | Z | m | V,W | Y | M | U | V | B | G | R | I | V-I | Obs. |
| 432r | $\beta$ Cas | i | 2.7† | F2 | F2 IV | +2.2 | -0.38 | -0.47 | -0.20 | -0.02 | +0.22 | +0.46 | -0.93 | 4 |
| 107192r* | NPS 2s | o | 6.28 | F2 | ..... | +3.0 | -0.50 | -0.47 | -0.20 | -0.02 | +0.22 | +0.45 | -0.92 | Stand. |
| 61421n | $\alpha$ CMi | o | 0.48 | F3 | F5 IV-V | +3.1 | -0.43 | -0.38 | -0.14 | -0.03 | +0.17 | +0.39 | -0.77 | 5 |
| 46136Bn | 20 Gem | i | 7.00 | F6 | ..... | +2.2 | -0.40 | -0.40 | -0.16 | -0.03 | +0.19 | +0.36 | -0.76 | 2 |
| 107113r | NPS 3s | o | 6.33 | F4 | ..... | +3.2 | -0.52 | -0.35 | -0.13 | -0.02 | +0.15 | +0.33 | -0.68 | Stand. |
| 48737n | $\xi$ Gem | o | 3.40 | F3 | F5 IV | +2.2 | -0.35 | -0.33 | -0.13 | -0.02 | +0.15 | +0.31 | -0.64 | 2 |
| 82328n | $\theta$ UMa | o | 3.26 | F4 | F6 IV | +3.3 | -0.40 | -0.33 | -0.11 | -0.02 | +0.13 | +0.28 | -0.61 | 2 |
| 11443n | $\alpha$ Tri | o | 3.9† | F2 | F6 IV | +2.4 | -0.33 | -0.30 | -0.10 | -0.03 | +0.13 | +0.28 | -0.58 | 2 |
| 224758n | HR 9078 | o | 6.38 | F5 | ..... | +3.2 | -0.30 | -0.28 | -0.07 | -0.03 | +0.10 | +0.21 | -0.49 | 1 |
| 90839n | 36 UMaA | o | 4.84 | F8 | F8 V | +3.5 | -0.40 | -0.25 | -0.08 | -0.02 | +0.10 | +0.22 | -0.47 | 3 |

Table 3 (Continued)

| HD | Name | Z | m | V, W | Y | M | U | V | B | G | R | I | V-I | Obs. |
|---|---|---|---|---|---|---|---|---|---|---|---|---|---|---|
| | | | | | | F Dwarfs (Continued) | | | | | | | | |
| 221356n | HR 8931 | o | 6.50 | F8 | ..... | +3.6 | -0.35 | -0.20 | -0.06 | -0.01 | +0.07 | +0.20 | -0.40 | 1 |
| 46136An | 20 Gem | i | 6.36 | F6 | ..... | +2.1 | -0.25 | -0.25 | -0.08 | -0.02 | +0.10 | +0.21 | -0.46 | 2 |
| 102870n | $\beta$ Vir | o | 3.80 | F8 | F8 V | +4.0 | -0.21 | -0.19 | -0.06 | -0.03 | +0.09 | +0.21 | -0.40 | 3 |
| 187691n | o Aql | ? | 5.22 | F8 | F8 V | +3.9 | -0.25 | -0.19 | -0.07 | -0.02 | +0.09 | +0.20 | -0.39 | 3 |
| 136064r | HR 5691 | o | 5.23 | F9 | F8 V | +3.1 | -0.24 | -0.21 | -0.07 | -0.01 | +0.08 | +0.18 | -0.39 | 3 |
| 200790n | 4 Eql | o | 6.03 | F7 | ..... | +3.1 | -0.30 | -0.18 | -0.07 | -0.02 | +0.09 | +0.18 | -0.36 | 2 |
| 121370n | $\eta$ Boo | o | 3.1† | F7 | G0 IV | +3.2 | -0.09 | -0.14 | -0.05 | -0.03 | +0.08 | +0.18 | -0.32 | 3 |
| 115383n | 59 Vir | o | 5.22 | F8 | F8 V | +3.7 | -0.18 | -0.15 | -0.05 | -0.01 | +0.07 | +0.17 | -0.32 | 1 |
| 142373r | $\chi$ Her | o | 4.61 | F7 | F9 V | +3.6 | -0.32 | -0.18 | -0.04 | -0.01 | +0.05 | +0.13 | -0.31 | 3 |
| 110897n | 10 CVn | o | 5.97 | F9 | ..... | +4.3 | -0.37 | -0.18 | -0.04 | -0.02 | +0.06 | +0.09 | -0.27 | 2 |
| 39587n | $\chi^1$Ori | i | 4.62 | F9 | G0 V | +4.0 | -0.24 | -0.12 | -0.02 | -0.01 | +0.03 | +0.12 | -0.24 | 2 |
| 142267n | 39 Ser | o | 6.16 | F9 | ..... | +3.7 | -0.21 | -0.11 | -0.01 | -0.01 | +0.01 | +0.12 | -0.23 | 1 |
| 189340n* | HR 7637 | o | 5.91 | F8 | ..... | +3.8 | (-0.19) | -0.11 | -0.04 | -0.02 | +0.06 | +0.12 | -0.23 | 2 |
| 165401n | ..... | i | 6.83 | F7 | ..... | +4.5 | -0.24 | -0.12 | -0.02 | 0.00 | +0.02 | +0.09 | -0.21 | 1 |
| | | | | | | G Dwarfs | | | | | | | | |
| 109358r | $\beta$ CVn | o | 4.32 | G0 | G0 V | +4.2 | -0.26 | -0.15 | -0.04 | -0.02 | +0.06 | +0.16 | -0.31 | 3 |
| 141004n | $\lambda$ Ser | o | 4.42 | G0 | G2 V | +4.4 | -0.13 | -0.10 | -0.03 | -0.01 | +0.03 | +0.17 | -0.27 | 1 |
| 190406n | 15 Sge | o | 5.89 | G1 | ..... | +4.4 | -0.21 | -0.11 | -0.05 | 0.00 | +0.05 | +0.14 | -0.25 | 2 |
| 19373n | $\iota$ Per | o | 4.17 | G1 | G0 V | +3.9 | -0.16 | -0.12 | -0.03 | -0.02 | +0.05 | +0.13 | -0.25 | 2 |
| 10307r | HR 483 | o | 5.10 | G0 | G2 V | +4.4 | -0.21 | -0.14 | -0.03 | -0.02 | +0.05 | +0.11 | -0.25 | 3 |
| 34411n | $\lambda$ Aur | i | 4.85 | G0 | G0 V | +4.4 | -0.14 | -0.09 | -0.02 | -0.01 | +0.03 | +0.13 | -0.22 | 2 |
| 95128n | 47 UMa | o | 5.14 | G0 | G0 V | +4.2 | -0.17 | -0.11 | -0.01 | -0.02 | +0.03 | +0.11 | -0.22 | 2 |
| 84737n | HR 3881 | o | 5.20 | G0 | G1 V | +3.8 | -0.13 | -0.09 | -0.02 | -0.02 | +0.04 | +0.12 | -0.21 | 2 |
| 199960n | 11 Aqr | o | 6.26 | G1 | ..... | +4.0 | -0.04 | -0.07 | -0.01 | -0.02 | +0.03 | +0.13 | -0.20 | 2 |
| 72905n | $\pi^1$UMa | o | 5.69 | G0 | ..... | +4.2 | -0.18 | -0.09 | -0.01 | -0.02 | +0.03 | +0.11 | -0.20 | 2 |
| 150680n | $\zeta$ Her | o | 3.00 | G0 | G0 IV | +3.7 | -0.05 | -0.10 | -0.01 | -0.02 | +0.03 | +0.10 | -0.20 | 2 |
| 221830n | ..... | o | 6.72 | G0 | ..... | +4.4 | -0.22 | -0.13 | -0.02 | -0.01 | +0.03 | +0.04 | -0.17 | 2 |
| 217014n | 51 Peg | o | 5.59 | G0 | ..... | +4.3 | +0.02 | -0.03 | -0.01 | -0.01 | +0.02 | +0.10 | -0.13 | 2 |
| 198802n* | HR 7994 | o | 6.40 | G1 | ..... | +3.8 | (-0.04) | -0.06 | 0.00 | -0.01 | +0.01 | +0.06 | -0.12 | 2 |
| 224930n* | 85 Peg | o | 5.85 | G1 | G2 V | +4.7 | -0.20 | -0.05 | +0.04 | -0.01 | -0.03 | -0.09 | +0.04 | 3 |
| 161797n | $\mu$ Her | o | 3.48 | G4 | G5 IV | +4.2 | +0.27 | +0.06 | +0.06 | -0.03 | -0.03 | 0.00 | +0.06 | 2 |
| 82210n* | 24 UMa | o | 4.57 | F9 | G2 IV | +3.7 | +0.30 | +0.11 | +0.07 | -0.02 | -0.05 | -0.08 | +0.19 | 2 |
| 103095n* | Gr 1830 | o | 6.46 | G5 | G8 Vp | +6.3 | +0.04 | +0.08 | +0.09 | -0.02 | -0.07 | -0.19 | +0.27 | 3 |
| 188512n | $\beta$ Aql | o | 3.90 | G8 | G8 IV | +4.0 | +0.47 | +0.23 | +0.11 | -0.01 | -0.10 | -0.19 | +0.42 | 24 |
| 191026n | 27 Cyg | i | 5.52 | G3 | ..... | +4.5 | +0.57 | +0.25 | +0.12 | -0.02 | -0.10 | -0.17 | +0.42 | 4 |

Table 3 (Continued)

| HD | Name | Z | m | V, W | Y | M | U | V | B | G | R | I | V-I | Obs. |
|---|---|---|---|---|---|---|---|---|---|---|---|---|---|---|
| | | | | | | G Dwarfs (Continued) | | | | | | | | |
| 198149n | $\eta$ Cep | i | 3.59 | G7 | K0 IV | +2.6 | +0.69 | +0.32 | +0.14 | -0.01 | -0.13 | -0.26 | +0.58 | 4 |
| | | | | | | K and M Dwarfs | | | | | | | | |
| 23249n | $\delta$ Eri | o | 3.72 | K0 | ..... | +3.0 | +0.78 | +0.32 | +0.14 | -0.04 | -0.10 | -0.22 | +0.54 | 2 |
| 201091n | 61 CygA | i | 5.57 | K6 | K5 V | +7.7 | +1.49 | +0.65 | +0.35 | +0.03 | -0.39 | -0.71 | +1.36 | 1 |
| 201092n | 61 CygB | i | 6.28 | M0 | K7 V | +8.6 | ..... | +0.97 | +0.49 | +0.04 | -0.53 | -1.04 | +2.01 | 1 |
| 60179Cn | YY Gem | o | 9.0 | M1e | ..... | +8.3 | ..... | +1.24 | +0.68 | -0.02 | -0.66 | -1.39 | +2.63 | 1 |
| 36395n | -37°1123 | i | 8.0 | M3 | ..... | .... | ..... | +1.11 | +0.63 | +0.03 | -0.66 | -1.58 | +2.69 | 2 |
| | | | | | | F Giants | | | | | | | | |
| 89025n | $\zeta$ Leo | o | 3.9† | F0 | F0 III | +1.3 | -0.29 | -0.50 | -0.20 | -0.03 | +0.23 | +0.45 | -0.95 | 2 |
| 23230n | $\nu$ Per | ? | 3.93 | cF4 | F5 II | -1.0 | -0.06 | -0.37 | -0.12 | -0.03 | +0.15 | +0.26 | -0.63 | 1 |
| 20902r | $\alpha$ Per | i | 1.90 | cF4 | F5 Ib | -1.2 | +0.10 | -0.28 | -0.11 | -0.02 | +0.13 | +0.22 | -0.50 | 7 |
| 8890r* | NPS 1s | o | 2.1 | cF7 | F8 Ib | -2.2 | +0.13 | -0.16 | -0.07 | -0.03 | +0.09 | +0.21 | -0.37 | Max. |
| 31964r | $\epsilon$ Aur | i | 3.3 | cF2 | F0 Iap | -1.7 | +0.14 | -0.22 | -0.03 | -0.02 | +0.05 | -0.06 | -0.16 | 3 |
| 194093r | $\gamma$ Cyg | i | 2.32 | cF7 | F8 Ib | -2.1 | +0.39 | -0.05 | -0.02 | -0.02 | +0.04 | +0.09 | -0.14 | 5 |
| 18925n* | $\gamma$ Per | i | 3.4 | cF7 | G8 III:+A3: | -0.3 | +0.34 | -0.01 | +0.06 | -0.01 | -0.05 | -0.11 | +0.10 | 2 |
| | | | | | | G Giants | | | | | | | | |
| 47138n | $\nu^1$CMa | o | 5.81 | G4 | ..... | +0.8 | +0.32 | +0.10 | +0.08 | -0.03 | -0.05 | -0.06 | +0.16 | 1 |
| 34029n | $\alpha$ Aur | i | 0.7† | G1 | G8 III:+F | +0.1 | +0.37 | +0.14 | +0.08 | -0.03 | -0.05 | -0.08 | +0.22 | 4 |
| 84441n | $\epsilon$ Leo | o | 3.12 | cG3 | G0 II | -1.3 | +0.46 | +0.18 | +0.07 | -0.03 | -0.04 | -0.08 | +0.26 | 3 |
| 215182n | $\eta$ Peg | o | 3.4† | G2 | G8 II:+F? | +0.6 | +0.61 | +0.20 | +0.11 | -0.02 | -0.09 | -0.16 | +0.36 | 2 |
| 71369n | o UMa | o | 3.47 | G1 | G5 III | +0.5 | +0.51 | +0.22 | +0.09 | -0.01 | -0.08 | -0.15 | +0.37 | 2 |
| 26659n | HR 1304 | o | 5.70 | G4 | ..... | +1.0 | +0.53 | +0.20 | +0.11 | -0.01 | -0.10 | -0.20 | +0.40 | 1 |
| 153751n | $\epsilon$ UMi | o | 4.7† | G1 | G5 III | +0.3 | +0.59 | +0.25 | +0.13 | -0.02 | -0.11 | -0.18 | +0.43 | 1 |
| 148387n | $\eta$ Dra | o | 2.89 | G6 | G8 III | +0.7 | +0.73 | +0.29 | +0.12 | -0.02 | -0.10 | -0.21 | +0.50 | 3 |
| 113226n | $\epsilon$ Vir | o | 2.95 | G6 | G9 II-III | +0.4 | +0.83 | +0.30 | +0.14 | -0.04 | -0.10 | -0.21 | +0.51 | 3 |
| 163993n | $\xi$ Her | o | 3.82 | G7 | G9 III | +0.6 | +0.79 | +0.31 | +0.15 | -0.03 | -0.12 | -0.22 | +0.53 | 2 |
| 150997n | $\eta$ Her | o | 3.61 | G4 | G7 III-IV | +1.0 | +0.64 | +0.28 | +0.13 | -0.02 | -0.11 | -0.25 | +0.53 | 3 |
| 204075r | $\zeta$ Cap | o | 4.2† | cG4 | G4 Ib?p | -1.3 | +0.74 | +0.40 | +0.14 | -0.03 | -0.11 | -0.15 | +0.55 | 3 |
| 148856n | $\beta$ Her | o | 3.1† | G5 | G8 III | +0.1 | +0.73 | +0.32 | +0.14 | -0.03 | -0.11 | -0.23 | +0.55 | 2 |
| 62345n | $\kappa$ Gem | o | 3.68 | G7 | G8 III | +0.6 | +0.79 | +0.32 | +0.14 | -0.03 | -0.11 | -0.24 | +0.56 | 3 |
| 219615n | $\gamma$ Psc | o | 3.85 | G4 | G7 III | +1.2 | +0.67 | +0.29 | +0.16 | -0.02 | -0.14 | -0.29 | +0.58 | 2 |
| 216131n | $\mu$ Peg | o | 3.67 | G6 | G8 III | +0.9 | +0.70 | +0.31 | +0.13 | -0.02 | -0.11 | -0.27 | +0.58 | 3 |

Table 3 (Continued)

| HD | Name | Z | m | V,W | Y | M | U | V | B | G | R | I | V-I | Obs. |
|---|---|---|---|---|---|---|---|---|---|---|---|---|---|---|
| | | | | | G Giants (Continued) | | | | | | | | | |
| 192947r | $\alpha^2$Cap | o | 4.1† | G8 | G9 III | +0.3 | +0.81 | +0.34 | +0.15 | -0.03 | -0.12 | -0.25 | +0.59 | 4 |
| 168723n | $\eta$ Ser | i | 3.42 | G8 | K0 III-IV | +1.4 | +0.72 | +0.33 | +0.16 | -0.03 | -0.13 | -0.28 | +0.61 | 3 |
| 202109n | $\zeta$ Cyg | o | 3.7† | G4 | G8 II | -0.6 | +0.91 | +0.40 | +0.16 | -0.04 | -0.12 | -0.24 | +0.64 | 3 |
| 146791n | $\epsilon$ Oph | o | 3.34 | G7 | G9 III | +0.7 | +0.92 | +0.37 | +0.17 | -0.03 | -0.14 | -0.28 | +0.65 | 2 |
| 27697n | $\delta$ Tau | i | 3.93 | G8 | K0 III | +0.6 | +0.96 | +0.39 | +0.14 | -0.01 | -0.13 | -0.26 | +0.65 | 2 |
| 196787n | 75 Dra | ? | 5.62 | G8 | ..... | +0.6 | +1.04 | +0.40 | +0.19 | -0.03 | -0.16 | -0.26 | +0.66 | 1 |
| 163917n | $\nu$ Oph | i | 3.50 | G9 | G9 III | +0.5 | +1.07 | +0.40 | +0.17 | -0.04 | -0.13 | -0.27 | +0.67 | 2 |
| 76294n | $\zeta$ Hya | o | 3.30 | G5 | K0 II-III | +0.3 | +1.00 | +0.42 | +0.18 | -0.03 | -0.15 | -0.29 | +0.71 | 3 |
| 62509n | $\beta$ Gem | o | 1.21 | G8 | Ko III | +0.9 | +1.03 | +0.41 | +0.17 | -0.03 | -0.14 | -0.31 | +0.72 | 3 |
| 28305n | $\epsilon$ Tau | i | 3.63 | G7 | K0 III | +0.7 | +1.05 | +0.44 | +0.16 | -0.03 | -0.13 | -0.29 | +0.73 | 2 |
| 180711n | $\delta$ Dra | o | 3.24 | G8 | G9 III | +0.4 | +0.94 | +0.41 | +0.18 | -0.02 | -0.16 | -0.32 | +0.73 | 2 |
| 40035n | $\delta$ Aur | o | 3.88 | G6 | K0 III | +0.8 | +1.02 | +0.43 | +0.18 | -0.03 | -0.15 | -0.31 | +0.74 | 3 |
| 183124n | ..... | o | 6.72 | G5 | ..... | ..... | +0.97 | +0.43 | +0.20 | -0.02 | -0.18 | -0.34 | +0.77 | 1 |
| 58207n | $\iota$ Gem | o | 3.89 | G7 | K0 III | +0.7 | +1.08 | +0.46 | +0.19 | -0.03 | -0.16 | -0.37 | +0.83 | 2 |
| 95689n | $\alpha$ UMa | o | 1.95 | G7 | K0 III | 0.0 | +1.15 | +0.49 | +0.22 | -0.02 | -0.20 | -0.40 | +0.89 | 3 |
| 192876r | $\alpha^1$Cap | o | 4.55 | cG5 | G3 Ib | -2.7 | +1.08 | +0.50 | +0.22 | -0.02 | -0.20 | -0.40 | +0.90 | 2 |
| 3712n | $\alpha$ Cas | i | 2.5 | G7 | K0 II-III | -0.4 | +1.49 | +0.65 | +0.27 | -0.04 | -0.23 | -0.46 | +1.11 | 3 |
| 48329n | $\epsilon$ Gem | o | 3.18 | cG8 | G8 Ib | -2.1 | ..... | +0.97 | +0.37 | -0.02 | -0.35 | -0.69 | +1.66 | 2 |
| | | | | | K Giants | | | | | | | | | |
| 47205n | $\nu^2$CMa | o | 4.14 | K1 | K1 IV | +0.7 | +1.15 | +0.50 | +0.22 | -0.03 | -0.19 | -0.35 | +0.85 | 1 |
| 197989n | $\epsilon$ Cyg | ? | 2.9† | K0 | K0 III | +0.7 | +1.08 | +0.49 | +0.20 | -0.02 | -0.18 | -0.37 | +0.86 | 2 |
| 157588n | HR 6474 | i | 6.26 | K1 | ..... | +0.8 | +1.50 | +0.50 | +0.25 | -0.02 | -0.23 | -0.41 | +0.91 | 2 |
| 199437n | HR 8016 | ? | 5.58 | K1 | ..... | +0.8 | +1.41 | +0.65 | +0.28 | -0.03 | -0.25 | -0.47 | +1.12 | 1 |
| 161096n | $\beta$ Oph | i | 2.94 | K1 | K2 III | +0.5 | +1.59 | +0.65 | +0.29 | -0.03 | -0.26 | -0.47 | +1.12 | 3 |
| 47442n | $\nu^3$CMa | ? | 4.65 | K1 | K1 II-III | +0.4 | +1.38 | +0.63 | +0.27 | -0.01 | -0.26 | -0.50 | +1.13 | 1 |
| 12929n | $\alpha$ Ari | o | 2.23 | K1 | K2 III | +0.4 | +1.40 | +0.64 | +0.25 | 0.00 | -0.25 | -0.52 | +1.16 | 2 |
| 140573n | $\alpha_2$Ser | o | 2.75 | K2 | K2 III | +0.5 | +1.77 | +0.69 | +0.27 | -0.02 | -0.25 | -0.48 | +1.17 | 2 |
| 73108n | $\pi^2$UMa | o | 4.76 | K2 | K2 III | +0.5 | +1.67 | +0.73 | +0.30 | -0.01 | -0.29 | -0.55 | +1.28 | 1 |
| 5848n | HR 285 | o | 4.52 | K2 | K2 III | +0.4 | +1.73 | +0.73 | +0.31 | -0.01 | -0.29 | -0.56 | +1.29 | 1 |
| 12533n* | $\gamma$ And | o | 2.28 | K3 | K3 II | -0.2 | +1.36 | +0.61 | +0.34 | -0.02 | -0.32 | -0.69 | +1.30 | 2 |
| 124897n | $\alpha$ Boo | o | 0.24 | K0 | K2 IIIp | +0.2 | +1.63 | +0.73 | +0.35 | +0.01 | -0.35 | -0.59 | +1.32 | 3 |
| 216446n | HR 8702 | ? | 4.97 | K3 | K3 III | +0.1 | +1.81 | +0.79 | +0.34 | 0.00 | -0.35 | -0.67 | +1.46 | 1 |
| 3627n | $\delta$ And | o | 3.49 | K4 | K3 III | +0.5 | ..... | +0.83 | +0.35 | -0.02 | -0.33 | -0.68 | +1.51 | 3 |
| 124294n* | $\kappa$ Vir | o | 4.31 | K2 | K3 III | +0.6 | ..... | ..... | +0.40 | 0.00 | -0.40 | -0.78 | ..... | 1 |
| 32068n* | $\zeta$ Aur | o | 4.4† | cK4 | K5 III+B | -2.5 | +0.78 | +0.66 | +0.47 | +0.01 | -0.48 | -1.08 | +1.74 | 2 |

Table 3 (Continued)

| HD | Name | Z | m | V, W | Y | M | U | V | B | G | R | I | V-I | Obs. |
|---|---|---|---|---|---|---|---|---|---|---|---|---|---|---|
| | | | | | | K Giants (Continued) | | | | | | | | |
| 217382n | HR 8748 | o | 4.96 | K5 | K4 III | +0.1 | ..... | +1.01 | +0.45 | 0.00 | -0.45 | -0.88 | +1.89 | 1 |
| 81797n | $\alpha$ Hya | o | 2.16 | K5 | K4 III | -0.8 | ..... | +1.08 | +0.45 | -0.07 | -0.38 | -0.83 | +1.91 | 1 |
| 131873n | $\beta$ UMi | o | 2.24 | K5 | K4 III | -0.5 | ..... | +1.07 | +0.48 | -0.01 | -0.47 | -0.93 | +2.00 | 3 |
| 206778r | $\epsilon$ Peg | o | 2.54 | cK0 | K2 Ib | -2.3 | ..... | +1.15 | +0.48 | -0.02 | -0.46 | -0.90 | +2.05 | 4 |
| 158996n | HR 6529 | o | 5.91 | K2 | ..... | ... | ..... | +1.09 | +0.51 | 0.00 | -0.51 | -0.98 | +2.07 | 1 |
| 47667n | HR 2450 | i | 4.97 | K5 | K3 III | -0.7 | ..... | +1.13 | +0.50 | -0.01 | -0.49 | -0.94 | +2.07 | 3 |
| 186791n | $\gamma$ Aql | ? | 2.80 | K4 | K3 II | -0.8 | ..... | +1.17 | +0.47 | -0.01 | -0.46 | -0.91 | +2.08 | 2 |
| 31398n | $\iota$ Aur | i | 2.90 | K3 | K3 II | -0.5 | ..... | +1.14 | +0.49 | -0.02 | -0.47 | -0.99 | +2.13 | 2 |
| 164058n | $\gamma$ Dra | o | 2.42 | K5 | K5 III | -0.1 | ..... | +1.19 | +0.51 | +0.02 | -0.53 | -1.11 | +2.30 | 3 |
| 159881n* | ..... | i | 7.02 | K5 | ..... | .... | ..... | (+1.48) | +0.86 | +0.04 | -0.90 | -2.00 | (+3.48) | 2 |
| | | | | | | M Giants | | | | | | | | |
| 102212n | $\nu$ Vir | o | 4.20 | M1 | M1 III | -0.5 | ..... | +1.16 | +0.56 | +0.04 | -0.60 | -1.31 | +2.47 | 2 |
| 6860n | $\beta$ And | o | 2.37 | M0 | M0 III | +0.2 | ..... | +1.26 | +0.59 | +0.01 | -0.60 | -1.30 | +2.56 | 2 |
| 51802r | NPS 1r | o | 5.3 | M0 | ..... | -0.1 | ..... | +1.28 | +0.62 | +0.03 | -0.65 | -1.42 | +2.70 | 4 |
| 18884n | $\alpha$ Cet | o | 2.82 | M2 | M2 III | -0.1 | ..... | +1.46 | +0.64 | +0.03 | -0.67 | -1.50 | +2.96 | 2 |
| 42995n | $\eta$ Gem | i | 3.2 | M3 | ..... | -0.8 | ..... | +1.30 | +0.69 | +0.08 | -0.77 | -1.80 | +3.10 | 2 |
| 183030r | NPS 2r | o | 6.55 | M1 | ..... | -0.3 | ..... | +1.35 | +0.69 | +0.07 | -0.76 | -1.76 | +3.11 | 4 |
| 217906n | $\beta$ Peg | o | 2.61 | M2 | M2 II-III | -0.6 | ..... | +1.43 | +0.72 | +0.07 | -0.79 | -1.83 | +3.26 | 3 |
| 44478n | $\mu$ Gem | i | 3.19 | M3 | ..... | -0.6 | ..... | +1.44 | +0.76 | +0.08 | -0.84 | -1.88 | +3.32 | 2 |
| 209772r | 18 Cep | i | 5.5 | M5 | ..... | 0.0 | ..... | +1.35 | +0.79 | +0.12 | -0.91 | -2.22 | +3.57 | 3 |
| 214665r | HR 8621 | i | 5.5 | M4 | ..... | -0.4 | ..... | +1.42 | +0.80 | +0.13 | -0.93 | -2.25 | +3.67 | 2 |
| 175588r | $\delta^2$ Lyr | o | 4.5 | M4 | ..... | -1.6 | ..... | +1.48 | +0.85 | +0.11 | -0.96 | -2.33 | +3.81 | 5 |
| 156014n | $\alpha$ Her | o | 3.6 | M5 | ..... | -1.9 | ..... | .... | +1.05 | +0.17 | -1.22 | -2.93 | ..... | 2 |

## NOTES TO TABLE 3

HD

5394—Magnitude and color variable
8890—Polaris, variable, colors at maximum
12533—Color is composite
14633—Included to complete list of bluest stars
18925—Color is composite
19356—Algol near maximum
32068—Color is composite
35439—Color agrees with spectral type B1
37468—Combined A, B, C, and D
44743—Small variation in magnitude and color
48915—Visual magnitude from photoelectric measures
82210—Color indicates G-type spectrum

HD

103095—Color apparently composite
107192—Keenan calls it a normal giant, F2 III
116656—Includes companion at 14″
124294—Violet missed
159561—Color agrees with spectral type A5
159881—Violet doubtful
189340—Ultraviolet discordant
194335—Included to complete list of bluest stars
198802—Ultraviolet discordant
205021—Variable, mean colors
224930—Color is composite

TABLE 4

RELATIVE COLORS REFERRED TO O-TYPE STARS

| V, W | Y | U | V | B | G | R | I | V−I | No. |
|---|---|---|---|---|---|---|---|---|---|
| O7.5.... | O8 | 0.000 | 0.000 | 0.000 | 0.000 | 0.000 | 0.000 | 0.000 | 2 |
| B0..... | O9.5 | +0.040 | +0.030 | +0.005 | .000 | −0.005 | −0.010 | +0.040 | 2 |
| B1.5.... | B1 | +0.155 | +0.020 | −0.005 | .000 | +0.005 | −0.020 | +0.040 | 2 |
| B1.7.... | B2 | +0.190 | +0.042 | 0.000 | − .002 | +0.002 | −0.018 | +0.060 | 3 |
| B3..... | B3 | +0.330 | +0.075 | +0.030 | − .005 | −0.025 | −0.135 | +0.210 | 2 |
| B6..... | B5 | +0.63 | +0.12 | +0.04 | .00 | −0.04 | −0.19 | +0.31 | 4 |
| A0.1.... | ..... | +1.31 | +0.24 | +0.10 | .00 | −0.10 | −0.39 | +0.63 | 4 |
| A7.7.... | ..... | +1.81 | +0.62 | +0.28 | + .02 | −0.30 | −0.79 | +1.41 | 6 |
| dF7.0.... | ..... | +1.96 | +0.94 | +0.46 | + .03 | −0.49 | −1.17 | +2.11 | 4 |
| dG1.5.... | ..... | +2.13 | +1.10 | +0.52 | + .04 | −0.56 | −1.33 | +2.43 | 4 |
| cG1.7.... | ..... | +2.78 | +1.36 | +0.61 | + .03 | −0.64 | −1.48 | +2.84 | 3 |
| dK1.7.... | ..... | +2.66 | +1.38 | +0.60 | + .07 | −0.67 | −1.57 | +2.95 | 3 |
| gK0.5.... | ..... | +3.27 | +1.64 | +0.74 | + .03 | −0.77 | −1.75 | +3.39 | 4 |
| dK5.7.... | ..... | +3.31 | +1.70 | +0.77 | + .08 | −0.85 | −1.92 | +3.62 | 3 |
| cK5.0.... | ..... | +4.86 | +2.41 | +1.07 | + .05 | −1.12 | −2.43 | +4.84 | 3 |
| dM0..... | ..... | ..... | +2.13 | +1.04 | + .10 | −1.14 | −2.47 | +4.60 | 3 |
| gM0..... | ..... | ..... | +2.44 | +1.15 | +0.07 | −1.22 | −2.75 | +5.19 | 4 |

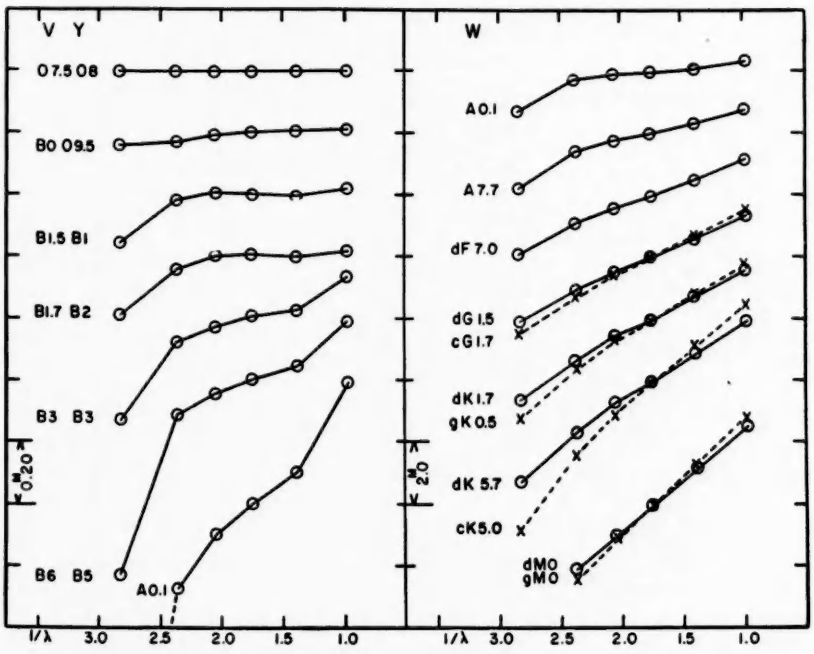


FIG. 1.—Colors referred to O type

TABLE 5

OBSERVATIONS OF B STARS BY HALL

| 1/λ | 1.54 | 1.44 | 1.34 | 1.26 | 1.19 | 1.12 | 1.07 | 1.02 |
|---|---|---|---|---|---|---|---|---|
| Obs. $\Delta m$..... | 0.288 | 0.238 | 0.205 | 0.200 | 0.180 | 0.110 | 0.032 | 0.000 |
| Comp. $\Delta m$..... | .288 | .230 | .179 | .133 | .095 | .059 | .029 | .000 |
| O−C..... | 0.000 | 0.008 | 0.026 | 0.067 | 0.085 | 0.051 | 0.003 | 0.000 |

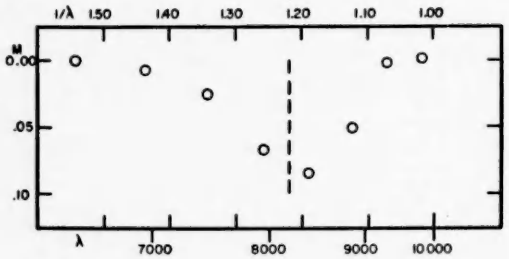


FIG. 2.—Paschen depression in A stars by J. S. Hall

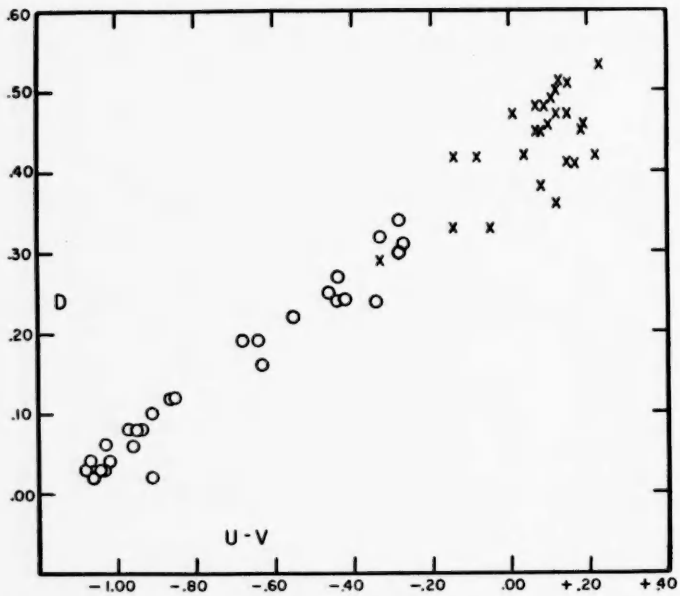


FIG. 3.—Relation between U − V and Barbier and Chalonge's *D; circles*, O and B stars; *crosses*, A stars.

is an obvious Paschen depression in the infrared. The Paschen limit at $\lambda = 8206$ A, $1/\lambda = 1.22$, is caught by the toe of the curve of the red filter. These two strong effects of hydrogen absorption will obviously complicate any effort to determine color temperatures from the six-color data.

From A0 on, the Balmer depression gets less until it is about gone at G0, but, from there, we have the well-known ultraviolet absorption like that of the sun in both dwarfs and giants. The over-all difference between dwarfs and giants, as shown in the figures, probably is greatest in the M's, but there our measures become less certain in the weak ultraviolet.

The Paschen depression in the near infrared was detected in the spectrum of Vega by Hall and Williams (1942) in a comparison of this A0 star with a standard lamp, but Hall (1941) had already measured infrared regions that showed the Paschen absorption differentially between A0 and early B stars. In Table 5 under each $1/\lambda$ the first line gives the mean $\Delta m$, referred to standard A0, of four stars averaging B1, taken from Hall's Table 7, with zero point at $1/\lambda = 1.02$. The second line gives the linearly interpolated values between $1/\lambda = 1.02$ and $1/\lambda = 1.54$. Hence the last line, (O − C), gives the deviations from a uniform continuum between those limits. These deviations are plotted in Figure 2, and the Paschen depression is shown even better than in the results for Vega by Hall and Williams. The first good spectrograms showing the Paschen series in A stars seem to have been obtained by Merrill (1934) and by Merrill and Wilson (1934).

The Balmer depression in our ultraviolet results is well correlated with the quantity $D$ that Barbier and Chalonge (1941) used to indicate the size of the Balmer discontinuity in their spectrophotometric measures. The relation between their $D$ and our U − V for nonreddened B and A stars is shown in Figure 3. When the types are later than A, the relation is complicated by the presence of metallic lines in the spectra and becomes confused. In Figure 3 the discordant star, 25 Orionis, at U − V = −0.91, may be anomalous, since it is known to have variable bright hydrogen lines (Dodson 1940).

In Paper III it was found that the combined light of the four stars in the Trapezium of Orion gave what appeared to be the only clear-cut case of deviation from the law of interstellar absorption that obtains in reddened early-type stars in other parts of the sky. These deviations are shown in Table 9 and Figure 4 of that paper. We now have two additional stars that show the same anomalous absorption, $\theta^2$ Orionis, not far from $\theta^1$ in the nebula, and $\phi$ Persei, previously overlooked as being in the same class. The color of the Trapezium stars was discussed by Baade and Minkowski (1937), but neither they nor we looked into the possibility that undetected late-type companions might be affecting the colors of the early-type primaries. All four components of $\theta^1$ seem to be spectroscopic binaries with single lines, and the same holds for both $\theta^2$ Orionis and $\phi$ Persei (Moore and Neubauer 1948). Although such redder companions might show little effect in the photographic and visual regions, their light could be conspicuous in the infrared at 10000 A. We can find by trial what combination of a yellow star and a small amount of reddening will change the light of an O or B star to the quality observed in one of these anomalous objects.

This procedure is exemplified in Table 6, where under the proper headings the first line gives the six colors of a normal O star referred differentially to the infrared. The second and third lines give six-color data for B0 and gK0 spectral types, while the fourth line gives the usual interstellar absorption when reduced to V − I = 1.00 (Stebbins and Whitford 1943). To represent the colors of $\theta^2$ Orionis, we add to the colors of the normal O star those of a K0 star, which is 0.75 mag. fainter in the infrared than the O star, as indicated in the column $\Delta m_i$ in the table. We then apply the absorption proportional to V − I = 0.25, as in the last column of the table, and when the resulting colors are referred to the mean of BGR, we have the computed values in the line below $\theta^2$ Orionis. The practically perfect agreement with the observed colors of this star could also have been obtained by assuming the companion to be a later K or an earlier G star, with dif-

ferent proportions of the magnitude difference and the absorption. Hence we find no need to draw upon anomalous absorption to satisfy the measured colors of $\theta^2$ Orionis.

The cases of $\theta^1$ Orionis and $\phi$ Persei are not so clear. Various trials for each of them always gave a discordant residual in the red. As noted, all four bright components of $\theta^1$ Orionis have spectroscopic companions, while the spectrum of $\phi$ Persei is anomalous (Hynek 1940) and has bright hydrogen lines of the Paschen series (Hiltner 1947). Therefore, until we can be sure that there is no effect of companions or of idiosyncrasies in the spectra, there is little point in attempting to evaluate a subtle deviation from the law of absorption for either of these stars.

The possibility that undetected companions may affect the colors of other O and B stars used to determine the law of interstellar absorption is always present, but it is

TABLE 6

EFFECTS OF COMPANIONS AND INTERSTELLAR ABSORPTION ON COLORS OF EARLY-TYPE STARS

| | U | V | B | G | R | I | V−I | $\Delta m_v$ | Absorption V−I |
|---|---|---|---|---|---|---|---|---|---|
| O | −3.64 | −2.57 | −1.93 | −1.44 | −0.80 | 0.00 | −2.57 | ... | ... |
| B0 | −3.59 | −2.53 | −1.92 | −1.43 | − .79 | .00 | −2.53 | ... | ... |
| gK0 | +1.38 | +0.82 | +0.56 | +0.34 | + .18 | .00 | +0.82 | ... | ... |
| Absorption | +1.22 | +1.00 | +0.82 | +0.61 | + .33 | .00 | +1.00 | ... | 1.00 |
| $\theta^2$ Orionis | −1.97 | −0.98 | −0.41 | −0.02 | + .43 | + .92 | −1.90 | ... | ... |
| O+K0+Abs. | −1.99 | −0.98 | −0.42 | −0.03 | + .44 | + .92 | −1.90 | 0.75 | 0.25 |
| O−C | +0.01 | 0.00 | +0.01 | +0.01 | − .01 | .00 | 0.00 | ... | ... |
| $\theta^1$ Orionis | −1.68 | −0.76 | −0.29 | +0.02 | + .27 | + .57 | −1.33 | ... | ... |
| B0+K0+Abs. | −1.68 | −0.77 | −0.31 | −0.01 | + .32 | + .56 | −1.33 | .00 | 0.50 |
| O−C | 0.00 | +0.01 | +0.02 | +0.03 | − .05 | + .01 | 0.00 | ... | ... |
| $\phi$ Persei | −1.88 | −0.91 | −0.36 | 0.00 | + .36 | + .80 | −1.71 | ... | ... |
| B0+K0+Abs. | −1.89 | −0.91 | −0.38 | −0.02 | + .41 | + .80 | −1.71 | 0.25 | 0.23 |
| O−C | +0.01 | 0.00 | +0.02 | +0.02 | −0.05 | 0.00 | 0.00 | ... | ... |

probably of little significance. The very blue B0 star, $\delta$ Orionis, is a single-lined binary showing eclipses (Stebbins 1915), but the companion has nearly the same surface brightness and hence nearly the same color as the primary. Since strong reddening by absorption is far greater than any possible effect of an unknown companion, we can dismiss the latter as of little importance in color comparisons.

## GENERAL REMARKS

The newly observed stars of the present study were added to round out the earlier list; two-thirds of them are brighter than visual magnitude 5.0, and about 50 are brighter than 3.0. Hence many can be studied spectroscopically with high dispersion. These additional early O–B3 stars strengthen the list at the top of each type, as shown in Table 4, but it is probable that a further search will uncover still bluer stars to serve as nonreddened standards in studies of space absorption. The additional stars of types A, F, G, and K do not furnish any striking differences from the conclusions in Paper III, but they are available for comparisons with color systems like that set up by Morgan, Harris, and Johnson (1953). The extra number of F and G dwarfs was obtained in order to place the sun on the stellar scale of colors, but this study will be the subject of another paper.

We are much indebted to Dr. W. W. Morgan for furnishing the latest classification of many of our stars on the revised system of the Yerkes spectral *Atlas*. The inauguration of this work at the Lick Observatory was supported by two grants from the American Philosophical Society.

## REFERENCES

Baade, W., and Minkowski, R. 1937, *Ap. J.*, **86**, 119; *Mt. W. Contr.*, No. 571.
Barbier, D., and Chalonge, D. 1941, *Ann. d'Ap.*, **4**, 30.
Dodson, H. W. 1940, *Ap. J.*, **91**, 126.
Hall, J. S. 1941, *Ap. J.*, **94**, 71.
Hall, J. S., and Williams, R. C. 1942, *Ap. J.*, **95**, 225.
Hiltner, W. A. 1947, *Ap. J.*, **105**, 212.
Hubble, E. P. 1934, *Ap. J.*, **79**, 41; *Mt. W. Contr.*, No. 485.
Hynek, J. A. 1940, *Perkins Pub.*, **2**, 1.
Merrill, P. W. 1934, *Ap. J.*, **79**, 183; *Mt. W. Contr.*, No. 486.
Merrill, P. W., and Wilson, O. C. 1934, *Ap. J.*, **80**, 19; *Mt. W. Contr.*, No. 494.
Moore, J. H., and Neubauer, F. J. 1948, *Lick Obs. Bull.*, **20**, 1 (No. 521).
Morgan, W. W., Harris, D. L., and Johnson, H. L. 1953, *Ap. J.*, **118**, 92; *McDonald Contr.*, No. 224.
Stebbins, J. 1915, *Ap. J.*, **42**, 133.
Stebbins, J., and Whitford, A. E. 1943, *Ap. J.*, **98**, 20; *Mt. W. Contr.*, No. 680.
———. 1945, *Ap. J.*, **102**, 318; *Mt. W. Contr.*, No. 712.

# VARIATIONS IN THE STELLAR LUMINOSITY FUNCTION
## VIII. A SUMMARY OF RESULTS

S. W. McCuskey
Case Institute of Technology, Warner and Swasey Observatory
*Received January 23, 1956*

ABSTRACT

Analyses over the last ten years of statistical data on spectral types and photographic magnitudes in selected regions of the Milky Way are summarized in this paper. Tables and charts present the local galactic structure within 1000 parsecs of the sun and, for the B8–A0 and B5 stars, the structure to 2500 parsecs. A similar chart shows the distribution of interstellar matter to a distance of 2500 parsecs. Maximum cosmic fluctuations in the general luminosity function with longitude and with distance amount to 0.6 in log $\phi(M)$. The average function derived for all longitudes and for distances within 500 parsecs of the sun agrees well with the standard function published by van Rhijn.

### INTRODUCTION

In 1945 the Warner and Swasey Observatory began the observation of eleven areas of the Milky Way for the study of local galactic structure and variations in the general stellar luminosity function. The statistical distributions of spectral type and apparent

TABLE 1

NUMBER OF SPECTRA CLASSIFIED IN THE LF REGIONS
(Average Limiting Mag. 12.2)

| LF Region | Spectral Class | | | | | | | | | | All | Area (Sq. Deg.) |
|---|---|---|---|---|---|---|---|---|---|---|---|---|
| | B0–B5 | B8–A0 | A2–A5 | F0–F5 | F8–G2 | dG5 | gG5 | dG8–K3 | gG8–K3 | K5–M | | |
| 1 | 10 | 343 | 90 | 95 | 118 | 56 | 53 | 17 | 136 | 28 | 946 | 14.3 |
| 2 | 28 | 481 | 334 | 274 | 361 | 52 | 42 | 61 | 290 | 49 | 1972 | 13.4 |
| 3 | 387 | 378 | 228 | 242 | 236 | 28 | 37 | 31 | 178 | 27 | 1772 | 10.8 |
| 3a | 184 | 358 | 183 | 111 | 132 | 18 | 41 | 11 | 113 | 10 | 1161 | 12.5 |
| 3b | 122 | 192 | 204 | 209 | 173 | 15 | 29 | 7 | 129 | 16 | 1096 | 9.9 |
| 4 | 303 | 1479 | 438 | 353 | 553 | 108 | 174 | 54 | 415 | 43 | 3920 | 16.9 |
| 5 | 230 | 203 | 156 | 107 | 117 | 10 | 18 | 1 | 71 | 12 | 925 | 11.3 |
| 6 | 53 | 299 | 86 | 73 | 138 | 19 | 34 | 12 | 91 | 11 | 816 | 16.2 |
| 7 | 119 | 787 | 161 | 152 | 253 | 24 | 69 | 20 | 190 | 18 | 1793 | 16.9 |
| 8 | 60 | 471 | 150 | 147 | 298 | 32 | 52 | 25 | 167 | 7 | 1409 | 17.3 |
| 9 | 129 | 781 | 245 | 196 | 396 | 45 | 54 | 16 | 329 | 32 | 2223 | 16.4 |
| Total | 1625 | 5772 | 2275 | 1959 | 2775 | 407 | 603 | 255 | 2109 | 253 | 18033 | 155.9 |

photographic magnitude for some 18000 stars have already appeared in the first eight papers of this series (McCuskey and Seyfert 1947; McCuskey 1949*a*, *b*, 1951, 1952, 1954; Nassau and MacRae 1949; Farnsworth and McCuskey 1955). Analyses of these data for stellar space density and for the fluctuations in the luminosity function in each area, together with a study of the absorption of photographic light, were also given. The present paper summarizes the conclusions to be drawn from the entire program and includes the results of a recalculation of some of the earlier data.

With the exception of areas in Cygnus which have a high population of early B stars

and a patchy pattern of interstellar absorption, the areas studied have been selected for an absence of conspicuous irregularities in the surface distribution of the stars. They were assumed to be normal representatives of the local galactic structure. Centers of these regions are listed in the first paper of the series (McCuskey and Seyfert 1947).

Table 1 indicates the scope of the program and gives the number of stars observed to an average limiting magnitude $m_{pg} = 12.2$. Figure 1 shows in histogram form these statistics as distributed along the galactic circle. A preliminary summary of the results from the first six of the LF regions was published earlier (McCuskey 1951).

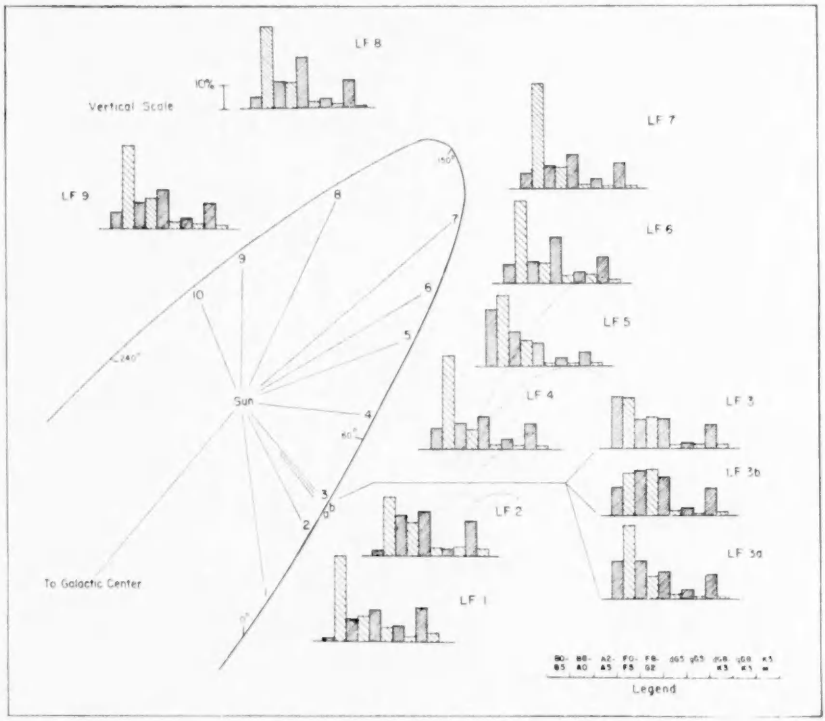


FIG. 1.—Distribution of spectral types in the LF regions as a function of galactic longitude. The average limiting photographic magnitude of the stars is 12.2.

## METHOD OF ANALYSIS

The observational data on spectral types and photographic magnitudes have been analyzed for stellar space density by numerical analysis to yield the function $D_s(r)$, the number of stars per 1000 cubic parsecs at distance $r$ parsecs from the sun for spectral type $s$. It has been assumed that within each spectral group the absolute-magnitude distribution is Gaussian, with parameters $M_s$ and $\sigma_s$ as exhibited in Table 2 ($M_s$ is the mean absolute photographic magnitude per unit volume of space). In view of the fact that the early calculations of density employed values of $M_s$ and $\sigma_s$ differing a little from the current ones, it has seemed wise to revise the earlier calculations for LF1, 2, 7, and

8 to make the results consistent with the work published later. In the description to follow, all space densities have been computed on a strictly comparable basis, namely, with $M_s$ and $\sigma_s$ as given in Table 2.

The order of accuracy to be expected in numerical solutions of the fundamental integral equation of stellar statistics is a matter of some concern in studies of the present type. In general ($m$, log $\pi$) analyses (Bok 1937) provide the most flexible calculational program for this purpose. With intervals of 0.5 in apparent magnitude and corresponding

TABLE 2

MEAN ABSOLUTE PHOTOGRAPHIC MAGNITUDES AND DISPERSIONS

| Spectral Type | $M_s$ | $\sigma_s$ | Spectral Type | $M_s$ | $\sigma_s$ |
|---|---|---|---|---|---|
| B0–B1 | −3.5 | ±0.8 | F0–F5 | +3.5 | ±0.8 |
| B2–B3 | −2.0 | .9 | dF8–G2 | +4.5 | .8 |
| B5 | −1.0 | .7 | dG5 | +6.0 | .7 |
| B8–A0 | +0.5 | .8 | dG8–K3 | +7.5 | .9 |
| A2–A5 | +2.0 | ±0.8 | gF8–K5 | +2.0 | ±0.8 |

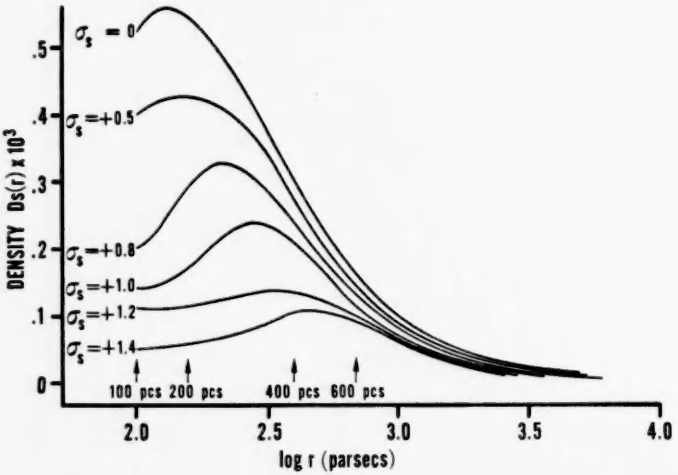


FIG. 2.—Variation in a calculated density function, $D_s(r)$, due to different adopted values of the dispersion $\sigma_s$.

intervals of 0.1 in log $\pi$ (or log $r$), it is apparent that a change of 0.5 in the mean absolute magnitude adopted for an analysis will change the computed densities by a factor of 2. The effect of varying $\sigma_s$ is not so easily visualized. An empirical test made recently indicates what happens when $\sigma_s$ is allowed to change. Figure 2 shows the density function $D_s(r)$ calculated for the B8–A0 stars in LF4 for values of $\sigma_s$ ranging from 0 to ±1.4. The same value of $M_s$ has been used for all curves. It is clear that the density maximum exhibited in this region moves farther from the sun by a considerable amount as the dispersion $\sigma_s$ is increased. There is not likely to be an uncertainty of more than ±0.2 in the value of $\sigma_s$ adopted for a given spectral class. Hence the uncertainty in $D_s(r)$ is not

likely to exceed a factor of 2, even in the critical region of space within 500 parsecs of the sun.

A second experiment indicates the order of uncertainty to be expected in the purely numerical process of solving an ($m$, log $\pi$) table for the function $D_s(r)$. Two computers, inexperienced in this kind of analysis, were asked to solve, independently, identical tables for the density function. Their resulting curves are shown in Figure 3 for $\sigma_s = \pm 0.5$ and $\sigma_s = \pm 1.0$. And in Figure 4 are shown the differences, $\Delta D_s(r)$, between their solutions as a function of log $r$ for a series of values of $\sigma_s$. The tolerance specified between the final computed values of log $A'(m)$ and the observed values was $\pm 0.05$, but in most instances these differences were less than $\pm 0.02$. Here $A'(m)$ is the number of stars per 100 square degrees with apparent magnitude $m - \frac{1}{4}$ to $m + \frac{1}{4}$. The data on which the experiment was performed were the B8–A0 stars in LF4. It seems clear that the inherent errors due to the computer are negligible compared to the errors due to uncertainties in $M_s$ and $\sigma_s$.

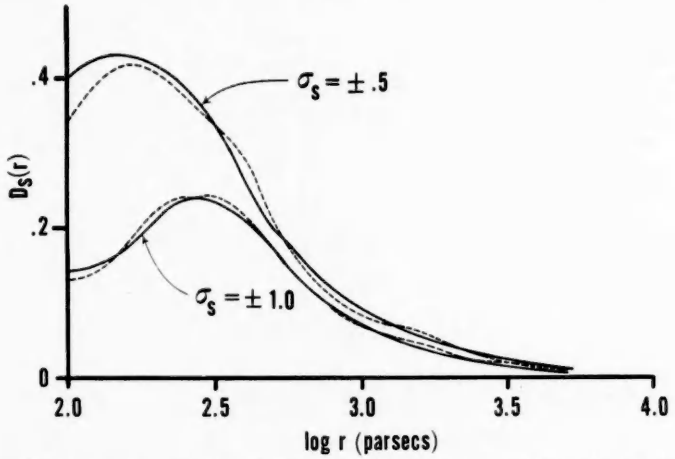


FIG. 3.—Density functions calculated independently by two computers. The ordinate is the density in stars per 1000 cubic parsecs. Two values of the dispersion were used on the same data.

While the *absolute* densities obtained in the type of analysis described here may be uncertain by as much as 50 per cent, the *relative* densities from region to region should be far more reliable. One source of uncertainty from region to region is the error likely to arise in evaluating the interstellar absorption. In order to investigate the order of magnitude of an error in the density functions due to this cause, three calculations of $D_s(r)$ for all spectral groups have been made in LF7, a representative region. For the first calculation the values of total absorption actually found for LF7 were used. For the second evaluation the observed absorption was increased by 10 per cent. For the third calculation the observed absorption was decreased by 10 per cent. The resulting density functions are shown in Table 3 for representative groups of stars. Columns A, B, and C refer, respectively, to our first, second, and third calculations. The changes in the functions $D_s(r)$ due to possible uncertainty in the corrections for absorption do not appear excessive. For all spectral groups in LF7 the average change in $D_s(r)$ for the 20 per cent change in the absorption values amounts to 13 per cent. It is unlikely that an uncertainty of more than $\pm 10$ per cent in the absorption is present. Hence the relative density functions to be presented in a succeeding section are probably reliable within 15 per cent.

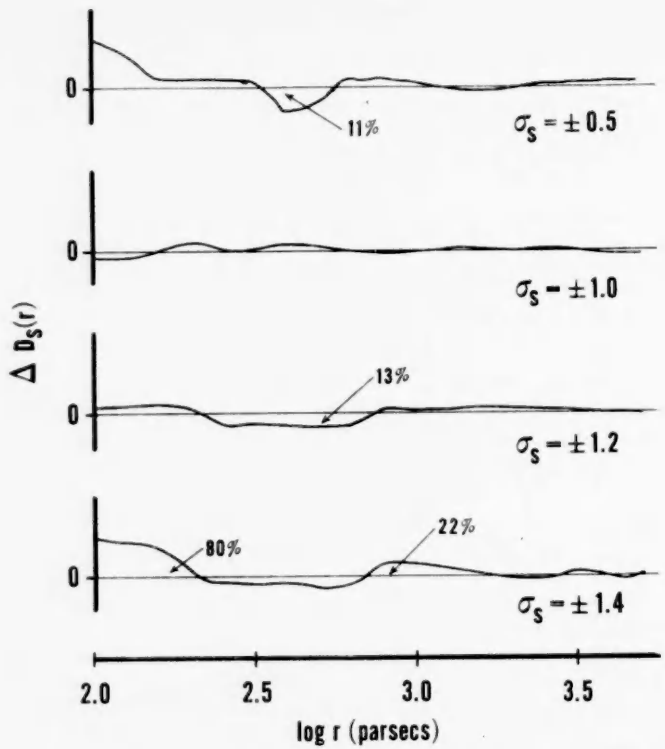


FIG. 4.—Differences between values of the density obtained independently from the same data by two computers. Various dispersions were used. Percentage differences are indicated at certain points.

TABLE 3

VARIATIONS IN DENSITY FUNCTIONS DUE TO ASSUMED CHANGES IN ABSORPTION
($D_s[r]$ in Stars per $10^3$ Cubic Parsecs)

| r (parsecs) | B8–A0 | | | A2–A5 | | | F0–F5 | | | gF8–M | | |
|---|---|---|---|---|---|---|---|---|---|---|---|---|
| | A | B | C | A | B | C | A | B | C | A | B | C |
| 200 | 0.140 | 0.140 | 0.140 | 0.184 | 0.184 | 0.184 | 0.95 | 0.95 | 0.95 | 0.380 | 0.380 | 0.380 |
| 400 | .134 | .146 | .122 | .145 | .158 | .133 | .53 | .526 | .525 | .260 | .280 | .228 |
| 600 | .139 | .146 | .131 | .129 | .131 | .126 | .29 | .292 | .281 | .224 | .227 | .214 |
| 800 | .151 | .158 | .141 | .116 | .113 | .113 | .062 | .059 | .060 | .220 | .228 | .210 |
| 1000 | .170 | .167 | .157 | .077 | .073 | .077 | .165 | .190 | .142 | .181 | .178 | .192 |
| 1200 | .180 | .188 | .172 | .069 | .072 | .066 | 0.264 | 0.281 | 0.246 | .149 | .157 | .153 |
| 1400 | .205 | .208 | .201 | .083 | .085 | .080 | ... | ... | ... | .329 | .411 | .258 |
| 1600 | 0.182 | 0.184 | 0.177 | 0.066 | 0.061 | 0.069 | ... | ... | ... | 0.897 | 0.880 | 0.771 |

THE INTERSTELLAR ABSORPTION

Preliminary to a discussion of the stellar space density in the LF regions, a summary of the interstellar absorption characteristics is required. As explained in detail in the series of papers already published, the absorption values have been determined from blue-red color indices of the stars of spectral types A5 and earlier in each LF region. To the best of our observational ability, the colors and magnitudes are on a uniform system. The mean error of a color index averages $\pm 0.09$ mag. for the areas concerned. In

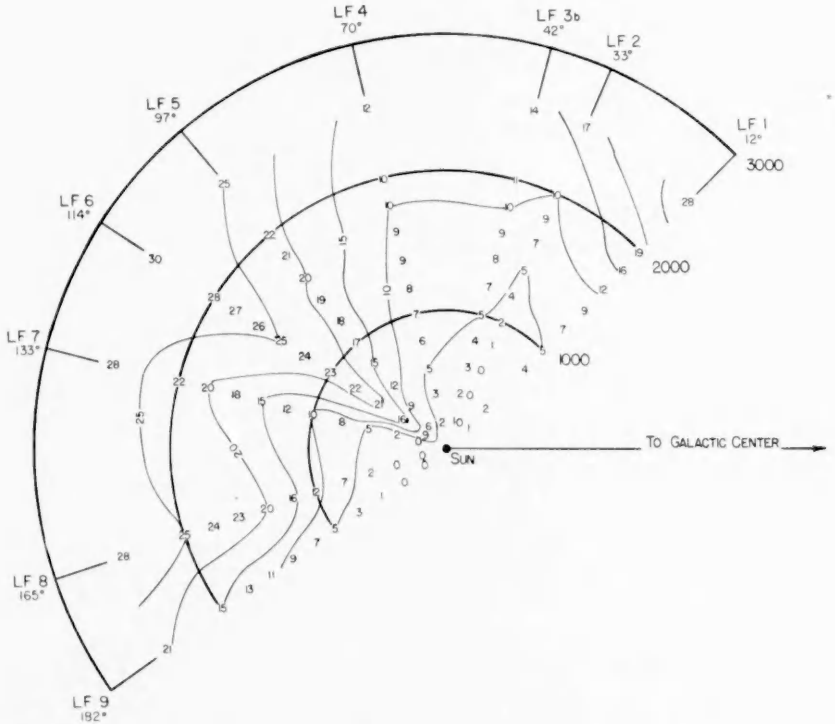


FIG. 5.—The distribution of interstellar matter in the galactic plane as determined from color data in the LF regions. The numbers are values of total absorption, $A_{pg}$, in tenths of a magnitude.

most regions photoelectric observations were used to confirm the magnitude sequences established photographically. The summarized results of a discussion of the colors and color excesses are shown in Table 4, where the total photographic absorption, $A_{pg}$, is given as a function of distance. The ratio $A_{pg}/E$ has been taken as 2.6. Figure 5 shows the distribution of interstellar matter in the galactic plane. Admittedly, extrapolation between LF regions to obtain contours of equal $A_{pg}$ is approximate at best. But the body of data here collected does have the strength of uniformity, and hence a picture of the absorption pattern in broad outline has seemed worth while presenting in this form.

As Table 4 and Figure 5 indicate, the LF regions, with the exception of LF6, exhibit no unusual absorption characteristics. In LF6 the interstellar material appears to be close by and quite dense. The average total absorption in the 2000-parsec interval covered by the data is about 0.9 mag/kpc.

### THE PERCENTAGE OF DWARF STARS

A second consideration entering into the calculation of space density for the late-type stars is the relative numbers of giants and dwarfs among them. For the bright stars particularly, the numbers are too small in a given region, or even in the sum total of all the LF regions, to permit a reliable estimate of the percentages of giants and dwarfs. Therefore, the separation of these two groups *in each region* has been made on the hypothesis that the space density is uniform within the 200 or so parsecs embracing the dwarf stars of $m_{pg} < 11$.

The observed number of dwarf stars with $9 < m_{pg} < 11$ can be reliably determined in each area. In this magnitude interval the spectroscopic evidence for distinguishing

TABLE 4

TOTAL ABSORPTION IN THE LF REGIONS
($A_{pg}$ [Mag.])

| DISTANCE (parsecs) | LF REGION..1 | 2 | 3b | 4 | 5 | 6 | 7 | 8 | 9 |
|---|---|---|---|---|---|---|---|---|---|
| | $l=12°$ | 33° | 42° | 70° | 97° | 114° | 133° | 165° | 182° |
| 250 | 0.1 | 0.0 | 0.1 | 0.2 | 0.7 | 1.1 | 0.0 | 0.0 | 0.0 |
| 500 | 0.3 | 0.0 | 0.2 | 0.4 | 1.0 | 2.0 | 0.4 | 0.0 | 0.0 |
| 750 | 0.4 | 0.0 | 0.4 | 0.6 | 1.4 | 2.2 | 0.7 | 0.6 | 0.2 |
| 1000 | 0.5 | 0.2 | 0.5 | 0.7 | 1.7 | 2.3 | 1.0 | 1.2 | 0.5 |
| 1500 | 1.0 | 0.6 | 0.8 | 0.9 | 2.0 | 2.5 | 1.6 | 2.2 | 1.0 |
| 2000 | 1.9 | 1.0 | 1.1 | 1.0 | 2.2 | 2.8 | 2.2 | 2.5 | 1.5 |
| 2500 | 2.8 | 1.7 | 1.4 | 1.2 | 2.5 | 3.0 | 2.8: | 2.8 | 2.1 |

giants from dwarfs is well defined. Hence by a linear formula in $\log A'(m)$ the numbers of dwarfs at brighter magnitudes may be calculated on the assumption of uniform space density. And from the values of $\log A'(m)$ for all stars follow the values of $\log A'(m)$ for the giants.

Such calculations yield the percentages of dwarf stars for the spectral groups F8–G2, G5, and G8–K3 shown in Table 5. The large fluctuation from area to area among the bright stars undoubtedly arises principally from the extrapolation process. But even among the fainter stars there is a regional variation in percentage of dwarfs which is pronounced. The number of dwarf G8–K3 stars in LF5 was too small for an adequate analysis.

By way of comparison, the percentages of dwarf stars (class V) actually observed in all nine LF regions may be found in Table 6. Here the columns give, respectively, the magnitude interval, the number of stars, the percentages in luminosity classes III (giants), IV (subgiants), and V (dwarfs), and the percentage of unclassifiable stars. If one compares the columns headed "V" with the mean values from the last column in Table 5 and makes due allowance for the variation with magnitude, one finds satisfactory agreement for $m_{pg} > 8$. All stars of classes K5–M8 were considered to be giants.

The agreement between the percentages of dwarfs found here and those found from proper-motion data is not too close, particularly among the brighter stars. The researches

of van Rhijn and Schwassman (1935), Oort (1936), van de Kamp and Vyssotsky (1936), Bok (1935, 1945), and others have shown that, on the average, the percentage of dwarfs among the G stars increases from 30 at $m_{pg} = 7$ to about 60 at $m_{pg} = 12$. And for the K stars these percentages are 5 and 30. But the figures for the G stars refer to the broad spectral range G0–G5, and there is evidence for a rapid decrease in the percentage of dwarfs with advancing spectral type among these stars (McCuskey 1952). Hence for the F8–G2 groups in particular the spectral-type observations yield considerably higher percentages than do the proper-motion studies.

TABLE 5

PERCENTAGE OF DWARF STARS

| $m$ | LF Region | | | | | | | | | Mean |
|---|---|---|---|---|---|---|---|---|---|---|
| | 1 | 2 | 3b | 4 | 5 | 6 | 7 | 8 | 9 | |
| *F8–G2:* | | | | | | | | | | |
| 6 | 29 | 32 | 70 | 64 | 87 | 28 | 37 | 43 | 75 | 52 |
| 8 | 30 | 32 | 74 | 36 | 89 | 42 | 48 | 48 | 85 | 54 |
| 10 | 72 | 82 | 76 | 60 | 90 | 58 | 55 | 60 | 95 | 72 |
| 12 | 81 | 87 | 82 | 75 | 90 | 98 | 80 | 95 | 95 | 87 |
| *G5:* | | | | | | | | | | |
| 6 | 14 | 20 | 23 | 15 | 7 | 10 | 6 | 23 | 22 | 16 |
| 8 | 20 | 20 | 23 | 15 | 8 | 11 | 13 | 17 | 32 | 18 |
| 10 | 36 | 37 | 31 | 17 | 17 | 29 | 34 | 36 | 60 | 33 |
| 12 | 58 | 47 | 42 | 25 | 35 | 63 | 59 | 74 | 60 | 51 |
| *G8–K3:* | | | | | | | | | | |
| 6 | 3 | 4 | 5 | 4 | ..... | 2 | 4 | 6 | 3 | 4 |
| 8 | 4 | 4 | 6 | 4 | ..... | 3 | 6 | 4 | 4 | 4 |
| 10 | 8 | 7 | 8 | 7 | ..... | 9 | 20 | 12 | 4 | 9 |
| 12 | 18 | 15 | 10 | 15 | ..... | 29 | 15 | 28 | 5 | 17 |

TABLE 6

OBSERVED PERCENTAGE DISTRIBUTION IN LUMINOSITY CLASS
(Area 135 Square Degrees)

| $m_{pg}$ | F8–G2 | | | | | G5 | | | | | G8–K3 | | | | |
|---|---|---|---|---|---|---|---|---|---|---|---|---|---|---|---|
| | No. | III | IV | V | Un. | No. | III | IV | V | Un. | No. | III | IV | V | Un. |
| 7–8 | 7 | 0 | 14 | 86 | 0 | 5 | 40 | 0 | 60 | 0 | 22 | 86 | 9 | 5 | 0 |
| 8–9 | 31 | 19 | 36 | 45 | 0 | 8 | 87 | 0 | 13 | 0 | 42 | 69 | 19 | 12 | 0 |
| 9–10 | 69 | 13 | 16 | 71 | 0 | 48 | 52 | 23 | 25 | 0 | 172 | 70 | 24 | 6 | 0 |
| 10–11 | 290 | 14 | 10 | 63 | 13 | 131 | 45 | 18 | 34 | 3 | 281 | 66 | 24 | 9 | 1 |

## THE LOCAL GALACTIC STRUCTURE

The density functions derived by the ($m$, log $\pi$) analyses and corrected for interstellar absorption are listed in Table 7. Stars earlier than B5 have been omitted in the analysis because of their relative scarcity and spotty distribution. The values of $D_s(r)$ are the numbers of stars per 1000 cubic parsecs. Parentheses indicate uncertain determinations.

## TABLE 7

SUMMARY OF DENSITY FUNCTIONS—LF REGIONS
($D_0[r]$ per $10^3$ Cubic Parsecs)

| $r$ (parsecs) | 1 | 2 | 3b | 4 | 5 | 6 | 7 | 8 | 9 |
|---|---|---|---|---|---|---|---|---|---|
| | B5 Stars | | | | | | | | |
| 50 | 0.0144 | 0.0200 | ..... | 0.0196 | 0.033 | ..... | 0.0200 | 0.016 | ..... |
| 100 | .0141 | .0155 | ..... | .0192 | .027 | 0.028 | .0200 | .016 | 0.0130 |
| 200 | .0087 | .0070 | ..... | .0099 | .015 | .026 | .0053 | .0070 | .0080 |
| 300 | .0055 | .0055 | 0.021 | .0060 | .012 | .021 | .0044 | .0031 | .0045 |
| 400 | .0041 | .0036 | .015 | .0046 | .012 | .013 | .0056 | .0025 | .0028 |
| 500 | .0029 | .0029 | .012 | .0041 | .012 | .0085 | .0097 | .0020 | .0018 |
| 600 | .0022 | .0024 | .010 | .0037 | .012 | .0056 | .0207 | .0067 | .0024 |
| 800 | .0021 | .0023 | .0075 | .0030 | .015 | .0042 | .0295 | .0167 | .0078 |
| 1000 | .0010 | .0022 | .0062 | .0031 | .019 | 0.0040 | .0149 | .0107 | .0123 |
| 1200 | .0007 | .0020 | .0055 | .0031 | .020 | ..... | .0092 | .0075 | .0135 |
| 1400 | .0008 | .0023 | .0048 | .0029 | .017 | ..... | .0067 | .0037 | .0105 |
| 1600 | .0009 | .0017 | .0043 | .0030 | .014 | ..... | .0048 | .0011 | .0078 |
| 1800 | .0006 | .0008 | ..... | .0032 | .010 | ..... | .0039 | .0009 | .0066 |
| 2000 | .0002 | .0006 | ..... | .0034 | .007 | ..... | .0029 | .0014 | .0064 |
| 2500 | 0.0009 | 0.0004 | 0.0041 | .0040 | .004 | ..... | 0.0017 | 0.0016 | .0052 |
| 3000 | ..... | ..... | ..... | 0.0052 | 0.004 | ..... | ..... | ..... | 0.0045 |
| | B8–A0 Stars | | | | | | | | |
| 50 | 0.100 | 0.088 | ..... | 0.109 | 0.129 | 0.163 | 0.100 | 0.088 | 0.090 |
| 100 | .105 | .104 | 0.120 | .125 | .220 | .435 | .100 | .110 | .120 |
| 200 | .133 | .130 | .174 | .228 | .394 | .310 | .100 | .132 | .140 |
| 300 | .118 | .138 | .174 | .239 | .355 | .138 | .144 | .126 | .122 |
| 400 | .074 | .140 | .162 | .236 | .250 | .109 | .134 | .120 | .110 |
| 500 | .064 | .131 | .144 | .218 | .143 | .100 | .136 | .110 | .112 |
| 600 | .057 | .134 | .120 | .197 | .076 | .100 | .139 | .118 | .150 |
| 800 | .047 | .122 | .080 | .127 | .084 | .100 | .151 | .078 | .134 |
| 1000 | .039 | .071 | .058 | .102 | .095 | 0.100 | .170 | .122 | .121 |
| 1200 | .033 | .038 | .041 | .082 | .093 | ..... | .180 | .166 | .145 |
| 1400 | .053 | .045 | 0.027 | .080 | .071 | ..... | .205 | .233 | .173 |
| 1600 | .073 | .045 | ..... | .083 | .044 | ..... | .182 | .303 | .204 |
| 1800 | .083 | .038 | ..... | .088 | .029 | ..... | .177 | .254 | .216 |
| 2000 | .090 | .036 | ..... | .090 | .032 | ..... | .160 | .135 | .200 |
| 2500 | 0.172 | 0.034 | ..... | .061 | .042 | ..... | 0.114 | 0.140 | 0.306 |
| 3000 | ..... | ..... | ..... | 0.042 | 0.056 | ..... | ..... | ..... | ..... |
| | A2–A5 Stars | | | | | | | | |
| 50 | 0.70 | 0.705 | (0.64) | 0.680 | 0.915 | (0.64) | 0.736 | 0.69 | 0.80 |
| 100 | .404 | .422 | .53 | .480 | .542 | .41 | .368 | .40 | .34 |
| 200 | .278 | .254 | .42 | .354 | .330 | .32 | .184 | .26 | .39 |
| 300 | .125 | .183 | .37 | .284 | .294 | .33 | .152 | .186 | .38 |
| 400 | .101 | .170 | .37 | .219 | .313 | .25 | .145 | .100 | .32 |
| 500 | .077 | .146 | .40 | .184 | .409 | .17 | .143 | .072 | .27 |
| 600 | .060 | .135 | .37 | .158 | .440 | 0.09 | .129 | .106 | .21 |
| 800 | .054 | .122 | (0.22) | .114 | .231 | ..... | .116 | .108 | .12 |
| 1000 | .035 | .117 | ..... | .090 | .155 | ..... | .077 | .121 | .071 |
| 1200 | .026 | .118 | ..... | .072 | .091 | ..... | .069 | .166 | .039 |
| 1400 | .053 | .143 | ..... | .141 | 0.055 | ..... | .083 | 0.266 | .039 |
| 1600 | 0.048 | .170 | ..... | .227 | ..... | ..... | .066 | ..... | 0.030 |
| 1800 | ..... | .210 | ..... | 0.325 | ..... | ..... | 0.028 | ..... | ..... |
| 2000 | ..... | 0.163 | ..... | ..... | ..... | ..... | ..... | ..... | ..... |
| 2500 | ..... | ..... | ..... | ..... | ..... | ..... | ..... | ..... | ..... |
| 3000 | ..... | ..... | ..... | ..... | ..... | ..... | ..... | ..... | ..... |

TABLE 7—*Continued*

| $r$ (parsecs) | 1 | 2 | 3b | 4 | 5 | 6 | 7 | 8 | 9 |
|---|---|---|---|---|---|---|---|---|---|
| | F0–F5 Stars | | | | | | | | |
| 50 | 1.90 | 1.93 | 2.4 | 1.96 | 2.60 | 2.1 | 2.7 | 1.9 | 1.67 |
| 100 | 1.41 | 1.48 | 1.65 | 1.70 | 3.15 | 1.60 | 1.8 | 1.5 | 1.20 |
| 200 | 0.88 | 0.92 | 1.28 | 1.46 | 0.20 | 1.20 | 0.95 | 0.9 | 2.00 |
| 300 | 0.44 | 0.654 | 1.15 | 1.05 | 0.87 | 1.02 | 0.84 | 0.42 | 1.28 |
| 400 | 0.30 | 0.570 | 1.08 | 0.87 | 1.63 | 0.92 | 0.53 | 0.35 | 0.90 |
| 500 | 0.15 | 0.526 | (1.05) | 0.75 | 1.23 | 0.83 | 0.35 | 0.30 | 0.45 |
| 600 | 0.16 | 0.456 | ..... | 0.66 | 1.10 | (0.80) | 0.29 | 0.324 | 0.30 |
| 800 | 0.15 | 0.464 | ..... | 0.50 | 0.85 | ..... | 0.062 | 0.167 | 0.14 |
| 1000 | 0.12 | 0.460 | ..... | 0.48 | 1.14 | ..... | 0.165 | 0.101 | 0.06 |
| 1200 | 0.12 | 0.512 | ..... | 0.44 | ..... | ..... | 0.264 | 0.207 | 0.05 |
| 1400 | 0.18 | 0.683 | ..... | 0.42 | ..... | ..... | ..... | ..... | 0.05 |
| 1600 | ..... | 0.886 | ..... | 0.39 | ..... | ..... | ..... | ..... | ..... |
| 1800 | ..... | 1.167 | ..... | ..... | ..... | ..... | ..... | ..... | ..... |
| 2000 | ..... | ..... | ..... | ..... | ..... | ..... | ..... | ..... | ..... |
| 2500 | ..... | ..... | ..... | ..... | ..... | ..... | ..... | ..... | ..... |
| 3000 | ..... | ..... | ..... | ..... | ..... | ..... | ..... | ..... | ..... |
| | dF8–G2 Stars | | | | | | | | |
| 50 | 1.00 | 0.99 | 3.4 | 0.55 | 2.8 | 1.62 | 1.25 | 1.08 | 2.5 |
| 100 | 1.02 | 1.07 | 3.4 | 1.85 | 2.8 | 1.62 | 1.25 | 1.08 | 2.9 |
| 200 | 1.15 | 2.08 | 3.4 | 2.52 | 3.0 | 1.62 | 1.44 | 1.08 | 3.4 |
| 300 | 0.94 | 1.91 | 3.4 | 1.40 | 3.4 | 1.62 | 1.81 | 1.08 | 4.0 |
| 400 | 0.73 | 1.90 | ..... | 3.59 | 3.5 | ..... | 1.93 | 1.08 | 4.4 |
| 500 | 0.53 | 1.92 | ..... | 4.28 | 3.5 | ..... | 1.69 | 1.08 | 5.0 |
| 600 | 0.37 | 1.93 | ..... | 3.78 | ..... | ..... | 0.59 | 2.59 | 7.3 |
| 800 | ..... | 2.53 | ..... | 1.32 | ..... | ..... | 0.39 | 5.31 | ..... |
| 1000 | ..... | (3.06) | ..... | ..... | ..... | ..... | ..... | ..... | ..... |
| | dG5 Stars | | | | | | | | |
| 50 | 3.2 | 3.05 | 2.8 | 3.27 | 1.4 | 1.48 | 2.6 | 3.7 | 5.2 |
| 100 | 3.2 | 3.05 | 2.8 | 3.65 | 1.4 | 1.48 | 2.6 | 3.7 | 7.5 |
| 200 | 3.2 | 3.05 | 2.8 | 4.52 | 1.6 | 1.48 | 2.6 | 2.9 | 3.5 |
| 300 | 4.0 | 3.05 | ..... | 4.44 | 2.4 | ..... | 3.6 | 1.0 | 1.8 |
| 400 | 4.3 | 3.05 | ..... | 4.92 | 3.1 | ..... | 4.4 | 1.0 | 0.9 |
| 500 | 4.6 | 3.05 | ..... | 5.56 | ..... | ..... | 5.6 | 1.0 | 0.5 |
| 600 | ..... | 3.05 | ..... | ..... | ..... | ..... | ..... | ..... | (0.4) |
| 800 | ..... | (4.00) | ..... | ..... | ..... | ..... | ..... | ..... | ..... |
| | dG8–K3 Stars | | | | | | | | |
| 50 | 8.1 | 17.8 | 15.2 | 12.0 | ..... | 4.68 | 26.0 | 17.8 | 10.0 |
| 100 | 8.1 | 17.8 | 15.2 | 13.2 | ..... | 4.68 | 6.0 | 17.8 | 8.7 |
| 200 | 9.4 | 17.8 | ..... | 8.9 | ..... | 4.68 | 2.0 | 17.8 | 2.0 |
| 300 | 10.1 | 17.8 | ..... | 8.4 | ..... | ..... | 5.5 | 17.8 | 0.9 |
| 400 | 11.0 | 17.8 | ..... | ..... | ..... | ..... | 3.4 | 17.8 | (0.5) |
| | gF8–G2 Stars | | | | | | | | |
| 50 | 0.065 | 0.053 | ..... | 0.084 | 0.018 | (0.04) | 0.25 | 0.055 | 0.020 |
| 100 | .091 | .054 | 0.030 | .048 | .016 | .098 | .059 | .048 | .020 |
| 200 | .091 | .064 | .030 | .089 | .019 | .163 | .050 | .047 | .017 |
| 300 | .051 | .055 | .030 | .119 | .023 | .165 | .064 | .041 | .013 |
| 400 | .033 | .040 | .030 | .081 | .026 | .058 | .056 | .040 | .011 |
| 500 | 0.014 | 0.025 | 0.030 | 0.015 | 0.026 | 0.033 | 0.062 | 0.030 | 0.010 |

TABLE 7—*Continued*

| r (parsecs) | 1 | 2 | 3b | 4 | 5 | 6 | 7 | 8 | 9 |
|---|---|---|---|---|---|---|---|---|---|
| | gF8–G2 Stars—*Continued* | | | | | | | | |
| 600 | 0.0080 | 0.011 | 0.030 | 0.015 | 0.025 | 0.028 | 0.062 | 0.043 | 0.011 |
| 800 | .0075 | .012 | 0.030 | .036 | .023 | (0.024) | .058 | .039 | .015 |
| 1000 | .0071 | .018 | ..... | .066 | .021 | ..... | .021 | .050 | .019 |
| 1200 | .0069 | .019 | ..... | .081 | .021 | ..... | .009 | .021 | .024 |
| 1400 | .012 | .023 | ..... | .051 | 0.021 | ..... | .013 | .033 | .028 |
| 1600 | .013 | .029 | ..... | .055 | ..... | ..... | (.173) | 0.040 | 0.032 |
| 1800 | .012 | .037 | ..... | .057 | ..... | ..... | (0.388) | ..... | ..... |
| 2000 | 0.020 | 0.048 | ..... | 0.056 | ..... | ..... | ..... | ..... | ..... |
| | gG5 Stars | | | | | | | | |
| 50 | 0.080 | 0.042 | ..... | 0.045 | 0.062 | (0.05) | 0.145 | 0.037 | 0.042 |
| 100 | .067 | .053 | 0.044 | .051 | .100 | .100 | .140 | .042 | .042 |
| 200 | .059 | .061 | .044 | .066 | .133 | .191 | .083 | .055 | .042 |
| 300 | .048 | .057 | .044 | .073 | .119 | .138 | .035 | .070 | .041 |
| 400 | .039 | .020 | .044 | .077 | .068 | .083 | .036 | .055 | .038 |
| 500 | .031 | .002 | .044 | .081 | .050 | .044 | .036 | .025 | .034 |
| 600 | .023 | .001 | .044 | .086 | .042 | .028 | .035 | .022 | .029 |
| 800 | .019 | .005 | 0.044 | .083 | .040 | (0.019) | .029 | .015 | .026 |
| 1000 | .024 | .015 | ..... | .086 | .038 | ..... | .041 | .020 | .026 |
| 1200 | .023 | .016 | ..... | .082 | .030 | ..... | .030 | .021 | .026 |
| 1400 | .034 | .025 | ..... | .084 | 0.025 | ..... | .028 | .033 | .028 |
| 1600 | .027 | .041 | ..... | .096 | ..... | ..... | .066 | 0.040 | 0.031 |
| 1800 | .026 | .058 | ..... | .110 | ..... | ..... | 0.028 | ..... | ..... |
| 2000 | 0.025 | 0.090 | ..... | 0.124 | ..... | ..... | ..... | ..... | ..... |
| | gG8–K3 Stars | | | | | | | | |
| 50 | 0.190 | 0.19 | 0.17 | 0.214 | 0.27 | (0.18) | 0.67 | 0.193 | 0.20 |
| 100 | .172 | .19 | .17 | .181 | .29 | .28 | .49 | .193 | .20 |
| 200 | .150 | .19 | .17 | .186 | .34 | .44 | .18 | .193 | .20 |
| 300 | .125 | .160 | .17 | .175 | .41 | .359 | .165 | .193 | .20 |
| 400 | .117 | .159 | .17 | .151 | .44 | .198 | .142 | .193 | .20 |
| 500 | .087 | .151 | .17 | .146 | .18 | .139 | .130 | .120 | .20 |
| 600 | .077 | .126 | .17 | .135 | .04 | .092 | .115 | .082 | .20 |
| 800 | .043 | .111 | 0.17 | .101 | .02 | (0.025) | .124 | .064 | .17 |
| 1000 | .047 | .100 | ..... | .098 | .05 | ..... | .112 | .080 | .15 |
| 1200 | .057 | .092 | ..... | .099 | .09 | ..... | .106 | .021 | .16 |
| 1400 | .118 | .105 | ..... | .105 | 0.14 | ..... | .284 | .033 | .18 |
| 1600 | .173 | .112 | ..... | .119 | ..... | ..... | .66 | 0.040 | 0.20 |
| 1800 | .154 | .140 | ..... | .135 | ..... | ..... | 0.28 | ..... | ..... |
| 2000 | 0.250 | 0.188 | ..... | 0.152 | ..... | ..... | ..... | ..... | ..... |
| | gK5–M Stars | | | | | | | | |
| 50 | 0.050 | 0.050 | ..... | 0.050 | 0.072 | ..... | 0.290 | ..... | 0.040 |
| 100 | .050 | .038 | ..... | .055 | .095 | ..... | .141 | ..... | .037 |
| 200 | .041 | .030 | ..... | .080 | .120 | ..... | .067 | ..... | .031 |
| 300 | .025 | .026 | ..... | .052 | .117 | ..... | .039 | ..... | .026 |
| 400 | .026 | .023 | ..... | .043 | .100 | ..... | .026 | ..... | .026 |
| 500 | .021 | .018 | ..... | .036 | .065 | ..... | .018 | ..... | .025 |
| 600 | .018 | .016 | ..... | .030 | .039 | ..... | .012 | ..... | .024 |
| 800 | .015 | .019 | ..... | .016 | .020 | ..... | .009 | ..... | .021 |
| 1000 | .010 | .018 | ..... | .011 | .020 | ..... | .007 | ..... | .018 |
| 1200 | .012 | .019 | ..... | .007 | .020 | ..... | .005 | ..... | .018 |
| 1400 | .012 | .022 | ..... | .007 | 0.020 | ..... | .004 | ..... | .018 |
| 1600 | .013 | .021 | ..... | .006 | ..... | ..... | .002 | ..... | 0.018 |
| 1800 | .015 | .020 | ..... | .006 | ..... | ..... | 0.003 | ..... | ..... |
| 2000 | 0.025 | 0.019 | ..... | 0.006 | ..... | ..... | ..... | ..... | ..... |

Figures 6*a*–6*d* portray the spatial distribution of the most prominent groups of stars in the local region of the Galaxy within 1000 parsecs of the sun. Noteworthy features exhibited by these maps are as follows:

*a*) The concentration of B8–A0 stars between longitudes 60° and 120° and within 500 parsecs of the sun.

*b*) The widespread concentration of A2–A5 stars in the same longitude range but at greater distances than in the case of the B8–A0 stars.

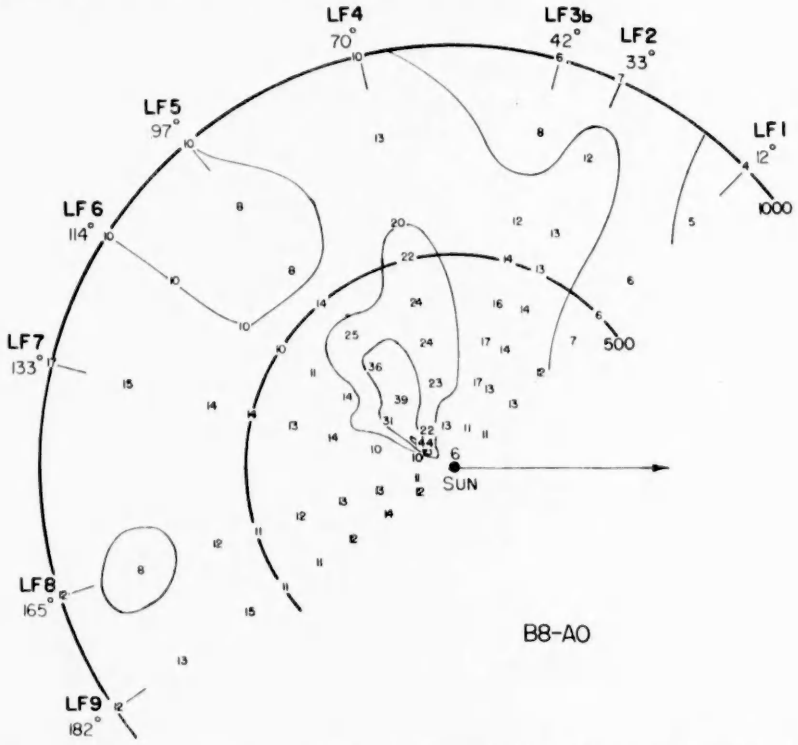


FIG. 6*a*.—The space distribution in the galactic plane of the B8–A0 stars within 1000 parsecs of the sun. The numbers give the density in units of stars per $10^8$ cubic parsecs. Contours of equal density are shown. The arrow points to the galactic center at $l = 327°$.

*c*) The rapid decrease in density of the F0–F5 stars at all longitudes except 42° and 97°. The negative gradient is less pronounced at $l = 70°$ but is present there. The reality of the maximum and dip near the sun at $l = 97°$ (LF5) is doubtful. The absorption characteristics of this region make the correction of densities at small distances uncertain.

*d*) The pronounced concentration of yellow giant stars, classes F8–K3, in the same area as that dominated by the B8–A0 stars.

It is difficult to compare the results found in this study with the work of other investigators because of the different groupings in spectral class. Pannekoek (1929), for example, studied the B8–A3 stars from the *Henry Draper Catalogue* and also the K0–K8 stars. To the limit of his survey, 300 parsecs, there appears to be a concentration of the

A stars more or less coinciding with the Cygnus concentration found here for the A2–A5 stars. While Pannekoek found very little correspondence between the clusterings of A stars and those of the K stars, we find a prominent matching of the large-scale aggregates of these two groups.

Malmquist and Hufnagel (1933) discussed the space-density distribution of the A0–A5 stars of the *Henry Draper Catalogue*. They also found the extended clustering of these stars in Cygnus shown in Figure 6*b* for the A2–A5 stars to extend at least to 800 parsecs.

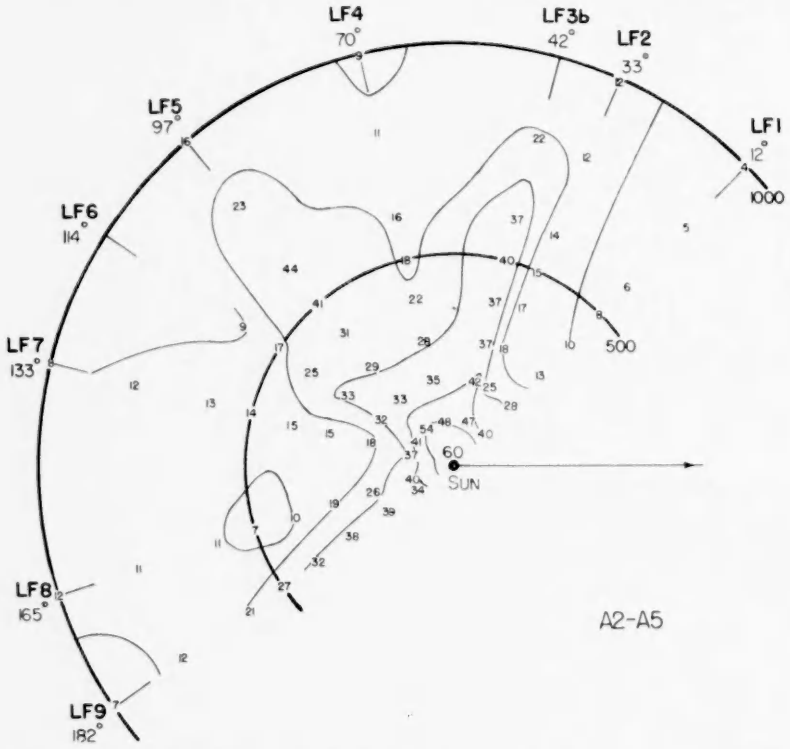


FIG. 6*b*.—The space distribution in the galactic plane of the A2–A5 stars within 1000 parsecs of the sun. See the caption for Fig. 6*a*.

The concentration of near-by A stars in Taurus is not shown on our charts because of the selection of the LF regions. However, an earlier study (McCuskey 1941) of the stellar distribution from the *Henry Draper Extension* indicated a concentration of B8–A3 stars at a distance of 250 parsecs in the Taurus area. In neither of the studies by Pannekoek and by Malmquist and Hufnagel were corrections for interstellar absorption applied. The distances concerned were small, but we have found in some longitudes that the absorption effects are quite large even near the sun.

Figures 7*a* and 7*b* show, respectively, the large-scale distribution in the galactic plane of the B8–A0 stars and the B5 stars. Contours indicate approximately the regions of high and low density. Between longitudes 130° and 180° there appears to be a high con-

centration of B8–A0 stars at distances of 1000–2000 parsecs. The space density averages four to five times that in the solar neighborhood. This aggregate of A stars coincides quite closely with the junction between the local spiral arm and the Perseus arm, as shown by Morgan (1955). In this region Morgan, Whitford, and Code (1953) have found a concentration of aggregates of blue supergiant stars. Along the local spiral arm toward Cygnus, however, the density of A stars remains low, gradually decreasing with distance. Between the local arm and the Perseus arm at $l = 100°$, the population of early A stars is very small. Clearly, one cannot, from this study, associate the early A stars with the spiral structure of the Galaxy in a definitive way.

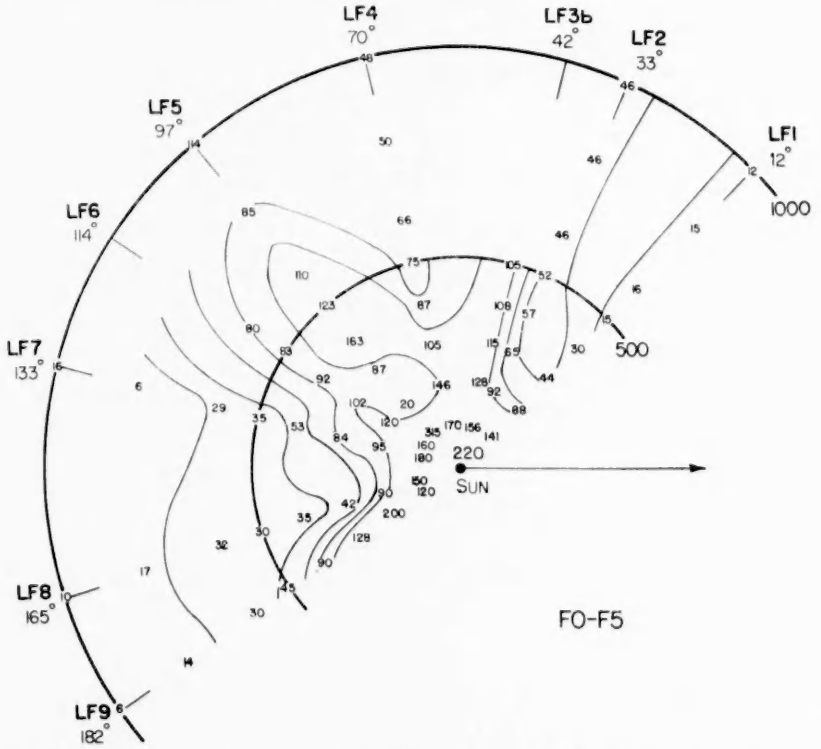


FIG. 6c.—The space distribution in the galactic plane of the F0–F5 stars within 1000 parsecs of the sun. See the caption for Fig. 6a.

The high density of A stars in regions LF8 and LF9 coincides with a high density of hydrogen gas as shown by van de Hulst, Muller, and Oort (1954). Furthermore, the very low space density of these stars in LF4 and LF5 between 1000 and 2000 parsecs coincides with a region of low density of hydrogen. But there appears in our analysis no increase in the A-star population between 2000 and 3000 parsecs comparable to the large increase in the density of hydrogen in these longitudes within the same distance interval.

In all these comparisons, the sampling nature of the results must be kept in mind. Interpolation between LF regions can be approximate at best, and the interpretation of

contours as shown in Figures 6 and 7 should be made accordingly. The general picture one gets of the distribution of the early A stars is a uniform space density of about 0.08 star per 1000 cubic parsecs, on which is superposed a concentration of twice or three times this in the anticenter region of the Galaxy. The correlation with the spiral structure shown by the hydrogen gas, with the O associations, with the early B-star distribution, and with the distribution of other types of objects is not clearly defined.

The B5 stars, as shown in Figure 7*b*, are numerous in LF5 and in LF7. The concentration at $l = 97°$ extends to a distance of 2000 parsecs, while that at $l = 133°$ is within

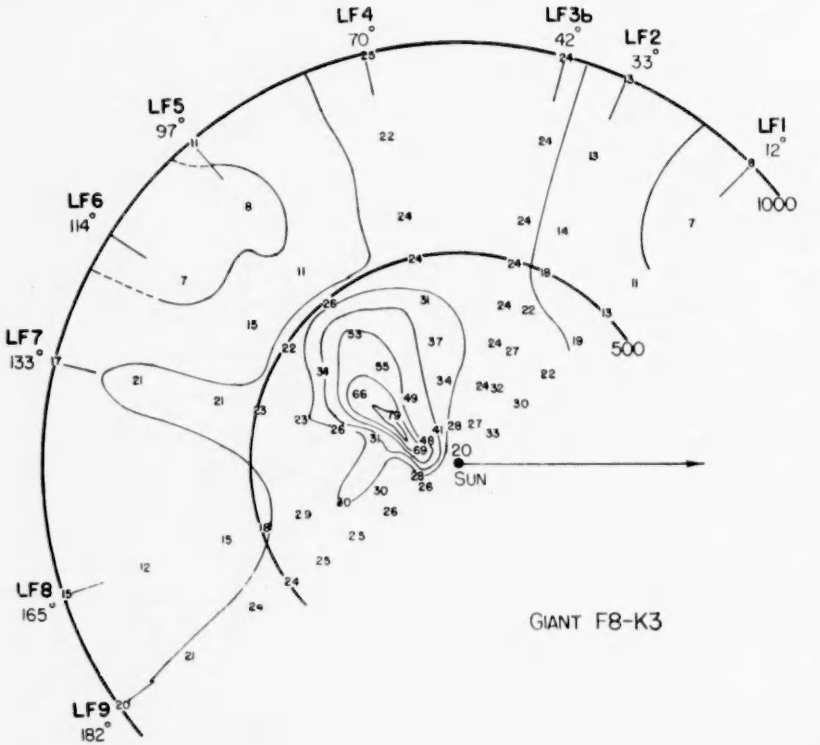


FIG. 6*d*.—The space distribution in the galactic plane of the giant F8–K3 stars within 1000 parsecs of the sun. See the caption for Fig. 6*a*.

1000 parsecs. Weaver (1953) has shown that there is evidence of an early B-star concentration between $l = 70°$ and $l = 100°$ and at a distance comparable with that found here for the B5 stars. But the near-by aggregate in LF7 falls approximately in the break in the early B-star distribution. The dearth of early B stars in the directions of LF1 and LF2 is noteworthy. This is apparent from the tabulation of data in Table 1 and shows clearly for the B5 stars in Figure 7*b*. The highly luminous OB stars studied by Nassau and Morgan (1951) are also very scarce in this region. These two LF regions lie in the gap between two spiral arms, as shown by Morgan, Whitford, and Code (1953).

THE LUMINOSITY FUNCTION

The density functions of Table 7 have been used to compute a general luminosity function for distances of 100, 200, 400, and 600 parsecs in each LF region. Let $D_s(r)$ be the density (stars per cubic parsec) at distance $r$ considered fixed and of spectral group $s$. Then

$$\phi(M) = \sum_s (2\pi\sigma_s^2)^{-1/2} \exp -\left(\frac{M - M_s}{\sqrt{2}\,\sigma_s}\right)^2 D_s(r) = \sum_s a_s(M)\, D_s(r), \qquad (1)$$

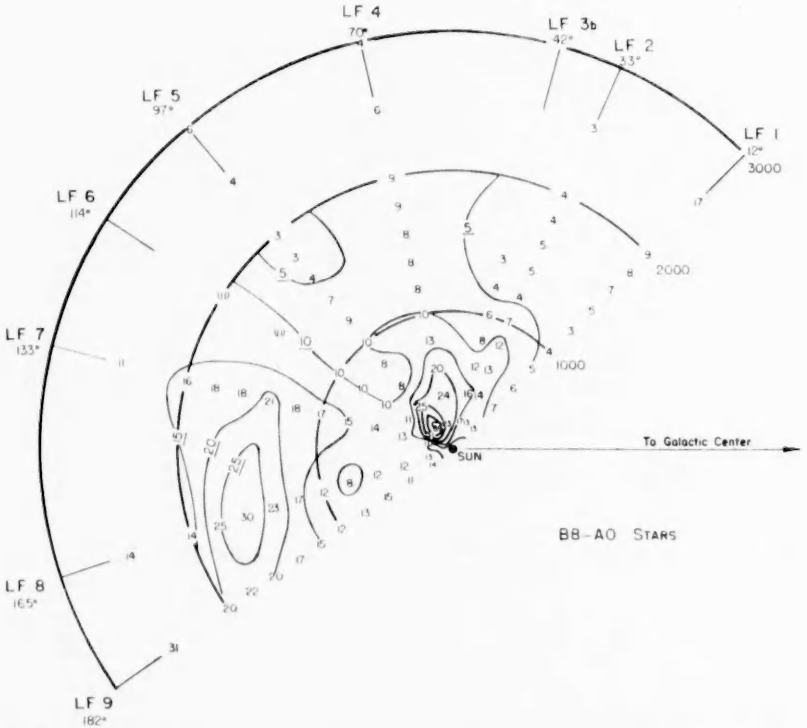


FIG. 7*a*.—The large-scale distribution of the B8–A0 stars in the galactic plane. Contours of equal density indicate approximately regions of high and low density. The units of density are stars per $10^6$ cubic parsecs.

where $\phi(M)$ is defined to be the number of stars at the distance concerned per cubic parsec with absolute photographic magnitude between $M - \frac{1}{2}$ and $M + \frac{1}{2}$. At a given $M$ it is apparent from equation (1) that $\phi(M)$ is a linear function of $D_s(r)$, with coefficients $a_s(M)$ calculable from the normal error function with dispersion $\sigma_s$ and mean $M_s$ listed in Table 2.

Table 8 gives the values of $\log \phi(M) + 10$ computed according to equation (1). Where an extrapolated value of $D_s(r)$ for the dwarf stars was used at 400 and 600 parsecs, the $\log \phi(M)$ is uncertain and is inclosed in parentheses. The last two columns give, respec-

tively, at each distance the average over all LF regions and the range in log $\phi(M) + 10$. Owing to the revised density functions in some regions, these luminosity functions differ somewhat from those already published in preceding papers of this series.

The functions, as defined by equation (1) and given in Table 8, *at a given distance* contain a general density factor common to all absolute magnitudes in a given region. The standard van Rhijn function (1936), with which we wish to compare our results, refers to the number of stars per cubic parsec *near the sun*. Before the changes in *shape*

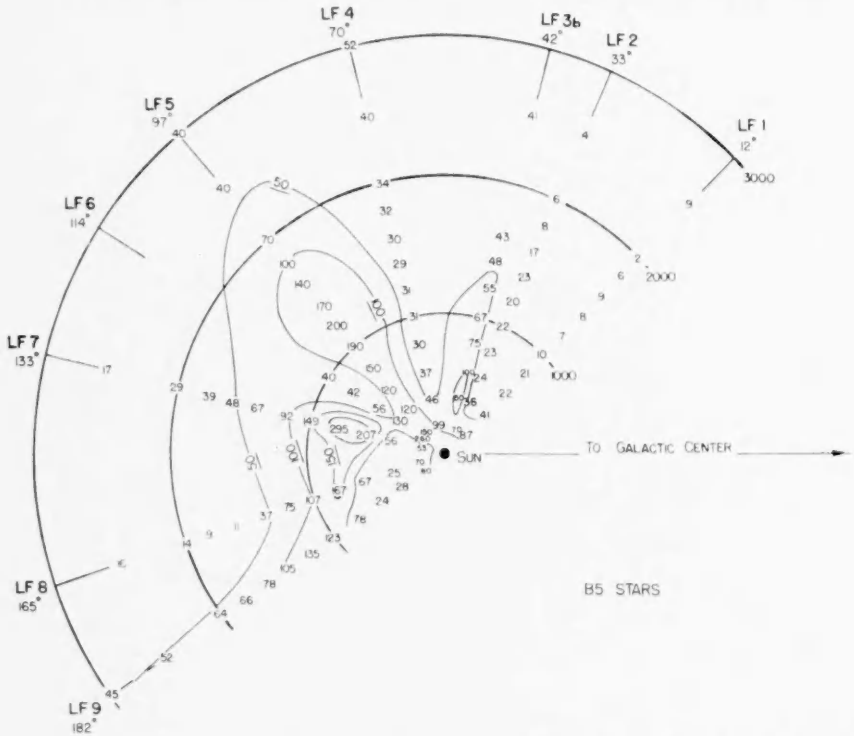


FIG. 7*b*.—The large-scale distribution in the galactic plane of the B5 stars. The density is expressed as the number of stars per $10^7$ cubic parsecs.

of the luminosity function can be exhibited free of this general density factor, the values of log $\phi(M)$ as computed must be referred to a common base, which we take to be the standard van Rhijn function. The average differences between the observed functions and the standard are shown in Table 9. These are taken in the sense log $\phi(M)$ (LF regions) *minus* log $\phi(M)$ (standard). By means of these differences, the observed functions were reduced to a form in which the general stellar density fluctuation had been eliminated.

Table 10 gives the maximum and minimum values of log $\phi(M)$ and the range, without reference to galactic longitude or distance. The final mean luminosity function and the standard van Rhijn function are given in the fifth and sixth columns, respectively. These

TABLE 8

LUMINOSITY FUNCTIONS IN THE GALACTIC PLANE
($\log \phi[M] + 10$)

| $M_{pg}$ | LF. . . . . 1 | 2 | 3b | 4 | 5 | 6 | 7 | 8 | 9 | Av. | RANGE |
|---|---|---|---|---|---|---|---|---|---|---|---|
| | Gal. Long. . . 12° | 33° | 42° | 70° | 97° | 114° | 133° | 165° | 182° | | |
| | At 100 Parsecs | | | | | | | | | | |
| −2 | 4.53 | 4.56 | ..... | 4.89 | 5.04 | 4.81 | 4.66 | 4.58 | 4.51 | 4.70 | 0.53 |
| −1 | 5.25 | 5.27 | ..... | 5.38 | 5.57 | 5.48 | 5.32 | 5.28 | 5.25 | 5.35 | .32 |
| 0 | 5.81 | 5.84 | 5.90 | 5.88 | 6.07 | 5.96 | 5.84 | 5.81 | 5.82 | 5.88 | .26 |
| +1 | 6.36 | 6.46 | 6.38 | 6.39 | 6.53 | 6.43 | 6.46 | 6.32 | 6.29 | 6.40 | .24 |
| +2 | 6.72 | 6.82 | 6.75 | 6.76 | 6.91 | 6.78 | 6.84 | 6.68 | 6.64 | 6.77 | .27 |
| +3 | 6.93 | 6.97 | 7.04 | 7.02 | 7.25 | 7.00 | 7.04 | 6.94 | 6.95 | 7.01 | .32 |
| +4 | 7.02 | 7.04 | 7.24 | 7.18 | 7.39 | 7.13 | 7.11 | 7.04 | 7.25 | 7.16 | .37 |
| +5 | 7.11 | 7.14 | 7.29 | 7.25 | 7.23 | 7.06 | 7.10 | 7.18 | 7.47 | 7.20 | .41 |
| +6 | 7.45 | 7.58 | 7.53 | 7.57 | 7.02 | 7.17 | 7.35 | 7.62 | 7.74 | 7.45 | .72 |
| +7 | 7.57 | 7.87 | 7.79 | 7.76 | ..... | 7.32 | 7.45 | 7.87 | 7.69 | 7.67 | 0.55 |
| | At 200 Parsecs | | | | | | | | | | |
| −2 | 4.38 | 4.30 | 4.94 | 4.76 | 5.06 | 4.82 | 4.19 | 4.31 | 4.36 | 4.57 | 0.87 |
| −1 | 5.24 | 5.20 | 5.55 | 5.43 | 5.66 | 5.62 | 5.09 | 5.20 | 5.23 | 5.36 | .59 |
| 0 | 5.84 | 5.83 | 5.99 | 6.06 | 6.27 | 6.19 | 5.73 | 5.83 | 5.86 | 5.96 | .54 |
| +1 | 6.28 | 6.29 | 6.37 | 6.44 | 6.58 | 6.59 | 6.20 | 6.27 | 6.33 | 6.37 | .39 |
| +2 | 6.58 | 6.60 | 6.68 | 6.73 | 6.73 | 6.84 | 6.54 | 6.57 | 6.72 | 6.67 | .30 |
| +3 | 6.77 | 6.84 | 6.97 | 7.00 | 6.74 | 6.95 | 6.80 | 6.77 | 7.10 | 6.88 | .36 |
| +4 | 6.94 | 7.10 | 7.18 | 7.23 | 7.13 | 7.08 | 7.01 | 6.93 | 7.35 | 7.11 | .42 |
| +5 | 7.12 | 7.24 | 7.28 | 7.34 | 7.20 | 7.05 | 7.09 | 7.12 | 7.36 | 7.20 | .31 |
| +6 | 7.47 | 7.59 | 7.53 | 7.58 | 7.07 | 7.17 | 7.26 | 7.57 | 7.40 | 7.40 | .52 |
| +7 | 7.62 | 7.87 | 7.79 | 7.64 | ..... | 7.32 | 7.11 | 7.86 | 7.17 | 7.55 | 0.76 |
| | At 400 Parsecs | | | | | | | | | | |
| −2 | 4.07 | 4.15 | 4.74 | 4.56 | 4.82 | 4.49 | 4.24 | 4.02 | 4.03 | 4.35 | 0.80 |
| −1 | 4.96 | 5.17 | 5.42 | 5.38 | 5.48 | 5.23 | 5.18 | 5.09 | 5.05 | 5.22 | 0.52 |
| 0 | 5.57 | 5.83 | 5.94 | 6.05 | 6.10 | 5.78 | 5.81 | 5.77 | 5.77 | 5.85 | 0.53 |
| +1 | 5.96 | 6.19 | 6.34 | 6.36 | 6.51 | 6.26 | 6.16 | 6.14 | 6.27 | 6.24 | 0.55 |
| +2 | 6.21 | 6.44 | 6.64 | 6.60 | 6.80 | 6.59 | 6.40 | 6.37 | 6.61 | 6.52 | 0.59 |
| +3 | 6.39 | 6.70 | 6.92 | 6.90 | 7.07 | ..... | 6.68 | 6.52 | 6.95 | 6.77 | 0.68 |
| +4 | 6.68 | 7.02 | 7.16 | 7.28 | 7.33 | ..... | 7.02 | 6.78 | 7.34 | 7.08 | 0.66 |
| +5 | 7.13 | 7.22 | 7.27 | 7.42 | 7.34 | ..... | 7.25 | 6.93 | 7.32 | 7.24 | 0.49 |
| +6 | 7.57 | 7.59 | 7.53 | 7.61 | 7.32 | ..... | 7.48 | 7.42 | 6.98 | 7.44 | 0.63 |
| +7 | 7.70 | 7.87 | ..... | 7.63 | ..... | ..... | 7.34 | 7.84 | (6.59) | 7.68 | 1.28 |
| | At 600 Parsecs | | | | | | | | | | |
| −2 | 3.86 | 4.08 | 4.61 | 4.41 | 4.73 | 4.19 | 4.69 | 4.28 | 4.06 | 4.32 | 0.87 |
| −1 | 4.81 | 5.13 | 5.28 | 5.30 | 5.16 | 5.07 | 5.38 | 5.16 | 5.16 | 5.16 | 0.57 |
| 0 | 5.43 | 5.79 | 5.84 | 5.97 | 5.67 | 5.67 | 5.84 | 5.74 | 5.86 | 5.76 | 0.54 |
| +1 | 5.74 | 6.09 | 6.30 | 6.26 | 6.23 | 5.99 | 6.13 | 6.03 | 6.24 | 6.11 | 0.56 |
| +2 | 5.94 | 6.31 | 6.63 | 6.48 | 6.61 | 6.31 | 6.32 | 6.24 | 6.49 | 6.37 | 0.69 |
| +3 | 6.12 | 6.63 | 6.90 | 6.84 | 6.95 | ..... | 6.40 | 6.62 | 6.93 | 6.67 | 0.83 |
| +4 | 6.43 | 7.01 | 7.15 | 7.28 | 7.29 | ..... | 6.63 | 7.08 | 7.49 | 7.05 | 1.06 |
| +5 | 7.07 | 7.22 | 7.27 | 7.45 | 7.34 | ..... | 7.17 | 7.17 | 7.49 | 7.27 | 0.42 |
| +6 | 7.56 | 7.59 | ..... | 7.65 | 7.32 | ..... | 7.55 | (7.45) | (6.96) | 7.44 | 0.69 |
| +7 | 7.70 | (7.87) | ..... | 7.64 | ..... | ..... | 7.39 | (7.84) | (6.48) | 7.49 | 1.39 |

results are exhibited graphically in Figure 8. The upper part of the figure shows the average reduced functions for the four distances concerned. The vertical lines indicate the variation in log $\phi(M)$ at integral absolute magnitudes. The mean curve for all LF regions at all distances is shown in the lower part of the figure, together with the van Rhijn function for comparison.

In the region within 500 parsecs of the sun the average fluctuation in log $\phi(M)$ is 0.6, which implies a variation by a factor of 4 in the relative proportions of stars of a given absolute magnitude. As Figure 8 shows, the variation is greatest for $M > +3$.

In general, the van Rhijn function and the mean of our functions are in very good agreement. In the LF regions there appears to be a preponderance of stars with $-1 <$

TABLE 9

AVERAGE DIFFERENCES IN LOG $\phi(M)$, LF REGION MINUS VAN RHIJN STANDARD
(Units: 0.01 in log $\phi[M]$)

| DISTANCE (parsecs) | LF REGION | | | | | | | | |
|---|---|---|---|---|---|---|---|---|---|
| | 1 | 2 | 3b | 4 | 5 | 6 | 7 | 8 | 9 |
| 100 | − 3 | + 5 | + 7 | +10 | +17 | 0 | + 1 | + 3 | +6 |
| 200 | − 8 | − 2 | +12 | +12 | +10 | + 6 | −19 | − 6 | −2 |
| 400 | −37 | −16 | + 5 | + 7 | +18 | − 5 | −16 | −30 | −8 |
| 600 | −60 | −22 | 0 | 0 | 0 | −28 | −18 | −21 | −4 |

TABLE 10

VARIATIONS IN LOG $\phi(M) + 10$ IN LF REGIONS

| $M_{pg}$ | Max. | Min. | Difference | Mean | Van Rhijn |
|---|---|---|---|---|---|
| −2 | 4.96 | 4.10 | 0.86 | 4.53 | 4.75 |
| −1 | 5.56 | 5.13 | .43 | 5.32 | 5.07 |
| 0 | 6.17 | 5.67 | .50 | 5.91 | 5.68 |
| +1 | 6.53 | 6.23 | .30 | 6.33 | 6.34 |
| +2 | 6.83 | 6.45 | .38 | 6.63 | 6.77 |
| +3 | 7.12 | 6.58 | .54 | 6.88 | 6.86 |
| +4 | 7.53 | 6.81 | .72 | 7.14 | 7.19 |
| +5 | 7.67 | 6.99 | .68 | 7.29 | 7.35 |
| +6 | 7.67 | 6.85 | .82 | 7.49 | 7.50 |
| +7 | 7.92 | 7.19 | 0.73 | 7.63 | 7.53 |

$M < +1$ compared to the standard function. A similar excess was found by Bok and Wright (1945), who compiled luminosity functions at 200 parsecs for seven fields ranging in galactic longitude from 40° to 332°. Miller and Hanna (1941) found fluctuations in log $\phi(M)$ somewhat smaller than those shown in Table 10.

Every effort has been made in this study to keep the magnitudes and colors for all LF regions on the same system, to make the spectral classifications consistent from region to region, and to keep the purely calculational errors in the density functions at a minimum. The *relative* changes in the values of $D_s(r)$ from region to region and at different distances in the same region should therefore reflect cosmic changes in the spatial contents of the Galaxy. Fluctuations in log $\phi(M)$ calculated from these densities should represent true variations of this important function.

There always exists, however, the possibility that combinations of errors in the basic data have yielded the variations in log $\phi(M)$ shown in Table 10 and Figure 8. The average range in log $\phi(M)$ for all LF regions corresponds to a mean error of $\pm 0.19$. From formula (1) we readily find that it would require an over-all fluctuation of $\pm 30$ per cent in the values of $D_s(r)$ to produce the observed fluctuation in log $\phi(M)$. It is not likely that the *relative* densities from region to region are so much in error. If we assume that a 15 per cent error from region to region is reasonable, then a residual dispersion of about $\pm 0.16$ in log $\phi(M)$ may be assigned to cosmic differences in the stellar population.

We conclude from this study that (1) the standard luminosity function derived by van Rhijn gives a good representation, on the average, of the stellar contents of space within 500 parsecs of the sun in the galactic plane; (2) there are fluctuations in log $\phi(M)$

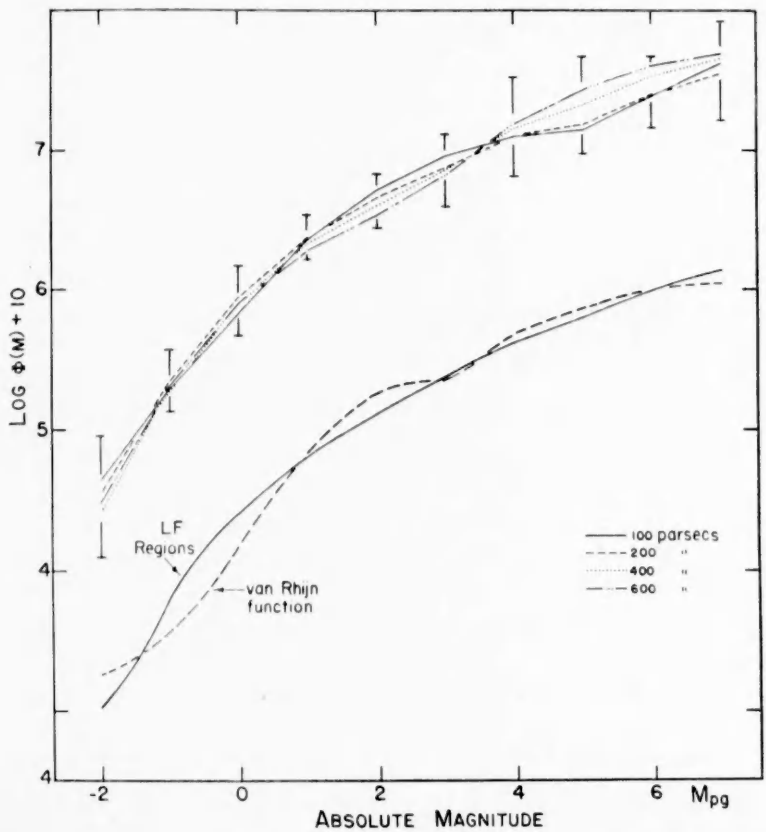


FIG. 8.—Variations in log $\phi(M) + 10$. The average luminosity functions for all LF regions at 100, 200, 400, and 600 parsecs are shown in the upper figure. Vertical lines indicate the range in log $\phi(M)$. The mean function for all regions and distances and the van Rhijn function are shown in the lower figure.

which may amount to a factor of 4 in $\phi(M)$ from region to region of this space; (3) for local studies, the values given in Table 8 may give a closer approximation to the actual state of affairs than would the use of the average function.

## REFERENCES

Bok, B. J. 1935, *Harvard Circ.*, No. 400.
———. 1937, *Distribution of the Stars in Space* (Chicago: University of Chicago Press).
———. 1945, *Ap. J.*, **101**, 293.
Bok, B. J., and Wright, F. W. 1945, *Ap. J.*, **101**, 311.
Farnsworth, A. H., and McCuskey, S. W. 1955, *Ap. J.*, **121**, 643.
Hulst, H. C. van de, Muller, C. A., and Oort, J. H. 1954, *B.A.N.*, **12**, 117.
Kamp, P. van de, and Vyssotsky, A. N. 1936, *A.J.*, **45**, 177.
McCuskey, S. W. 1941, *Ap. J.*, **94**, 468.
———. 1949*a*, *ibid.*, **109**, 139.
———. 1949*b*, *ibid.*, p. 414.
———. 1949*c*, *ibid.*, p. 423.
———. 1951, *ibid.*, **113**, 672.
———. 1951, *Pub. Obs. U. Michigan*, **10**, 67.
———. 1952*a*, *Ap. J.*, **115**, 479.
———. 1952*b*, *A.J.*, **57**, 147.
———. 1954, *Ap. J.*, **120**, 130.
McCuskey, S. W., and Seyfert, C. K. 1947, *Ap. J.*, **106**, 1.
Malmquist, K. G., and Hufnagel, L. 1933, *Pub. Stockholm Obs.*, Vol. 11, No. 9.
Miller, F. D., and Hanna, S. 1941, *A.J.*, **49**, 174.
Morgan, W. W. 1955, *Scient. American*, **192**, No. 5, 43.
Morgan, W. W., Whitford, A. E., and Code, A. D. 1953, *Ap. J.*, **118**, 318.
Nassau, J. J., and MacRae, D. A. 1949, *Ap. J.*, **110**, 40.
Nassau, J. J., and Morgan, W. W. 1951, *Pub. Obs. U. Michigan*, **10**, 43.
Oort, J. H. 1936, *B.A.N.*, **8**, 75.
Pannekoek, A. 1929, *Pub. Astr. Inst. Amsterdam*, No. 2.
Rhijn, P. J. van. 1936, *Groningen Pub.*, Vol. **47**.
Rhijn, P. J. van, and Schwassman, A. 1935, *Zs. f. Ap.*, **10**, 161.
Weaver, H. F. 1953, *A.J.*, **58**, 177.

# CORRELATION PROBLEMS IN THE STUDY OF THE BRIGHTNESS OF THE MILKY WAY

ALLADI RAMAKRISHNAN AND S. K. SRINIVASAN
Department of Physics, University of Madras, India
*Received August 8, 1955*

ABSTRACT

The problem of the fluctuations in the brightness of the Milky Way is studied from a new point of view—the correlation between the contributions to brightness from different parts of the astrophysical system. Besides extending the results obtained by Münch, this paper points out the relevance to the phenomenological theory of stochastic integration recently developed by one of us (R).

## INTRODUCTION

The problem of fluctuations in the brightness of the Milky Way, first formulated by Chandrasekhar and Münch (1950), has received considerable attention in the last few years. The solution of the fundamental integrodifferential equation of the problem was obtained by them under various conditions, while the stochastic features were stressed and explained by one of us (Ramakrishnan 1952, 1954*a*, *b*, 1955). But in view of Münch's recent paper (1955), fresh problems have arisen in investigating the correlation between the contributions to brightness from various parts of the astrophysical system.

Quite independently, in a different context, one of us (Ramakrishnan 1955*b*) dealt with similar correlation problems in the recent formulation of the phenomenological interpretation of integrals of random functions representing evolutionary stochastic processes. The theory finds direct application to the present case, and it is our present object to show that Münch's results are particular cases of our more general treatment. Incidentally, I had already obtained Münch's solution for $\Phi_n$ (see eq. [22] of his paper) (Ramakrishnan 1953) by a simpler method. Since this paper is in a sense a continuation of the previous work, familiarity with the general features and notation of the problem will be assumed. But as we are viewing the stochastic process from the point of view of integrals of random functions, we shall adopt a formulation suited to that purpose.

## FORMULATION OF THE PROBLEM

Assuming the astrophysical system to be one-dimensional, we suppose that the observer is at $A$ (see Fig. 1) and the system extends from $A$ to $B$, where $AB = t$. We

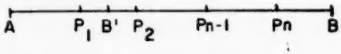


FIG. 1.—Realization of random clouds at $P_1, P_2, \ldots, P_n$. $AP_i = \tau_i$, $AB' = \kappa$

shall call $B$ the terminal point of the system. Any element of the system of length $d\tau$ at a distance $\tau$ from the observer emanates radiation of magnitude $\beta d\tau$ ($\beta$ can be set equal to unity by suitably choosing the unit of radiation), which, before reaching the observer, is intercepted by clouds occurring in a Poisson distribution, each cloud having a transparency factor between $q$ and $q + dq$, with probability $\psi(q)dq$. A case of particular physical interest is when the transparency factor is exactly $q$, i.e., $\psi(q') = \delta(q' - q)$, where $\delta$ is the Dirac delta function.

Let a typical realization of random clouds be represented by the occurrence of $n$ clouds in $AB$, the first between $\tau_1$ and $\tau_1 + d\tau_1$, the second between $\tau_2$ and $\tau_2 + d\tau_2, \ldots,$

the $n$th between $\tau_n$ and $\tau_n + d\tau_n$, where the $\tau$'s are measured from $A$. The corresponding transparency factors of the $n$ clouds lie between $q_1$ and $q_1 + dq_1$, $q_2$ and $q_2 + dq_2$, . . . , $q_n$ and $q_n + dq_n$, respectively. The probability of such a realization is given by

$$\lambda^n e^{-\lambda t} d\tau_1 d\tau_2 \ldots d\tau_n \psi(q_1)\psi(q_2)\ldots\psi(q_n)\, dq_1 dq_2 \ldots dq_n ,$$

$\lambda$ being the parameter of the Poisson distribution. Also $\lambda$ can be set equal to unity by choosing a suitable unit of $\tau$. The intensity as measured by the observer at $A$ is given by

$$I(t) = (t - \tau_n)\, q_1 q_2 \ldots q_n + (\tau_n - \tau_{n-1})\, q_1 q_2 \ldots q_{n-1} + \ldots + \tau_1 \qquad (t > \tau_n > \tau_{n-1} > \ldots > \tau_1) . \tag{1}$$

Thus $I(t)$ is a stochastic variate, and it is with its probability frequency function that all treatments of the problem have hitherto been concerned. We shall now deal with new features which present themselves when we consider the correlation problems relating to the stochastic process represented by $I(t)$.

The introduction of the concept of a stochastic process represented by $I(t)$ includes the idea of "evolution" with respect to the one-dimensional parameter $t$; to realize the process, we have to vary $t$ from an initial zero value to any value which we shall call the "duration" of the process. If the process is homogeneous in $t$, this variation can be made in two ways by moving either of the end-points of the interval $t$.[1] In the present case of astrophysical interest, this dual concept of evolution can be introduced by keeping the observer fixed at $A$ and moving the terminal point $B'$ of the partial system $AB'$ from $A$ to $B$ or by moving the observer from $B$ to $A$. The problem considered by Münch corresponds to the first case, but in view of the mathematical interest of the dual formulation we shall develop the theory in the two cases, which yield strikingly different results.

### CASE I: OBSERVER AT $A$ STATIONARY: PROCESS EVOLVES AS $B'$, TERMINAL POINT OF PARTIAL SYSTEM $AB'$, IS MOVED FROM $A$ TO $B$

In Case I, $B'$ is the terminal point of the partial system $AB' = \tau$; we are interested in $I(\tau)$, the amount of radiation from $AB'$ which reaches the observer at $A$. The function $I(\tau)$ does not evolve in a Markovian manner with $\tau$, for, if we were to increase $\tau$ to $\tau + d\tau$, the amount of radiation from the element reaching the observer would depend on the cumulative transparency factor $Q(\tau)$[2] of the clouds occurring in $AB'$, which in a sense implies the need for the knowledge of the history of the process before $\tau$. However, $Q(\tau)$ represents a Markovian process, and $\pi(Q;\ \tau)$, the probability frequency function (p.f.f.) of $Q(\tau)$, satisfies the equation[3]

$$\frac{\partial \pi(Q;\ \tau)}{\partial \tau} = -\pi(Q;\ \tau) + \int_q \pi\left(\frac{Q}{q};\ \tau\right)\frac{\psi(q)}{q}\, dq . \tag{2}$$

Using the Markovian property of $Q(\tau)$, we immediately obtain the joint probability that $Q(\tau_1)$ lies between $Q_1$ and $Q_1 + dQ_1$; $Q(\tau_2)$ lies between $Q_2$ and $Q_2 + dQ_2$, . . . , and $Q(\tau_n)$ lies between $Q_m$ and $Q_m + dQ_m$ as

$$\pi(Q_1, Q_2, \ldots, Q_m;\ \tau_1, \tau_2, \ldots, \tau_m)\, dQ_1 dQ_2 \ldots dQ_m = \pi(Q_1;\ \tau_1)\,\pi\left(\frac{Q_2}{Q_1};\ \tau_2 - \tau_1\right)\ldots\pi\left(\frac{Q_m}{Q_{m-1}};\ \tau_m - \tau_{m-1}\right)\frac{dQ_1 dQ_2 \ldots dQ_m}{Q_1 Q_2 \ldots Q_{m-1}} . \tag{3}$$

[1] We shall not be concerned with the practical difficulties in increasing $t$, a problem which falls within the province of physical experiment.

[2] Münch has used the notation $Q$ to denote an entirely different quantity. We are constrained to adopt the present notation to be in conformity with my earlier papers.

[3] In this paper $\int_x$ denotes integration over the whole domain of the variable $x$. Moreover, we shall use $\pi$ to denote any p.f.f.; the distinction between two functions will be apparent from the context.

The correlation function of $Q(\tau)$ can be obtained directly, once the foregoing expression is known. We have

$$E[Q(\tau_1)Q(\tau_2)\ldots Q(\tau_m)] = E[Q^m(\tau_1)]E[Q^{m-1}(\tau_2-\tau_1)]\ldots E[Q(\tau_m-\tau_{m-1})], \quad (4)$$

where $E$ denotes the expectation value of the product inside the brackets.

As one of us observed (Ramakrishnan 1954*b*), we can symbolically write

$$I(\tau) = \int_0^\tau Q(\tau'')\, d\tau''. \quad (5)$$

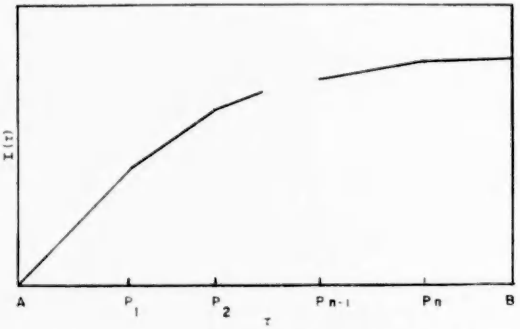


FIG. 2.—Realization of $I(\tau)$ as observed from $A$ when the terminal point $B'$ is moved from $A$ to $B$

If $I^R(\tau)$ is the realized value of $I(\tau)$, it describes a "trajectory" as $\tau$ varies from 0 to $t$, corresponding to a realization of random clouds at $P_1, P_2, \ldots, P_n$, as shown in Figure 1. The equation for $I^R(\tau)$ in the interval $(0, t)$ is given by

$$I^R(\tau) = (\tau-\tau_n)\, q_1q_2\ldots q_nH(\tau-\tau_n) + (\tau_n-\tau_{n-1})\, q_1q_2\ldots q_{n-1}H(\tau-\tau_{n-1}) + \ldots + \tau_1H(\tau-\tau_1), \quad (6)$$

where $H(x)$ is the Heaviside unit function. Accordingly, $H(x) = 0$ if $x < 0$; $H(x) = 1$ if $x > 0$. The trajectory of $I^R(\tau)$ is continuous for all $\tau$; however, its slope is discontinuous at $P_1, P_2, \ldots, P_n$ (see Fig. 2).

By the application of the theorem established by one of us (Ramakrishnan 1954*a*), the correlation functions $E[I(\tau_1)I(\tau_2)\ldots I(\tau_n)]$ can be obtained from the correlation functions of $Q(\tau)$:

$$E[I(\tau_1)\, I(\tau_2)\ldots I(\tau_m)] = \int_0^{\tau_1}\int_0^{\tau_2}\ldots\int_0^{\tau_m} E[Q(\tau_1'')\, Q(\tau_2'')\ldots Q(\tau_m'')] \times d\tau_1''\, d\tau_2''\ldots d\tau_m''. \quad (7)$$

[4] We have used $\tau''$ instead of $\tau'$ to denote the variable of integration, since in the next section $\tau'$ is used to denote the distance as measured from the end $B$.

Though it is difficult to obtain explicitly an expression for the correlation function of degree $m$ of $I(\tau)$ for a general $m$, it is quite easy to obtain the same for any given $m$. After some calculation, we obtain

$$E[I(\tau_1)\,I(\tau_2)]$$

$$= 2\left\{\frac{1-\exp-[\tau_1(1-q_2)]}{(1-q_1)(1-q_2)} - \frac{\exp-[\tau_1(1-q_1)]-\exp-[\tau_1(1-q_2)]}{(1-q_1)(q_1-q_2)}\right\}$$
$$+\frac{1}{(1-q_1)(q_1-q_2)}\{1-\exp-[\tau_1(q_1-q_2)]\}\{\exp-[\tau_1(1-q_1)]$$
$$-\exp-[\tau_2(1-q_1)]\}, \tag{8}$$

where

$$q_n = \int_0^1 q^n \psi(q)\,dq\,; \tag{9}$$

$$E[I(\tau_1)\,I(\tau_2)\,I(\tau_3)]$$

$$= 6\left\{\frac{1-\exp-[\tau_1(1-q_3)]}{(1-q_1)(1-q_2)(1-q_3)} - \frac{\exp-[\tau_1(1-q_2)]-\exp-[\tau_1(1-q_3)]}{(1-q_1)(1-q_2)(q_2-q_3)}\right\}$$
$$+4\,\frac{\exp-[\tau_1(1-q_1)]-\exp-[\tau_2(1-q_1)]}{(1-q_1)(q_1-q_2)}\left\{\frac{1-\exp-[\tau_1(q_1-q_3)]}{q_1-q_3}\right.$$
$$\left.-\frac{\exp-[\tau_1(q_1-q_2)]-\exp-[\tau_1(q_1-q_3)]}{q_2-q_3}\right\}$$
$$+2\,\frac{1-\exp-[\tau_1(q_2-q_3)]}{(1-q_1)(q_2-q_3)}\left\{\frac{\exp-[\tau_1(1-q_2)]-\exp-[\tau_2(1-q_2)]}{1-q_2}\right.$$
$$\left.-\frac{\exp-[\tau_2(1-q_1)]}{q_1-q_2}(\exp-[\tau_1(q_1-q_2)]-\exp-[\tau_2(q_1-q_2)])\right\} \tag{10}$$
$$+2\,\frac{\exp-[\tau_2(1-q_1)]-\exp-[\tau_3(1-q_1)]}{(1-q_1)(q_1-q_2)}\left\{\frac{1-\exp-[\tau_1(q_1-q_3)]}{q_1-q_2}\right.$$
$$\left.-\frac{\exp-[\tau_1(q_1-q_2)]-\exp-[\tau_1(q_1-q_3)]}{q_2-q_3}\right\}+\frac{1-\exp-[\tau_1(q_2-q_3)]}{q_2-q_3}$$
$$\times\frac{\exp-[\tau_1(q_1-q_2)]-\exp-[\tau_2(q_1-q_2)]}{q_1-q_2}$$
$$\times\frac{\exp-[\tau_2(1-q_1)]-\exp-[\tau_3(1-q_1)]}{1-q_1}.$$

In the particular case when $\psi(q') = \delta(q'-q)$, equation (8) reduces to a result obtained by Münch.

A complete description of the stochastic process is given if we are able to obtain the joint p.f.f. of $I(\tau_1), I(\tau_2), \ldots, I(\tau_m)$; to achieve this, we have to obtain the more detailed function, $\pi(I_1, I_2, \ldots, I_m; Q_1, Q_2, \ldots, Q_m; \tau_1, \tau_2, \ldots, \tau_m)$, representing the joint p.f.f. of the aggregate $I(\tau_i)$ and $Q(\tau_i)$ $(i = 1, 2, \ldots, m)$. This is readily obtained

by using standard probability arguments, which follow from studying the stochastic variate $I(t)$ as defined in equation (1):

$$\pi(I_1, I_2, \ldots, I_m; Q_1, Q_2, \ldots, Q_m; \tau_1, \tau_2, \ldots, \tau_m)\, dI_1 dI_2 \ldots \times dI_m dQ_1 dQ_2 \ldots dQ_m = \pi(I_1, Q_1; \tau_1)\, \pi\left(\frac{I_2 - I_1}{Q_1}, \frac{Q_2}{Q_1}; \tau_2 - \tau_1\right) \ldots \times \pi\left(\frac{I_m - I_{m-1}}{Q_{m-1}}, \frac{Q_m}{Q_{m-1}}; \tau_m - \tau_{m-1}\right) \frac{dI_1 dI_2 \ldots dI_m}{Q_1 Q_2 \ldots Q_{m-1}} \frac{dQ_1 dQ_2 \ldots dQ_m}{Q_1 Q_2 \ldots Q_{m-1}}. \tag{11}$$

The joint p.f.f. of the aggregate $I(\tau_i)$ alone can be obtained by integrating formula (11) over all $Q_i$'s. In principle, any kind of information about $I(t)$ can be obtained from formula (11).

In the case when $\psi(q') = \delta(q' - q)$, since $Q(\tau)$ can be written as $q^{n(\tau)}$, where $n(\tau)$, the number of random clouds in an interval of length $\tau$, is a stochastic variable which has a Poisson distribution, it is possible to define a function $\pi(I_1, I_2, \ldots, I_m; n_1, n_2, \ldots, n_m; \tau_1, \tau_2, \ldots, \tau_m)$, the joint p.f.f. of $n(\tau_i)$ and $I(\tau_i)$. By simple arguments we obtain

$$\pi(I_1, I_2, \ldots, I_m; n_1, n_2, \ldots, n_m; \tau_1, \tau_2, \ldots, \tau_m)\, dI_1 dI_2 \ldots dI_m = \pi(I_1, n_1; \tau_1)\, \pi\left(\frac{I_2 - I_1}{q^{n_1}}, n_2 - n_1; \tau_2 - \tau_1\right) \ldots \times \pi\left(\frac{I_m - I_{m-1}}{q^{n_{m-1}}}, n_m - n_{m-1}; \tau_m - \tau_{m-1}\right) q^{-(n_1 + n_2 + \ldots + n_{m-1})}\, dI_1 dI_2 \ldots dI_m \tag{12}$$

where $\pi(I, n; t)dI$ is the joint probability that $I(t)$ lies between $I$ and $I + dI$ and $n$ clouds occur between 0 and $t$. The function $\Phi_n$, defined by Münch, and $\pi(I, n; t)$ are connected by the relation

$$\pi(I, n; t) = \Phi_n(I; t)\, \frac{e^{-t} t^n}{n!}. \tag{13}$$

The quantity $\pi(I, n; t)$ has already been explicitly obtained by one of us (Ramakrishnan 1953), using the regeneration-point method; in that paper the notation $\pi_n(I; t)$ was used:

$$\pi(I, n; t) = -\frac{e^{-t}}{(n-1)!} \sum_{k=0}^{l-1} A_k^n (I - tq^k)^{n-1} \qquad (tq^l < I < tq^{l-1}),$$
$$A_k^n = \prod_{\substack{j=0 \\ j \neq k}}^{n} (q^j - q^k)^{-1}. \tag{14}$$

### CASE II: TERMINAL POINT $B$ STATIONARY: PROCESS EVOLVES AS OBSERVER AT $B'$ MOVES FROM $B$ TO $A$

We now deal with the evolution of the system from the following point of view. The observer is situated at $B'$, a point in the interval $AB = t$, and he measures the intensity $I^*(\tau')$ of the partial system $BB' = \tau'$ (the significance of the star notation will be explained presently), as distinguished from $AB'$ in the previous case. The system evolves as we move $B'$ from $B$ to $A$, keeping the end $B$ fixed. The realized trajectory of $I^*(\tau')$ as $\tau'$ varies from 0 to $t$, $\tau'$ being measured from the end $B$ corresponding to a realization

of random clouds at $P_1, P_2, \ldots, P_n$, is as shown in Figure 3,[5] i.e., $BP_n = \tau_1'$, $BP_{n-1} = \tau_2', \ldots, BP_1 = \tau_n'$.

The trajectory of $I^*(\tau')$ is characterized by a constant slope of magnitude unity except at the points $P_i$, where the realized value of $I^*(\tau')$ jumps down to $q_i$ times its value. Thus the mode of evolution of $I^*(\tau')$, which is characterized by the nature of its typical trajectory, is entirely different from that of $I(\tau)$. *However, the p.f.f. of* $I^*(\tau')$ *is identical with that of* $I(\tau)$ *if* $\tau = \tau'$, since both represent the intensity, as measured by an observer, of radiation from a system extending up to a distance $\tau$ from the observer. However, we note that $I^*(\tau')$ *evolves in a Markovian manner unlike* $I(\tau)$ *but in a direction*

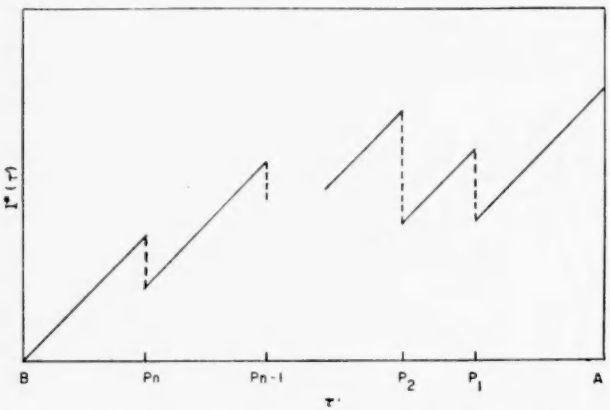


FIG. 3.—Realization of $I^*(\tau')$ as the observer at $B'$ is moved from $B$ to $A$

*opposite* to that of $I(\tau)$. The forward differential equation for the p.f.f. of $I^*(\tau')$ is obtained by studying the variation of $I^*(\tau')$ in the infinitesimal interval $(t < \tau' < t + \Delta)$, and this is precisely the well-known Chandrasekhar-Münch equation,

$$\frac{\partial \pi(I; t)}{\partial t} = -\pi(I; t) + \int_q \pi\left(\frac{I}{q}; t\right) \frac{\psi(q)\, dq}{q} - \frac{\partial \pi(I; t)}{\partial I}. \tag{15}$$

It represents, of course, the backward differential equation of the p.f.f. of $I(t)$.

While the distinction between the two processes $I(\tau)$ and $I^*(\tau')$ does not lead to distinct p.f.f.'s, it plays a fundamental role in computing the joint p.f.f. of $I^*(\tau')$ at various points—say at distances $\tau_1', \tau_2', \ldots, \tau_m'$ from the end $B$. Denoting the joint p.f.f. of $I^*(\tau')$ at $\tau_1', \tau_2', \ldots, \tau_m'$ by $\pi^*(I_1, I_2, \ldots, I_m; \tau_1', \tau_2', \ldots, \tau_m')$, we recognize that, in view of the Markovian nature of the evolution of $I^*(\tau')$, $\pi^*$ is given by

$$\begin{aligned}\pi^*(I_1, I_2, \ldots, I_m; \tau_1', \tau_2', \ldots, \tau_m') &= \pi(I_1; \tau_1')\, \pi(I_2 | I_1; \tau_2' - \tau_1') \ldots \\ &\quad \times \pi(I_m | I_{m-1}; \tau_m' - \tau_{m-1}'),\end{aligned} \tag{16}$$

where $\pi(I_i | I_{i-1}; \tau_i' - \tau_{i-1}')dI_i$ denotes the probability that the stochastic variate $I^*(\tau_i' - \tau_{i-1}')$ assumes a value between $I_i$ and $I_i + dI_i$, provided that at $\tau_i' - \tau_{i-1}' = 0$ it assumed the value $I_{i-1}$. We have to distinguish these functions from $\pi(I; \tau')$, the p.f.f. of $I^*(\tau_i' - \tau_{i-1}')$, the initial condition of which is specified by saying that $I^*(0)$ exactly as-

[5] Since in graphs, it is customary to have the origin of the abscissa to left, $B$ in Fig. 3 is situated to the left of $A$. Note that $P_n$ is the first random point when counted from $B$.

sumes the value 0. It is easily seen that $\pi(I_i|I_{i-1};\tau_i'-\tau_{i-1}')$ is the p.f.f. of the stochastic variate $I^*(\tau_i')+I_{i-1}Q(\tau_i'-\tau_{i-1}')$. It satisfies the same type of equation (13) with the initial condition that it assumes the value $I_{i-1}$ at $\tau_i'-\tau_{i-1}'=0$.

There is a more convenient way of obtaining $\pi^*$ by defining $\pi^*(I_1, I_2, \ldots, I_m; Q_1, Q_2, \ldots, Q_m; \tau_1', \tau_2', \ldots, \tau_m')$ as the joint p.f.f. of the aggregate $I^*(\tau_i')$ and $Q(\tau_i')$ $(i=1, 2, \ldots, m)$, the $\tau_i'$'s being measured from $B$, for which an expression can be immediately written in terms of the function $\pi(I, Q; t)$ as in case I:

$$\pi(I_1, I_2, \ldots, I_m, Q_1, Q_2, \ldots, Q_m; \tau_1', \tau_2', \ldots, \tau_m')\, dI_1 dI_2 \ldots$$

$$\times dI_m dQ_1 dQ_2 \ldots dQ_m = \pi(I_1, Q_1; \tau_1')\, \pi\left(I_2 - I_1\frac{Q_2}{Q_1}, \frac{Q_2}{Q_1}; \tau_2'-\tau_1'\right)\ldots \tag{17}$$

$$\times \pi\left(I_m - I_{m-1}\frac{Q_m}{Q_{m-1}}, \frac{Q_m}{Q_{m-1}}; \tau_m'-\tau_{m-1}'\right)\frac{dI_1 dI_2 \ldots dI_m dQ_1 dQ_2 \ldots dQ_m}{Q_1 Q_2 \ldots Q_{m-1}}.$$

Every kind of information about $I^*(\tau')$ can be obtained from formula (16).

As before in the special case when $\psi(q')=\delta(q'-q)$, we can define $\pi^*(I_1, I_2, \ldots, I_m, n_1, n_2, \ldots, n_m; \tau_1', \tau_2', \ldots, \tau_m')$, the joint p.f.f. of $I^*(\tau_i')$ and $n(\tau_i')$. Using simple probability arguments, we obtain

$$\pi^*(I_1, I_2, \ldots, I_m, n_1, n_2, \ldots, n_m; \tau_1', \tau_2', \ldots, \tau_m')\, dI_1 dI_2 \ldots dI_m$$

$$= \pi(I_1, n_1; \tau_1)\, \pi(I_2 - I_1 q^{n_2-n_1}, n_2-n_1, \tau_2'-\tau_1')\ldots \tag{18}$$

$$\times \pi(I_m - I_{m-1}q^{n_m-n_{m-1}}, n_m-n_{m-1}, \tau_m'-\tau_{m-1}')\, dI_1 dI_2 \ldots dI_m.$$

As we are in possession of an explicit expression for $\pi(I, n; t)$, we have formally obtained the joint p.f.f. of $I^*(\tau')$ at $\tau_i'(i=1, 2, \ldots, m)$. It is interesting to note the striking difference between formulae (18) and (12) except in the simple case $m=1$, when they are identical.

In my notation, $I^*(\tau')$ can be symbolically represented by the integral

$$I^*(\tau') = \int^{\tau'} Q(\tau'-\tau'')\, d\tau'', \tag{19}$$

as distinguished from $I(\tau)$ as given by equation (5), to suggest that in the case of $I^*(\tau')$, the $Q$'s are computed from a moving origin as the $I^*(\tau')$ process evolves with $\tau'$. The details of the dual formulation of the stochastic integration of $Q$ or other processes associated with a basic Poisson distribution of points along the $\tau$-axis are given in the author's (Ramakrishnan 1956) comprehensive treatment of the phenomenological interpretation of integrals of random functions. The present problem of astrophysical interest is a direct illustration of a particular aspect of that theory.

## REFERENCES


Chandrasekhar, S., and Münch, G. 1950, *Ap. J.*, **112**, 380.
Münch, G. 1955, *Ap. J.*, **121**, 291.
Ramakrishnan, Alladi. 1952, *Ap. J.*, **115**, 141.
———. 1953, *Proc. Cambridge Phil. Soc.*, **49**, 473.
———. 1954*a*, *Ap. J.*, **119**, 443.
———. 1954*b*, *ibid.*, p. 682.
———. 1955, *ibid.*, **122**, 24.
———. 1956, *Proc. Kon. Ned. Akad. Wetensch*, **58**, 470, 634, and **59**, 120.

# ON THE OPTICAL PROPERTIES OF INTERSTELLAR DUST

JOHN R. PLATT
University of Chicago
*Received November 5, 1955; revised December 14, 1955*

ABSTRACT

Solid particles of less than 10 A in radius grown by random accretion from interstellar gas would be expected to be generally opaque and highly reflecting in the visible region and paramagnetic and quasi-metallic, even if formed from light atoms, because their energy bands will, in general, be unfilled. Their ellipticity and optical anisotropy is estimated. It appears that interstellar reddening and polarization might be explainable by the quantum-mechanical optical and statistical properties of such tiny particles, with normal cosmic composition, provided that they have random geometrical and electronic structure.

The apparently peculiar combination of properties empirically indicated for interstellar dust particles (Greenstein 1951)—high visible absorption coefficient per unit mass, high albedo, and considerable magnetic moment and ellipticity—becomes less peculiar and is, in fact, just what is expected for tiny particles ($3 \times 10^{-3}\ \lambda$) of normal cosmic composition as soon as it is assumed that *their electronic energy bands are usually unfilled*.

There is no reason to suppose that small particles grown by random low-temperature accretion from a gas plasma containing many ions and radicals will be any more chemically stable or electrically neutral than the gas molecules themselves or that they will generally have filled energy bands such as are required to form a dielectric, for example. The optical properties of a particle should not depend very much on its exact state of charge; but they should depend strongly on whether the number of electrons present does or does not fill the energy bands of the system in its particular geometrical atomic arrangement. Even if a system does have a filled energy band at one instant, there are more ways of losing this property than of preserving it during a random gain or loss of electrons, ions, or atoms, so that the energy bands of intrastellar particles would be expected to be unfilled most of the time. Optically, the most comparable terrestrial species will therefore be radicals and unsaturated compounds. Applying the evidence on such molecules to the interstellar dust problem suggests the following conclusions.

A. *The longest wave length, $\lambda$, of strong allowed absorption parallel to the largest diameter, $l$, of a particle will probably be of the order of $gl$, where $g$ is about 400.*

Empirically, radicals, even small ones, usually have strong visible absorption. Unsaturated organic compounds containing first-row atoms show a first strong absorption wave length that generally increases as the molecular diameter parallel to the direction of polarization increases. This is shown in Figure 1 for chain dyes and two-dimensional conjugated organic compounds containing hydrogen, carbon, nitrogen, and oxygen and the three-dimensional decaborane, $B_{10}H_{14}$ (Platt and Klevens 1950, 1954, 1956). The heavy points are for the strongest allowed transitions. Numerous chain dyes fall on a line with $g = 410$; for example, an even-electron amidinium ion with only 9 conjugated atoms and about 12 A long absorbs near 5000 A with a molar extinction coefficient of nearly 200000 and an oscillator strength of nearly 2.

These results have been accounted for theoretically in terms of a free-electron approximation like that for metals. The transition energies far from the top of an energy band can be estimated from the free-electron energy-level density. For a rectangular particle of dimensions $l$, $w$, and $h$, the orbital energies are

$$\epsilon = \frac{h^2}{8m}\left(\frac{n_l^2}{l^2} + \frac{n^2}{w^2} + \frac{n_h^2}{h^2}\right).$$

The allowed transitions parallel to each co-ordinate will be given by $\Delta n = \pm 1$ in that co-ordinate, with energies of the order of

$$E_l \simeq \frac{h^2}{8m}\frac{2n_L}{l^2} = 154\,\frac{2n_L}{L^2} \times 10^3 \text{ cm}^{-1},$$

and so on. Here $n_L$ is the largest occupied value of $n_l$; $L$ is the number of atoms in $l$; and the numerical coefficient is for an interatomic distance of 1.40 A. There may, of course, be numerous forbidden transitions at still lower energies.

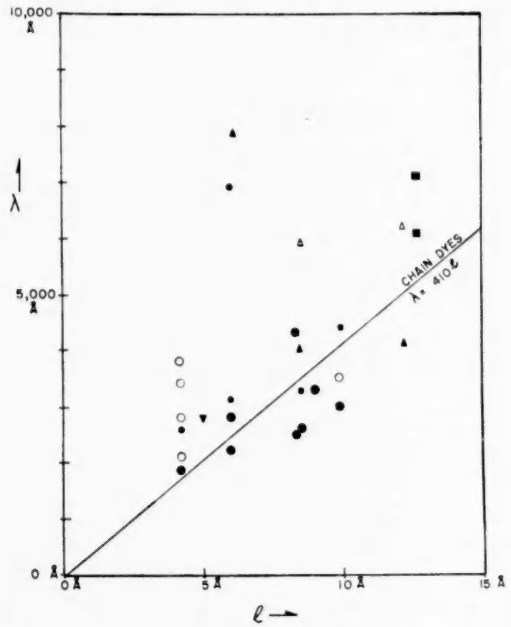


FIG. 1.—First absorption wave lengths versus molecular diameter parallel to the direction of polarization, for molecules with unfilled energy bands. Small and hollow points show different classes of forbidden transitions; large solid points indicate allowed transitions. *Circles*, condensed-ring hydrocarbons; *triangles*, porphyrins; *squares*, other dyes; *inverted triangle*, decaborane.

For a single line of atoms like the chain dyes with one optical electron per atom, $2n_L = L$. The wave length of strong allowed absorption is then proportional to the length,

$$\lambda \sim 650\, L \text{ angstroms} = 460\, l,$$

the numerical coefficient of $L$ being the reciprocal of that above, for the same interatomic distance; so that, theoretically, $g$ is 460. (It is easily seen that the value of $g$ is a small multiple of 137, because an electron oscillating from side to side in the solid travels more slowly by about this factor than the light-wave it is emitting or absorbing.)

For a three-dimensional system the numerical values should still be of the same order of magnitude, but larger for larger interatomic distances and smaller for more optical electrons per atom. (In Fig. 1 the wave lengths for the two-dimensional systems spread

on each side of those for the linear systems of the same dimensions.) The quasi-classical proportionality between wave length and molecular size would be generally expected from dimensional arguments. It is true that, in a macroscopic piece of metal such as an antenna, the electronic interaction has a classical retarded potential that shortens the absorption wave length to only twice the largest diameter or antenna length and so brings $g$ down to a classical value of 2; but, in molecules a few angstroms across, the interaction only reduces the quantum-mechanical value of $g$ as given previously by the order of 10 per cent, empirically and theoretically. This makes a difference by a factor of about 200 between the wave lengths involved in a classical theory of absorption or scattering by molecular-size particles and those in a quantum-mechanical theory.

The general numerical agreement of Figure 1 with the quantum-mechanical expectations makes it possible to extrapolate with some confidence to the case of interstellar dust particles with unfilled energy bands. With $g$ of the order of 400, a roughly spherical particle of about 6 A in radius, containing about 500 atoms, would, in general, be large enough to absorb intensely in the visible; and one of only 25 A in radius and less than $10^5$ atoms would absorb to about 2 $\mu$. At these wave lengths there might also be weaker forbidden transitions of even tinier objects. (As a prototype of this class, perhaps one might think of the $C_3$ radical, less than 3 A long, which is now supposed to be a cosmically important continuous ultraviolet absorber and emitter.) Such particle dimensions are smaller than is often supposed in discussions based on classical scattering or reflection theory, and they permit a decrease by several powers of 10 in the bulk of "dust" assumed necessary to account for interstellar reddening.

The particles are still large enough to have a statistical distribution of structures and to make a fairly uniform statistical distribution of spectra. Figure 1 shows that, even for particles of similar type and similar size, there will probably be a distribution of long-wave-length absorption limits over a factor of 2 or more in wave length because of their different particular structures. This spread would have to be taken into account in estimating particle sizes from reddening curves. It may be that particular polyatomic small particles or compounds will recur often enough and will have sharp enough spectra to give discrete structure to the interstellar absorption-curve, as, of course, some of the diatomics do.

Unfortunately, there appears to be no present theory that will give more exactly the wave-length dependence of extinction or polarization for the structurally random particles postulated here. The LCAO molecular-orbital theory gives results for particular structures but is neither simple nor accurate; for example, the predicted intensities of the first absorption in a number of important cases are too high by a factor of 100. This would be of little astronomical importance, since there is usually a second absorption band within a few hundred A and of high intensity; but it weakens confidence in the reliability of the theory when applied to unknown structures. Both the empirical and the theoretical locations of the first absorption bands are very sensitive to local structural details, with wave lengths of conjugated compounds being two or three times longer when an odd-membered ring system is present than when it is not. Much more theoretical work would be needed before the wave-length dependence of structurally random particles of a given size could be estimated reliably; and detailed inferences about the size distribution of the present type of particles from the interstellar reddening-curve must therefore be postponed. The aim here is only to show the order of magnitude of the sizes and how much it differs from the classical expectations.

B. *The absorption cross-section of the particles is likely to be roughly constant and equal to the geometrical cross-section down into the ultraviolet.*

Braude (1950) has pointed out that the peak absorption cross-section of planar unsaturated molecules is approximately the geometrical cross-section. For hydrocarbons in solution, the absorption rarely falls by more than a factor of 10 in any minimum after the first peak. Consequently, a particle ten layers thick should also reach approximately

geometrical absorption cross-sections even in the minima. If each layer were a different size, as in the approximately spherical carbon-smoke particles of graphite structure, where each layer is a condensed-ring system, each would absorb at different peak wave lengths and produce opacity over a wide range of wave lengths. These are artificial models of the dust but may give a qualitative picture of its properties.

The intensity of absorption should then be, like the free-electron wave length of absorption, quasi-metallic in character. The opaque colored crystals of organic dyes are frequently described as having a metallic sheen. These may contain only hydrogen, carbon, nitrogen, and oxygen, the commonest interstellar combining elements. An abundance of heavy atoms is not necessary to give a metallic character.

C. *The albedo in the visible region may be large, perhaps near unity.*

After absorption, a small isolated particle should lose infrared or visible light-energy principally by reradiation, since chemical dissociation usually requires more energy. Reradiation of the same frequency will be fast, with lifetimes of the order of $10^{-9}$ seconds for strong allowed transitions in the visible. The only competing processes will involve thermal degradation, with radiation of infrared vibrational frequencies combined with lower-energy electronic emission. The frequency factor will make the latter processes slow; and, for small particles with only a few strong dipole vibrational modes, this degradation may not compete in probability with nondegraded reradiation. Macroscopically, reradiation is equivalent to random reflection and will give the dust particles a high albedo. Greenstein inferred that the degree of forward scattering was also high in interstellar dust. The present particles reradiate isotropically and do not show this feature.

D. *Most of the particles will be paramagnetic.*

All the odd-electron systems and those even-electron systems that have unpaired electrons will be paramagnetic. The orbital energies for a three-dimensional particle will be close together, much closer than indicated by the allowed transition energy. With close-packed orbitals, the Hund rule will commonly give rise to ground states of high total spin with many unpaired electrons. Stable paramagnetic systems and highly colored systems are easy to produce in light-atom solids, even in the laboratory and at room temperature, by the random processes of radiation damage. Again, the assumption of heavy or metallic atoms in the particles is unnecessary.

E. *The particles will not be perfectly spherical and should give several per cent polarization if aligned with their long axes (or short axes) all parallel.*

The present remarks do not bear on the problem of how alignment comes about, except to say that for very small particles it is transformed into a quantum-mechanical problem. If there is any mechanism that would align large metal-containing (not necessarily ferromagnetic) particles in a weak magnetic field (Davis and Greenstein 1951), it should have an equally valid analogue for the present paramagnetic particles. (The analogue of the Davis-Greenstein mechanism of paramagnetic energy dissipation by rotation in a field would apparently be dissipation by radiative transitions between the rotational Zeeman levels.) Likewise, if the particles are not exactly spherical, dynamical alignment of the axes of rotation after collision with a streaming gas cloud might produce some degree of optical anisotropy, as Gold (1952, 1955) has suggested.

Regardless of the mechanism, if alignment does take place, the order of magnitude of the optical anisotropy of the present particles can be estimated by estimating their eccentricity. For simplicity, consider a hypothetical solid cube formed from a simple cubic lattice in which the lengths of each row, column, and file have been allowed to grow at random to an average length of $n$ atoms, with a total volume of $n^3$ or $N$ atoms. The root-mean-square variation in each such line of atoms will be $n^{1/2}$. The average variation in one dimension of the cube will be less by the square root of the number, $n^2$, of parallel lines of atoms; it will be $n^{-1/2}$. The relative r.m.s. variation in any dimension will then be $n^{-3/2}$ or $N^{-1/2}$.

For a near-spherical particle of $N$ atoms, the relative variation in an arbitrary average diameter will be of the same order, perhaps a little larger, since the diameters are longer than $n$ atoms; and the maximum variation between the axes of the prolate ellipsoid that fits the particle best will be of the same order, or perhaps a little larger, since the r.m.s. maximum variation will be larger than the r.m.s. variation between random axes.

If a 500-atom particle has a strong allowed absorption in the visible, its relative r.m.s. variation of axes should then be of the order of $500^{-1/2}$, or 0.045, or perhaps larger. If many such particles could be lined up with their longest (or shortest) axes parallel, conclusion A shows that the first strong parallel absorption should be at wave lengths averaging about 4.5 per cent (or more) longer than the first perpendicular absorption. Call this wave length variance $\delta\lambda$. The variation in absorption coefficient, $\delta k$, in the two directions will then be $\delta\lambda dk/d\lambda$, and the relative polarization, $\delta k/k$ will be about

$$\frac{\delta k}{k} = \frac{1}{k}\frac{dk}{d\lambda}\,\delta\lambda .$$

If $k$ varies about as $1/\lambda$, which is the observed approximate interstellar dependence in the visible region, $\delta k/k$ will be also about 0.045, or perhaps larger. This is of the order of magnitude observed for the maximum interstellar relative polarization (Greenstein 1951; Davis and Greenstein 1951). If still smaller particles are sufficiently numerous for their weak long-wave-length forbidden bands to contribute importantly to the visible absorption, they would have substantially larger values of $\delta k/k$ and would not require complete alignment to give the observed maximum relative polarization.

The wave-length dependence of the polarization for perfectly aligned, but structurally random, particles of a given size is as difficult to predict theoretically as that of the absorption coefficient. The ratio of polarization to extinction for allowed transitions, according to the present assumptions, should certainly decrease with increasing wave length for perfectly aligned particles, contrary to the observations; but how the alignment depends on particle size and wave length depends on the alignment mechanism, a question that will have to be re-examined for quantum-mechanical particles. In any case, the order-of-magnitude numerical agreement shown here for allowed transitions in the visible region gives an upper limit and shows that the particles cannot be more than a few angstroms in diameter if they are randomly quasi-spherical; and, subject to this assumption, it gives independent support to the dimensions estimated from wave-length arguments in conclusion A. In order for larger particles than those assumed here to be sufficiently nonspherical to give the right order of polarization, there must be some very nonisotropic mechanism of formation; such processes are available, equilibrium molecular crystallization being one, for example, but it would be satisfying not to have to invoke them generally in interstellar space.

I am indebted to Dr. B. D. Donn for helpful discussions of some of these questions. Some of his studies on initial particle chemistry, which seem to have a bearing on the present ideas, are to be published shortly.

## REFERENCES

Braude, E. A. 1950, *J. Chem. Soc.*, **1950**, 379.
Davis, L., Jr., and Greenstein, J. L. 1951, *Ap. J.*, **114**, 206.
Gold, T. 1952, *Nature*, **169**, 322.
———. 1955, *Mém. Soc. R. Sci. Liège*, **15**, 591.
Greenstein, J. L. 1951, *Astrophysics*, ed. J. A. Hynek (New York: McGraw-Hill Book Co.), chap. xiii.
Klevens, H. B., and Platt, J. R. 1954, *Survey of Vacuum Ultraviolet Spectra* (ONR Technical Report, Department of Physics, University of Chicago).
Platt, J. R. 1950, *J. Chem. Phys.*, **18**, 1168.
———. 1954, *ibid.*, **22**, 1448.
———. 1956, *ibid.*, **24** (in press).

# NONTHERMAL RADIO EMISSION OF THE GALAXY AND THE ORIGIN OF COSMIC RADIATIONS*

C. Y. FAN
Yerkes Observatory, University of Chicago
*Received January 5, 1956*

ABSTRACT

Based on the general scheme of Fermi's theory of the origin of cosmic radiation, the possibility of the acceleration of high-energy electrons required for the production of the nonthermal radio emission of the Galaxy is investigated. It is found that the energy spectrum of these electrons assumes the form of $(w_m - w)^{s-1}/(w - w_i)^{s+1}$, where $w_m$ is the maximum energy attainable and $w_i$ is the minimum initial energy (the injection energy) for which an electron can be accelerated. A particular set of data which is compatible with the present knowledge of the galactic structures yields $w_m = 14$ Bev, $w_i = 0.06$ Bev, and $s = 1.6$. The total number of such high-energy electrons sufficient for the production of the observed intensity of radio emission is of the order of $10^{-12}$/cm.$^3$ The spectrum of the radio emission is $1/\nu$ when the tentatively chosen data are used. These results seem to be compatible with observations.

## I. INTRODUCTION

In 1949 Fermi published his first version of the origin of cosmic radiation (Fermi 1949); later, in 1954, he revised his theory (Fermi 1954) to meet the demand of the similarity of the energy spectra of protonic and nuclear components which had been discovered in the meantime. The basis of Fermi's revised theory is expressed in the following assumptions: (1) The cosmic-ray particles are accelerated in the Galaxy. (2) A cosmic-ray particle, regardless of its charge, gains its energy at the rate

$$\frac{dw}{dt} = \frac{w}{A_0}, \tag{1}$$

where $w$ is the energy of the particle, including the rest-mass, and $A_0$ is the time scale of the acceleration; $A_0$ must be comparable to the mean life of a heavy cosmic-ray nucleus as determined by nuclear collisions with interstellar particles. (3) The cosmic-ray particles are eliminated from the Galaxy at a rate governed by the statistical law,

$$p\,(t)\,dt = \frac{dt}{B}\exp\left(-\frac{t}{B}\right). \tag{2}$$

On these assumptions, the power law,

$$\frac{dn}{dw} \sim \frac{1}{w^{1+s_0}}, \tag{3}$$

where

$$s_0 = \frac{A_0}{B}, \tag{4}$$

readily follows. The exponent $s_0$ is the same for both the protonic and the nuclear components. In developing his theory, Fermi suggested that cosmic-ray particles are accelerated by interactions with interstellar magnetic fields and that they are eliminated from the Galaxy by straightforward leakage. The set of values $A_0 = 4 \times 10^6$ years, $B = A_0/1.4$ years yields the observed spectrum.

* The research reported in this paper has been supported in part by the Geophysical Research Directorate of the Air Force Cambridge Research Center.

Within the framework of Fermi's theory, efforts have been made by various authors to make his acceleration mechanisms meet the demands of efficiency implied by the short-time scale $A_0$. Recent investigations by Davis (1956) and by Fan (1956) (referred to hereafter as "Paper I") indicated that a mechanism seems to exist which is compatible with our present knowledge of the galactic structure. The question then arises as to whether or not the mechanism is also efficient enough to accelerate high-energy electrons. It will be seen that this question has a bearing on the origin of cosmic radiation, on the one hand, and on the origin of the nonthermal radio emission of the Galaxy, on the other.

The distribution of the sources of radio emission in the Galaxy is now fairly well established (see Brown 1954), and the following picture emerges: (1) concentrated emission toward the galactic center; (2) a distribution away from the galactic plane and almost uniformly around the galactic center in a sphere of a radius of the order of 10 kpc (the "galactic halo"); and (3) discrete sources associated with extended nebulosities with fine filamentary structures and high internal motions.

In radio-frequency measurements the power $P$ of the radio emission in a frequency band $\Delta\nu$ at frequency $\nu$ received by a radio telescope is customarily expressed in terms of an effective aerial temperature, $T_A$. This is essentially equal to the temperature of a black body, which will emit the same power as the source in a frequency band $\Delta\nu$ at $\nu$. An aerial inside a box at temperature $T$ receives power at the rate of

$$P = ATv^2\Delta\nu\,, \tag{5}$$

where $A$ is a constant. Thus

$$T_A \sim \left(\frac{P}{\Delta\nu}\right)\lambda^2\,, \tag{6}$$

where $\lambda$ is the wave length of the radio emission considered. It is found (Pawsey and Bracewell 1955) that the galactic radio emission in the wave-length region 1–20 meters has the spectrum

$$T_A \sim \lambda^x\,, \tag{7}$$

where $x$ has a value between 2.5 and 2.8. This power law cannot be explained in terms of thermal emission from the interstellar gas.

It was suggested by Alfvén and Herlofson (1950) and independently by Kiepenheuer (1950) that the radio emission could be synchrotron radiation, that is, radiation from high-energy electrons spiraling around magnetic lines of force. Recent investigations on the Crab Nebula by Shklovsky (1953*a*), Vashakidze (1954), Dombrosvsky (1954), and Oort and Walraven (1956) have shown that the optical emission is polarized to a surprisingly high degree. Now a high degree of polarization is one of the characteristic features of synchrotron radiation. This discovery suggests that the earlier interpretation of the general radio emission as synchrotron radiation is likely to be correct. The strongest argument in its favor is its high efficiency. Therefore, a mechanism for the acceleration of high-energy electrons is needed.

On the other hand, there is definite evidence that primary cosmic radiation contains practically no electrons of energy higher than 5 Bev. The critical problem is whether or not the mechanism which fits Fermi's general scheme for the acceleration of cosmic radiation is capable of accelerating electrons to energies high enough to account for the nonthermal radio emission of the Galaxy but not too high to conflict with the measurements of cosmic radiation. This paper is devoted to an examination of this question; earlier considerations of this problem are due to Shklovsky (1953*b*), Pikel'ner (1953), and Ginsberg (1953). It is found that the mechanism does seem to fulfil both the requirements; and this fact may be considered as lending support to a galactic origin for the cosmic rays.

## II. ENERGY SPECTRUM OF COSMIC-RAY ELECTRONS

The general equation describing the rate of energy gain of a cosmic-ray electron differs in several respects from equation (1) because energy losses, which can be neglected in considering the acceleration of cosmic-ray ions, must now be taken into account. First, there is the energy loss by synchrotron radiation; this is inversely proportional to the fourth power of the mass of a charged particle and proportional to the square of its kinetic energy (Schwinger 1949). This produces a high-energy cutoff, $w_m$, in the energy spectrum. Second, there is the energy loss due to bremsstrahlung, which is inversely proportional to the square of the mass and directly proportional to its kinetic energy. This reduces the rate of energy gain of a cosmic-ray electron (see Bethe and Ashkin 1953). Third, there is the energy loss due to inelastic collisions with interstellar particles; this determines the required minimum initial energy (the injection energy), $w_i$, for which an electron can be accelerated. The value of $w_i$ for the acceleration of an electron is comparable with the injection energy for the acceleration of a proton; however, since $w_i$ is several hundred times higher than the rest-energy of the electron (see Sec. IV) and since the energy spectrum of cosmic-ray electrons is limited to only several Bev in the range $(w_i, w_m)$, the injection energy must be included in considering the energy spectrum of cosmic-ray electrons, although it is often ignored in considering the spectra of protonic and nuclear components. Including these various factors, we may write the general equation governing the rate of energy gain of a cosmic-ray electron in the form

$$\frac{dw}{dt} = 2\alpha_0 w - 2\alpha_1 w - k^2 w^2 - k_0^2 = 2\alpha w - k^2 w^2 - k_0^2 , \tag{8}$$

where $2\alpha_0 = 1/A_0$, $\alpha = (\alpha_0 - \alpha_1)$, and $-k^2w^2$, $-2\alpha_1 w$, and $-k_0^2$ represent the energy loss per unit time due to synchrotron radiation, bremsstrahlung, and inelastic collisions, respectively. To a sufficient approximation, $k$, $\alpha_1$, and $k_0$ can be regarded as constants.

Let

$$b = (\alpha^2 - k^2 k_0^2)^{1/2} \tag{9}$$

and

$$w_i = \frac{a - b}{k^2} \qquad \text{and} \qquad w_m = \frac{a + b}{k^2} \tag{10}$$

be the two roots of the quadratic expression in $w$ on the right-hand side of equation (8), which can then be rewritten as

$$\frac{dw}{dt} = k^2 (w - w_i)(w_m - w) . \tag{11}$$

It can be seen that if $\alpha > 0$ and $\alpha^2 - k^2 k_0^2 > 0$, an electron with its initial energy $w_0$ in the range $(w_i, w_m)$ will be accelerated; $w_i$ is thus the injection energy, and $w_m$ is the maximum energy attainable by an electron.

A simple integration of equation (11) yields

$$\frac{w - w_i}{w_m - w} = \frac{w_0 - w_i}{w_m - w_0} e^{2bt} . \tag{12}$$

Now let the process which eliminates cosmic-ray ions from the Galaxy also be responsible for the elimination of electrons; and let the constant $B$ in equation (2), governing the rate of this elimination, also be the same. Then the energy spectrum of cosmic-ray electrons with $w_0$ as a parameter is readily found to be

$$\frac{dn_e}{dw} \sim \frac{s (w_0 - w_i)^s (w_m - w_i)}{(w_m - w_0)^s} \frac{(w_m - w)^{s-1}}{(w - w_i)^{s+1}} , \tag{13}$$

where

$$s = \frac{1}{2\,bB}. \tag{14}$$

The complete energy spectrum cannot be determined without a knowledge of the spectrum of initial energies. However, if we assume that the initial-energy spectrum has a negligible amount of electrons of energy higher than $w_c(>w_i)$, then the energy spectrum for $w \geq w_c$ will be quite accurately given by

$$\frac{dn_e}{dw} = J_0 \frac{(w_m - w)^{s-1}}{(w - w_i)^{s+1}} \qquad (w_m \geq w \geq w_c)\,, \tag{15}$$

where $J_0$ is a constant.

## III. THE EVALUATION OF THE CONSTANTS

For evaluating the constants $a_0$, $k^2$, $a_1$, and $k_0^2$, we need the density distribution of the interstellar medium, the strength of the galactic magnetic field, and a description of the motion of electrons in interstellar space. The following set of data, which was used for the calculation of the acceleration of cosmic-ray ions in Paper I as compatible with our present astronomical knowledge, will also be used here.

*a*) *Composition and density of interstellar medium between interstellar clouds.*—Protons, 0.6/cm³; helium, 0.04/cm³; ions of atomic charge $Z = 10$, 0.0005/cm³. The composition of interstellar clouds is assumed to be the same as the interstellar medium, but with a density sixteen times higher (10 protons/cm³). The clouds fill about 7 per cent of the space of the spiral arm of the Galaxy.

*b*) *Interstellar magnetic fields.*—The general magnetic field, $H_0$, is taken to be $10^{-5}$ gauss, and the magnetic field in interstellar clouds, $H_1$, is assumed to be $4 \times 10^{-5}$ gauss, in accordance with the concept of equipartition of kinetic and magnetic energies.

*c*) *The motion of a cosmic-ray particle in interstellar space.*—It was shown in Paper I that during the process of acceleration the angle between the momentum vector of the particle and the general galactic magnetic field $H_0$ will gradually reach an equilibrium angle $\theta_e$, which is of the order of $\sin^{-1}(H_0/H_1)^{1/2}$. With the present assigned values of $H_0$ and $H_1$, $\theta_e = 30°$. On this simplified model, the particle spirals along the magnetic lines of force with an angle of pitch, $\theta$, equal to 30° in the space between interstellar clouds and equal to $\pi/2$ when in the clouds (cf. Paper I). The fraction of time the particle finds itself inside the interstellar clouds will be assumed to be the fraction of the space occupied by the clouds, which is 7 per cent. With the foregoing data, the evaluation of the constants is straight-forward.

From the observed spectrum of the cosmic rays, we take

$$2a_0 = \frac{1}{A_0} = 8.1 \times 10^{-15}/\text{sec}\,; \qquad B = \left(\frac{A_0}{1.4}\right) \text{sec}\,. \tag{16}$$

The energy loss per unit time due to synchrotron radiation is given by (Schwinger 1949)

$$-\left(\frac{dw}{dt}\right)_H = \frac{2\,c}{3}\left(\frac{e}{m\,c^2}\right)^4 w^2 H^2 \sin^2\theta\,, \tag{17}$$

where $e$ is the electronic charge, $c$ is the velocity of light, and $m$ is the electronic mass. With the values of $H$ and $\theta$ given in the preceding paragraph, the average value of $H^2 \sin^2\theta$ is $1.35 \times 10^{-10}$ gauss². Thus

$$k^2 = 3.2 \times 10^{-13}\ (\text{erg sec})^{-1}. \tag{18}$$

The energy loss per unit time due to bremsstrahlung (Bethe and Ashkin 1953) is

$$-\left(\frac{dw}{dt}\right)_{\text{rad}} = cN\Phi_{\text{rad}}w, \tag{19}$$

where $N$ is the particle density and

$$\Phi_{\text{rad}} = (4\log 183Z^{-1/3} + \tfrac{2}{9})Z(Z+1) \times 5.79 \times 10^{-28}\ \text{cm}^2. \tag{20}$$

For the assumed interstellar density and composition, the average value of $N\Phi_{\text{rad}}$ is $1.75 \times 10^{-26}$ cm$^2$ in the regions between the clouds and sixteen times higher in the clouds themselves. Therefore,

$$2a_1 = 1.1 \times 10^{-15}\ \text{sec}. \tag{21}$$

The energy loss per unit time due to inelastic collisions is given by (Bethe and Ashkin 1953)

$$-\left(\frac{dw}{dt}\right)_i = \frac{2\pi N e^4 Z}{mc}\left(\log\frac{w^3}{2mc^2I^2Z^2} + \frac{1}{8}\right), \tag{22}$$

where $I$ (=13.6 ev) is the ionization potential of a hydrogen atom. Neglecting the logarithmic dependence on $w$ and $Z$, we obtain

$$-\left(\frac{dw}{dt}\right)_i = 4.8 \times 10^{-19}NZ \tag{23}$$

as the average energy loss for the high-energy electrons. The average value of $NZ$ is 0.68 for the regions between clouds and 10.9 in the clouds. Thus

$$k_0^2 = 6.7 \times 10^{-19}\ \text{erg/sec}. \tag{24}$$

Using the foregoing values, from equations (9), (10), and (14) we obtain

The injection energy $w_i = 0.94 \times 10^{-4}$ erg = 0.06 Bev,

The maximum energy $w_m = 2.2 \times 10^{-2}$ erg = 14 Bev,

And $s = 1.6$.

Thus the energy spectrum of cosmic-ray electrons (eq. [15]) becomes

$$\frac{dn_e}{dw} = J_0\frac{(w_m - w)^{0.6}}{(w - w_i)^{2.6}} \qquad (w_m \geq w \geq w_c). \tag{25}$$

Table 1 gives the numerical values of the differential spectrum (apart from a multiplicative constant), with $w$ measured in units of $w_m$. The spectrum with $0.03 \leq w/w_m \leq 0.7$ can be represented by the simple power law,

$$\frac{dn_e}{dw} = \frac{J}{w^3}, \tag{26}$$

TABLE 1

| $w/w_m$ | 0.01 | 0.03 | 0.05 | 0.1 | 0.2 | 0.3 | 0.4 | 0.5 | 0.6 | 0.7 | 0.8 | 0.9 |
|---|---|---|---|---|---|---|---|---|---|---|---|---|
| $dn_e/dw$ | 9.3 $\times 10^6$ | 1.6 $\times 10^4$ | 3.4 $\times 10^3$ | 4.6 $\times 10^2$ | 6.5 $\times 10$ | 2.0 $\times 10$ | 8.4 | 4.1 | 2.2 | 1.2 | 0.65 | 0.31 |

where $J$ is a constant related to the total number of electrons per cubic centimeter, and $n_e$ in the energy range $(w_c, w_m)$ by

$$J = 2w_c^2 n_e \,. \tag{27}$$

The energy $5 \times 10^{-4}$ erg will be assumed to be the $w_c$ for the calculations in the next section.

## IV. SPECTRUM OF THE NONTHERMAL RADIO EMISSION

With equation (26) as the energy spectrum of the cosmic-ray electrons, the spectrum of the nonthermal radio emission can be easily calculated. The emission of an electron of energy $w$ in a magnetic field $H$ is characterized by the frequency

$$\nu_c = QHw^2 \sin\theta \,, \tag{28}$$

where

$$Q = \frac{3e}{4\pi m^3 c^5} = 6.26 \times 10^{18} \text{ c.g.s.} \tag{29}$$

For the adopted data, the averaged value of $H \sin\theta$ is $0.75 \times 10^{-5}$ gauss. Thus the average value of $\nu_c$ for $w = 0.3$ Bev and 10 Bev are $\nu_1 = 10$ and $\nu_2 = 12000$ Mc/s, respectively. The power emitted in a unit frequency interval at $\nu$ is given by (Schwinger 1949)

$$\frac{P}{\Delta\nu} = RHF(\eta) \sin\theta \,, \tag{30}$$

where

$$R = \frac{3^{1/2} e^3}{m c^2} = 2.34 \times 10^{-22} \text{ c.g.s.} \tag{31}$$

and

$$\eta = \frac{\nu}{\nu_c} \quad \text{and} \quad F(\eta) = \eta \int_\eta^\infty K_{5/3}(y)\, dy \,, \tag{32}$$

$K_{5/3}(y)$ being the Airy integral. The function of $F(\eta)$ has been tabulated by Oort (1955).

Using equations (26), (28), (30), and (32), we find after a simple transformation that the total power emitted per cubic centimeter per unit frequency interval at $\nu$ is given by

$$\frac{P}{\Delta\nu} = \tfrac{1}{2} JRQ (H^2 \sin^2\theta) \nu^{-1} \int_{\eta_2}^{\eta_1} F(\eta)\, d\eta \,, \tag{33}$$

where $\eta_1 = \nu/\nu_1$ and $\eta_2 = \nu/\nu_2$. The value of the integral in equation (33) depends, of course, on the frequency $\nu$. But, since the function $F(\eta)$ decreases very rapidly for higher values of $\eta$, the integral is fairly constant, provided that $\nu$ is in the range, say, of $(2\nu_1, 0.1\nu_2)$, or 20–1000 Mc/s. For this frequency range the integral is approximately constant and has the numerical value 1.5. Thus

$$\frac{P}{\Delta\nu} = \frac{1.5}{2} JRQ (H^2 \sin^2\theta) \nu^{-1} \tag{34}$$

for frequencies between 20 and 1000 Mc/s. From equation (6) we find that the effective temperature, $T_A$, is proportional to $\lambda^3$ compared with the observed spectrum $T_A \sim \lambda^{2.5-2.8}$.

The total flux of cosmic-ray electrons can be estimated from equation (34), provided that $p/\Delta\nu$ per unit volume is known. Hey, Parsons, and Phillips (1949) found that the radio emission in the galactic plane at 64 Mc/s is of the order of $10^{-40}$ erg/cm$^3$/sec$^2$. With the values of $R$, $Q$, $\nu$, and the averaged value of $H^2 \sin^2\theta$, we obtain $n_e \sim 10^{-12}$/cm$^3$ for $w$ in (0.3–10 Bev); this is about 1 per cent of the total intensity of cosmic radiation.

It should be emphasized that the calculations presented are of a tentative nature. Nevertheless, Fermi's mechanism does seem to fulfil the requirements for the acceleration of cosmic radiation and for the emission of the nonthermal radio emission of the Galaxy. An interesting question then arises as to whether or not the "galactic halo" is an indication of the leakage of cosmic radiation from the galactic plane, as postulated by Morrison *et al.* (1954). Further acceleration may be needed in order to explain the fair uniformity of the emission (Burbidge 1956).

The author wishes to express his sincere thanks to Professor Chandrasekhar for his interest in this work and his guidance and to Dr. Prendergast for reading the manuscript and offering several suggestions.

## REFERENCES

Alfvén, H., and Herlofson, N. 1950, *Phys. Rev.*, **78**, 616.
Bethe, H., and Ashkin, J. 1953, *Experimental Nuclear Physics* (New York: John Wiley & Sons, Inc.), **1**, 252–269.
Brown, R. H. 1955, *Occasional Notes, R. Astr. Soc.*, **3**, No. 16, 57.
Burbidge, G. R. 1956, *Ap. J.*, **123**, 178.
Davis, L., Jr. 1956, *Phys. Rev.*, **101**, 351.
Dombrovsky, V. A. 1954, *Doklady Akad. Nauk U.S.S.R.*, **94**, 1021.
Fan, C. Y. 1956, *Phys. Rev.*, **101**, 314 (referred to as "Paper I").
Fermi, E. 1949, *Phys. Rev.*, **75**, 1169.
———. 1954, *Ap. J.*, **119**, 1.
Ginsberg, V. 1953, *Uspekhi phys. Nauk*, **51**, 343.
Hey, J. S., Parsons, S. J., and Philips, J. W. 1947, *Proc. R. Soc. London, A*, **192**, 425.
Kiepenheuer, K. O. 1950, *Phys. Rev.*, **79**, 738.
Morrison, P., Olbert, S., and Rossi, B. 1954, *Phys. Rev.*, **94**, 440.
Oort, J. H., and Walraven, J. H. 1956, *B.A.N.*, No. 462.
Pawsey, J. L., and Bracewell, R. M. 1955, *Radio Astronomy* (Oxford: Oxford University Press), pp. 259–260.
Pikel'ner, S. B. 1953, *Doklady Akad. Nauk U.S.S.R.*, **88**, No. 2, 229.
Schwinger, J. 1949, *Phys. Rev.*, **75**, 1912.
Shklovsky, I. S. 1953*a*, *Doklady Akad. Nauk U.S.S.R.*, **90**, 983.
———. 1953*b*, *Astr. J. U.S.S.R.*, **30**, 15.
Vashakidze, M. A. 1954, *Abastumani Astr. Circ.*, No. 147, p. 11.

# THE EQUILIBRIUM OF A SELF-GRAVITATING INCOMPRESSIBLE FLUID SPHERE WITH A MAGNETIC FIELD. I

KEVIN H. PRENDERGAST
Yerkes Observatory
*Received January 23, 1956*

ABSTRACT

It is shown that the introduction of a toroidal, as well as a poloidal, field makes possible an exact solution of the equations of hydromagnetic equilibrium.

## I. INTRODUCTION

Several investigators in recent years have dealt with the problem of the equilibrium of magnetic stars. Fermi and Chandrasekhar (1953) derived the virial theorem for an infinitely conducting fluid with a magnetic field and showed that it is necessary for dynamic stability that the magnetic energy be less than the gravitational energy. They also demonstrated that an incompressible fluid sphere with a uniform internal field is not in equilibrium and tends to contract in the direction of the field. Miss Gjellestad (1954) determined the optimum eccentricity of an incompressible oblate spheroid with a uniform field. This configuration, however, is unstable with respect to all deformations except those which transform the spheroid into another spheroid of different eccentricity. Ferraro (1954) gave a general condition which must be satisfied by any poloidal magnetic field in equilibrium with an incompressible fluid. He used this result for a first-order calculation of the eccentricity of an equilibrium spheroid with a magnetic field of a particular type. Roberts (1955) has extended this work by obtaining a series expansion for the equation of the surface of a body with Ferraro's field, but there is some doubt about the convergence of the series. Starting from a different point of view, Lüst and Schlüter (1954) studied the case in which the magnetic field and the electric current are everywhere parallel. Such a field can be imbedded in any conducting fluid, since it exerts no force. Chandrasekhar (1956) has given explicit expressions for a large class of such fields.

None of the magnetic fields which have been suggested so far satisfies the equilibrium conditions in an unequivocal way, with the exception of the force-free fields. These were postulated by Lüst and Schlüter for the region outside a star where the density is low but where the conductivity may still be high. They argued that in such a region the magnetic forces must vanish, as there are no compensating forces of comparable magnitude. This reasoning is not applicable to the interior of a star, where the magnetic force can, at most, be comparable to the gravitational and pressure forces. Under these circumstances there is no reason to believe that the magnetic field is force-free, and it is necessary to consider the more general case. The purpose of this paper is to exhibit an equilibrium configuration in which the magnetic forces do not vanish.

## II. THE EQUILIBRIUM CONDITIONS

The equations of equilibrium which must be satisfied in the interior of an infinitely conducting mass of fluid with a prevalent magnetic field are

$$0 = -\operatorname{grad} p + \rho \operatorname{grad} V + \boldsymbol{J} \times \boldsymbol{H} , \tag{1}$$

$$\nabla^2 V = -4\pi G\rho , \tag{2}$$

$$\operatorname{curl} \boldsymbol{H} = 4\pi \boldsymbol{J} , \tag{3}$$

and

$$\operatorname{div} \boldsymbol{H} = 0 , \tag{4}$$

where $\boldsymbol{H}$ is the magnetic field, $\boldsymbol{J}$ the current, $p$ the pressure, $\rho$ the density (which will be assumed constant), and $V$ the gravitational potential. Outside the fluid, if it is in vacuum, we must have

$$\nabla^2 V = 0 , \tag{5}$$

$$\operatorname{div} \boldsymbol{H} = 0 , \tag{6}$$

and

$$\operatorname{curl} \boldsymbol{H} = 0 . \tag{7}$$

If the body is surrounded by extremely tenuous, but highly conducting, material, equation (7) should, according to the ideas of Lüst and Schlüter, be replaced by

$$\operatorname{curl} \boldsymbol{H} \times \boldsymbol{H} = 4\pi \boldsymbol{J} \times \boldsymbol{H} = 0 , \tag{8}$$

which is the condition that the magnetic force vanishes.

At the surface of the body, the gravitational force,

$$\boldsymbol{F} = \operatorname{grad} V , \tag{9}$$

and the normal component of the magnetic field must be continuous. In addition, we must require that the sum of the fluid and magnetic pressures be continuous across the boundary; that is,

$$p + \frac{|\boldsymbol{H}_i|^2}{8\pi} = \frac{|\boldsymbol{H}_0|^2}{8\pi} , \tag{10}$$

where $\boldsymbol{H}_i$ and $\boldsymbol{H}_0$ are the values of the magnetic field inside and outside the surface, respectively.

Roberts (1955) has distinguished two types of equilibrium with respect to the way in which equation (10) is satisfied. In "true equilibrium," $p$ goes to zero at the surface, and $\boldsymbol{H}$ is continuous. In "quasi-equilibrium," $p$ does not go to zero, and there is a surface current,

$$\boldsymbol{K} = \frac{\boldsymbol{n} \times (\boldsymbol{H}_0 - \boldsymbol{H}_i)}{4\pi} , \tag{11}$$

where $\boldsymbol{n}$ is the unit normal out of the surface. The magnetic field exerts an unbalanced force on the fluid at the surface, but the resulting motion leaves the shape of the boundary unchanged. Quasi-equilibrium configurations will not be considered in this paper.

## III. POSSIBLE MAGNETIC FIELDS

It is evident that equation (1) imposes a rather stringent restriction on the magnetic field, for, on taking the curl, we find

$$\operatorname{curl} (\boldsymbol{J} \times \boldsymbol{H}) = \frac{1}{4\pi} \operatorname{curl} (\operatorname{curl} \boldsymbol{H} \times \boldsymbol{H}) = 0 . \tag{12}$$

The preceding equation implies that in an equilibrium configuration the Lorentz force,

$$\mathfrak{L} = \boldsymbol{J} \times \boldsymbol{H} , \tag{13}$$

must be the gradient of a scalar, for only then can it be balanced by pressure and gravitational forces alone. Before proceeding with the equilibrium problem, it is necessary to discuss the general class of magnetic fields satisfying this condition; these will be referred to as "possible magnetic fields."

If we consider only the axisymmetric case (all physical variables independent of the azimuthal angle $\phi$), the magnetic field may be written in the form

$$\boldsymbol{H} = \mathbf{1}_z \times \boldsymbol{r} T + \operatorname{curl} (\mathbf{1}_z \times \boldsymbol{r} P) , \tag{14}$$

where $\mathbf{1}_z$ is a unit vector along the axis and $\boldsymbol{r}$ is the radius vector from the origin; this representation of the field is automatically divergence-free. The necessary and sufficient conditions on $T$ and $P$ so that $\boldsymbol{H}$ may be a possible magnetic field have been given by Chandrasekhar and Prendergast (1956). They have shown that in cylindrical co-ordinates $(\varpi, \phi, z)$, the poloidal function $P$ must be a solution of

$$\Delta_5 P + \frac{1}{\varpi^2} G (\varpi^2 P) = \Phi (\varpi^2 P) , \tag{15}$$

where $G$ and $\Phi$ are arbitrary; the differential operator is the five-dimensional axisymmetric Laplacian

$$\Delta_5 = \frac{\partial^2}{\partial \varpi^2} + \frac{3}{\varpi} \frac{\partial}{\partial \varpi} + \frac{\partial^2}{\partial z^2} . \tag{16}$$

When a solution of equation (15) has been obtained, the appropriate toroidal function $T$ is readily found (cf. Chandrasekhar and Prendergast 1956, eq. [26]) from

$$\frac{d}{d (\varpi^2 P)} (\varpi^4 T^2) = 2G (\varpi^2 P) . \tag{17}$$

The determination of a possible magnetic field therefore involves a choice of the arbitrary functions $G$ and $\Phi$ and the solution of a second-order (generally nonlinear) equation.

Certain special cases of equation (15) are of interest. The most general force-free fields are obtained by setting $\Phi = 0$. The case in which $G(\varpi^2 P) = \alpha^2 \varpi^2 P$, with $\alpha$ a constant, has been discussed by Lüst and Schlüter (1954) and solved explicitly by Chandrasekhar (1956). The equation with $G = 0$, $\Phi \neq 0$, is identical with Ferraro's condition for poloidal fields, and the case investigated by Ferraro (1954) and Roberts (1955) is a solution of equation (15) with $\Phi =$ Constant.

The simplest linear equation which involves both $G$ and $\Phi$ is obtained by setting

$$G = \alpha^2 \varpi^2 P , \tag{18}$$

where $\alpha$ is a constant, and

$$\Phi = \kappa = \text{Constant} . \tag{19}$$

In spherical co-ordinates $(r, \mu = \cos \theta, \phi)$, equation (15) becomes

$$\Delta_5 P = \frac{\partial^2 P}{\partial r^2} + \frac{4}{r} \frac{\partial P}{\partial r} + \frac{1 - \mu^2}{r^2} \frac{\partial^2 P}{\partial \mu^2} - \frac{4\mu}{r^2} \frac{\partial P}{\partial \mu}$$

$$= - \alpha^2 P + \kappa . \tag{20}$$

It will be shown that the solution of this equation determines a magnetic field which can be adjusted to fit the boundary conditions on the surface of a sphere.

The solution of the homogeneous part of equation (20) which is finite at the origin (cf. Chandrasekhar 1956, eq. [17]) is

$$P_0 = \sum_{n=0}^{\infty} A_n \frac{J_{n+3/2} (\alpha r)}{(\alpha r)^{3/2}} C_n^{3/2} (\mu) , \tag{21}$$

where $J_{n+3/2}(\alpha r)$ is the Bessel function of order $n + \frac{3}{2}$ and $C_n^{3/2}(\mu)$ is the Gegenbauer polynomial of order $n$ and index $\frac{3}{2}$, as defined by Magnus and Oberhettinger (1949). The general solution of equation (20) which is finite at the origin is, therefore,

$$P = \frac{\kappa}{\alpha^2} + \sum_{n=0}^{\infty} A_n \frac{J_{n+3/2}(\alpha r)}{(\alpha r)^{3/2}} C_n^{3/2}(\mu) . \tag{22}$$

The associated toroidal function $T$ is obtained from equation (17). Since $G = \alpha^2 \varpi^2 P$, we immediately have

$$\varpi^4 T^2 = \alpha^2 \varpi^4 P^2 + K . \tag{23}$$

The evaluation of the constant of integration, $K$, follows from the requirement that the magnetic field be regular on the $z$-axis. In spherical co-ordinates, equation (14) for the magnetic field is

$$\boldsymbol{H} = -\frac{\partial}{\partial \mu}[(1-\mu^2) P]\, \mathbf{1}_r - \frac{\sqrt{(1-\mu^2)}}{r} \frac{\partial}{\partial r}(r^2 P)\, \mathbf{1}_\theta + r\sqrt{(1-\mu^2)}\, T \mathbf{1}_\phi , \tag{24}$$

where $\mathbf{1}_r$, $\mathbf{1}_\theta$, and $\mathbf{1}_\phi$ are unit vectors. It is evident that $H_\phi$ is singular on the axis unless $K = 0$. We then have simply

$$T = \alpha P , \tag{25}$$

and consequently

$$\boldsymbol{H} = -\frac{\partial}{\partial \mu}[(1-\mu^2) P]\, \mathbf{1}_r - \frac{\sqrt{(1-\mu^2)}}{r} \frac{\partial}{\partial r}(r^2 P)\, \mathbf{1}_\theta + \alpha r \sqrt{(1-\mu^2)}\, P \mathbf{1}_\phi . \tag{26}$$

This magnetic field, where $P$ is given by equation (22), is a solution of equation (12) and therefore gives rise to a Lorentz force which is the gradient of a scalar.

The general expression for the current in terms of $T$ and $P$ is

$$4\pi \boldsymbol{J} = \operatorname{curl} \boldsymbol{H} = -\frac{\partial}{\partial \mu}[(1-\mu^2) T]\, \mathbf{1}_r - \frac{\sqrt{(1-\mu^2)}}{r} \frac{\partial}{\partial r}(r^2 T)\, \mathbf{1}_\theta - r\sqrt{(1-\mu^2)}\, \Delta_5 P \mathbf{1}_\phi . \tag{27}$$

Since $T = \alpha P$ and since our choice of the functions $G$ and $\Phi$ makes

$$\Delta_5 P = -\alpha^2 P + \kappa , \tag{28}$$

equation (27) reduces to

$$4\pi \boldsymbol{J} = -\alpha \frac{\partial}{\partial \mu}[(1-\mu^2) P]\, \mathbf{1}_r - \frac{\alpha\sqrt{(1-\mu^2)}}{r} \frac{\partial}{\partial r}(r^2 P)\, \mathbf{1}_\theta + r\sqrt{(1-\mu^2)}\,(\alpha^2 P - \kappa)\, \mathbf{1}_\phi . \tag{29}$$

Comparing this result with equation (26), we see that

$$4\pi \boldsymbol{J} = \alpha \boldsymbol{H} - \kappa r \sqrt{(1-\mu^2)}\, \mathbf{1}_\phi . \tag{30}$$

The Lorentz force is therefore

$$\mathfrak{L} = \boldsymbol{J} \times \boldsymbol{H} = -\frac{\kappa}{4\pi} r \sqrt{(1-\mu^2)}\, \mathbf{1}_\phi \times \boldsymbol{H} , \tag{31}$$

or, in terms of the poloidal function $P$,

$$\mathfrak{L} = -\frac{\kappa}{4\pi} \frac{\partial}{\partial r}[(1-\mu^2)\, r^2 P]\, \mathbf{1}_r + \frac{\kappa}{4\pi} \frac{\sqrt{(1-\mu^2)}}{r} \frac{\partial}{\partial \mu}[1-\mu^2)\, r^2 P]\, \mathbf{1}_\theta . \tag{32}$$

But this is the same as

$$\mathfrak{L} = -\frac{\kappa}{4\pi} \operatorname{grad} [\,(1-\mu^2)\, r^2 P]\,, \tag{33}$$

and we have verified that $\mathfrak{L}$ is the gradient of a scalar.

## IV. THE EQUILIBRIUM SPHERE

The integration of the fundamental equation of equilibrium is now straightforward. From equations (1) and (33) we have

$$0 = -\operatorname{grad} p + \rho \operatorname{grad} V - \frac{\kappa}{4\pi} \operatorname{grad} [\,(1-\mu^2)\, r^2 P]\,, \tag{34}$$

or

$$-p + \rho V - \frac{\kappa}{4\pi} r^2 (1-\mu^2) P(r, \mu) = \mathfrak{S}\,. \tag{35}$$

It must now be shown that the boundary conditions can be satisfied on the surface of a sphere. For a true equilibrium configuration, the pressure must go to zero on the surface, and the magnetic field must be continuous. Since the gravitational potential is

$$V = 2\pi G\rho R^2 - \tfrac{2}{3}\pi G\rho r^2\,, \tag{36}$$

where $R$ is the radius of the sphere, the vanishing of the pressure requires that

$$\tfrac{4}{3}\pi G\rho^2 R^2 - \frac{\kappa}{4\pi} R^2 (1-\mu^2) P(R, \mu) = \mathfrak{S}\,. \tag{37}$$

Then

$$P(R, \mu) = \frac{D}{1-\mu^2}\,, \tag{38}$$

where $D$ is a constant. But, from equation (26), this would mean that

$$H_\phi(R, \mu) = \alpha R \sqrt{(1-\mu^2)}\, P(R, \mu) = \frac{\alpha R D}{\sqrt{(1-\mu^2)}}\,, \tag{39}$$

which is clearly impossible, unless $D \equiv 0$: the $\phi$-component of the magnetic field must vanish on the axis ($\mu = \pm 1$). It follows that

$$\mathfrak{S} = \tfrac{4}{3}\pi G\rho^2 R^2 \tag{40}$$

and

$$P(R, \mu) = 0 \qquad \text{for all } \mu\,. \tag{41}$$

From the general expression for $P$ (cf. eq. [22]), we have

$$P(R, \mu) = \frac{\kappa}{\alpha^2} + \sum_{n=0}^{\infty} A_n \frac{J_{n+3/2}(\alpha R)}{(\alpha R)^{3/2}} C_n^{3/2}(\mu) \equiv 0\,, \tag{42}$$

which can be satisfied if and only if

$$\begin{aligned} A_0 &= -\frac{\kappa}{\alpha^2} \frac{(\alpha R)^{3/2}}{J_{3/2}(\alpha R)}\,, \\ A_1, \ldots, A_n, \ldots &= 0\,. \end{aligned} \tag{43}$$

Then

$$P(r, \mu) = \frac{\kappa}{a^2}\left[1 - \left(\frac{R}{r}\right)^{3/2} \frac{J_{3/2}(ar)}{J_{3/2}(aR)}\right], \tag{44}$$

and the entire configuration has been determined, except for the constant $a$. In particular, the magnetic field is now

$$\begin{aligned} \boldsymbol{H} = \frac{2\kappa}{a^2}\,\mu\left[1 - \left(\frac{R}{r}\right)^{3/2} \frac{J_{3/2}(ar)}{J_{3/2}(aR)}\right]\mathbf{1}_r \\ - \frac{\kappa}{a^2}\sqrt{(1-\mu^2)}\left[2 + \frac{(aR)^{3/2}}{J_{3/2}(aR)}\left\{\frac{J_{5/2}(ar)}{(ar)^{1/2}} - 2\,\frac{J_{3/2}(ar)}{(ar)^{3/2}}\right\}\right]\mathbf{1}_\theta \\ + \frac{\kappa}{a}\,r\sqrt{(1-\mu^2)}\left[1 - \left(\frac{R}{r}\right)^{3/2}\frac{J_{3/2}(ar)}{J_{3/2}(aR)}\right]\mathbf{1}_\phi . \end{aligned} \tag{45}$$

It remains to show that this magnetic field can be made continuous with an external field $\boldsymbol{H}_0$, satisfying

$$\operatorname{div} \boldsymbol{H}_0 = 0 \tag{46}$$

and[1]

$$\operatorname{curl} \boldsymbol{H}_0 = 0 . \tag{47}$$

It may be remarked that it is just this final condition which has frustrated several earlier attempts at a solution. The reason is the following. The external field is completely determined by the condition that the normal component of $\boldsymbol{H}$ be continuous across the boundary. However, for a true equilibrium configuration, as Roberts (1955) has emphasized, the tangential component must also be continuous, and we cannot generally expect to satisfy both boundary conditions on $\boldsymbol{H}$ simultaneously. The difficulty is not materially lessened by considering quasi-equilibrium states. Once a possible magnetic field has been chosen for the interior of the fluid, the external magnetic field and the fluid pressure $p$ have been completely determined—the latter apart from an additive constant. But we must still satisfy the condition that the total pressure $p + |\boldsymbol{H}|^2/8\pi$ be continuous across the boundary.

Fortunately, in our case it is possible to achieve a true equilibrium configuration. We note that the radial and $\phi$-components of $\boldsymbol{H}$ are automatically zero on the boundary (cf. eq. [45]), and that the $\theta$-component can be made zero by choosing $a$ such that

$$J_{5/2}(a_j R) = 0 , \tag{48}$$

where the subscript $j$ refers to the $j$th root of the Bessel function; that is,

$$a_1 R = 5.7635 , \qquad a_2 R = 9.0950 , \qquad a_3 R = 12.3229 , \qquad \text{etc.} \tag{49}$$

With this choice of $a$, the magnetic field lies wholly within the fluid, and all boundary conditions have been met.

## V. THE TOTAL MAGNETIC ENERGY

The only free parameter in this solution is $\kappa$, which is related to the strength of the magnetic field. The condition for dynamical stability given by Fermi and Chandrasekhar imposes an upper limit on $\kappa$, since it requires that the magnetic energy,

$$\mathfrak{M} = \frac{1}{8\pi}\int_{\mathfrak{B}} |\boldsymbol{H}|^2 d\tau , \tag{50}$$

[1] The case in which the external field is a force-free field will not be considered here.

be less than the gravitational energy,

$$|\Omega| = \frac{1}{2}\int_{\mathfrak{B}} \rho V \, d\tau . \tag{51}$$

Since the toroidal and the poloidal components of $\boldsymbol{H}$ are orthogonal and since $T = \alpha P$, we have

$$\mathfrak{M} = \frac{\alpha^2}{8\pi}\int_{\mathfrak{B}} |\, \mathbf{1}_z \times \boldsymbol{r}\,|^2 P^2 d\tau + \frac{1}{8\pi}\int_{\mathfrak{B}} |\operatorname{curl}(\mathbf{1}_z \times \boldsymbol{r} P)\,|^2 d\tau . \tag{52}$$

For the purpose of evaluating the second integral, we introduce a vector,

$$\boldsymbol{S} = \mathbf{1}_z \times \boldsymbol{r} P , \tag{53}$$

whose Cartesian components will be denoted by $S_k$. Then

$$\int_{\mathfrak{B}} |\operatorname{curl}(\mathbf{1}_z \times \boldsymbol{r} P)\,|^2 d\tau = \int \left(\frac{\partial S_k}{\partial x_j}\right)^2 d\tau - \int_{\mathfrak{B}} \frac{\partial S_k}{\partial x_j}\frac{\partial S_j}{\partial x_k}\, d\tau . \tag{54}$$

The first of these integrals is

$$\int_{\mathfrak{B}} \left(\frac{\partial S_k}{\partial x_j}\right)^2 d\tau = \int_{\mathfrak{S}} S_k \frac{\partial S_k}{\partial x_j}\, d\sigma - \int_{\mathfrak{B}} S_k \frac{\partial^2 S_k}{\partial x_j^2}\, d\tau , \tag{55}$$

and the surface integral vanishes, since $S_k$ is zero on the boundary. The second integral in equation (54) may be written

$$-\int_{\mathfrak{B}} \frac{\partial S_k}{\partial x_j}\frac{\partial S_j}{\partial x_k}\, d\tau = -\int_{\mathfrak{S}} S_k \frac{\partial S_j}{\partial x_k}\, d\sigma + \int_{\mathfrak{B}} S_k \frac{\partial^2 S_j}{\partial x_j \partial x_k}\, d\tau . \tag{56}$$

The surface integral again vanishes, and the volume integral is also zero by virtue of the fact that div $\boldsymbol{S} = 0$. Collecting these results, we see that

$$\int_{\mathfrak{B}} |\operatorname{curl}(\mathbf{1}_z \times \boldsymbol{r} P)\,|^2 d\tau = \int_{\mathfrak{B}} P\, \mathbf{1}_z \times \boldsymbol{r} \cdot \operatorname{curl}\operatorname{curl}(\mathbf{1}_z \times \boldsymbol{r} P)\, d\tau . \tag{57}$$

But from equations (14) and (29),

$$\operatorname{curl}\operatorname{curl}(\mathbf{1}_z \times \boldsymbol{r} P) = r\sqrt{(1-\mu^2)}\,(\alpha^2 P - \kappa)\,\mathbf{1}_\phi . \tag{58}$$

The complete expression for the magnetic energy is therefore

$$\mathfrak{M} = \frac{\alpha^2}{4\pi}\int_{\mathfrak{B}} r^2 (1-\mu^2) P^2 d\tau - \frac{\kappa}{8\pi}\int_{\mathfrak{B}} r^2 (1-\mu^2) P\, d\tau . \tag{59}$$

The integrations with respect to $\mu$ and $\phi$ are readily performed, leaving

$$\mathfrak{M} = \frac{2\alpha^2}{3}\int_0^R r^4 P^2 dr - \frac{\kappa}{3}\int_0^R r^4 P\, d\tau , \tag{60}$$

where

$$P = \frac{\kappa}{\alpha^2}\left[1 - \left(\frac{R}{r}\right)^{3/2}\frac{J_{3/2}(\alpha r)}{J_{3/2}(\alpha R)}\right] . \tag{61}$$

Finally, the integrals appearing in equation (60) are evaluated with the aid of the relations (cf. Watson 1944, pp. 132 and 135)

$$\int_0^z z^{\nu+1} J_\nu(z)\, dz = z^{\nu+1} J_{\nu+1}(z) \tag{62}$$

and

$$\int_0^z zJ_\nu^2(kz)\,dz = \tfrac{1}{2}z^2\left[J_\nu^2(kz) - J_{\nu-1}(kz)\,J_{\nu+1}(kz)\right]. \tag{63}$$

The result is

$$\mathfrak{M} = \frac{2}{5}\frac{\kappa^2}{a^2}R^5, \tag{64}$$

and, since the gravitational energy of a uniform sphere is

$$|\Omega| = \tfrac{16}{15}\pi^2 G\rho^2 R^5, \tag{65}$$

the Fermi-Chandrasekhar limit on the total magnetic energy requires that

$$\frac{\kappa^2}{a^2} < \tfrac{8}{3}\pi^2 G\rho^2. \tag{66}$$

This inequality may also be written as

$$\kappa^2 < \tfrac{3}{2}x_j^2\frac{GM^2}{R^3}, \tag{67}$$

where $x_j$ is the $j$th root of $J_{5/2}(x)$ and $M$ is the total mass.

## VI. THE MAGNETIC LINES OF FORCE

The equations for the magnetic lines of force are

$$\frac{dr}{H_r} = -\frac{r\,d\mu}{\sqrt{(1-\mu^2)}\,H_\theta} = \frac{r\sqrt{(1-\mu^2)}\,d\phi}{H_\phi}. \tag{68}$$

The first of these can be integrated explicitly to give

$$F(r,\mu) = r^2(1-\mu^2)\left[\frac{J_{3/2}(aR)}{(aR)^{3/2}} - \frac{J_{3/2}(ar)}{(ar)^{3/2}}\right] = \text{Constant}, \tag{69}$$

which is the equation of a family of toroids concentric with the axis of the field. The intersections of these surfaces with a meridional plane for the case where $aR$ is the first root of $J_{5/2}(x)$ is plotted in Figure 1. The second of equations (68) is easily reduced to

$$d\phi = \frac{a\,dr}{\mu}, \tag{70}$$

where $r$ and $\mu$ are related to each other by equation (69). Since $dr/\mu$ does not change sign in a complete circuit of the curve $F(r, \mu) =$ Constant, it is evident from equation (70) that a typical line of force resembles a helix wrapped on the surface of a torus, as shown in Figure 2. The sense of spiraling depends on the sign of $\kappa$. It should be noted that such a line does not necessarily close on itself.

## VII. CONCLUSION

At least two features of the present model are somewhat unexpected. The first is that it is possible to have both a toroidal and a poloidal field inside an infinitely conducting fluid and yet have no field either on the surface or outside it. The second is that the introduction of a toroidal field makes possible a spherical equilibrium configuration. Presumably the only way in which a field such as the one considered could be detected is

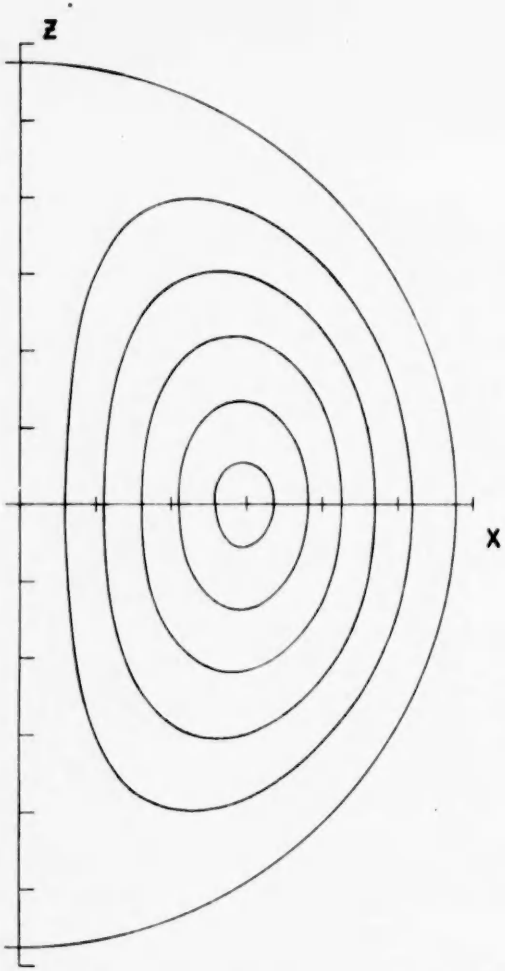


FIG. 1.—The intersections of the surfaces $F(r, \mu)$ = Constant with the $(x, z)$ plane for the case where $\alpha_1 R$ is the lowest root of $J_{5/2}(x)$. A single division represents a change of 1 in the dimensionless quantity $\alpha_1 r$.

FIG. 2.—A schematic diagram to illustrate the way in which lines of force spiral around a toroidal surface $F(r, \mu)$ = Constant.

through its effects on the pulsations of the sphere. If it is legitimate to extrapolate these conclusions to the compressible case, we might infer that a magnetic field of considerable strength may be concealed in an otherwise normal star; this is obviously a question which cannot be decided on the basis of the present material alone. It may be remarked that some of the results derived in this paper may be extended, at least formally, to the compressible case.

The question of the stability of the model appears to be one of considerable difficulty. In order to establish stability, it is necessary to show that an arbitrary infinitesimal perturbation produces no first-order change in the total gravitational plus magnetic energy and that the second-order change in this quantity is positive. The alternative to this procedure is to show that all the eigen-values of the pulsation equation are real.

A more general question arises as to the uniqueness of an equilibrium configuration. In obtaining the present model, we made an arbitrary choice of the functions $G$ and $\Phi$ and an equally arbitrary choice of the shape of the surface. But any choice of $G$ and $\Phi$ leads to a possible magnetic field, and it is not known which of these will be realized in a given mass of fluid. It is hoped to discuss some of these questions in the future.

*Note added in proof:* It has recently been found that a variational principle exists for axisymmetric oscillations of this model.

The author wishes to thank Professor S. Chandrasekhar for many helpful discussions in the course of this work. The research reported in this paper was supported in part by the Geophysics Research Directorate of the Air Force Cambridge Research Center, Air Research and Development Command, under Contract AF 19(604)-299 with the University of Chicago.

## REFERENCES

Chandrasekhar, S. 1956, *Proc. Nat. Acad. Sci.*, **42**, 1–5.
Chandrasekhar, S., and Prendergast, K. H. 1956, *Proc. Nat. Acad. Sci.*, **42**, 5–9.
Fermi, E., and Chandrasekhar, S. 1953, *Ap. J.*, **118**, 116–141.
Ferraro, V. C. A. 1954, *Ap. J.*, **119**, 407–412.
Gjellestad, G. 1954, *Ap. J.*, **119**, 14–33.
Lüst, R., and Schlüter, A. 1954, *Zs. f. Ap.*, **34**, 263–282.
Magnus, W., and Oberhettinger, F. 1949, *Special Functions of Mathematical Physics* (New York: Chelsea Publishing Co.), p. 76.
Roberts, P. H. 1955, *Ap. J.*, **122**, 508–512.
Watson, G. N. 1944, *A Treatise on the Theory of Bessel Functions* (Cambridge: At the University Press), pp. 132 and 135.

# THE EXTERNAL ELECTRIC FIELD OF A ROTATING MAGNET*

GEORGE BACKUS
Physics Department, University of Chicago
*Received December 16, 1955*

ABSTRACT

The electromagnetic fields outside rigidly rotating magnets in vacuum are computed in two cases: for a nonconducting magnet with dielectric constant unity the electric and magnetic fields are given exactly in terms of retarded potentials; for a conducting magnet the electric and magnetic fields are computed in the region of space where the displacement current can be neglected. In the former case the rotation of the magnet has no effect unless its stationary magnetic field is axially asymmetric. One example of the latter case is that a uniformly magnetized conducting sphere rotating about its axis of magnetization produces an external electric quadrupole field. These results contradict Alfvén's results for the same problem (1950, see p. 8) but agree with the experimental results he cites in favor of his theory.

## I. INTRODUCTION

It is the purpose of this paper to discuss a formula of Alfvén (1950, see p. 8) for the electric field outside a rotating rigid magnet. If the magnet's angular velocity is $\boldsymbol{\omega}$ and if, when the magnet is not rotating, its magnetic field is $\boldsymbol{B}$, then at the point $\boldsymbol{r}$ inside or outside the magnet Alfvén gives, for the electric field $\boldsymbol{E}$ due to the rotating magnet,

$$\boldsymbol{E} = -(\boldsymbol{\omega} \times \boldsymbol{r}) \times \boldsymbol{B} . \tag{1}$$

He obtains this formula by asserting that in the reference frame rotating with the magnet the electric field vanishes and the magnetic field has its stationary value; formula (1) is then the result of a Lorentz transformation into the frame of the nonrotating observer.

The present writer doubts Alfvén's assumption about the electromagnetic field in the rotating reference frame, which leads to formula (1). Two reasons for this doubt are the following: if $\boldsymbol{E}$ is given by formula (1), then, in the vacuum outside the magnet, $\nabla \cdot \boldsymbol{E} = -2\boldsymbol{B} \cdot \boldsymbol{\omega}$, which is not generally zero; and if the "magnet" is a ring of charge rotating with angular velocity $\boldsymbol{\Omega}$ about the $z$-axis, which "magnet" is given an angular velocity $\boldsymbol{\omega}$ about the $z$-axis, the ring will simply rotate with angular velocity $\boldsymbol{\Omega} + \boldsymbol{\omega}$, producing no effects except an increase in the external magnetic field.

The electric field can be calculated from Maxwell's equations in the nonrotating frame of reference, and it disagrees with formula (1) but gives the same results as formula (1) in all the experiments cited by Alfvén in support of that formula. This paper is devoted to verifying these assertions.

## II. ELECTRICALLY INERT MAGNETS

If the magnet is neither a conductor nor a dielectric but simply a rigid current distribution $\boldsymbol{j}(r, \theta, \phi)$ in a volume $V$, where $r$, $\theta$, and $\phi$ are the spherical polar co-ordinates of the vector $\boldsymbol{r}$, then at time $t$ the current distribution in the rotating magnet is $U(\omega t)\boldsymbol{j}(r, \theta, \phi - \omega t)$, where $U(\omega t)$ is the matrix of rotation through an angle $\omega t$ about the $z$-axis. The usual retarded current integral for the vector potential, $\boldsymbol{A}$,

$$\boldsymbol{A}(\boldsymbol{r}, t) = \mu_0 \int_V \frac{U(\omega t - \omega |\boldsymbol{r} - \boldsymbol{r}'| / c)\, \boldsymbol{j}(r, \theta, \phi - \omega t + \omega |\boldsymbol{r} - \boldsymbol{r}'| / c)}{|\boldsymbol{r} - \boldsymbol{r}'|}\, d^3\boldsymbol{r}' , \tag{2}$$

gives the exact electric and magnetic fields at all points. In particular, from equation (2) it is evident that if $\boldsymbol{j}$ is invariant under rotations about the $z$-axis, then $-\partial \boldsymbol{A}/\partial t = \boldsymbol{E} = \boldsymbol{0}$. This is already a violation of formula (1). Now suppose that in the expansion

$$\boldsymbol{j}(r, \theta, \phi) = \sum_{m=-\infty}^{\infty} \boldsymbol{j}_m(r, \theta)\, e^{im\phi} \tag{3}$$

* The research reported in this paper has in part been supported by the Geophysics Research Directorate of the Air Force Cambridge Research Center, Air Research Development Command, under Contract AF 19(604)-299 with the University of Chicago.

the coefficients $j_m(r, \theta)$ with $m > m_0$ are negligible compared with the others. If the semidiameter $a$ of the magnet satisfies $m_0\omega a \ll c$ and if $\boldsymbol{r}$ is any point for which $m_0\omega r \ll c$, then $\boldsymbol{A}(\boldsymbol{r}, t)$ differs by terms of the order of $m_0\omega r/c$ from the field obtained by rotating the static vector potential through an angle $\omega t$ about the $z$-axis. Neglecting these terms corresponds to neglecting the displacement current.

## III. AN EXAMPLE OF A CONDUCTING MAGNET

Suppose that a stationary electrically uncharged iron sphere of radius $a$ is magnetized so that $\boldsymbol{B}$ is symmetric under rotations about the $z$-axis and lies in meridian planes. Let $\boldsymbol{k}$ be a unit vector in the $z$-direction and start the sphere rotating with angular velocity $\boldsymbol{\omega} = \omega\boldsymbol{k}$. Suppose it is possible for the conduction electrons to distribute themselves so that their static electric field $-\boldsymbol{\nabla}V$ just cancels the Lorentz field $(\boldsymbol{\omega} \times \boldsymbol{r}) \times \boldsymbol{B}$ seen by the interior of the sphere. Then, neglecting the displacement current (Sec. II describes when this is justified), inside the sphere we have

$$\boldsymbol{\nabla}V = \boldsymbol{u} \times \boldsymbol{B} \qquad \text{where} \qquad \boldsymbol{u} = \boldsymbol{\omega} \times \boldsymbol{r}\,,$$

$$\boldsymbol{\nabla}^2 V = -\frac{\rho}{\epsilon_0}, \qquad \text{and} \qquad \boldsymbol{\nabla} \times \boldsymbol{H} = \rho\boldsymbol{u}\,.$$

Thus

$$\boldsymbol{\nabla}V = (\boldsymbol{\omega} \times \boldsymbol{r}) \times \boldsymbol{B}\,, \tag{4}$$

and

$$\boldsymbol{\nabla} \times \boldsymbol{B} = -\epsilon_0\mu_0\boldsymbol{\omega} \times \boldsymbol{r}\boldsymbol{\nabla}^2 V \tag{5}$$

inside the sphere. Taking the divergence of equation (4) and substituting the resulting value for $\boldsymbol{\nabla}^2 V$ in equation (5), one obtains

$$\boldsymbol{\nabla} \times \boldsymbol{B} = -\epsilon_0\mu_0\boldsymbol{\omega} \times \boldsymbol{r}\boldsymbol{\nabla} \cdot [(\boldsymbol{\omega} \times)\boldsymbol{r} \times \boldsymbol{B}]\,. \tag{6}$$

In neglecting the displacement current we have neglected terms of the order of $u/c$; hence we can neglect the right side of equation (6). This amounts to neglecting the effect on the magnetic field of the current produced by the motion of the induced volume charge in the sphere. If the surface charge is not too inhomogeneously distributed, since its total magnitude is that of the volume charge, it also will have a negligible effect on $\boldsymbol{B}$, so that, neglecting terms of order $(a\omega/c)^2$, the magnetic field is unaffected by the rotation. But then equation (4) can be used to compute $V$ inside the sphere by substituting for $\boldsymbol{B}$ the field of the nonrotating sphere, and the external potential can be computed by fitting the general exterior solution of Laplace's equation to the interior potential at the surface of the sphere. For example, if

$$\boldsymbol{B} = B\boldsymbol{k} \tag{7}$$

inside the sphere, then, from equation (4),

$$V = -\tfrac{1}{3}B\omega a^2 + \tfrac{1}{2}B\omega r^2 \sin^2\theta \qquad \text{inside the sphere,} \tag{8}$$

and

$$V = -\tfrac{1}{3}B\omega a^5 r^{-3} P_2(\cos\theta) \qquad \text{outside the sphere.} \tag{9}$$

Here $P_2$ is the second Legendre polynomial. Where equation (1) predicts an $r^{-2}$ dependence for $\boldsymbol{E}$ outside the sphere, equation (9) predicts an $r^{-4}$ dependence. Equations (8) and (9) give the surface charge on the sphere as $\frac{1}{2}\epsilon_0 B\omega a(1 + \cos^2\theta)$, whose effect on $\boldsymbol{B}$ is of the order of $(\omega a/c)^2$, as asserted.

## IV. THE GENERAL CONDUCTING MAGNET, NEGLECTING DISPLACEMENT CURRENT

Consider a conducting permanent magnet of maximum diameter $2a$, rotating rigidly with angular velocity $\omega$. Let $-\boldsymbol{\nabla}V$ be the electrostatic field due to the displacement of charges and $\boldsymbol{E}_b$ the electric field induced by the time variation of $\boldsymbol{B}$. Then, if it is pos-

sible to distribute the charges so that $-\nabla V + \boldsymbol{E}_b + \boldsymbol{u} \times \boldsymbol{B} = \boldsymbol{0}$, where $\boldsymbol{u} = \boldsymbol{\omega} \times \boldsymbol{r}$, there will be no eddy currents. Therefore, the condition for the absence of eddy currents is $\nabla \times \boldsymbol{E}_b + \nabla \times (\boldsymbol{u} \times \boldsymbol{B}) = \boldsymbol{0}$, or

$$\nabla \times (\boldsymbol{u} \times \boldsymbol{B}) = \frac{\partial \boldsymbol{B}}{\partial t}. \tag{10}$$

But $\nabla \times (\boldsymbol{u} \times \boldsymbol{B}) = (\boldsymbol{B} \cdot \nabla)\boldsymbol{u} - (\boldsymbol{u} \cdot \nabla)\boldsymbol{B}$ and $\partial \boldsymbol{B}/\partial t + (\boldsymbol{u} \cdot \nabla)\boldsymbol{B} = D\boldsymbol{B}/Dt$ is the time rate of change of $\boldsymbol{B}$ at a point moving with the magnet. Furthermore, $(\boldsymbol{B} \cdot \nabla)\boldsymbol{u} = \boldsymbol{\omega} \times \boldsymbol{B}$, so that equation (10) can be written

$$\frac{D\boldsymbol{B}}{Dt} = \boldsymbol{\omega} \times \boldsymbol{B}. \tag{11}$$

But equation (11) is simply the condition that the magnetic field rotate rigidly with the magnet, which it will certainly do, since it is produced by the permanent magnetization, the eddy currents rotating rigidly with the magnet and the currents due to the translation of volume and surface charges fixed in the magnet.

Now, since we are neglecting the displacement current, $\boldsymbol{E}_b = -\partial \boldsymbol{A}/\partial t$, where $\boldsymbol{A}$ is the vector potential vanishing at infinity and satisfying

$$\boldsymbol{B} = \nabla \times \boldsymbol{A} \qquad \text{and} \qquad \nabla \cdot \boldsymbol{A} = 0. \tag{12}$$

Then Maxwell's equations inside the conductor are

$$\nabla \times \nabla \times \boldsymbol{A} = \mu_0 \rho \boldsymbol{u} \qquad \text{where} \qquad \boldsymbol{u} = \boldsymbol{\omega} \times \boldsymbol{r}, \qquad \text{and} \tag{13}$$

$$\nabla^2 V = -\frac{\rho}{\epsilon_0}, \tag{14}$$

while we also have $-\nabla V + \boldsymbol{E}_b + \boldsymbol{u} \times \boldsymbol{B} = \boldsymbol{0}$, or

$$\nabla V = -\frac{\partial \boldsymbol{A}}{\partial t} + \boldsymbol{u} \times (\nabla \times \boldsymbol{A}). \tag{15}$$

We know that $\boldsymbol{A}$ is obtained by rigidly rotating some static $\boldsymbol{A}$ at angular velocity $\boldsymbol{\omega}$, so that $\partial \boldsymbol{A}/\partial t = \boldsymbol{\omega} \times \boldsymbol{A} - (\boldsymbol{u} \cdot \nabla)\boldsymbol{A}$. Hence, from equation (15), $\nabla V = \nabla(\boldsymbol{u} \cdot \boldsymbol{A})$, or, inside the magnet,

$$V = C + \boldsymbol{u} \cdot \boldsymbol{A}, \tag{16}$$

where $C$ is a constant to be determined by the requirement that the exterior potential fit equation (16) at the surface of the magnet and vanish at infinite distance.

The only remaining task is to show that the $\boldsymbol{A}$ of equation (12), which is used in equation (16), can be computed with an error $(\omega a/c)^2$ by rigidly rotating with angular velocity $\boldsymbol{\omega}$ the static $\boldsymbol{A}$ of the stationary magnet; that is, the contribution to $\boldsymbol{A}$ of the currents produced by the motion of the static charges induced in and on the surface of the magnet is of the order of $(\omega a/c)^2$. To see this for the volume charge, take the divergence of equation (15), obtaining $\nabla^2 V = \nabla \cdot [\boldsymbol{u} \times (\nabla \times \boldsymbol{A})]$. Then from equations (14) and (13), $\nabla \times \nabla \times \boldsymbol{A} + \epsilon_0 \mu_0 \boldsymbol{u}[\nabla \cdot (\boldsymbol{u} \times \boldsymbol{A})] = \boldsymbol{0}$; and $\epsilon_0 \mu_0 = c^{-2}$, which justifies the neglect of the right side of equation (13). To see why the surface charge affects $\boldsymbol{A}$ only to order $(\omega a/c)^2$, observe that the surface density of charge is

$$\sigma = \epsilon_0 \left[ \left( \frac{\partial V}{\partial n} \right)_{\text{inside}} - \left( \frac{\partial V}{\partial n} \right)_{\text{outside}} \right],$$

where $\partial/\partial n$ means the normal derivative at the surface of the magnet. By means of Green's function for Laplace's equation chosen to vanish on the surface of the magnet, $V_{\text{outside}}$ can be computed from $V_{\text{inside}}$, so that

$$\left|\left(\frac{\partial V}{\partial n}\right)_{\text{outside}}\right| \leq f \max\left|\left(\frac{\partial V}{\partial n}\right)_{\text{inside}}\right|,$$

where $f$ is a dimensionless factor which depends only on the shape of the magnet's surface. Then $|\sigma| \leq (f+1)\epsilon_0 \max |(\partial V/\partial n)_{\text{inside}}|$. But, from equation (15),

$$\max\left|\left(\frac{\partial V}{\partial n}\right)_{\text{inside}}\right| \leq \max\left|\frac{\partial \boldsymbol{A}}{\partial t}\right| + \max|\boldsymbol{u}\times\boldsymbol{B}|.$$

If in the dependence of $\boldsymbol{A}$ on azimuthal angle $\phi$, all harmonics above the $m$th can be neglected, then

$$\max\left|\frac{\partial \boldsymbol{A}}{\partial t}\right| \leq m\omega \max|\boldsymbol{A}|.$$

Furthermore, $a \max|\boldsymbol{B}| = b \max|\boldsymbol{A}|$, where $b$ is a dimensionless number which depends only on the shape of the magnet's static field. Then

$$\max\left|\left(\frac{\partial V}{\partial n}\right)_{\text{inside}}\right| \leq (m+b)\,\omega \max|\boldsymbol{A}|.$$

The contribution of the surface current $\boldsymbol{u}\sigma$ to $\boldsymbol{A}$ is

$$|\delta\boldsymbol{A}| = \mu_0\left|\int_S \frac{\sigma'\boldsymbol{u}'}{|\boldsymbol{r}-\boldsymbol{r}'|}\,d^2\boldsymbol{r}'\right| \leq \mu_0 a\omega\,(\max|\sigma|)\int_S \frac{d^2\boldsymbol{r}'}{|\boldsymbol{r}-\boldsymbol{r}'|}.$$

This last integral is $\epsilon_0^{-1}$ times the potential at the point $\boldsymbol{r}$ inside the magnet, due to unit surface-charge density on the magnet's surfaces, and is $\leq da$, where $d$ is a dimensionless number determined by the shape of the surface. Combining all the foregoing results, we obtain

$$|\delta\boldsymbol{A}| \leq \left(\frac{a\omega}{c}\right)^2 (f+1)\,d\,(m+b)\max|\boldsymbol{A}|.$$

This justifies neglecting the contribution of the surface currents to $\boldsymbol{A}$.

## V. DISCUSSION OF THE EXPERIMENTS

Alfvén (1950, see pp. 6–10) cites experiments with unipolar inductors in support of his formula; but the theory presented here predicts the same results in these experiments as does Alfvén's. The first unipolar inductor described by Alfvén is a cylindrical permanent iron magnet rotating about its geometrical axis, which is also its dipole axis (see Fig. 1). The emf between points $A$ and $C$ around the circuit $ABC$ is found experimentally to be

$$-\int_{ABC}(\boldsymbol{u}\times\boldsymbol{B})\cdot d\boldsymbol{l},$$

where $\boldsymbol{u} = \boldsymbol{\omega}\times\boldsymbol{r}$. Now if $\boldsymbol{B}$ is cylindrically symmetric, equation (15) shows that $\boldsymbol{u}\times\boldsymbol{B}$ is the gradient of some potential function $V_1$, which agrees with the true electric potential $V$ in the interior of the magnet. But then, clearly,

$$\int_{ABC}\boldsymbol{\nabla}V_1\cdot d\boldsymbol{l} = \int_{ABC}\boldsymbol{\nabla}V\cdot d\boldsymbol{l},$$

since the two end-points of the path of integration lie in the magnet and both integrals are $V_1(C) - V_1(A)$. This argument applies as well when the rotating cylinder is copper and the magnetic field is externally supplied as in the second unipolar inductor cited by Alfvén.

Finally, Alfvén reports the experimental result that if the circuit $ABC$ is rigidly connected to the conductor and rotates with it, no potential is observed from $A$ to $C$. He concludes that the induced electric field $\boldsymbol{u} \times \boldsymbol{B}$ in the moving wire must just cancel the electric field $\boldsymbol{E}$ due to the rotating magnet, so that $\boldsymbol{E} = -\boldsymbol{u} \times \boldsymbol{B}$. Actually, all that is required to explain the experimental result is that the line integrals along $ABC$ of these two electric fields cancel, which is just the result we have derived above.

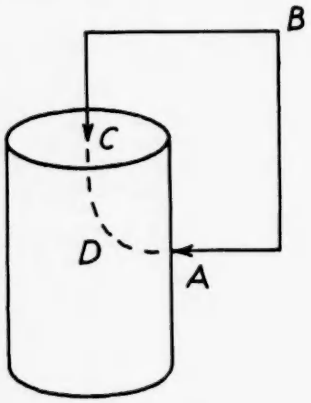


FIG. 1.—A unipolar inductor

## VI. CONCLUSION

As Alfvén has emphasized (1953), the medium outside the stars is a good conductor, so that the results of this paper cannot be applied to the computation of the electric field outside a rotating magnetic star; this paper does show, however, that formula(1) is not universally applicable. Leverett Davis (1947, 1948) obtains formulae (8) and (9) for a uniformly magnetized sphere rotating *in vacuo* and shows that, if the space surrounding the sphere contains charged particles constrained to move along the magnetic lines of force, then a charge density will accumulate which will provide exactly the electric field of formula (1) predicted by Alfvén. This picture assumes that the effects of electron pressure and ordinary conduction current can be ignored near a star, an assumption challenged by Schlüter (1955).

In conclusion the author should like to express his gratitude to Professor Alfvén for the references to the work of Leverett Davis, and to Professor Chandrasekhar and Dr. Kevin Prendergast for their helpful discussion of and interest in this paper.

## REFERENCES

Alfvén, H. 1953, *Cosmical Electrodynamics* (London: Oxford University Press).
Davis, Leverett. 1947, *Phys. Rev.*, **72**, 632.
———. 1948, *ibid.*, **73**, 536.
Schlüter, A. 1955, *Gas Dynamics of Cosmic Clouds* (Amsterdam: North Holland Publishing Co.), pp. 46–50.

# MODEL ATMOSPHERES FOR A-TYPE STARS

KIYOTERU OSAWA*
Yerkes Observatory
*Received October 10, 1955; revised January 24, 1956*

ABSTRACT

Model stellar atmospheres with $T_e = 8900°$ and $7560°$ and log $g = 3.5$, 4.0, and 4.5 were calculated, taking into account the continuous absorption by H, $H^-$, and $H_2^+$. The constancy of the net flux was secured to about 1 per cent. The colors and Balmer discontinuities of these models are consistent with the observations for A3 and A9 stars. The profiles of Hγ were calculated and compared with observations. It is possible to interpret qualitatively the empirical luminosity effect of Balmer lines for A-type stars.

## I. CALCULATION OF THE MODELS

Model stellar atmospheres considered in the present investigation are completely specified by the effective temperature $T_e$ (determined by the quantity of outward net flux of energy per unit area), the surface gravity $g$, and the relative abundance of elements. The values of $T_e$ and log $g$ chosen for our models were $T_e = 8900°$ and $7560°$ and log $g = 3.5$, 4.0, 4.5, respectively. The parameter log $A$, specifying the relative abundance of hydrogen with respect to heavier elements, was assumed to be 3.8 for all the model atmospheres considered. Radiative equilibrium was assumed. Further, the atmospheres were taken to be in hydrostatic equilibrium (cf. earlier work on model atmospheres for A stars: Aller 1942 and Strömgren 1944). Under these circumstances we have

$$\frac{dp}{d\tau} = \frac{g}{\bar{\kappa}}, \tag{1}$$

where $p$, $\tau$, and $\bar{\kappa}$ denote the pressure, optical depth, and opacity (Rosseland mean), respectively. Here $\bar{\kappa}$ depends upon the temperature function $\theta$ and electron pressure $p_e$, which in turn depends on $\theta$ and $p$. A table of log $p_e$ as a function of $\theta$ and log $p$ was published in a paper by Strömgren (1944). Tables of $\bar{\kappa}$, as well as a set of tables of $\kappa_\nu/\kappa$ for twenty-three standard wave lengths, were compiled by Strömgren and were lent to the author for the present investigation. These tables greatly facilitated the calculation. The absorption by neutral hydrogen and negative hydrogen ions (Chandrasekhar and Breen 1946), as well as the absorption by hydrogen molecules (Wildt 1947; Bates 1952), was taken into account. For the model atmospheres considered here the effect of electron scattering is so small that it can be neglected.

As the first approximation, a temperature distribution for a gray atmosphere was assumed, namely,

$$\theta_{\text{first}} = \theta_0 \left[ \tfrac{3}{4} (\tau + q) \right]^{-1/4}, \tag{2}$$

where $\theta_0$ is a constant specifying the effective temperature of the model and $q$ is a function of $\tau$ tabulated by Mark (1947). By integrating equation (1) numerically, the distributions of $p$, $p_e$, and $\bar{\kappa}$ were obtained as functions of $\tau$.

The next step is to calculate $F_\nu$, the net flux of energy as the function of $\tau$ and $\nu$. We have

$$\tau_\nu = \int_0^\tau \frac{\kappa_\nu}{\bar{\kappa}} \, d\tau \tag{3}$$

and

$$F_\nu(\tau_\nu) = 2\int_{\tau_\nu}^{\infty} B_\nu(t_\nu) E_2(t_\nu - \tau_\nu) \, dt_\nu - 2\int_0^{\tau_\nu} B_\nu(t_\nu) E_2(\tau_\nu - t_\nu) \, dt_\nu, \tag{4}$$

* On leave of absence from Tokyo Astronomical Observatory.

where $B_\nu$ and $E_2$ are the Planck radiation function and the integral-exponential function of the second order, respectively. Actual numerical calculations of these integrals were carried out by means of the method of representative points (Chandrasekhar 1950; Aller 1953). For $\tau = 0$, the three-point approximation

$$F_\nu(0) = 0.767B_\nu(0.287) + 0.2265B_\nu(1.814) + 0.0065B_\nu(5.385) \quad (5)$$

was used, and for the other values of $\tau$, namely, $\tau = 0.5$, 1.0, 1.5, and 2.0, the two-point approximation was used,

$$F_\nu(\tau_\nu) = 0.8839B_\nu(\tau_\nu + 0.397) + 0.1161B_\nu(\tau_\nu + 2.723) - d_1B_\nu(t_1) - d_2B_\nu(t_2), \quad (6)$$

where the weighting coefficients $d_1$ and $d_2$ and the representative points $t_1$ and $t_2$ are also tabulated by Strömgren (unpublished).

It is necessary to ascertain that the integrated flux,

$$F = \int_0^\nu F_\nu d\nu, \quad (7)$$

is constant with $\tau$. In order to secure this constancy of $F$, the temperature distribution of our first approximation (2) has to be improved by some amount, say $\Delta\theta$. This correction $\Delta\theta$ was obtained by means of a method suggested by Strömgren. The method has been described by Swihart (1956). With this new temperature distribution,

$$\theta_{\text{second}} = \theta_{\text{first}} + \Delta\theta, \quad (8)$$

all the calculation, namely, the integrations of equations (1), (3), (5), (6), and (7), were repeated as before. In all the seven atmospheres considered in the present paper the constancy of the net flux of energy was reached to an error of about 1 per cent by the second approximation. Therefore, in no case was it necessary to perform the calculations for the third approximation. It should be emphasized that the Rosseland mean was used only as a convenient unit in the first approximation and that no assumption concerning a mean absorption coefficient is involved in obtaining the final solution.

TABLE 1

FIRST AND SECOND APPROXIMATIONS

| $\tau$ | $\theta_{\text{first}}$ (Gray) | $F\times10^{-11}$ (First Approx.) | $\Delta\theta$ | $F\times10^{-11}$ (Second Approx.) | $\tau_{5050}$ |
|---|---|---|---|---|---|
| 0.0 | 0.700 | 1.155 | +0.045 | 1.134 | 0.00 |
| 0.1 | .694 | ..... | + .021 | ..... | 0.075 |
| 0.5 | .677 | 1.088 | + .002 | 1.137 | 0.37 |
| 1.0 | .535 | 1.090 | − .001 | 1.127 | 0.74 |
| 1.5 | .501 | 1.095 | − .002 | 1.123 | 1.14 |
| 2.0 | 0.476 | 1.097 | −0.002 | 1.123 | 1.57 |

As an illustrative example, an extract from the calculation of our model No. 1 ($T_e = 8900$, $\log g = 3.5$) is shown in Table 1. The final results, thus obtained, of $\theta$, $\log p$, $\log p_e$, $\bar{\kappa}$, and $\tau_{5050}$ (optical depth for $\lambda$ 5050) of our model atmospheres are shown in Table 2. Model No. 5′ is a special model which neglects the continuous absorption by hydrogen molecules but is otherwise the same as model No. 5.

## TABLE 2

### MODEL ATMOSPHERES

MODEL NO. 1 ($T_e = 8900°$; LOG $g = 3.5$)

| $\tau$ | $\theta$ | log $p$ | log $p_e$ | log $\bar{\kappa}$ | $\tau_{5050}$ |
|---|---|---|---|---|---|
| 0.00 | 0.745 | ... | ... | ... | ... |
| 0.01 | .734 | 2.39 | 0.78 | 9.27 | ... |
| 0.02 | .725 | 2.59 | 0.94 | 9.40 | ... |
| 0.03 | .718 | 2.70 | 1.05 | 9.49 | ... |
| 0.04 | .712 | 2.78 | 1.13 | 9.56 | ... |
| 0.06 | .700 | 2.88 | 1.27 | 9.68 | ... |
| 0.08 | .690 | 2.94 | 1.37 | 9.77 | ... |
| 0.10 | .681 | 2.99 | 1.46 | 9.86 | 0.073 |
| 0.15 | .663 | 3.06 | 1.64 | 0.04 | ... |
| 0.20 | .647 | 3.10 | 1.78 | 0.18 | 0.15 |
| 0.3 | .623 | 3.15 | 1.98 | 0.41 | 0.22 |
| 0.4 | .604 | 3.18 | 2.13 | 0.57 | ... |
| 0.5 | .588 | 3.20 | 2.25 | 0.72 | 0.37 |
| 0.75 | .557 | 3.23 | 2.47 | 0.99 | 0.55 |
| 1.0 | .533 | 3.25 | 2.61 | 1.18 | 0.74 |
| 1.5 | .499 | 3.27 | 2.79 | 1.40 | 1.14 |
| 2.0 | .473 | 3.28 | 2.86 | 1.48 | 1.57 |
| 3 | .437 | 3.30 | 2.96 | 1.47 | 2.57 |
| 4 | .412 | 3.33 | 3.01 | 1.41 | 3.74 |
| 6 | .377 | 3.39 | 3.08 | 1.23 | 6.70 |
| 8 | .353 | 3.46 | 3.16 | 1.12 | ... |
| 10 | 0.336 | 3.53 | 3.23 | 1.05 | ... |

MODEL NO. 2 ($T_e = 8900°$; LOG $g = 4.0$)

| $\theta$ | log $p$ | log $p_e$ | log $\bar{\kappa}$ | $\tau_{5050}$ |
|---|---|---|---|---|
| 0.744 | ... | ... | ... | ... |
| .734 | 2.77 | 0.97 | 9.39 | ... |
| .726 | 2.98 | 1.13 | 9.51 | ... |
| .720 | 3.09 | 1.24 | 9.60 | ... |
| .714 | 3.16 | 1.32 | 9.67 | ... |
| .703 | 3.26 | 1.45 | 9.78 | ... |
| .694 | 3.33 | 1.55 | 9.87 | ... |
| .685 | 3.38 | 1.64 | 9.95 | 0.082 |
| .667 | 3.45 | 1.81 | 0.11 | ... |
| .652 | 3.50 | 1.95 | 0.25 | 0.16 |
| .627 | 3.56 | 2.16 | 0.46 | 0.24 |
| .609 | 3.59 | 2.31 | 0.62 | ... |
| .593 | 3.61 | 2.43 | 0.76 | 0.39 |
| .561 | 3.65 | 2.72 | 1.09 | 0.58 |
| .537 | 3.66 | 2.84 | 1.25 | 0.78 |
| .502 | 3.68 | 3.05 | 1.50 | 1.18 |
| .476 | 3.69 | 3.19 | 1.67 | 1.61 |
| .439 | 3.71 | 3.32 | 1.76 | 2.60 |
| .414 | 3.72 | 3.38 | 1.73 | 3.78 |
| .378 | 3.76 | 3.45 | 1.59 | 6.72 |
| .354 | 3.80 | 3.50 | 1.46 | ... |
| 0.337 | 3.85 | 3.55 | 1.38 | ... |

MODEL NO. 3 ($T_e = 8900°$; LOG $g = 4.5$)

| $\tau$ | $\theta$ | log $p$ | log $p_e$ | log $\bar{\kappa}$ | $\tau_{5050}$ |
|---|---|---|---|---|---|
| 0.00 | 0.744 | ... | ... | ... | ... |
| 0.01 | .735 | 3.16 | 1.16 | 9.51 | ... |
| 0.02 | .728 | 3.35 | 1.32 | 9.64 | ... |
| 0.03 | .722 | 3.47 | 1.42 | 9.72 | ... |
| 0.04 | .716 | 3.54 | 1.50 | 9.79 | ... |
| 0.06 | .706 | 3.64 | 1.62 | 9.89 | ... |
| 0.08 | .697 | 3.71 | 1.72 | 9.97 | ... |
| 0.10 | .689 | 3.76 | 1.81 | 0.05 | 0.086 |
| 0.15 | .672 | 3.84 | 1.98 | 0.20 | ... |
| 0.20 | .657 | 3.89 | 2.11 | 0.32 | 0.17 |
| 0.3 | .632 | 3.95 | 2.33 | 0.54 | 0.26 |
| 0.4 | .613 | 3.99 | 2.49 | 0.69 | ... |
| 0.5 | .596 | 4.01 | 2.62 | 0.85 | 0.42 |
| 0.75 | .564 | 4.05 | 2.88 | 1.09 | 0.62 |
| 1.0 | .540 | 4.07 | 3.06 | 1.30 | 0.83 |
| 1.5 | .504 | 4.09 | 3.31 | 1.60 | 1.24 |
| 2.0 | .477 | 4.10 | 3.47 | 1.79 | 1.69 |
| 3 | .440 | 4.11 | 3.65 | 1.98 | 2.70 |
| 4 | .414 | 4.12 | 3.73 | 2.01 | 3.89 |
| 6 | .378 | 4.14 | 3.81 | 1.92 | 6.83 |
| 8 | .354 | 4.17 | 3.85 | 1.80 | ... |
| 10 | 0.337 | 4.20 | 3.89 | 1.71 | ... |

MODEL NO. 4 ($T_e = 7560°$; LOG $g = 3.5$)

| $\theta$ | log $p$ | log $p_e$ | log $\bar{\kappa}$ | $\tau_{5050}$ |
|---|---|---|---|---|
| 0.837 | ... | ... | ... | ... |
| .829 | 2.88 | 0.34 | 8.81 | ... |
| .823 | 3.07 | 0.47 | 8.91 | ... |
| .818 | 3.19 | 0.57 | 8.99 | ... |
| .813 | 3.27 | 0.65 | 9.05 | ... |
| .804 | 3.37 | 0.77 | 9.15 | ... |
| .796 | 3.44 | 0.86 | 9.23 | ... |
| .788 | 3.49 | 0.94 | 9.29 | 0.095 |
| .722 | 3.58 | 1.11 | 9.44 | ... |
| .757 | 3.63 | 1.25 | 9.55 | 0.19 |
| .733 | 3.70 | 1.45 | 9.73 | 0.28 |
| .712 | 3.74 | 1.63 | 9.88 | ... |
| .695 | 3.77 | 1.76 | 0.01 | 0.46 |
| .659 | 3.81 | 2.05 | 0.28 | 0.68 |
| .631 | 3.83 | 2.27 | 0.51 | 0.88 |
| .590 | 3.85 | 2.59 | 0.84 | 1.28 |
| .559 | 3.86 | 2.81 | 1.10 | 1.67 |
| .516 | 3.87 | 3.10 | 1.45 | 2.48 |
| .485 | 3.88 | 3.28 | 1.68 | 3.33 |
| .443 | 3.88 | 3.46 | 1.86 | 5.28 |
| .415 | 3.89 | 3.53 | 1.85 | ... |
| 0.394 | 3.89 | 3.56 | 1.79 | ... |

TABLE 2—*Continued*

| Model No. 5 ($T_e = 7560°$; log $g = 4.0$) | | | | | | Model No. 6 ($T_e = 7560°$; log $g = 4.5$) | | | | |
|---|---|---|---|---|---|---|---|---|---|---|
| $\tau$ | $\theta$ | log $p$ | log $p_e$ | log $\bar{\kappa}$ | $\tau_{5000}$ | $\theta$ | log $p$ | log $p_e$ | log $\bar{\kappa}$ | $\tau_{5000}$ |
| 0.00 | 0.839 | ..... | ..... | ..... | ..... | 0.841 | ..... | ..... | ..... | ..... |
| 0.01 | .832 | 3.24 | 0.50 | 8.93 | ..... | .834 | 3.60 | 0.67 | 9.08 | ..... |
| 0.02 | .826 | 3.44 | 0.64 | 9.05 | ..... | .828 | 3.80 | 0.82 | 9.20 | ..... |
| 0.03 | .821 | 3.55 | 0.74 | 9.13 | ..... | .823 | 3.91 | 0.92 | 9.28 | ..... |
| 0.04 | .817 | 3.63 | 0.81 | 9.19 | ..... | .819 | 3.98 | 0.99 | 9.34 | ..... |
| 0.06 | .808 | 3.73 | 0.93 | 9.29 | ..... | .810 | 4.09 | 1.11 | 9.43 | ..... |
| 0.08 | .800 | 3.80 | 1.02 | 9.36 | ..... | .802 | 4.16 | 1.20 | 9.51 | ..... |
| 0.10 | .793 | 3.86 | 1.10 | 9.43 | 0.095 | .795 | 4.21 | 1.27 | 9.57 | 0.104 |
| 0.15 | .777 | 3.94 | 1.26 | 9.56 | ..... | .778 | 4.30 | 1.43 | 9.70 | ..... |
| 0.20 | .762 | 4.00 | 1.39 | 9.67 | 0.20 | .764 | 4.36 | 1.57 | 9.81 | 0.22 |
| 0.3 | .737 | 4.07 | 1.61 | 9.85 | 0.29 | .739 | 4.43 | 1.78 | 9.99 | 0.32 |
| 0.4 | .717 | 4.11 | 1.79 | 0.00 | ..... | .718 | 4.47 | 1.96 | 0.13 | ..... |
| 0.5 | .699 | 4.14 | 1.93 | 0.12 | 0.48 | .701 | 4.50 | 2.10 | 0.24 | 0.54 |
| 0.75 | .662 | 4.18 | 2.13 | 0.32 | 0.71 | .663 | 4.54 | 2.40 | 0.49 | 0.78 |
| 1.0 | .634 | 4.21 | 2.45 | 0.60 | 0.94 | .635 | 4.57 | 2.63 | 0.70 | 1.02 |
| 1.5 | .592 | 4.23 | 2.77 | 0.92 | 1.37 | .592 | 4.59 | 2.96 | 1.01 | 1.49 |
| 2.0 | .561 | 4.24 | 3.00 | 1.16 | 1.78 | .561 | 4.60 | 3.18 | 1.24 | 1.94 |
| 3 | .517 | 4.25 | 3.32 | 1.52 | 2.62 | .517 | 4.62 | 3.52 | 1.60 | 2.83 |
| 4 | .486 | 4.26 | 3.52 | 1.77 | 3.51 | .486 | 4.62 | 3.73 | 1.84 | 3.77 |
| 6 | .444 | 4.27 | 3.75 | 2.02 | 5.49 | .444 | 4.63 | 4.00 | 2.12 | 5.84 |
| 8 | .415 | 4.27 | 3.86 | 2.09 | ..... | .415 | 4.64 | 4.14 | 2.27 | ..... |
| 10 | 0.394 | 4.27 | 3.90 | 2.08 | ..... | 0.394 | 4.64 | 4.32 | ..... | ..... |

| Model No. 5′ ($T_e = 7560°$; log $g = 4.0$, $H_2^+$ Neglected) | | | | | | Model No. 5′ ($T_e = 7560°$; log $g = 4.0$, $H_2^+$ Neglected) | | | | | |
|---|---|---|---|---|---|---|---|---|---|---|---|
| $\tau$ | $\theta$ | log $p$ | log $p_e$ | log $\bar{\kappa}$ | $\tau_{5000}$ | $\tau$ | $\theta$ | log $p$ | log $p_e$ | log $\bar{\kappa}$ | $\tau_{5000}$ |
| 0.00 | 0.834 | ..... | ..... | ..... | ..... | 0.4 | 0.720 | 4.11 | 1.77 | 9.99 | ..... |
| 0.01 | .828 | 3.22 | 0.52 | 8.95 | ..... | 0.5 | .703 | 4.14 | 1.90 | 0.09 | 0.47 |
| 0.02 | .823 | 3.42 | 0.66 | 9.06 | ..... | 0.75 | .666 | 4.19 | 2.20 | 0.36 | 0.69 |
| 0.03 | .819 | 3.54 | 0.75 | 9.14 | ..... | 1.0 | .638 | 4.21 | 2.42 | 0.57 | 0.90 |
| 0.04 | .815 | 3.62 | 0.82 | 9.20 | ..... | 1.5 | .595 | 4.23 | 2.74 | 0.89 | 1.31 |
| 0.06 | .807 | 3.72 | 0.93 | 9.29 | ..... | 2.0 | .564 | 4.25 | 2.98 | 1.14 | 1.71 |
| 0.08 | .800 | 3.80 | 1.02 | 9.35 | ..... | 3 | .519 | 4.26 | 3.31 | 1.50 | 2.53 |
| 0.10 | .792 | 3.85 | 1.10 | 9.42 | 0.094 | 4 | .488 | 4.26 | 3.51 | 1.75 | 3.39 |
| 0.15 | .778 | 3.94 | 1.25 | 9.55 | ..... | 6 | .446 | 4.27 | 3.74 | 2.01 | 5.34 |
| 0.20 | .764 | 4.00 | 1.38 | 9.65 | .19 | 8 | .417 | 4.27 | 3.86 | 2.09 | ..... |
| 0.3 | 0.740 | 4.07 | 1.59 | 9.83 | 0.28 | 10 | 0.396 | 4.28 | 3.91 | 2.09 | ..... |

Table 3 shows the values of $F_\nu$ at $\tau = 0$. The absorption by hydrogen molecules is important for the visual and violet regions, especially at lower temperatures. It amounts to about 10 per cent of the absorption by H and $H^-$ at maximum. Comparing the values of $F_\nu$ for models Nos. 5 and 5′ with each other, we note an increased radiation in the violet region, accompanied by a decrease in red and ultraviolet regions in No. 5′. This effect causes the color of model No. 5′ to be bluer than that of No. 5. The agreement with observation is better for model No. 5 than for model No. 5′, as will be shown in the following section.

## II. COLOR TEMPERATURE, COLOR, AND BALMER DISCONTINUITY

Table 4 contains the effective temperature, color temperature, color $(B - V)$, the discontinuity at the Balmer limit, and the residual intensity (at $\Delta\lambda = 10$ A) of the Hγ line calculated for our model atmospheres. These results will be discussed in this and the following sections.

Effective temperatures were calculated from the net flux of energy by means of the Stefan-Boltzmann formula. According to Kuiper (1938), the effective temperatures of

TABLE 3

SPECTRAL ENERGY DISTRIBUTION OF MODEL ATMOSPHERES

| λ (A) | $F_\nu \times 10^6$ | | | | | | |
|---|---|---|---|---|---|---|---|
| | Model 1 | Model 2 | Model 3 | Model 4 | Model 5 | Model 6 | Model 5′ |
| 912 | 5.0 | 4.7 | 4.3 | 0.19 | 0.19 | 0.25 | 0.21 |
| 1002 | 6.9 | 6.9 | 7.6 | 0.84 | 1.11 | 1.49 | 1.10 |
| 1122 | 8.4 | 8.6 | 9.2 | 1.44 | 1.75 | 2.16 | 1.78 |
| 1269 | 9.9 | 10.2 | 10.7 | 2.18 | 2.63 | 3.02 | 2.54 |
| 1458 | 11.0 | 11.9 | 12.5 | 3.04 | 3.63 | 4.12 | 3.48 |
| 1716 | 13.2 | 14.3 | 15.6 | 4.45 | 5.14 | 5.89 | 5.00 |
| 2084 | 16.7 | 18.1 | 19.6 | 7.04 | 8.18 | 9.08 | 7.91 |
| 2652 | 25.0 | 26.5 | 29.4 | 12.7 | 14.2 | 15.9 | 13.9 |
| 3647⁻ | 40.8 | 43.5 | 45.3 | 24.4 | 25.8 | 28.0 | 25.9 |
| 3647⁺ | 165 | 154 | 142 | 70.6 | 63.3 | 58.1 | 66.1 |
| 4235 | 152 | 144 | 136 | 71.8 | 66.2 | 62.2 | 67.8 |
| 5050 | 138 | 132 | 127 | 72.8 | 70.0 | 66.8 | 70.0 |
| 6250 | 118 | 116 | 113 | 72.2 | 69.7 | 68.0 | 69.6 |
| 8206⁻ | 90 | 89 | 92 | 65.7 | 64.6 | 63.7 | 64.5 |
| 8206⁺ | 113 | 109 | 105 | 71.6 | 68.6 | 66.5 | 67.3 |
| 9214 | 98 | 96 | 94 | 66.5 | 63.7 | 62.9 | 64.4 |
| 10503 | 84 | 83 | 82 | 60.5 | 59.0 | 57.8 | 59.3 |
| 12213 | 69 | 68 | 68 | 53.2 | 52.5 | 51.9 | 52.6 |
| 14588⁻ | 53.2 | 54.1 | 53.9 | 44.5 | 44.3 | 44.4 | 44.7 |
| 14588⁺ | 57.7 | 57.3 | 57.1 | 46.2 | 45.7 | 45.6 | 46.0 |
| 19450 | 35.5 | 35.6 | 35.4 | 30.2 | 29.7 | 29.7 | 29.9 |
| 29176 | 17.2 | 17.2 | 17.3 | 14.9 | 14.8 | 14.7 | 14.8 |
| 58353 | 4.8 | 4.8 | 4.8 | 4.2 | 4.1 | 4.2 | 4.2 |
| log g | 3.5 | 4.0 | 4.5 | 3.5 | 4.0 | 4.5 | 4.0 |
| $T_e$ | 8900° | 8900° | 8900° | 7560° | 7560° | 7560° | 7560° |

A0, A5, and F0 are 10700°, 8530°, and 7500°, respectively. Therefore, our models correspond to types around A3 and A9. The values of log $g$ of our models cover luminosity classes III, IV, and V. (The value of log $g$ for an A-type main-sequence star is about 4.3.)

The color temperatures were calculated from the ratios of the net fluxes for the specified wave lengths. In general, the color temperatures are higher for the smaller surface gravities. This agrees with the observations.

The color $(B - V)$ in Harold Johnson's system were calculated by the following formula:

$$(B - V) = 2.5 \log \left( \frac{I_V}{I_B} \right), \tag{9}$$

where

$$I_V = \int_0^\infty (1 - \eta) F_\nu R_V d\nu \tag{10}$$

and

$$I_B = \int_0^\infty (1 - \eta)\, F_\nu R_B\, d\nu, \tag{11}$$

where $R_V$ and $R_B$ denote the standard spectral response of the photometer, and $\eta$ measures the reduction of the flux by absorption lines. Values of $R_V$ and $R_B$ were taken from the paper by Johnson and Morgan (1951); values of $\eta$ were taken from a paper of Milford (1948) by interpolating the values between $\alpha$ CMa (A1 V) and $\alpha$ CMi (F5 IV). The zero-point color $(B - V)$ was determined by the color of the sun; $F_\nu$ of the sun was taken from Pettit (1940), and $(B - V) = 0.63$ was adopted for the sun.

According to Morgan, Harris, and Johnson (1953), the colors $(B - V) = 0.07$–$0.11$ correspond to spectral type A3, and $(B - V) = 0.24$ and 0.30 correspond to A7 and F0, respectively. It is interesting to see that the color $(B - V)$ is sensitive to a change of $g$ at lower temperature.

We cannot calculate the color $(U - B)$ for our models because accurate values of $\eta$ for the ultraviolet region are not available at present. We can get reasonable values of $(U - B)$—for example, $(U - B) = 0.027$—for our model No. 2 by adopting $\eta = 0.38$,

TABLE 4

OBSERVABLE CHARACTERS OF MODEL ATMOSPHERES

| Model no. | 1 | 2 | 3 | 4 | 5 | 6 | 5′ |
|---|---|---|---|---|---|---|---|
| $T_e$ | 8900° | 8900° | 8900° | 7560° | 7560° | 7560° | 7560° |
| log $g$ | 3.5 | 4.0 | 4.5 | 3.5 | 4.0 | 4.5 | 4.0 |
| Color temp. from $F_{2652}:F_{3647^-}$ | 10400 | 10300 | 10800 | 9290 | 9620 | 9810 | 9400 |
| Color temp. from $F_{3647^+}:F_{5050}$ | 15650 | 14820 | 13860 | 11500 | 10620 | 10220 | 11150 |
| Color temp. from $F_{4235}:F_{5050}$ | 14370 | 13920 | 13170 | 10700 | 9780 | 9520 | 10300 |
| Color temp. from $F_{5050}:F_{6250}$ | 13320 | 12290 | 11870 | 9220 | 9180 | 8810 | 9080 |
| Color $(B-V)$ | 0.07 | 0.09 | 0.11 | 0.24 | 0.27 | 0.30 | 0.24 |
| Balmer discontinuity $(D)$ | 0.61 | 0.55 | 0.49 | 0.46 | 0.39 | 0.32 | 0.41 |
| Residual intensity $(\Delta\lambda = 10\,\text{A})$ of Hγ | 0.72 | 0.71 | 0.69 | 0.81 | 0.82 | 0.82 | ..... |

but this coincidence should not be emphasized. It is intended to make a more detailed comparison with spectrophotometric observations in a future investigation.

The Balmer discontinuities, $D$, computed for our models can be compared with the observational results of Chalonge and Divan (1952). Comparing their values with our theoretical values in Table 4, we notice good agreement between them, except perhaps for a slight tendency for the theoretical values to be larger than the observed values. If we had not included the continuous absorption by hydrogen molecules, the discrepancy would have been a little larger.

### III. THE PROFILE OF THE Hγ LINE

Kolb (1956*a*) has modified the theory of Stark-effect broadening of the hydrogen lines. Jugaku, Elste, and Aller (1956) have applied a preliminary version of this theory (Kolb 1956*b*) to model B-star atmospheres and have shown that it gives deeper wings than those calculated according to the classical Holtsmark theory.

The profiles of the Hγ line in our models were also computed by this same preliminary theory. The residual intensity, $r$, was calculated with the assumption of pure absorption, namely,

$$r = \frac{\int_0^\infty B_\nu(t_\nu)\, E_2(t_\nu)\, dt_\nu}{\int_0^\infty B_\nu(\tau_\nu)\, E_2(\tau_\nu)\, d\tau_\nu}, \tag{12}$$

where

$$t_\nu = \int_0^\infty \frac{\kappa_\nu + l_\nu}{\kappa_\nu} d\tau_\nu . \tag{13}$$

The results of these calculations are shown in Table 5, together with some observational results, $\beta$ Leo by Williams (1932), 95 Leo by Chamberlain and Aller (1951), $\alpha$ CMi by Hiltner and Williams (1946).

We see from this table that the theoretical profiles have deeper wings than the observed ones. The Holtsmark theory predicts too shallow wings for Balmer lines, in contrast to our result (Underhill 1952; Hunger 1955). As a matter of fact, computed according to the Holtsmark theory, the residual intensity at $\Delta\lambda = 30$ A for model No. 2 would be 0.96 instead of 0.91, and that of model No. 5 would be 0.98 instead of 0.95.

There may also be an observational difficulty in estimating the continuous background of the spectrum for wings of strong Fraunhofer lines. Comparison of observed profiles of Balmer lines by different observers (Günther 1933) clearly shows this difficulty. It is

TABLE 5

PROFILES OF Hγ (RESIDUAL INTENSITIES)

| MODELS OR STARS | THEORY | | | | | | OBSERVATION | | |
|---|---|---|---|---|---|---|---|---|---|
| | 1 | 2 | 3 | 4 | 5 | 6 | | | |
| | $T_e = 8900°$ | | | $T_e = 7560°$ | | | $\beta$ Leo (A3 V) | 95 Leo (A3 V) | $\alpha$ CMi (F5 IV) |
| | log $g = 3.5$ | 4.0 | 4.5 | 3.5 | 4.0 | 4.5 | | | |
| $\Delta\lambda = 5$ A | 0.56 | 0.56 | 0.56 | 0.70 | 0.71 | 0.71 | 0.48 | 0.50 | 0.71 |
| 10 | .72 | .71 | .69 | .81 | .82 | .82 | .66 | .70 | .85 |
| 20 | .88 | .85 | .83 | .90 | .90 | .91 | .85 | .88 | .95 |
| 30 | 0.94 | 0.91 | 0.89 | 0.94 | 0.94 | 0.95 | 0.94 | 0.95 | 0.99 |

outside the scope of the present paper to go further into the discussion of this matter, but we may safely conclude that the results of Table 5 have made progress toward the solution of the problem of Balmer lines.

We note an interesting luminosity effect in the theoretical profiles of Hγ. At $T_e = 8900°$ (type A3), the wings are deeper for decreasing values of $g$ (i.e., for increasing luminosity). On the other hand, at $T_e = 7560°$ (type A9), this effect is quite small but in the opposite sense. The appearance of the wings of the Balmer lines are currently used as the powerful criterion of luminosity class for B and early A stars, but the practical limit of applicability of this criterion is reached at about A3 (Morgan, Keenan, and Kellman 1942). For later subclasses of A and F, Balmer lines show little luminosity effect except for supergiants, until at later types they show the luminosity effect again but in the opposite sense as compared with the earlier types. Our results agree with this empirical fact.

## IV. CONCLUDING REMARKS

By the discussion in the preceding sections, the various observable characters of the model atmospheres considered in the present investigation were proved to be in fair agreement with the observational results. We also saw that this agreement was improved by the inclusion of continuous absorption by hydrogen molecules. We may conclude that

these models represent the normal A3 and A9 atmospheres to a good approximation. The models can therefore be used for a quantitative analysis of the stellar spectra and probably of some kinds of peculiar objects frequently encountered in A-type stars.

We assumed in our models that practically the whole mass of the atmospheric matter is contributed by hydrogen. If we have to consider an atmosphere in which increased content of helium or heavier elements contribute appreciably to weight, then the correct values of $p$ and $p_e$ are obtained by dividing $g$ by $X$, where $X$ is the hydrogen content by weight of the atmospheric matter, as was shown by Strömgren (1944).

In conclusion the author wishes to express his cordial thanks to Dr. B. Strömgren for helpful discussions and kind advice while this work was carried out. He is very much indebted to Dr. L. H. Aller and Mr. A. Kolb for communicating, in advance of publication, the preliminary formulae for the Hγ absorption coefficient in a form suitable for astrophysical applications. He also is deeply grateful to the United States Educational Commission in Japan for a Fulbright Travel Grant and the International Astronomical Union for a grant which partly supported the author's stay in the United States.

## REFERENCES

Aller, L. H. 1942, *Ap. J.*, **96**, 321.
———. 1953, *Atmospheres of the Sun and Stars* (New York: Ronald Press), p. 204.
Bates, D. R. 1952, *M.N.*, **112**, 40.
Chalonge, D., and Divan, L. 1952, *Ann. d'ap.*, **15**, 201.
Chamberlain, J. W., and Aller, L. H. 1951, *Ap. J.*, **114**, 52.
Chandrasekhar, S. 1950, *Radiative Transfer* (Oxford: Oxford University Press), pp. 65–69.
Chandrasekhar, S., and Breen, F. H. 1946, *Ap. J.*, **104**, 430.
Elste, G., Jugaku, J., and Aller, L. H. 1956, *A.J.* (in press).
Günther, S. 1933, *Zs. f. Ap.*, **7**, 106.
Hiltner, W. A., and Williams, R. C. 1941, *Photometric Atlas of Stellar Spectra* (Ann Arbor: University of Michigan Press).
Hunger, K. 1955, *Zs. f. Ap.*, **36**, 42.
Johnson, H. L., and Morgan, W. W. 1951, *Ap. J.*, **114**, 522.
Kolb, A. 1956*a*, Thesis, University of Michigan (in preparation).
———. 1956*b*, *Pub. A.S.P.* (in press). This preliminary theory represents an improvement over the Holtsmark theory but has recently been superseded by a more precise theory in which nonadiabatic effects are taken into account.
Kuiper, G. P. 1938, *Ap. J.*, **88**, 429.
Mark, C. 1947, *Phys. Rev.*, **72**, 558.
Milford, N. 1949, *Ann d'ap.*, **12**, 243.
Morgan, W. W., Harris, D. L., and Johnson, H. L. 1953, *Ap. J.*, **118**, 92.
Morgan, W. W., Keenan, P. C., and Kellman, E. 1942, *An Atlas of Stellar Spectra* (Chicago: University of Chicago Press).
Pettit, E. 1940, *Ap. J.*, 91, 159.
Strömgren, B. 1944, *Pub. Copenhagen Obs.*, No. 127.
———. "Tables for Computing Flux and Mean Intensity" (unpublished).
Swihart, T. L. 1956, *Ap. J.*, **123**, 139.
Underhill, A. B. 1952, *Ap. J.*, **116**, 446.
Wildt, R. 1947, *Relation entre les phénomènes solaires et géophysiques* (Paris: Centre national de la Recherche scientifique), p. 7.
Williams, E. G. 1932, *Ann. Solar Phys. Obs. Cambridge*, Vol. 2, Part II.

# CLASSIFICATION OF EMISSION LINES λ 5694 AND λ 5446 IN THE SOLAR CORONA

F. ROHRLICH
Department of Physics, State University of Iowa, Iowa City
*Received September 29, 1955; revised January 16, 1956*

ABSTRACT

The contradictions in the literature concerning the theoretical classification of the coronal lines λ 5694 and λ 5446 are resolved, and the experimental result:

$$\text{Ca XV: } 2s^2 2p^2\,, \qquad {}^3P_2 - {}^3P_1 \rightarrow \lambda\,5446\,,$$
$$\text{Ca XV: } 2s^2 2p^2\,, \qquad {}^3P_1 - {}^3P_0 \rightarrow \lambda\,5694\,,$$

is confirmed. The semiempirical parameters associated with the Ca XV spectrum are obtained on the basis of the linear theory with configuration interaction in intermediate coupling. The parameter set used by Layzer (1954) is criticized.

## I. HISTORY OF THE PROBLEM

The classification of λ 5694 has been in doubt ever since Edlén's famous paper (1942), in which he identified most of the emission lines in the solar corona known at that time. In particular, he found by extrapolation of the C I isoelectronic sequence that for the $2s^2 2p^2$ configuration of Ca XV the $^3P$ term has two approximately equal energy intervals, $E(21) \equiv {}^3P_2 - {}^3P_1$ and $E(10) \equiv {}^3P_1 - {}^3P_0$, for which he computed the value of 17.7 kK,[1] i.e., 5650 A. He therefore surmised that λ 5694 should be identified with one of these two transitions.

The line λ 5446 was discovered by Waldmeier (1947), who later suggested (1951) that it might be the other one of the two Ca XV $^3P$ transitions. Being slightly higher in energy and lower in intensity, the classification

$$E(21) = 5446\,\text{A} = 18.355\,\text{kK} \qquad \text{and} \qquad E(10) = 5694\,\text{A} = 17.566\,\text{kK} \quad (1)$$

was adopted.

With this classification, the experimental intensity ratio was $I_{10}/I_{21} \sim 6$, whereas Shklovsky (1950) showed that theory predicts 1.05–1.53. This discrepancy was resolved by Pecker, Billings, and Roberts (1954), who found that the intensity of λ 5446.5 ±0.3 was underestimated, because that line is blended with two absorption lines, λ 5445.92 and λ 5446.93. The corrected ratio of about 1.6 is in fairly good agreement with theory.

In the same work Pecker, Billings, and Roberts also showed that a comparison of Doppler widths of λλ 6374, 5303, and 5694, when associated with the same kinetic temperature, results in an estimate for the atomic weight of the element responsible for λ 5694, and found $A = 40 \pm 2$. This is consistent with identification (1) in Ca XV but does not exclude neighboring elements like argon ($A = 39.9$) or potassium ($A = 39.1$).

Since Ca XV lines are associated with the highest ionization potential (814 ev) of all the coronal emission lines, the next two highest being 655 ev of λ 4086 from Ca XIII and 589 ev of λ 3328 from Ca XII, a check on the proposed classification was very desirable. Furthermore, since a laboratory experiment is out of the question, it is necessary to calculate the $2s^2 2p^2\ {}^3P_{0,1,2}$ levels of Ca XV on theoretical grounds. This was done by Garstang (1952), who took into account spin-orbit, spin-spin, and spin–other orbit interactions and to some extent configuration interaction also. He found

$$E(21) = 5380\,\text{A} = 18.58\,\text{kK} \qquad \text{and} \qquad E(10) = 5480\,\text{A} = 18.24\,\text{kK}\,. \quad (2)$$

[1] $1\,\text{kK} = 10^3\,\text{K} = 10^3\,\text{cm}^{-1}$.

He estimated the error of his calculation to be about $\pm 50$ A, so that his result and classification (1) are incompatible.

Another attempt to estimate the Ca XV levels was made by Naqvi and Talwar(1955), who, by least-squares methods, tried to fit a polynomial to the energy levels of the isoelectronic sequence based on C I of which Ca XV is a member. Extrapolation of the known levels (C I to Si IX) in this way yielded

$$E(21) = 4998\,\text{A} \quad \text{and} \quad E(10) = 6055\,\text{A}. \tag{3}$$

Again, an estimated error of about $\pm 50$ A was given. Thus all three results, equations (1), (2), and (3), are incompatible with one another.

It was then shown by Layzer (1954) that the interaction between the configurations $2s^2 2p^2$ and $2p^4$, not satisfactorily included by Garstang, is important enough to modify Garstang's results (eq. [2]) by much more than $\pm 50$ A. He found

$$E(21) = 5456\,\text{A} = 18.327\,\text{kK} \quad \text{and} \quad E(10) = 5650\,\text{A} = 17.701\,\text{kK}. \tag{4}$$

With a possible error of $\pm 50$ A (Layzer does not give errors on his results), these wave lengths are in very good agreement with classification (1), but they do not explain the very different results of Naqvi and Talwar.

More recently, Edlén (1954) studied the problem again along the same lines as those in his original paper on the coronal emission lines (1942). But he admitted interactions neglected in the earlier paper, by permitting two different values of the spin-orbit interaction parameter, $\zeta_{2-1}$ and $\zeta_{1-0}$, respectively. The extrapolation of these parameters leads to the assignment of equation (1) within an error that does not seem to exceed $\pm 50$ A by very much. In any case, assignment (1) is seen to be consistent with the isoelectronic sequence from C I to Si IX. Thus, together with Layzer's result (4), there seems to be strong evidence in favor of classification (1).

## II. PURPOSE AND METHOD OF THE PRESENT INVESTIGATION

The foregoing historical outline shows that the theoretical approach to the solution of this classification problem was governed by confusion. Only the recent work by Layzer (1954) and Edlén (1954) seems to lead to consistent results. In the light of this situation a *careful* theoretical analysis is very desirable.

For the purpose of such an analysis it is essential that the theory of atomic spectra be used in an approximation accurate enough for the problem at hand. None of the previous theoretical work—with the exception of Layzer's—has used such an approximation. In its place a relatively poor approximation of the theory was used, and the corresponding parameters were determined in such a manner that these approximate equations reproduce *exactly* the observed energy levels. The result was that the parameters were forced to take on values which in some cases were quite far from the correct values (*distorted* set of parameters). After all, these parameters are not arbitrary but can, in principle, be computed by determining the atomic wave functions. Since such a determination is not practical—even a self-consistent field calculation, including exchange and configuration interaction, is not accurate enough[2] (Hartree, Hartree, and Swirles 1940)—we are forced to use a semiempirical method, but one that involves a sufficiently high approximation to render the correct parameter values.

Until very recently such a method was not available, so that a satisfactory theoretical treatment was previously not possible. The discovery of the polarization effect by Layzer (1950) and Trees (1951*a*, *b*) and the generalization of the Bacher-Goudsmit method by Meshkov and Ufford (1954) finally led to the so-called *linear theory* (Trees 1954). This theory is essentially the old Slater method augmented by the polarization effect, but

[2] Recent work by Zirin (1955) belongs in the same class. His results for $\zeta$ and $\eta$ are not accurate enough to be useful for the Ca XV problem.

with Slater integrals $F_k$ and $G_k$ which are linear functions of the degree of polarization, $q$, and the number of equivalent electrons in the outer subshells. This author succeeded in showing that this linear theory in combination with configuration interaction can account very well for the energy levels of the first short period and its isoelectronic sequences (Rohrlich 1956). Therefore, we want to make full use of this method in the Ca XV problem.

In addition to this general background as the main incentive for the present paper there are two more specific but related reasons:

*a*) In the case of Ca XV one can show that the polarization effect is very small, so that Layzer's method for this case involves the same equations as the afore-mentioned linear theory augmented by configuration interaction. However, Layzer's determination of the parameter $\phi$ for configuration interaction is subject to criticism and also affects the values for the parameters $\zeta$ and $\eta$ which he used. Thus his parameters $\phi$, $\zeta$, and $\eta$ may not be consistent. Since the levels are very sensitive to these parameters, his final result is subject to doubt.

*b*) It must be shown that the methods used by Garstang (1952) and by Naqvi and Talwar (1955) are indeed incapable of yielding correct results.

## III. THE SENSITIVITY OF LAYZER'S RESULT

The $2s^22p^2$ configuration consists of the terms $^3P$, $^1D$, and $^1S$ in this order. When spin-orbit coupling (characterized by the parameter $\zeta$) and spin-spin and spin–other orbit coupling (both characterized by the parameter $\eta$) are taken into account, the energy matrix consists of the two $2 \times 2$ matrices for $J = 2$ ($^3P_2$, $^1D_2$) and $J = 0$ ($^3P_0$, $^1S_0$) and a single term for $J = 1$ ($^3P_1$). These matrices were studied by Garstang (1951). When configuration interaction with $2p^4$ is included, the terms of that configuration (which are the same as those of $2s^22p^2$) will interact with those of $2s^22p^2$ in pairs, since that interaction commutes with $L^2$, $S^2$, and the parity. The result is an energy matrix consisting of two $4 \times 4$ matrices (for $J = 2$ and 0) and one $2 \times 2$ matrix (for $J = 1$), as was shown explicitly by Layzer (1954).

Whereas the case $J = 1$ evidently does not offer any difficulties, the fourth-order secular equations must be solved by suitable approximation methods. Layzer used fifth-order Schrödinger perturbation theory, which should give an accuracy of 1 in $10^4$ in this case. However, the method is complicated and does not easily lend itself to improvement. We have therefore adopted a different method. We first solve the $2 \times 2$ subdeterminants, which involve the configuration interaction, thereby reducing the matrix to two $2 \times 2$ matrices (quadratic approximation). Solving these, we obtain a zeroth approximation. From here on, one can use the Newton-Raphson method or similar methods of equally good accuracy. In our case the zeroth approximation is already good to 1 in $10^3$, and the next approximation is better than fifth-order perturbation theory. This can be seen in Table 1, where the experimental results and those of Garstang (1952) and Layzer (1954) are also given.

The parameters which represent the radial integrals are $f = 3F_2$, $\zeta$, $\eta$, $\phi$, and $L$. They are, respectively, the Slater coefficient $F^2(2p, 2p)$ times $\frac{3}{25}$, the spin-orbit interaction parameter, the spin-spin and spin–other orbit interaction parameter, the configuration interaction parameter, and a parameter that characterizes the separation of the two configurations $2s^22p^2$ and $2p^4$. Layzer's work also involves the parameters $f^*$, $\zeta^*$, and $\eta^*$ (of $2p^4$), which, in general, are different from $f$, $\zeta$, and $\eta$ (of $2s^22p^2$).

In order to compute the sensitivity of the energy levels on these parameters we derive a simple formula. Let

$$f(\lambda) = \sum_{m=0}^{N} a_m \lambda^{N-m} = 0 \qquad (a_0 = 1)$$

be a polynomial equation with $N$ real roots $\lambda_i (i = 1, \ldots, N)$. These roots can be expressed in terms of the $a_m$. Therefore, if these $a_m$'s depend on a parameter $p$,

$$\delta \lambda_i = \sum_m \frac{\partial \lambda_i}{\partial a_m} \frac{\partial a_m}{\partial p} \delta p .$$

On the other hand, we obtain, by differentiation of $f(\lambda)$ at $\lambda = \lambda_i$,

$$\frac{\partial \lambda_i}{\partial a_m} = - \frac{\lambda_i^{N-m}}{f'(\lambda_i)} ,$$

where

$$f'(\lambda_i) \equiv \left[ \frac{df(\lambda)}{d\lambda} \right]_{\lambda = \lambda_i} = \prod_{j \neq i} (\lambda_i - \lambda_j) .$$

TABLE 1*

$^3P$ SPLITTING IN VARIOUS APPROXIMATIONS BASED ON GARSTANG-LAYZER PARAMETERS

| | *a* | *b* | *c* | *d* | *e* | *f* |
|---|---|---|---|---|---|---|
| $E(21)$ . . . . | 18.58† | 18.327 | 18.054 | 18.287 | 18.288 | 18.355 |
| $E(10)$ . . . . | 18.24 | 17.701 | 18.143 | 17.671 | 17.669 | 17.556 |

* The column heads have the following meanings:
*a*: Configuration interaction included empirically (Garstang 1952).
*b*: Configuration interaction included theoretically, using fifth-order perturbation theory (Layzer 1955).
*c*: Same as *b*, but solving the secular equations in "quadratic approximation" (zeroth approximation).
*d*: Same as *c* in first approximation.
*e*: Same as *c* in second approximation.
*f*: Experimental.

† All energies are in kK = $10^3$ cm$^{-1}$.

TABLE 2

SENSITIVITY TO PARAMETERS OF $^3P$ LEVEL INTERVALS

| | $\Delta\zeta = 1$ Per Cent | $\Delta\eta = 1$ Per Cent | $\Delta\phi = 1$ Per Cent | $\Delta L = 1$ Per Cent |
|---|---|---|---|---|
| $\Delta E(21)$ . . . . | 0.163 | −0.0135 | −0.00563 | 0.0028 |
| $\Delta E(10)$ . . . . | 0.296 | +0.00053 | +0.00487 | 0.0056 |

It follows, therefore, that

$$\delta \lambda_i = - \frac{\sum_{m=1}^{N} \lambda_i^{N-m} (\partial a_m / \partial p)}{\prod_{j \neq i} (\lambda_i - \lambda_j)} \delta p . \qquad (5)$$

With the help of this formula we can compute by how much the $E(ij)$'s are affected because of an error of 1 per cent in any one of these parameters. The results are shown in Table 2 for the parameters $\zeta$, $\eta$, $L$, and $\phi$. The sensitivity of $E(ij)$ to the other parameters is small and will be discussed later. This calculation is based on the Garstang-Layzer parameters.

A comparison of columns *e* and *f* of Table 1 with Table 2 shows that a 1 per cent accuracy in $E(ij)$ requires that the error in $\zeta$ be, at most, about $\frac{1}{2}$ per cent. In fact, if Garstang's $\zeta$ were too small by 3 per cent, the corrected value of $E(10)$ would agree with the experimental value attributed to $E(21)$, and classification (1) would be completely overthrown. A similar situation would arise if $\eta$ were too small by 50 per cent. Such considerations also apply to the other parameters, though the classification depends less critically on them.

From Table 2 we also learn that the sensitivities of $E(21)$ and $E(10)$ with respect to $\phi$ are opposite in sign but of approximately the same magnitude. Thus a calculation which ignores configuration interaction (corresponding to $\phi = 0$) should give too large a value for $E(21)$ and too small a value for $E(10)$ but should not affect $E(20) = E(21) + E(10)$ very much. With this in mind, we can now understand the difference between the results of Garstang and those of Layzer (Table 1, cols. *a* and *b*).

The term separations in $2p^4$ and in $2s^22p^2$ are small compared to the separation of the two configurations. Therefore, the $J = 2$ and $J = 1$ levels (in particular, $^3P_2$ and $^3P_1$ of $2s^22p^2$) will be shifted by about the same amount by configuration interaction (the corresponding off-diagonal matrix elements being $\phi$ in both cases). Thus, in a first approximation, $E(^1D_2) - E(^3P_2)$ is not affected by $\phi$. On the other hand, the matrix elements of configuration interaction between the $^1S_0$ levels are $2\phi$ and between the $^3P_0$ levels they are only $\phi$. The $^1S_0$ and the $^3P_0$ levels of $2s^22p^2$, in turn, interact via $\zeta$ and $\eta$. Thus, $E(^1S_0) - E(^3P_0)$ will be affected strongly by configuration interaction, and the $^3P_0$ level of $2s^22p^2$ will be pushed down relatively farther than the $^3P_1$ and $^3P_2$ levels. It then follows (cf. Layzer's eqs. [3.1]) that Garstang's empirical term difference $DP$ must be equal to $6F_2$ in good approximation, whereas his $SP$ must be less than the Slater value $15F_2$. This can be seen formally from Layzer's equations (3.5). It is then not surprising that Garstang's value of $E(21)$ differs from the experimental value by only 66 A, whereas his $E(10)$ differs by 214 A.

We can now repeat Garstang's calculations but ignore configuration interaction,[3] by replacing his empirical value of $SP$ by $\frac{15}{6}\,DP$. This does not affect $E(21)$ but yields a smaller $E(10)$:

$$E(21) = 18.58\,\mathrm{kK} = 5380\,\mathrm{A} \quad \text{and} \quad E(10) = 17.48\,\mathrm{kK} = 5720\,\mathrm{A}\,, \tag{6}$$

in much better agreement with (1) than his value (2). The level separation (6) is smaller than Layzer's $E(10)$, in agreement with $\delta E(10)/\delta\phi > 0$ and with the fact that $E(20)$ is about the same as Layzer's (Table 2).

When we now compare the result (6) with that computed by Layzer (eq. [4]), we find that the inclusion of configuration interaction did not improve the agreement significantly. In the next section I want to show that this is due to a poor choice of parameters in Layzer's calculation, viz., that the parameters he adopted are not strictly consistent.

## IV. THE PARAMETERS AND THEIR ERRORS

The sensitivity of Layzer's results on $\zeta$ and $\eta$ raises the question of the accuracy of these parameters. There are two types of errors to be considered—errors due to the extrapolation and errors due to the inaccuracy of the parameters on which the extrapolation is based.

In extrapolating the semiempirical values of $\zeta$ for the low $Z$ members of the isoelectronic sequence of C I to $\zeta$ for Ca XV, Garstang used the semitheoretical result that $\zeta^{1/4}$ should be a linear function of $Z$. If this fourth-power law for $Z$ were exact, a least-squares calculation could establish $\zeta$(Ca XV) with an accuracy of 0.2 per cent, as can be verified explicitly. But this law is rigorously valid only for hydrogen-like atoms or in the

[3] This, of course, is not strictly true because his values of $\zeta$ and $\eta$ also depend on his method and therefore include $\phi$ to some extent.

limit $Z \to \infty$. In general, this law must therefore be regarded as the leading term in an expansion for large $Z$. But it follows from Garstang's semiempirical analysis (1951) that the fourth-power law is satisfied much more accurately than might be anticipated. The explanation of this fact may be sought in connection with the linear theory mentioned in Section II. In this theory it is shown that the Slater parameters depend linearly on the degree of ionization $q$ (and therefore also on $Z$) not only for very large $q$ (as discussed in the asymptotic form by Layzer, 1954) but even for $q \geq 2$ or 3. An explicit verification of this assertion was made recently for s and p electrons (Rohrlich 1956). Since this variation must be due to a corresponding dependence on $q$ of the wave functions, it is not so surprising that $\zeta$ and $\eta$ also take on their asymptotic $q$ dependence in the third or fourth spectrum.

The error in $\zeta$(Ca XV) due to possible systematic errors in the values of $\zeta$ on which the extrapolation is based can be much more serious. Garstang included the interaction between the configuration $2s^22p^2$ and $2p^4$ only in a certain sense, and the parameters for $2s^22p^2$ are undoubtedly affected thereby. Since configuration interaction is of increasing relative importance with increasing $\zeta$ and the extrapolation has to be carried quite far (from Si IX to Ca XV), the error in $\zeta$ can be appreciable. An estimate shows errors of the order of 1 per cent (cf. eqs. [20] and [22]). The situation with respect to $\eta$ is similar in every respect except that the *percentage* errors in $\eta$ are even much larger.

An accurate calculation of $\zeta$ and $\eta$ can be made only by a simultaneous analysis of $2s^22p^2$ and $2p^4$, including configuration interaction and otherwise following the linear theory. Unfortunately, the experimental data on $2p^4$ are much too scant for this purpose. For this reason a completely satisfactory theoretical classification of the lines in question cannot be made at the present time.

Nevertheless, it is possible to obtain a fairly reliable check on classification (1) by the following procedure. We know that a calculation with correct parameters (including $\zeta$, $\eta$, and $\phi$) can predict energy levels to very good accuracy. This accuracy can be estimated. Knowing all the parameters except $\zeta$ and $\eta$, we can now *assume* the correctness of classification (1) and compute from it $\zeta$ and $\eta$ to high accuracy. If we are then able to determine the dependence of $\zeta$ and $\eta$ on $\phi$, we can find the effective value of $\phi$ that corresponds to Garstang's analysis, $\phi_G$, such that his parameter values $\zeta_G$ and $\eta_G$, together with $\phi_G$, form a consistent (though distorted) set of parameters. Using this set, we must then be able to compute classification (1) within the accuracy of the parameters, provided that the original assumption of the validity of (1) is correct. This argument is not circular, because the dependence of $\zeta$ and $\eta$ on $\phi$ can be obtained without the use of Garstang's values, $\zeta_G$ and $\eta_G$, and because the functional form of $\zeta(\phi)$ and $\eta(\phi)$ is independent of assumption (1).

We now turn to the determination of all the necessary parameters other than $\zeta$ and $\eta$. These parameters are the Slater parameters $f$ and $f^*$ (the unstarred parameters refer to $2s^22p^2$, the starred ones to $2p^4$); the configuration interaction parameter $\phi$; the parameter $L$, which gives the energy difference between the two configurations; and the parameters $\zeta^*$ and $\eta^*$ of $2p^4$.

Some of these parameters can be obtained from a study of the first short period and its isoelectronic sequences (Rohrlich 1956). For example, the parameter $f$ is found to be given by

$$f(2s^m2p^n) = 2.3374q + 1.4743(n + 2m) - 3.4470 \text{ kK},$$

where $q$ is the degree of polarization. This formula fits the results of 50 terms of various configurations with a standard deviation of

$$\Delta = \pm 0.164 \text{ kK}.$$

For the cases of interest here ($q = 14$), this formula yields

$$f \equiv f\,(2s^2 2p^2) = 38.12 \pm 0.16\,\text{kK}\,, \tag{7}$$

$$f^* \equiv f\,(2p^4) = 35.17 \pm 0.16\,\text{kK}\,. \tag{8}$$

The same study also shows the importance of the so-called "polarization effect" for the calculation of term separations. However, the characteristic parameter, $\Lambda$, approaches zero for large $q$, and we can ignore the effect within the error of these calculations. For this reason we can identify the parameters $f$ and $\frac{3}{25}F^2(2p, 2p)$.

Equation (7) gives practically the same value for $f$ as is obtained from Garstang's $DP$ difference (38.2 kK) and which was adopted by Layzer. This is not surprising in view of the discussion preceding equation (6) and since it is known that configuration interaction has little effect on the Slater parameter $F_2$ (Hartree, Hartree, and Swirles 1940; Rohrlich 1956). The value of $f^*$ is about 8 per cent smaller than that of $f$. We shall see that $E(21)$ and $E(10)$ are quite insensitive to $f^*$, so that Layzer's assumption $f = f^*$ is indeed a good one.

The most important result for the present work that can be obtained from the general analysis of the first short period is an estimate of the configuration interaction parameter $\phi$. This parameter is actually identical with the Slater parameter $G_1(2s, 2p)$,

$$\phi = G_1\,(2s, 2p) = \tfrac{1}{3}G^1\,(2s, 2p)\,. \tag{9}$$

A semiempirical analysis now gives a very precise formula for the $q$ and $n$ dependence of $G_1(2s^2 2p^{n-2} - 2p^n)$, but its absolute value is most reliably obtained from the relation[4]

$$G_1\,(2s^2 2p^{n-2} - 2p^n) = G_1\,(2s2p^{n-1})\,. \tag{10}$$

The latter was found to be (Rohrlich 1956)

$$G_1\,(2s2p^n) = 6.6098q + 4.7002n + 7.0533\,\text{kK}\,, \tag{11}$$

with a standard deviation,

$$\Delta = \pm 0.239\,\text{kK}\,, \tag{12}$$

on 36 points. Thus

$$\phi = G_1\,(2s2p^3;\ q = 14) = 113.69 \pm 0.24\,\text{kK}\,. \tag{13}$$

This result is to be compared with Layzer's

$$\phi = 101.31\,\text{kK}\,, \tag{14}$$

which is considerably lower. This low value was obtained by applying a formula for the level separation $^3P_1(2p^4) - {}^3P_1(2s^2 2p^2)$ to the only observed $^3P_1(2p^4)$ levels, viz., those for $q = 2, 3, 4$, and 5, and by extrapolating the result to $q = 14$, assuming a linear variation of $L$ and $\phi$. We regard this to be a rather daring procedure. The result (13) is consistent with 21 values of configuration interaction of $2p^n$ with $2s^2 2p^{n-2}$, which range up to atoms with $q = 10$.

Once a value of $\phi$ is known, it is easy to find an estimate for $L$. As we shall see, $L$ need not be very accurate, since the $E(ij)$ are not very sensitive to it. If we ignore the effect of $\zeta$ and $\eta$ on the term separations, the $^3P(2p^4)$ and the $^3P(2s^2 2p^2)$ terms interact so that

$$L'^2 = L^2 + 4\phi^2\,, \tag{15}$$

where $L'$ is the observed $^3P$ separation and $L$ is the $^3P$ separation that would be there if $\phi = 0$. Layzer found, for Ca XV,

$$L = 1036.8\,\text{kK}\,, \tag{16}$$

[4] I am indebted to Professor Racah for a communication on this point.

from which we obtain, with equations (14) and (15),

$$L' = 1056\,\text{kK} . \tag{17}$$

This result is in good agreement with an independent extrapolation of the observed $^3$P terms which yields $L' = 1050$ kK. In any case, the internal consistency of Layzer's derivation of $\phi$ and $L$ guarantees that equation (17) is fairly accurate, even though Layzer's parameters are distorted. From equations (13), (15), and (17) we find

$$L = 1031.1 \pm 0.2\,\text{kK} . \tag{18}$$

The error is due to the error in $\phi$. The error in $L'$ is difficult to estimate, since only four $^3$P($2p^4$) are observed, as was mentioned previously. However, even a conservative estimate of $\pm 20$ kK will not affect $E(ij)$ unreasonably, as we shall see later.

We shall follow Layzer and assume $\zeta^* = \zeta$ and $\eta^* = \eta$. The error in $\eta^*$ due to this approximation will be seen to have a negligible effect on $E(ij)$, even when $\eta^*$ differs from $\eta$ by a factor of 2. On the other hand, $E(ij)$ is quite sensitive to $\zeta^*$. For lack of a better estimate, we notice that $f^*$ differs from $f$ by about 10 per cent, and we shall assume the same for $\zeta^*$ compared to $\zeta$. This is definitely the weakest point in our error estimate.

Following our program, we now take the best values of $\zeta$ and $\eta$ which are available, viz., those obtained by Garstang (1952),

$$\zeta_G = 24.21\,\text{kK} \quad \text{and} \quad \eta_G = 0.091\,\text{kK} , \tag{19}$$

and, using these as first approximations, compute the energy levels with these chosen parameters. The fourth-order secular equations are again solved by the method described in connection with Table 1. The first iteration is again sufficient for our purpose. The results are given in Table 3.

TABLE 3

$^3$P LEVEL SPACINGS AND THEIR SENSITIVITY

| | $E$ | $\partial E/\partial\zeta$ | $\partial E/\partial\eta$ | $\partial E/\partial\phi$ | $\partial E/\partial L$ | $\partial E/\partial f$ | $\partial E/\partial f^*$ | $\partial E/\partial\zeta^*$ | $\partial E/\partial\eta^*$ |
|---|---|---|---|---|---|---|---|---|---|
| $E(21)$ . . | 18.154 | 0.6236 | −14.930 | −0.00623 | 0.00092 | +0.112 | −0.0132 | −0.0088 | −0.080 |
| $E(10)$ . . | 17.735 | 1.0774 | +0.7722 | +0.00851 | 0.00028 | −0.154 | +0.0115 | −0.0143 | +0.0110 |

From this table and the foregoing discussion of the parameters we conclude that the errors $\epsilon(ij)$ of the energies $E(ij)$ due to the errors in all the parameters except $\zeta$ and $\eta$ are

$$\epsilon(21) \sim \epsilon(10) \sim \pm 0.05\,\text{kK} . \tag{20}$$

Within these errors the parameters $\zeta$ and $\eta$ can now be determined, assuming assignment (1). From

$$\Delta E(ij) = \Delta\zeta \frac{\partial E(ij)}{\partial\zeta} + \Delta\eta \frac{\partial E(ij)}{\partial\eta}$$

and Table 3 it follows that

$$\zeta - \zeta_G \equiv \Delta\zeta = -0.143 \pm 0.050\,\text{kK} , \qquad \eta - \eta_G \equiv \Delta\eta = -0.0194 \pm 0.0053\,\text{kK} ,$$

and, with equations (19) and (20),

$$\zeta = 24.07 \pm 0.05\,\text{kK} \quad \text{and} \quad \eta = 0.072 \pm 0.005\,\text{kK} . \tag{21}$$

This result means that the linear theory, augmented by configuration interaction, which for Ca XV leads to parameters (7), (8), (13), and (18), would yield parameters

(21) in intermediate coupling, provided that assignment (1) is correct. This set of parameters is not distorted, since it was obtained from a sufficiently accurate approximation of the theory. The fact that parameters (21) are not very different from those obtained by Garstang (eq. [19]), which we took as our first approximation, shows that the first derivatives are indeed sufficient for estimate (21).

From the sensitivities in Table 2 we conclude that, in the first approximation, a change of $\phi$ will affect only the parameters $\zeta$ and $\eta$,

$$\frac{\partial E(ij)}{\partial \phi} + \frac{\partial E(ij)}{\partial \zeta}\frac{d\zeta}{d\phi} + \frac{\partial E(ij)}{\partial \eta}\frac{d\eta}{d\phi} = 0\,, \tag{22}$$

where $\phi$ is regarded as the independent variable. From Table 3 one easily computes

$$\frac{d\zeta}{d\phi} = -0.00737 \qquad \text{and} \qquad \frac{d\eta}{d\phi} = -0.000725\,. \tag{23}$$

In order to determine the functions $\zeta(\phi)$ and $\eta(\phi)$, we notice that $\phi$ is a linear function of $Z$ (cf. eq. [11]). On the other hand, $\zeta^{1/4}$ and $\eta^{1/3}$ are also linear functions of $Z$. It follows, therefore, that the functions $\zeta^{1/4}[\phi(Z), Z]$ and $\eta^{1/3}[\phi(Z), Z]$ must be of the form

$$\zeta^{1/4} = \alpha\phi + \beta(Z)\,, \qquad \eta^{1/3} = \gamma\phi + \delta(Z)\,,$$

where $\alpha$ and $\gamma$ are constants and $\beta(Z)$ and $\delta(Z)$ are linear functions of $Z$. Using equations (21) and (23), we easily find

$$\zeta^{1/4} = -0.0001696\phi + 2.234\,\mathrm{kK}^{1/4}\,, \qquad \eta^{1/3} = -0.001397\phi + 0.575\,\mathrm{kK}^{1/3}\,. \tag{24}$$

If we use $\zeta_G$ and $\eta_G$ in these equations, we find $\phi = 93.2$ and $\phi = 89.5$, respectively. This is not surprising, since there is no reason why Garstang's empirical way of including configuration interaction should yield values $\zeta_G$ and $\eta_G$ consistent with one definite $\phi$. On the other hand, the fact that the two values of $\phi$ are actually fairly close shows that Garstang's method takes account of configuration interaction almost correctly except for the effective magnitude of $\phi$. Let us take $\phi_G = 90 \pm 3$kK. This error will cause a smaller error in $E(ij)$ than the errors due to $\zeta$ and $\eta$ in equation (21), and we shall ignore it from now on: $\phi_G = 90$ yields $\zeta(90) = 24.23 \pm 0.05$ and $\eta(90) = 0.0907 \pm 0.005$, which are well within the errors of $\zeta_G$ and $\eta_G$.

The parameters $\zeta_G$, $\eta_G$, and $\phi_G$ are a consistent set, and we conclude that Layzer's value of $\phi$ ($\phi_L = 101.31$) is 11.15 per cent too high to be consistent with $\zeta_G$ and $\eta_G$. Tables 1 and 2 permit us to correct this situation, since $\delta E(ij)/\delta\phi$ was computed there. We obtain

$$\begin{aligned} E(21) &= 18.351 \pm 0.082\ \mathrm{kK} = 5449 \pm 24\,\mathrm{A} \\ E(10) &= 17.615 \pm 0.063\ \mathrm{kK} = 5677 \pm 20\,\mathrm{A}\,. \end{aligned} \tag{25}$$

Though this result is obtained with a distorted parameter set, it provides evidence for the correctness of classification (1), because the set is internally consistent. I want to emphasize again that the result, equations (25), is meaningful even though we have assumed classification (1) in the derivation of equations (21). The reason for this fact was mentioned earlier in this section. In addition, we can easily verify how the assumption of a classification different from equations (1) would affect the result (eq. [25]). For example, we may assume that the empirical Ca XV $^3P_1 - {}^3P_2$ transitions are 0.789 kK larger than in equations (1):

$$E(21) = 19.144\,\mathrm{kK}\,, \qquad E(10) = 18.355\,\mathrm{kK} \tag{1'}$$

This corresponds to the assumption that λ 5694 is not due to Ca XV, that λ 5446 is the $^3P_1-{}^3P_0$ transition in Ca XV, and that $^3P_2-{}^3P_0$ is the same as before. One then finds, instead of equations (21),

$$\zeta = 24.82 \pm 0.05\,\mathrm{kK}\,, \qquad \eta = 0.050 \pm 0.005\,\mathrm{kK}\,. \tag{21'}$$

As before, we can determine the $\zeta(\phi)$ and $\eta(\phi)$,

$$\zeta^{1/4} = 0.0001657\phi + 2.251\,\mathrm{kK}^{1/4}\,, \qquad \eta^{1/3} = -0.001785\phi + 0.571\,\mathrm{kK}^{1/3}\,; \tag{24'}$$

and we finally obtain the values of $\phi$ corresponding to $\zeta_G$ and $\eta_G$. These are $\phi_G = 196.7$ kK and $\phi_G = 67.8$ kK; they are vastly different from each other as well as from the correct value (eq. [13]). Neither value reproduces classification (1′) by a computation analogous to equations (25).

## V. ON THE METHOD OF NAQVI AND TALWAR

It remains to be explained why the results in equation (3) differ from and seem, in fact, incompatible with classification (1). The essential difference between the work of Naqvi and Talwar (1955) and that of the other authors who used extrapolation lies in their method. They do not use theoretical formulae for their extrapolation, but they fit the known level separations to a polynomial and extrapolate it to Ca XV. If the extrapolation is large, the power of the polynomial need not be very high to yield results which are extremely sensitive to the underlying formula,

In order to illustrate this point, we studied the parameter $\zeta$ which is characteristic of the level spacings. We compared that formula,

$$\zeta = \alpha\,(Z-\sigma)^{4.00}\,,$$

which was used by Garstang, with the formula

$$\zeta = \alpha'\,(Z-\sigma')^{3.80}\,.$$

The extrapolation of the known $\zeta$-values in the C I sequence yields 24.20 ± 0.05 kK and 23.04 ± 0.10 kK, respectively. The resulting 5 per cent error would be much too large for the question of assignment, as we showed in the previous section.

If we use a fourth-order polynomial, the same extrapolation yields $\zeta = 21.86$ kK by the method of least squares. This value is even further remote from the correct value. But here the fallacy of the extrapolation method is particularly apparent. The fourth differences of the given $\zeta$-values show random fluctuations around zero. The coefficient of the leading power of the polynomial will therefore be poorly determined. However, the extrapolated value of $\zeta$ will receive its main contributions from the largest power in the polynomial. The error will therefore increase rapidly with $Z$. For the case in point it will be much too large to permit any classification. From Table 3 we find $\epsilon(21) = \pm 440$ A and $\epsilon(10) = \pm 770$ A. Within these errors, equations (1) and (3) are consistent. The fact that the method is successful in some cases but not in others depends on the sensitivity of the level spacings to the parameters and on how far one extrapolates. It would be coincidental if the complicated $Z$-dependence of the level spacings were represented by a simple polynomial to 1 per cent accuracy. These examples show that it is absolutely essential to base extrapolations of this kind on theoretical formulae.

## VI. SUMMARY OF RESULTS

1. The extrapolation method employed by Naqvi and Talwar is in error by about ten times more than was estimated by these authors, removing the apparent contradiction between their result and the experimental classification (1).

2. Layzer's results are criticized, because they are so sensitive to the parameters that

the crude method of parameter determination employed by him is not justified. In fact, his results, which include configuration interaction, are theoretically not much better than Garstang's calculation when configuration interaction is eliminated, because the parameters adopted by him are not consistent.

3. Although at the present time it is not possible to make a completely satisfactory theoretical classification of the lines in question, because the experimental data on the $2p^4$ configuration of the isoelectronic sequence of C I are missing, one can, by an indirect argument, obtain a consistent set of parameters, $\zeta_G$, $\eta_G$, and $\phi_G$, which confirm that $\lambda$ 5446 and $\lambda$ 5694 are indeed the $^3P_2-{}^3P_1$ and $^3P_1-{}^3P_0$ transitions of $2s^22p^2$ in Ca XV (cf. eq. [25]).

4. The most important (undistorted) parameters are

$$\zeta = 24.07 \pm 0.05\,\mathrm{kK}\,, \qquad \eta = 0.072 \pm 0.005\,\mathrm{kK}\,, \qquad \phi = 113.7 \pm 0.2\,\mathrm{kK}\,. \quad (26)$$

5. Finally, we learn from our analysis that a consistent set of parameters based on a poorer theoretical approximation can give a good or even better result than a poorly determined set of parameters based on a good theoretical approximation. For this reason, the extrapolation method employed by Edlén gives very good results, even though the theoretical formulae used are poor approximations. However, in such cases the parameters may differ considerably from their true values (distorted parameter set), thereby compensating in part for the errors in the approximation. Improved agreement can then be obtained by allowing greater variability of the parameters.

In conclusion, I should like to thank Dr. W. O. Roberts for drawing my attention to this problem and Dr. R. H. Garstang for a clarifying correspondence regarding his work. I am also indebted to Dr. D. Layzer for sending me a copy of his manuscript and for showing me Edlén's paper prior to its publication.

## REFERENCES

Edlén, B. 1942, *Zs. f. Ap.*, **22**, 30.
———. 1954, *M.N.*, **114**, 700.
Garstang, R. H. 1951, *M.N.*, **111**, 115.
———. 1952, *Ap. J.*, **115**, 569.
Hartree, D. R., Hartree, W., and Swirles, B. 1940, *Phil. Trans. R. Soc. London, A*, **238**, 229.
Layzer, D. 1950, thesis, Harvard.
———. 1954, *M.N.*, **114**, 692.
Meshkov, S., and Ufford, C. W. 1954, *Phys. Rev.*, **94**, 75.
Naqvi, A. M., and Talwar, S. P. 1955, *Ap. J.*, **121**, 287.
Pecker, Ch., Billings, D. E., and Roberts, W. O. 1954, *C.R.*, **238**, 1101.
Rohrlich, F. 1956, *Phys. Rev.*, **101**, 69.
Shklovsky, I. 1950, *Ann. Crim. Ap. Obs.*, **5**, 109.
Trees, R. E. 1951*a*, *Phys. Rev.*, **83**, 756.
———. 1951*b*, *ibid.*, **84**, 1089.
———. 1954, *J. Res. Nat. Bureau Stand.*, **53**, 35.
Waldmeier, M. 1947, *Astr. Mitt. Zürich*, No. 151.
———. 1951, *Zs. f. Ap.*, **29**, 29.
Zirin, H., 1955, *Ap. J.*, **121**, 528.

# CORONAL TEMPERATURE DETERMINATION FROM EMISSION LINES*

DONALD E. BILLINGS, SABINE HIRSCH, AND CARLOS VARSAVSKY
High Altitude Observatory
*Received January 5, 1956*

ABSTRACT

Coronal temperatures derived from widths of emission lines are compared with those derived from the relative brightness of the lines. In the majority of cases studied, temperatures from the two methods showed a definite correspondence, indicating that the widths of the coronal lines are primarily thermal.

Temperatures of the solar corona are derived from emission lines by two different means. One method is based on the relative intensities of the lines from two different stages of ionization of the same element (usually Fe X and Fe XIV). The other method is to compute from line profiles the thermal motion of the ions involved. The former, or degree-of-ionization method, has been applied by Waldmeier (1952*a*) and Elwert (1952), who obtained temperatures restricted to the rather narrow range 400000°–800000°.

The line-profile method of computing temperatures has been used by Lyot (1937), Waldmeier (1947), Dollfus and Lyot (partly published by Dollfus, 1953), and Pecker, Billings, and Roberts (1954). This method has yielded values from 1.8 million degrees upward to several million degrees, with the great majority of coronal regions manifesting temperatures in the vicinity of 2 million degrees. Waldmeier (1952*b*), noting the several hundred thousand degrees computed from line-intensity ratios, has attributed line broadening to macroscopic motions within the corona. In view of the violent motions exhibited by prominence material within the same localities, over active sunspot centers, where the line emission is most intense, it is certainly reasonable to expect considerable nonthermal motion in the corona. Indeed, the λ 6374 profile shown in Figure 1, traced from a High Altitude Observatory coronal spectrogram, clearly shows large-scale motion (Billings, Pecker, and Roberts 1954). The strongly Dopper-displaced emission arises from a relatively small portion of the corona and indicates motion in the same direction as that of a knot of prominence material which we could detect moving along the same line of sight.

We have now traced line profiles of a number of lines from the spectrograms made with the Climax coronagraph, paying special attention to those that appeared, on visual inspection, to be broadened. One important generalization has emerged: the type of line profile shown in Figure 1, in which large-scale motion is clearly evidenced, is the exception rather than the rule. Most of the profiles are Gaussian within the limits of resolution of the plates. Dollfus (1953) has drawn the same conclusion for lines of normal width. This strongly suggests that the Doppler broadening of most coronal lines may be primarily thermal. The work of Pecker, Billings, and Roberts (1954) tended to verify this suggestion. They found that by assuming the λλ 5303, 6374, and 5694 line widths in a very active region to be entirely thermal, they could compute the atomic weight of the ion emitting λ 5694 to be 40. Layzer (1955), Edlén (1955), and Rohrlich (1955) later gave theoretical evidence fully confirming Edlén's (1942) identification of the λ 5694 ion as Ca XV. Thus the assumption of thermal broadening appeared to be justified, although the line widths were equivalent to a temperature greater than 3000000°.

* This work was supported by the Office of Naval Research under Contract Nonr.-393(04).

In order to pursue further the idea that the widths of the coronal lines may arise primarily from thermal broadening, we have chosen coronal spectrograms from the past several years in which both λ 5303 and λ 6374 emission showed pronounced maxima, but for which the point on the limb of maximum λ 5303 emission is displaced at least 5° from the point of maximum λ 6374 emission. From each of such spectrograms we have made line-profile tracings of λ 5303 and λ 6374 at points of maximum emission for both lines. Next we used both the degree-of-ionization and the line-width method to compute the temperature at each point analyzed. For computing temperatures from degree of ionization we used tables given by Waldmeier (1952). The temperature at a given point

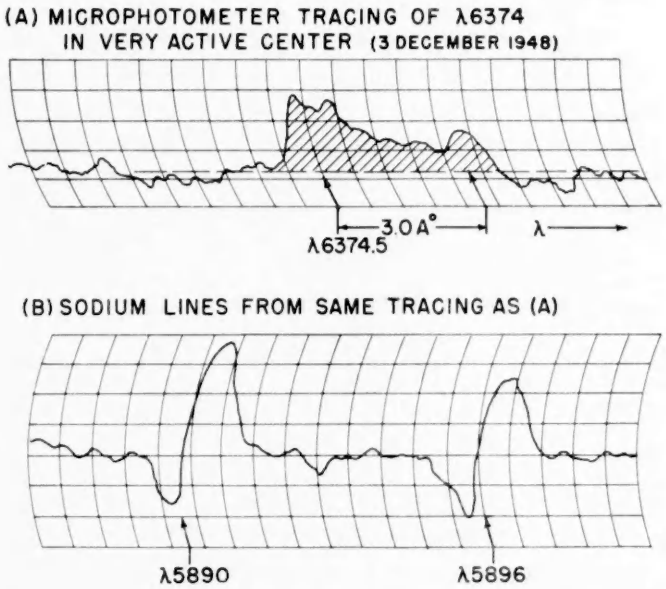


FIG. 1.—Microphotometer tracing of a 6374 coronal-line profile that shows large-scale Doppler distortion.

obtained by one method is plotted, in Figure 2, against the temperature at the same point obtained by the other method. Points representing positions on the limb of maximum λ 6374 emission are connected by arrows to points representing positions of maximum λ 5303 emission on the same spectrograms. We consider the directions of these arrows to be more significant than the positions of the individual points in Figure 2, because the line-width temperatures obtained from our older spectrograms are influenced by our evaluation of instrument broadening, whereas the relation between temperatures at two points on the same spectrogram should be more nearly independent of this parameter.

We note that five of the thirteen arrows in Figure 2 are almost exactly parallel and that, of the eight remaining, three are quite nearly parallel to these five. Thus differences in temperature between two near-by regions of the corona, when computed from line widths, appear to be proportional in the great majority of cases to those computed from

line-intensity ratios. (The one point in Fig. 2 showing a temperature less than $10^6$ degrees from line width was a very weak line, which the adjacent absorption line in the scattered-light continuum probably narrowed.) Hence only four of the thirteen pairs of points studied in the corona showed line-broadening temperatures that did not correspond to temperatures based on intensity ratios. We consider this as evidence that the Doppler broadening of coronal lines is primarily thermal. One arrow, shown by the heavy line, connects two points from the new spectrograph now in use in Climax, which has a dispersion of approximately 2.5 A/mm (more than three times as great as the instrument used for obtaining the other points) and a correspondingly small instrumental profile.

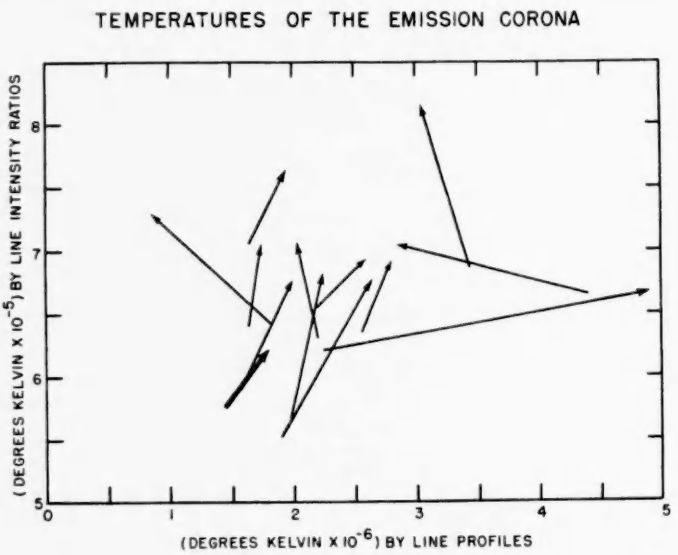


FIG. 2.—Relation between temperature of the emission corona as determined by line-intensity ratios and that determined by line widths. Temperatures determined by ratio of λ 5303 to λ 6374 intensities are plotted against temperatures determined by line width at the same position in the corona. Each arrow is drawn from a point representing temperatures at a position in the corona in which λ 6374 has a maximum intensity to a point corresponding to a position, shown on the same spectrogram, for which λ 5303 is maximum.

If we consider only the twelve pairs of points from the older spectrograph, we estimate the chance probability of finding four arrows as closely aligned as those in Figure 2 to be $2.54 \times 10^{-4}$. Similarly, we estimate the chance probability of finding seven of the twelve arrows as closely aligned as these to be $2.35 \times 10^{-4}$. The smallness of these chance probabilities, as well as the confirmation of the observed trend by the more precise instrument, strongly suggests that the line-profile broadenings are primarily thermal.

The authors wish to express their appreciation to Dr. Walter Orr Roberts, Dr. Harold Zirin, and Mr. Sanford B. Schwartz for many stimulating discussions of the question of coronal temperatures, and to Dr. Zirin for aid in the estimation of the statistical significance of the results.

## REFERENCES

Billings, D. E., Pecker, J. C., and Roberts, W. O. 1954, *C.R.*, **238**, 1194.
Dollfus, A. 1953, *C.R.*, **236**, 996.
Edlén, B. 1942, *Zs. f. Ap.*, **22**, 30.
———. 1954. *M.N.*, **114**, 700.
Elwert, G. 1952, *Zs. f. Naturforsch.*, **7A**, 432.
Layzer, D. 1955, *M.N.*, **114**, 692.
Lyot, B. 1937, *Astronomie*, **51**, 203.
Pecker, J. C., Billings, D. E., and Roberts, W. O. 1954, *Ap. J.*, **120**, 509.
Rohrlich, F. 1956, *Ap. J.*, **123**, 521.
Waldmeier, M. 1947, *Astr. Mitt. Eidgen. Sternw. Zürich*, No. 149.
———. 1952*a*, *Zs. f. Ap.*, **30** 137.
———. 1952*b*, *Trans. 11th Volta Cong.* (Rome: Acad. Lincei), pp. 171–184.

# THE HELIUM EQUILIBRIUM IN PROMINENCES AND THE CHROMOSPHERE

HAROLD ZIRIN
High Altitude Observatory
*Received December 23, 1955; revised January 19, 1956*

ABSTRACT

The equilibrium of helium in a gas suspended above the photosphere is analyzed by computing in detail the various atomic processes involved and writing down the equilibrium equations. These equations are solved for the occupation numbers of He III, He II, and the various important He I levels, in order to predict the relative intensity of helium lines. The triplet levels are in equilibrium (referred to the $2^3S$ state) with the photospheric radiation with the proper dilution factor. This gives good agreement with the 5876/10830 ratio measured by Severny. Particular attention is paid to the ratio of the lines 6678/5876. This is found to vary with temperature only, and the observed ratio should be a good measure of the temperature of helium.

## I. INTRODUCTION

The equilibrium of neutral helium in prominences, as well as in the chromosphere, is of peculiar interest to us because we are able to observe two separate series of lines—singlet and triplet—running parallel to each other. In particular, the transitions $3^3D-2^3P(5876)$ and $3^1D-2^1P(6678)$ are visible on most coronagraph spectra, and the strong line $2^3P-2^3S(10830)$ is now within the range of our instruments. It is therefore useful to analyze the processes involved in producing these lines and to predict their relative intensities.

Two salient facts govern the equilibrium of neutral helium: first, the ground configuration lies extremely low, 20 volts below the next lowest, and, second, ordinary optical transitions between the singlet and triplet series are strongly forbidden because of the change of multiplicity involved. We can divide the atomic processes which occur into three types: processes involving changes of multiplicity, processes of excitation and de-excitation, and processes of ionization and recombination. These will interconnect four groups of states: the singlet and triplet states of neutral helium and singly and doubly ionized helium. After determining the rates of these processes, we shall be able to write down and solve the equilibrium equations. The analogous problem in gaseous nebulae has already been considered by Goldberg (1941).

## II. PROCESSES INVOLVING CHANGES IN MULTIPLICITY

Since radiative processes involving changes in multiplicity are forbidden, these involve only collisions. In electron collisions with atoms it is possible, by exchange interaction, to change the multiplicity of the states involved. The cross-section for the excitation of the metastable $2^3S$ state from the ground state of helium has been calculated by Massey and Moiseiwitsch (1954), using distorted waves determined by variational methods, and measured in the laboratory by Maier-Leibnitz (1935), both results being in good agreement. The cross-section has a sharp peak at the threshold, due to the fact that the slowest electrons produce the greatest exchange effect. The highest part of the peak is too narrow to affect our problem much, so we may approximate the variation of the cross-section with energy by an exponential

$$\sigma(E) = 0.03\pi a_0^2 e^{-(E-E_0)/16\,\mathrm{ev}}, \tag{1}$$

$E_0$ being the threshold energy, and $a_0$ the Bohr radius. The number of collisional excitations per second per cubic centimeter is therefore (we designate all levels by the quantum numbers $nLS$; thus $2^3S$ is 201)

$$N_{100}N_eC_{100\text{-}201} = N_{100}N_e\int_{E_0}^{\infty} v\,f\,(v)\,\sigma\,(v)\,dv\,, \tag{2}$$

where $N_{100}$ is the number of atoms per cubic centimeter in the ground state, $N_e$ the electron density, and $f(v)$ the distribution of electron velocities. Putting in equation (1) and the Maxwellian distribution, we find

$$\begin{aligned} C_{100\text{-}201} &= 0.03\pi a_0^2 4\pi\left(\frac{m}{2\pi kT}\right)^{3/2}\int_{v_0}^{\infty} v^3\, e^{-mv^2/2kT}\, e^{-(mv^2-mv^2)/32\,\mathrm{ev}}\,dv \\ &= 8.48\times 10^{20}T^{-3/2}\beta^{-2}\left(\frac{m\beta}{2}v_0^2+1\right)\exp-\left(\frac{2.3\times 10^5}{T}+\frac{m\beta v_0^2}{2}\right), \end{aligned} \tag{3}$$

where $\beta = (1/kT + 1/16\ \mathrm{ev})$. This quantity is tabulated in Table 1.

TABLE 1

RATES OF VARIOUS PROCESSES IN HELIUM

| PROCESS | $T_e$ | | | | TO BE MULTIPLIED BY |
|---|---|---|---|---|---|
| | 25000 | 50000 | 100000 | 200000 | |
| $C_{\mathrm{II-III}}$ | $0.451\times10^{-20}$ | $1.97\times10^{-15}$ | $1.539\times10^{-12}$ | $5.16\times10^{-8}$ | $N_eN_{\mathrm{II}}$ |
| $F_{\mathrm{III-II}}$ | $1.22\times10^{-12}$ | $0.796\times10^{-12}$ | $0.447\times10^{-12}$ | $0.25\times10^{-12}$ | $N_eN_{\mathrm{III}}$ |
| $C_{100\text{-II}}$ | $2.4\times10^{-14}$ | $1.13\times10^{-11}$ | $3.4\times10^{-10}$ | $2.7\times10^{-9}$ | $N_eN_{100}$ |
| $C_{201\text{-II}}$ | $1.07\times10^{-10}$ | $5.85\times10^{-10}$ | $2.04\times10^{-9}$ | $6.45\times10^{-9}$ | $N_eN_{201}$ |
| $C_{100\text{-}201}$ | $2.03\times10^{-12}$ | $1.37\times10^{-10}$ | $8.73\times10^{-10}$ | $1.61\times10^{-9}$ | $N_eN_{100}$ |
| $C_{201\text{-}100}$ | $6.70\times10^{-9}$ | $4.55\times10^{-9}$ | $2.91\times10^{-9}$ | $1.69\times10^{-9}$ | $N_eN_{200}$ |
| $C_{100\text{-}210}$ | $6.42\times10^{-13}$ | $1.13\times10^{-10}$ | $2.13\times10^{-9}$ | $1.41\times10^{-8}$ | $N_eN_{100}$ |
| $\sum_{nL} F_{\mathrm{II}-nL0}$ | $3.51\times10^{-13}$ | $1.03\times10^{-13}$ | $0.583\times10^{-13}$ | $0.358\times10^{-13}$ | $N_eN_{\mathrm{II}}$ |
| $\sum_{nL} F_{\mathrm{II}-nL1}$ | $1.81\times10^{-13}$ | $0.882\times10^{-13}$ | $0.343\times10^{-13}$ | $0.225\times10^{-13}$ | $N_eN_{\mathrm{II}}$ |
| $F_{\mathrm{II}-6678}$ | $1.64\times10^{-14}$ | $0.81\times10^{-14}$ | $0.383\times10^{-14}$ | $0.176\times10^{-14}$ | $N_eN_{\mathrm{II}}$ |
| $F_{\mathrm{II}-5876}$ | $5.14\times10^{-14}$ | $2.53\times10^{-14}$ | $1.212\times10^{-14}$ | $0.547\times10^{-14}$ | $N_eN_{\mathrm{II}}$ |

The rate of the inverse process, collisional de-excitation, is determined by the condition that the two processes must establish a Boltzmann distribution when in equilibrium. Therefore,

$$C_{201\text{-}100} = \tfrac{1}{3}\exp\left(\frac{E_{100}-E_{201}}{kT}\right)C_{100\text{-}201}\,. \tag{4}$$

The collision rates for other intersystem transitions are unknown. The processes $2^1S \rightarrow 2^3S$ or $2^1P \rightarrow 2^3P$ may be important in populating the metastable levels, but we simply cannot guess as to their significance.

## III. PROCESSES OF EXCITATION AND DE-EXCITATION

Excitation may be produced by either absorption of radiation or electron collisions. The most significant process of excitation for $n > 2$ in the triplet series (and this process also plays a role in the singlet series) is the absorption of photospheric radiation. There

are insufficient high-energy photons in the 6000° photospheric black-body radiation to produce any effect on the ground state of helium.

The rate of absorption by an atom in state $n$ of the radiation field $u_\nu$, where $\nu$ corresponds to the frequency of the transition $n \rightarrow m$, is

$$N_n F_{nm} = N_n B_{nm} u_\nu \,. \tag{5}$$

The $B$'s are taken from the spontaneous transition probabilities computed by Goldberg (1939) and by Hylleraas (1937). For $u_\nu$ we use a black body at 6000°, with a dilution factor of $\frac{1}{2}$, which neglects limb darkening.

De-excitation is produced exclusively by spontaneous downward transitions, except when the prominence is optically deep in the line in question. As we shall see, this is not the case.

Since these two effects are the dominant ones in the triplet series, we see immediately that the triplet levels will have, relative to the $2^3S$ level, a Boltzmann distribution corresponding to a temperature of 6000° with a dilution factor of $\frac{1}{2}$. To this may be added a small correction for recombinations. The occupation number $N_{nLS}$ of the $n$th triplet level will therefore be

$$N_{nL1} = \tfrac{1}{2}\,(2L+1)\,\exp\left\{-\frac{h\nu}{8.28\times 10^{-13}}\right\} N_{203}\,. \tag{6}$$

This result can immediately be checked by observations of the relative intensities D3:10830 in prominence spectra. Use of equation (6) together with the proper transition probabilities gives 0.089 for this ratio. Measurements by Severny (1954) give the value 0.095. So, allowing for the difficulties of photometry, we must be close to the right track. This result also implies that the prominence *is not optically deep in the triplet lines*. It explains why prominences appear dark in λ 10830, even though their kinetic temperature is greater than 6000°. For certain levels (e.g., $3^3P$) photoexcitation requires ultraviolet quanta. In these cases the excitation will be given by the Boltzmann formula with a temperature equal to the radiation temperature of the pertinent part of the spectrum —say, 4500° in the near ultraviolet.

For the higher members of the triplet series the photoionization becomes comparable to the sum of all downward transition probabilities. Then the occupation number $N_{nL1}$ will be diminished by the factor

$$\left(\frac{1+F_{nL3-11}}{\sum_{n'L'} A_{nL3-n'L'3}}\right)^{-1}. \tag{7}$$

Although photospheric radiation excites the triplet states, the 6000° black body cannot effectively dig out electrons from the ground state to excite the singlet levels. This must be done by collisions. We are primarily interested in the $3^1D$ level, whence the λ 6678 transition originates. Collisions, however, will excite only P states from the $^1S$ ground state. Thus a double process must occur—first, collisional excitation of a P state and then a radiative process of some sort. Collisional excitation of the $3^1P$, $4^1P$, and higher levels is not useful, for the transition probability from these levels to $3^1D$ is very small. We must rely on collisional excitation of $2^1P$ with subsequent absorption of photospheric radiation to reach the $3^1D$ level.

There are, unfortunately, no experimental data on the cross-section $\sigma_{100-200}$, since the resulting downward transition is in the ultraviolet. But there are extensive data on the excitation of $3^1P$, $4^1P$, etc., given by Massey and Burhop (1952). Normally one would suppose that, since these are permitted transitions, their cross-sections would be proportional to the respective dipole matrix elements $1^1S-3^1P$ to $1^1S-4^1P$, which is, from Hylleraas, 2.64. The observed ratios of cross-sections obtained by Lees and Thieme and

quoted by Massey and Burhop are 4.65 by Lees and 4.76 by Thieme at 60 ev. The good agreement between the two experimental results is almost tragic; one does not wish to abandon the tried (but perhaps not altogether true) dipole form but is driven to do so. The ratio of dipole matrix elements $1^1S-2^1P/1^1S-3^1P$ is, according to Hylleraas, 5.36. Since the ratios of the experimental relative cross-sections to relative matrix elements of $1^1S-3^1P/1^1S-4^1P$ and $1^1S-4^1P/1^1S-5^1P$ are 1.8 and 2.3, we can guess that the same ratio for the lowest three states is about 1.3, and therefore

$$\sigma_{100\text{-}210} = 1.3 \times 5.36 \sigma_{100\text{-}310} = 7\,\sigma_{100\text{-}310}\,. \tag{8}$$

The cross-section $\sigma_{100\text{-}310}$ (actually Lees measures the cross-section for excitation of the $2^1S-3^1P$ transition) is quoted from Lees by Massey and Burhop. It rises almost linearly from 20 to 80 ev, peaks at 100 ev, and falls off slowly thereafter. Since we never deal with $kT > 16$ ev, the behavior of the curve after 80 ev concerns us little, and therefore we use a straight line for the cross-section. Parallel to equation (2), the rate of collisions from $1^1S$ to $2^1P$ is

$$\begin{aligned} N_e N_{100} C_{100\text{-}210} &= 7\, N_e N_{100} \int_{20\ ev}^{\infty} v\, \sigma_{100\text{-}310} f(v)\, dv \\ &= 4.67 \times 10^{-18} 4\pi \left(\frac{m}{2\pi kT}\right)^{3/2} \int_{140a/m}^{\infty} \frac{m v^2}{2a - 20} v^3 e^{-mv^2/2kT} dv \end{aligned} \tag{9}$$

$$= 4.67 \times 10^{-18} N_e N_{100} \times 4 \left(\frac{2kT}{\pi m}\right)^{1/2} e^{-20a/kT} \left(\frac{10 + kT}{a}\right), \tag{10}$$

where $a = 1$ ev $= 1.6 \times 10^{-12}$ erg. Values of $C_{100\text{-}110}$ are given in Table 1 for several temperatures.

Since this collisional excitation is by far the predominant source of electrons for $2^1P$, the number of atoms per cubic centimeter in that state will be

$$\begin{aligned} N_{210} &= \frac{N_{100} N_e C_{100\text{-}210}}{A_{210\text{-}100}} \\ &= 4.27 \times 10^{-10} C_{100\text{-}210} N_{100} N_e\,. \end{aligned} \tag{11}$$

Atoms in the $2^1P$ state absorb photospheric radiation and are raised to the $3^1D$ state, whence they radiate 6678. The rate of this process is obtained by evaluating equation (5), viz.,

$$\begin{aligned} N_{210} F_{210\text{-}320} &= N_{210} \times 2.04 \times 10^{20} \times \tfrac{1}{2} u_{6000} \\ &= 1.61 \times 10^{7} N_{210} \\ &= 6.87 \times 10^{-3} C_{100\text{-}210} N_{100} N_e\,. \end{aligned} \tag{12}$$

## IV. PROCESSES OF IONIZATION AND RECOMBINATION

Ionization of helium is produced both by electron collisions and by the photoeffect. In the singlet series the first mechanism is predominant, for almost all the electrons are in the ground state. In the triplet series the latter is most important, for the levels are accessible to the photospheric radiation flux. We also want to consider the equilibrium He II–He III.

The cross-section for collisional ionization of neutral helium is easier to measure than that of hydrogen. Mott and Massey (1949) give the experimental results of Smith. These may be closely approximated by a straight line rising from zero at 24.6 volts to 0.035 $\pi a_0^2$ at 75 volts. Then the calculation is exactly analogous to equations (9) and (10), and

(since almost all singlet electrons are in the ground state, we concern ourselves with this only) we find

$$C_{100\text{-II}} = 0.007\pi a_0^2 4\pi \left(\frac{m}{2\pi kT}\right)^{3/2} \int_{24.6\,ev} \left(\frac{m v^2}{2a - 24.6}\right) v^3 e^{-mv^2/2kT} dv \tag{13}$$

$$= 7.58 \times 10^{-13} \sqrt{T}\, e^{-24.6a/kT} \left(\frac{12.3 + kT}{a}\right),$$

$a$ again being 1 ev. This quantity is tabulated in Table 1 for various temperatures.

We have no data on the rate of collisional ionization of He II. We can, however, estimate an average cross-section of $\sigma_{\text{II-III}} = 0.01\pi a_0^2$. Then the rate of ionization will be roughly $\sigma$ times the number of electrons with energies greater than 54.4 ev times the velocity of an electron at 54.4 ev, or

$$C_{\text{II-III}} = 0.8725 \times 10^{-7} \times 0.089 \times 4.4 \times 10^8\, v\, \frac{\sqrt{54.4a}}{kT} e^{-54.4a/kT} \tag{14}$$

$$= 0.342 \times 10^{-9}\, \frac{\sqrt{54.4a}}{kT} e^{-54.4a/kT}.$$

Since almost all the He II atoms are in the ground state, we need compute ionization only from that state.

The collisional ionization from the $2^3S$ state may be computed in the same way as $C_{100\text{-II}}$. The two cross-sections will be related, approximately, as their respective dipole matrix elements to the continuum. This ratio is about 5; hence the rate of ionization by collisions from $2^3S$ is

$$N_e N_{201} C_{201\text{-II}} = 8.66 \times 10^{-13} \sqrt{T} N_e e^{-4.7a/kT} \left(2.35 + \frac{kT}{a}\right). \tag{15}$$

Here we have made a somewhat more serious error in letting the integration run to infinity. However, we shall see below that the rate of collisional ionization of the triplet states is insignificant compared to the rate of photoionization.

Photoionization of the triplet series may be treated as a hydrogenic problem, since the largest effect is in the upper levels. The absorption coefficient is

$$a_n = \frac{16\pi^2 e^6}{3\sqrt{3}h^3} \frac{Z^4}{\nu^3 n^5} 2R \tag{16}$$

$$= 0.280 \times 10^{30} Z^4 n^{-5} \nu^{-3}.$$

Since the levels are essentially hydrogenic, we let $Z = 1$. Then the rate of photoionization per atom in the $nLS$ state is

$$F_{nLS} = \tfrac{1}{2} \int \frac{c u_\nu}{h\nu} \times 0.28 \times 10^{30} Z^4 n^{-5} \nu^{-3} d\nu \tag{17}$$

$$= 0.391 \times 10^{10} n^{-5} \int_{\nu_n}^{\infty} \frac{1}{\nu} \frac{1}{e^{h\nu/kT} - 1}\, d\nu$$

$$= 0.391 + 10^{10} n^{-5} \int_{h\nu_n/kT}^{\infty} \frac{dx}{x\,(e^x - 1)}. \tag{18}$$

This integral cannot be evaluated in closed form. We may use two approximations, with $T = 6000°$. (Although the temperature of the sun is much less than 6000° in the ultraviolet, photoionization from $n = 2$, which requires ultraviolet quanta, is virtually zero. The levels of $n \geq 3$ may be ionized by infrared radiation, which is about 6000° in intensity. For $n = 2$ and $n = 3$, $h\nu_n/kT \gg 1$, and the integral is closely approximated by $-Ei(-h\nu_n/kT)$. For $n > 3$ we may use series No. 764 of Pierce (1929) and integrate

term by term. To obtain the total rate of ionization, we simply take the sum of $N_{nL3}F_{nL3\text{-II}}$ over all contributing levels, $N_{nL3}$ being taken from equations (6) and (7). The summation, carried up to $n = 30$, gives the value $18.3 \times 10^4$/atom/sec for the rate of triplet photoionizations. This number is independent of density and temperature.

We must now compute recombination rates for several cases: (*a*) recombination in the singlet and triplet series, respectively, (*b*) recombinations leading to the emission of 6678 and D3 directly, and (*c*) recombination of He III. Fortunately, all these formulae are well known.

The recombination formula is given by Cillié (1936) as

$$F_{\text{II-}nLS} = 3.29 \times 10^{-6} N_e Z^4 T^{-3/2} \frac{(2L+1)(2S+1)}{Zn^5} - Ei\left(-\frac{\chi_n}{kT}\right). \tag{19}$$

It is necessary to compute this quantity up to at least $n = 15$. Both

$$\sum_{n,L} F_{\text{II-}nL0} \quad \text{and} \quad \sum_{n,L} F_{\text{II-}nL1}$$

are given in Table 1.

To determine the recombinations and cascade to the $3^1$D and $3^3$D levels, we must consider the following: Any electron landing in a level with $L = n - 1$ will cascade through all levels of $L = n - 1$, since $\Delta L$ must equal 1; hence $\Delta n = 1$, and it cannot reach any state of $L < n - 1$ (except for transitions $\Delta n = 0$, for which the probability is quite small). Therefore, at least $(2n - 1)/n^2$ of the electrons landing in any level of $n \geq 3$ will eventually reach 3D (these arguments hold for either singlets or triplets). Furthermore, a large fraction of electrons landing in the *f*-state will preferentially cascade to 3D, because the transition to the lowest level of $\Delta L = -1$ is most probable. This fraction is, very roughly, $\frac{1}{2}$, depending on $n$. The number of electrons landing in the *f*-state, however, also includes those landing in states of $L > 4$, up to $L = n - 2$ (since we have already counted $L = n - 1$). So an additional fraction,

$$\sum_{L=4}^{n-2} \frac{1}{2} \frac{2L-1}{n^2},$$

of the electrons recombining in $n > 4$ pass through 3D. All other electrons landing in $L \leq 3$ do not reach 3D, for transition probabilities are overwhelmingly in favor of transitions with $\Delta L = -1$. Totaling everything up, it turns out that a large fraction of recombining electrons cascade to participate in the λ 6678 or λ 5876 transitions. These rates, which we designate $F_{\text{II-6678}}$ or $F_{\text{II-5876}}$, are given in Table 1.

Finally, it is necessary to compute the $F_{\text{III-II}}$, the rate of recombination from He III to He II. This poses no difficulty and is carried out by inserting the proper numbers in equation (20) and summing over a sufficient number of terms. This quantity, too, is set forth in Table 1.

## V. EQUILIBRIUM EQUATIONS

We now can write down and solve the equilibrium equations for helium, counting only processes that we have found to be important. First, we obtain the collisional ionization-recombination equilibrium between He II and He III from the equation

$$N_e N_{\text{III}} \sum_n F_{\text{III-II}n} = N_e N_{\text{II}} C_{\text{II-III}}. \tag{20}$$

The ratio He II:He III is given in Table 2.

Now we consider the three-level equilibrium between He II and the two ground levels of He I, $1^1$S and $2^3$S. The level $1^1$S receives electrons by recombinations from He II and collisional de-excitation from $2^3$S, while losing electrons by collisional ionization to He II

and by collisional excitation to $2^3S$. Therefore, the number of atoms per cubic centimeter in $1^1S$ is

$$N_{100} = \frac{N_{II}\sum_{nL} F_{II-1,nL0} + N_{201}C_{201-100}}{C_{100-II} + C_{100-201}}, \tag{21}$$

where we have canceled out the electron densities.

The $2^3S$ state receives electrons by recombination in all triplet states and by collisional excitation; it loses electrons by collisional de-excitation and ionization and by photoionization, which is far more rapid than the other two processes. Thus the number of atoms per cubic centimeter in the $2^3S$ state (actually, this is the number in all triplet states, but these are almost all in the ground state) is

$$N_{201} = \frac{N_{II}\sum_{nL} R_{II-nL1} + N_{100}C_{100-201}}{C_{201-II} + C_{201-100} + \sum_{nL} F_{nL1-II}/N_e}. \tag{22}$$

We can, therefore, obtain from equations (20), (21), and (22) the relative numbers of helium atoms in various stages of ionization and multiplicity.

TABLE 2

SOLUTION OF HELIUM EQUILIBRIUM EQUATIONS

| | $T$ | | | |
|---|---|---|---|---|
| | 25000° | 50000° | 100000° | 200000° |
| $N_{II}/N_{III}$ | $2.71\times10^{8}$ | 404 | 0.291 | 0.00484 |
| $N_{100}/N_{II}$ | 0.17 | $7\times10^{-4}$ | $4.8\times10^{-5}$ | $8.3\times10^{-6}$ |
| $N_{201}/N_{II}$ | $2.85\times10^{-18}\,N_e$ | $0.954\times10^{-18}\,N_e$ | $0.416\times10^{-18}\,N_e$ | $0.196\times10^{-18}\,N_e$ |
| 5876 emissions/cm³ | $0.861\times10^{-12}\,N_{II}N_e$ | $0.289\times10^{-12}\,N_{II}N_e$ | $0.126\times10^{-12}\,N_{II}N_e$ | $0.060\times10^{-12}\,N_{II}N_e$ |
| 6678 emissions/cm³ | $1.72\times10^{-14}\,N_{II}N_e$ | $0.86\times10^{-12}\,N_{II}N_e$ | $0.453\times10^{-14}\,N_{II}N_e$ | $0.302\times10^{-14}\,N_{II}N_e$ |
| Ratio 5876/6678 | 50.0 | 33.6 | 27.9 | 19.7 |

The solution of equations (20), (21), and (22) shows us the following: the relative amounts of $N_I$, $N_{II}$, and $N_{III}$ are determined by temperature only, since the electron density cancels out. On the other hand, the chief mechanism for depopulating the triplet series is photoionization, which is independent of density, and therefore the ratio $N_{201}/N_{II}$ is proportional to $N_e$.

The occupation number of $3^3D$ may be obtained from equation (6), with the addition of recombinations; to obtain the rate of D3 radiation, we simply multiply by the downward transition probability $A_{321-211}$. The rate of radiation of 6678 is the total number of electrons entering the $3^1D$ level and therefore is equal to the sum of equation (12) and the recombination $F_{II-6678}$. The rate of D3 emission is proportional to $N_{201}$, and therefore proportional to $N_eN_{II}$. The rate of emission of 6678, since it depends on recombinations and collisions, also is proportional to $N_eN_{II}$, and therefore the ratio D3/6678 depends on temperature only. This quantity is computed and set forth in Table 2.

## VI. DISCUSSION AND CONCLUSION

The results of Table 2 show that there is a significant change in the ratio D3/6678 with temperature. It is necessary to consider just how accurate this result is, and whether

or not it may be checked with observation. The theoretical intensity of D3 depends, first of all, on the relative populations of the $3^3D$ and $2^3S$ levels. Our theory for this has few likely flaws and gives good agreement with Severny's results. The population of $2^3S$ depends, in turn, on three factors: recombination, the collision process $C_{100-201}$, and photoionization. The recombinations come from well-known formulae, which can scarcely be in error at all. For the collisional excitation we have both experimental and theoretical data giving good agreement, so that the rate can scarcely be in error by more than a factor of 2. The photoionization is again given by a standard formula.

The theoretical intensity of 6678 comes from somewhat different sources. Recombination, which provides most of the electrons, is determined from an exact formula. The chain of processes $1^1S-2^1P-3^1D$ is not so well determined, principally because we do not have the cross-sections for $C_{100-210}$. The values we use are probably not off by more than a factor of 3, but this process is not important. Putting both errors together, we see that the maximum probable error in the D3/6678 ratio given in Table 1 is a factor of 3; but most probably the error is not more than 50 per cent. The *change* in the ratio, however, is surely very little in error, because the shapes of the various cross-section curves are better established than their absolute values.

The ratios for D3/6678 given here appear to agree fairly well with the ratio in many prominences, although precise photometry is not available. They also agree with the ratios found on eclipse plates (R. G. Athay, private communication). It will now be useful to carry out precise photometry on the spectra of prominences obtained with the coronagraph. Determination of the temperature of the prominences by Doppler profiles (Billings 1956) would enable us to check directly the results of Table 2. If our results prove correct by such a check, then we can feel that we have a reasonably good notion of the physical processes important in the helium equilibrium in the prominences and chromosphere.

It should finally be noted that we have here ignored the ionizing radiation of the corona. This could well play an important role, particularly when the temperature is low. But we know little about the exact nature of this radiation, in particular because of the variability of the corona. When we have learned more about the corona and the relation between coronal activity and prominences, then we can put in the effect of coronal ultraviolet radiation.

This work was initiated and partly completed while the author was at Harvard College Observatory, supported by the Air Force Cambridge Research Center, Geophysical Research Directorate, through contract AF 19(604)146. I am greatly indebted to Professor D. H. Menzel for support and encouragement. Work done since my arrival at High Altitude Observatory has been supported by Air Force Cambridge Research Center, Geophysical Research Directorate, under contract AF 19(604)969. I have also had valuable discussions with Professor Leo Goldberg.

## REFERENCES

Billings, D. E. 1956, *H.A.O. Solar Research Memoir*, No. 56.
Cillié, C. G. 1936, *M.N.*, **96**, 771.
Goldberg, L. 1939, *Ap. J.*, **90**, 414.
———. 1941, *ibid.*, **93**, 236.
Hylleraas, E. 1937, *Zs. f. Phys.*, **106**, 395.
Maier-Leibnitz. 1935, *Zs. f. Phys.*, **95**, 499.
Massey, H. S. W., and Burhop, E. H. S. 1952, *Electronic and Ionic Impact Phenomena* (London: Oxford University Press).
Massey, H. S. W., and Moiseiwitsch, B. L. 1954, *Proc. R. Soc. London, A*, **227**, 38.
Mott, N. F., and Massey, H. S. W. 1949, *The Theory of Atomic Collisions* (Oxford: Clarendon Press).
Severny, A. B., 1954, *Izv. Crim. Ap. Obs.*, **12**, 33.

# AN INVESTIGATION OF FAINT LINES IN THE SOLAR SPECTRUM BETWEEN 5000 A AND 6000 A

ROMUALD ZALUBAS
Georgetown College Observatory, Washington, D.C.
*Received January 4, 1956*

ABSTRACT

In the solar spectrum between 5000 and 6000 A, 234 new faint lines are recorded, and 4072 lines, which are present in the second revision of *Rowland's Table* (now in progress) have been remeasured. The present measurements have been compared with the Rowland lines retained in the second revision and with the Utrecht *Atlas*. The number of lines to be omitted as unreal makes only 1.5 per cent of the total; therefore, it is concluded that there are almost no spurious lines in the *Revised Rowland* in this interval.

The question of the reality of the faintest lines in the solar spectrum, listed in Rowland's classical paper (1895–1897), has long attracted the attention of many astronomers. It is well known that Rowland's observations at the extreme ends of his range, i.e., less than 3060 A and greater than 6600 A, were incomplete because of the inadequate sensitivity of photographic emulsions available at that time for these spectral regions (Babcock and Moore 1947; Babcock, Moore, and Coffeen 1948). Between these limits, however, it is worth while to investigate the reality of the faintest lines recorded by Jewell (1905), who measured Rowland's spectrograms. The region from 5000 to 6000 A has been selected as the present test region. The results obtained here have been compared with those in the *Revised Rowland Table* (*RRT*) (St. John *et al.* 1928), the second revision of Rowland's Table (SRRT) (Moore *et al.* unpublished), and the *Photometric Atlas of the Solar Spectrum* (Utrecht *Atlas*) (Minnaert, Mulders, and Houtgast 1940).

A 21-foot concave grating, having 20000 lines to the inch, was used. This grating was ruled by Rowland and is set up in a Wadsworth mounting at Georgetown Observatory. The plates were taken in the second order, which gives a dispersion about 1.4 A/mm. A Corning yellow-glass filter was used to cut off the radiation shorter than 4200 A. Kodak spectroscopic plates of types II F(3), III F(3), and IV F(2) were used and also a Hilger measuring engine with measuring screw 8 cm long, on which readings can be made to 0.001 mm.

The usual procedure of measuring and calculating wave lengths was adopted, as described in Glazebrook's *Dictionary of Applied Physics* (1923). The standards of solar wave lengths were taken from the *Transactions of the International Astronomical Union* (1928; see also Burns, Meggers, and Kiess 1928). The effects of orbital and diurnal motion of the earth were accounted for in the usual way (Babcock, Moore, and Hoge 1936). Necessary corrections were applied to the known terrestrial lines, because the solar standards were used. The accuracy of the wave lengths is about 0.01 A. The resulting wave lengths are mean values of measurements on three plates; only those new lines, which are present on all three Georgetown plates but not in *RRT* or SRRT, are proposed as new lines.

A detailed account of added and rejected lines is given in Table 1. Rowland's intensity scale is used throughout. The change in the number of the lines of intensity 3, 1, −1, −2, and −3 in the fourth line of the table is a result of change of estimated intensities. A small difference may exist between the SRRT data cited here and those which will be published, because work is still in progress on that table. There are, however, 224 faint lines added in the SRRT, which were not given in the *RRT*, of which 205 are present on the Georgetown plates. In addition to these new lines, 234 other faint lines have been measured here.

A review of the present identifications is given in Table 2. Counts of completely or partially identified lines have been made from the manuscript ledger of the SRRT. Although the identifications are not yet final, they are probably adequate to furnish a general picture in the selected test region. Revised molecular identifications are not yet available for inclusion in the counts. This may well explain the increasing percentage of unidentified lines with increasing faintness of the solar lines, indicated in the last row

TABLE 1

REVIEW OF NUMBERS OF LINES IN REGION 5000–6000 A

| LINES | NUMBER OF LINES OF CORRESPONDING ROWLAND INTENSITIES | | | | | | | TOTAL |
|---|---|---|---|---|---|---|---|---|
| | >3 and 3 | 2 | 1 | 0 | −1 | −2 | −3 | |
| In *RRT* | 267 | 123 | 186 | 290 | 465 | 1076 | 1555 | 3972 |
| Dropped in SRRT | ... | ... | ... | 1 | 1 | 4 | 57 | 63 |
| Added in SRRT | ... | ... | ... | ... | ... | ... | 224 | 224 |
| Total no. in SRRT | 273 | 123 | 187 | 289 | 455 | 1087 | 1719 | 4133 |
| Not detected here but present in SRRT | ... | ... | ... | ... | ... | ... | 61 | 61 |
| New lines present on Georgetown plates | ... | ... | ... | ... | ... | 12 | 222 | 234 |
| Total no. present on Georgetown plates | 273 | 123 | 187 | 289 | 455 | 1099 | 1880 | 4306 |

TABLE 2

REVIEW OF IDENTIFICATIONS IN REGION 5000–6000 A

| LINES | NUMBER OF LINES OF CORRESPONDING ROWLAND INTENSITIES | | | | | | | TOTAL |
|---|---|---|---|---|---|---|---|---|
| | >3 and 3 | 2 | 1 | 0 | −1 | −2 | −3 | |
| Identified in *RRT* | 267 | 122 | 178 | 254 | 303 | 642 | 539 | 2305 |
| Atomic identified in *RRT* | 248 | 109 | 138 | 187 | 212 | 362 | 259 | 1515 |
| Per cent atomic identified since 1928 | 1.6 | 0.9 | 5.0 | 3.2 | 2.7 | 27.2 | 35.9 | 17.5 |
| Per cent identified in SRRT (revised molecular identifications not included) | 99.3 | 92.2 | 99.0 | 90.3 | 79.4 | 67.2 | 32.9 | 58.9 |
| Per cent unidentified | 0.7 | 0.8 | 1.0 | 9.7 | 20.6 | 32.8 | 67.1 | 41.1 |

of Table 2. The number of identified atomic lines has been increased by 17.5 per cent since 1928.

In Table 3 there are listed 234 new lines which have been measured on Georgetown plates and not recorded in the SRRT. In the Utrecht *Atlas* 165 of these lines are detectable. Seventeen of them were listed in the *RRT* but are rejected in the SRRT. None of these lines coincides with calculated Rowland's ghosts. The first column of Table 3 contains the integral parts of the wave lengths in angstrom units. The second contains the decimal parts of the wave lengths as observed at Georgetown. In the third column are

TABLE 3

NEW LINES OBSERVED IN REGION 5000–6000 A

| Wave Length (A) | Decimal of Observed Wave Length | | | Estimated Intensity | Wave Length (A) | Decimal of Observed Wave Length | | | Estimated Intensity |
|---|---|---|---|---|---|---|---|---|---|
| | Georgetown | Rowland | Utrecht | | | Georgetown | Rowland | Utrecht | |
| 5004 | .630 | | .58–.66 | –3 | 5492 | .566 | | | –3 |
| 5007 | .922 | | .88–.94 | –3 | 5507 | .951 | | .95 | –3 |
| 5008 | .809 | | .79–.84 | –3 | 5509 | .331 | | .25–.33 | –3 |
| 5015 | .787 | | .70–.90 | –3 | 5518 | .980 | | .97 | –3 |
| 5024 | .376 | | .36 | –3 | 5524 | .108 | | .11 | –3 |
| 5030 | .237 | | | –3 | 5526 | .313 | | .30 | –3 |
| 5043 | .988 | | .99 | –2 | 5528 | .700 | | | –3 |
| 5065 | .561 | | | –3 | 5529 | .467 | | .47 | –3 |
| 5066 | .984 | | .98 | –3 | 5530 | .086 | | .05 | –3 |
| 5067 | .335 | | .35 | –3 | 5531 | .444 | | .42–.50 | –3 |
| 5093 | .050 | .050 | .05 | –3 | 5541 | .908 | | .92 | –3 |
| 5110 | .171 | | .16 | –3 | 5548 | .617 | | .62 | –3 |
| 5134 | .855 | | .79–.95 | –3 | 5561 | .718 | | .72 | –3 |
| 5176 | .345 | | | –3 | 5571 | .228 | | .15–.25 | –3 |
| 5182 | .602 | .594 | | –3 | 5571 | .718 | | .71 | –3 |
| 5187 | .701 | | | –3 | 5582 | .573 | | .57? | –3 |
| 5229 | .473 | | .47? | –3 | 5583 | .269 | | .26 | –3 |
| 5237 | .980 | | | –3 | 5584 | .922 | | .91 | –3 |
| 5244 | .426 | | | –3 | 5591 | .534 | | .54? | –3 |
| 5245 | .120 | | .12–.20? | –3 | 5591 | .650 | | .66 | –3 |
| 5251 | .728 | | | –3 | 5596 | .591 | | .60 | –3 |
| 5252 | .325 | | | –3 | 5597 | .471 | | .45–.50 | –3 |
| 5267 | .822 | | | –3 | 5599 | .147 | | .15 | –3 |
| 5270 | .746 | | .70–.75 | –3 | 5599 | .464 | | .46 | –3 |
| 5272 | .692 | | | –3 | 5600 | .695 | | .69–.74 | –3 |
| 5286 | .745 | | | –3 | 5604 | .099 | | .96–.99 | –3 |
| 5296 | .972 | | | –3 | 5610 | .601 | | .59 | –3 |
| 5299 | .338 | | .35–.40 | –3 | 5611 | .056 | | .05 | –3 |
| 5307 | .789 | | .75–.92 | –3 | 5611 | .988 | | | –3 |
| 5314 | .075 | | | –3 | 5621 | .797 | | .80 | –3 |
| 5325 | .386 | .391 | .39 | –3 | 5623 | .375 | | .25–.35 | –3 |
| 5330 | .742 | | | –3 | 5626 | .422 | | .42 | –3 |
| 5345 | .370 | | .37 | –2 | 5629 | .564 | | | –3 |
| 5353 | .170 | .164 | .16 | –3N | 5630 | .482 | | | –3 |
| 5372 | .273 | | .25 | –3 | 5634 | .351 | | .35 | –3 |
| 5372 | .642 | | .63 | –3 | 5634 | .874 | | .84–.88 | –3 |
| 5386 | .100 | .104 | | –3 | 5638 | .605 | | .61? | –3 |
| 5388 | .166 | .163 | .17? | –3 | 5639 | .064 | | .06 | –3 |
| 5389 | .309 | .307 | .31 | –3 | 5642 | .916 | | .92 | –3 |
| 5392 | .154 | | .15 | –2 | 5645 | .292 | | .29 | –3 |
| 5395 | .863 | | .86 | –3 | 5646 | .963 | | .96 | –3 |
| 5413 | .410 | .412 | | –3 | 5649 | .245 | | | –3 |
| 5427 | .024 | | .00–.08 | –3 | 5652 | .192 | | .20 | –3 |
| 5438 | .925 | | .92 | –3 | 5653 | .514 | | .51? | –3 |
| 5443 | .907 | .902 | .91 | –3 | 5654 | .380 | | .29–.42 | –2 |
| 5444 | .237 | | | –3 | 5654 | .663 | | .66 | –3 |
| 5447 | .366 | | .30–.37 | –3 | 5656 | .019 | | | –3 |
| 5458 | .558 | | .52 | –3 | 5665 | .766 | | .70–.77 | –3 |
| 5461 | .144 | .146 | | –3N | 5666 | .219 | | | –3 |
| 5464 | .473 | .476 | .42–.50 | –3 | 5671 | .267 | | .25–.32 | –3 |
| 5469 | .179 | | .18? | –3 | 5676 | .105 | | .05–.15 | –3 |
| 5469 | .763 | .763 | .77 | –3 | 5676 | .186 | | | –3 |
| 5471 | .409 | .398 | .40 | –3 | 5682 | .809 | | .81 | –3 |
| 5471 | .926 | .926 | .91–.00 | –3 | 5687 | .322 | | .28–.32 | –3 |
| 5476 | .745 | .745 | | –3 | 5688 | .872 | | .87 | –3 |
| 5479 | .614 | | .62? | –3 | 5690 | .811 | | .81 | –3 |
| 5488 | .772 | | .77 | –3 | 5690 | .957 | | .96 | –3 |
| 5489 | .111 | | .11 | –3 | 5691 | .143 | | .15 | –3 |

TABLE 3—*Continued*

| Wave Length (A) | Decimal of Observed Wave Length | | | Estimated Intensity |
|---|---|---|---|---|
| | Georgetown | Rowland | Utrecht | |
| 5691 | .335 | ... | .32 | −3 |
| 5692 | .136 | ... | 13 | −3 |
| 5693 | .770 | ... | .70–.80? | −3 |
| 5693 | .952 | ... | ... | −3 |
| 5696 | .499 | ... | ... | −2 |
| 5703 | .882 | .88 | .87 | −2 |
| 5706 | .533 | ... | .53? | −2 |
| 5710 | .297 | ... | .30 | −3 |
| 5710 | .494 | ... | .45–.54 | −3 |
| 5713 | .684 | ... | .68? | −3 |
| 5716 | .723 | ... | .61–.71 | −2 |
| 5718 | .763 | ... | .76–.82 | −3 |
| 5728 | .336 | ... | .33 | −3 |
| 5730 | .141 | ... | .14 | −3 |
| 5738 | .724 | ... | .73–.80 | −3 |
| 5741 | .400 | ... | .41 | −3 |
| 5744 | .732 | ... | .75 | −3 |
| 5744 | .864 | ... | .87 | −2 |
| 5746 | .992 | ... | .99 | −3 |
| 5749 | .485 | ... | .45–.50 | −3 |
| 5750 | .830 | ... | .85 | −3 |
| 5751 | .615 | ... | .61 | −3 |
| 5752 | .445 | ... | ... | −3 |
| 5752 | .719 | ... | .72–.76 | −3 |
| 5752 | .951 | ... | .95 | −3 |
| 5757 | .267 | ... | ... | −3 |
| 5757 | .554 | ... | ... | −2 |
| 5759 | .924 | ... | .93 | −3 |
| 5760 | .116 | ... | ... | −3 |
| 5765 | .329 | ... | .33 | −3 |
| 5765 | .578 | ... | .55 | −3 |
| 5766 | .118 | ... | .12 | −3 |
| 5770 | .305 | ... | .30 | −3 |
| 5776 | .978 | ... | .97 | −3 |
| 5778 | .635 | ... | .58 | −3 |
| 5779 | .098 | ... | .09 | −3 |
| 5784 | .198 | ... | .18 | −2 |
| 5784 | .520 | ... | ... | −3 |
| 5786 | .306 | ... | .29 | −3 |
| 5793 | .275 | ... | .20–.27 | −3 |
| 5794 | .078 | ... | ... | −3 |
| 5798 | .771 | ... | .77 | −3 |
| 5801 | .072 | ... | ... | −2 |
| 5802 | .874 | ... | .87 | −3 |
| 5806 | .960 | .960 | .96 | −3 |
| 5810 | .155 | ... | ... | −3 |
| 5810 | .378 | ... | .39 | −3 |
| 5814 | .415 | ... | ... | −3 |
| 5821 | .534 | ... | ... | −3 |
| 5823 | .956 | ... | .95 | −3 |
| 5825 | .476 | ... | ... | −3 |
| 5828 | .639 | ... | ... | −3 |
| 5829 | .147 | ... | .10–.14 | −3 |
| 5836 | .925 | ... | .93 | −3 |
| 5840 | .586 | ... | .60–.65 | −3 |
| 5841 | .046 | ... | .05 | −3 |
| 5850 | .431 | ... | .43 | −2 |
| 5855 | .688 | ... | ... | −3 |
| 5857 | .048 | ... | ... | −3 |
| 5857 | .608 | ... | .60 | −3 |
| 5859 | .747 | ... | .75? | −3 |
| 5860 | .379 | ... | .38 | −3 |
| 5860 | .639 | ... | .64 | −3 |
| 5861 | .483 | ... | ... | −3 |
| 5862 | .012 | ... | .02 | −3 |
| 5862 | .977 | ... | .98? | −3 |
| 5865 | .026 | ... | .96–.05 | −3 |
| 5865 | .273 | ... | ... | −2 |
| 5867 | .248 | ... | .25 | −3 |
| 5868 | .442 | ... | .46 | −3 |
| 5872 | .939 | ... | .94 | −3 |
| 5886 | .537 | ... | .51 | −3 |
| 5886 | .883 | ... | ... | −3 |
| 5888 | .557 | ... | ... | −3 |
| 5898 | .883 | ... | .88 | −3 |
| 5899 | .772 | ... | .77 | −3 |
| 5912 | .841 | ... | .84 | −3 |
| 5919 | .958 | ... | .96? | −3 |
| 5921 | .480 | ... | ... | −3 |
| 5923 | .753 | ... | .76 | −3 |
| 5924 | .121 | ... | ... | −3 |
| 5924 | .409 | ... | ... | −3 |
| 5931 | .279 | ... | .24 | −3 |
| 5934 | .840 | ... | ... | −3 |
| 5935 | .014 | ... | ... | −3 |
| 5936 | .674 | ... | .67 | −3 |
| 5937 | .635 | ... | ... | −3 |
| 5939 | .626 | ... | .62 | −3 |
| 5940 | .258 | ... | ... | −3 |
| 5944 | .091 | ... | ... | −3 |
| 5944 | .458 | ... | ... | −3 |
| 5946 | .181 | ... | .19 | −3 |
| 5950 | .687 | ... | ... | −3 |
| 5955 | .290 | ... | .29 | −3 |
| 5957 | .707 | ... | .70 | −3 |
| 5960 | .869 | ... | ... | −3 |
| 5963 | .708 | ... | .71 | −3 |
| 5963 | .983 | ... | .98 | −3 |
| 5964 | .281 | ... | .26 | −3 |
| 5964 | .800 | ... | .80 | −3 |
| 5965 | .659 | ... | ... | −3 |
| 5966 | .821 | ... | ... | −3 |
| 5969 | .370 | ... | .35 | −3 |
| 5970 | .824 | ... | ... | −3 |
| 5972 | .110 | ... | .00–.12 | −3 |
| 5973 | .628 | ... | .62 | −3 |
| 5974 | .033 | ... | ... | −3 |
| 5977 | .970 | ... | .98 | −3 |
| 5979 | .009 | ... | .01? | −3 |
| 5979 | .580 | ... | .59–.69 | −3 |
| 5979 | .812 | ... | ... | −3 |
| 5983 | .186 | ... | ... | −3 |
| 5985 | .911 | ... | ... | −3 |
| 5986 | .329 | ... | .32 | −3 |
| 5989 | .812 | .81 | ... | −3 |
| 5992 | .494 | ... | .49 | −3 |
| 5997 | .952 | ... | ... | −3 |
| 5999 | .860 | ... | .85 | −3 |

listed the decimal parts of those wave lengths which were given in the *RRT* but dropped in the SRRT. The fourth column contains the estimated wave lengths from the Utrecht *Atlas;* the fifth, the estimated intensities of these lines.

The present measurements have been compared with the Rowland lines retained in the SRRT and with the Utrecht *Atlas*. Observations made with three different gratings have, therefore, been studied, and consequently the likelihood of ghosts is minimized. In each of the recent investigations there are many more lines to be added than omitted. An increase in the number of lines is to be expected, because higher-sensitivity and higher-resolution techniques enable us to resolve close doublets. It is also to be expected that still fainter lines will be measured. The number of lines to be omitted as unreal makes up only 1.5 per cent of the total, which is unimportant and indicates that there are almost no spurious lines in this region of the *RRT*. The reality of the new lines observed at Georgetown should be confirmed by observers using different gratings. It is hoped that the present results will stimulate further similar investigations in this important phase of solar spectrum work.

I am very grateful to Dr. C. C. Kiess for suggesting this investigation and for his helpful advice. I am also grateful to Dr. F. J. Heyden, S.J., for his help and interest. I should like also to thank Mrs. C. E. Moore-Sitterly for use of unpublished data of the second revision of *Rowland's Table* and for the valuable suggestions she has made.

## REFERENCES

Babcock, H. D., and Moore, C. E. 1947, *The Solar Spectrum, 6600 to 13495* ("Carnegie Institution of Washington Publications," No. 579).
Babcock, H. D., Moore, C. E., and Coffeen, M. F. 1948, *Ap. J.*, **107**, 187; *Mt. W. Contr.*, No. 745.
Babcock, H. D., Moore, C. E., and Hoge, W. P. 1936, *Ap. J.*, **83**, 21; *Mt. W. Contr.*, No. 534.
Burns, K., Meggers, W. F., and Kiess, C. C. 1928, *Standard Solar Wave Lengths (3592–7148)* ("Nat. Bur. Standards Res. Papers," Vol. **1**, No. 11).
Glazebrook, R. 1923, *Dictionary of Applied Physics* (London: Macmillan).
Jewell, L. E. 1905, *Ap. J.*, **21**, 28.
Minnaert, M., Mulders, G. F. W., and Houtgast, J. 1940, *Photometric Atlas of the Solar Spectrum* (Utrecht: Utrecht Observatory).
Moore, C. E., Minnaert, M., and his collaborators, now preparing the second revision of *Rowland's Table of the Solar Spectrum*.
Rowland, H. A. 1895–1897, *Ap. J.*, Vols. **1–5**.
St. John, C. E., Moore, C. E., Ware, L. W., Adams, E. F., Babcock, H. D. 1928, *Revision of Rowland's Preliminary Table of Solar Spectrum Wavelengths with an Extension to the Present Limit of Infra-red* ("Carnegie Institution of Washington Publications," No. 396).
*Transactions of the International Astronomical Union*, **3**, 93, 1928.

# NOTES

## ON THE SPACE REDDENING OF DELTA CEPHEI AND ETA AQUILAE

In an earlier note (Harris 1954) it was suggested that the peculiarities in the six-color observations of $\eta$ Aquilae as observed by Stebbins, Kron, and Smith (1952) could be explained by assuming a small amount of interstellar reddening. In particular, it was noted that at phase $0.05P$ the colors of $\delta$ Cephei agreed very well with those of $\alpha$ Persei, a normal F5 I*b* star. It was also shown that the colors of $\eta$ Aquilae at phase $0.00P$ agreed

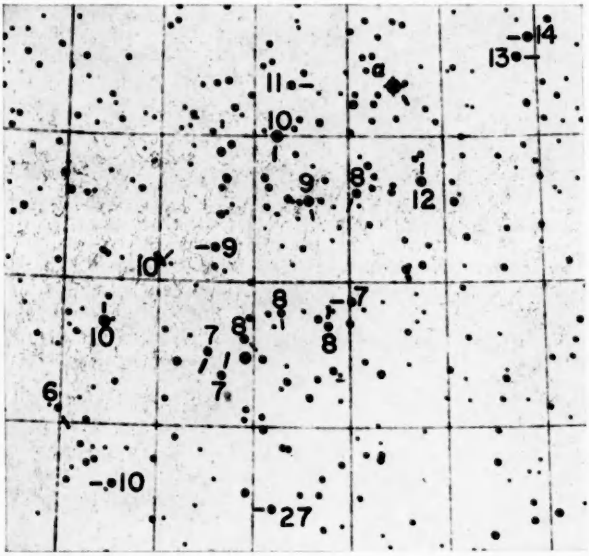


FIG. 1.—The region of $\alpha$ Persei. Color excesses of members earlier than A0 are given in hundredths of a magnitude.

well with $\alpha$ Persei, if the assumption was made that $\eta$ Aquilae was reddened by 0.32 mag. on the $V - I$ scale. This indicated a total visual absorption of 0.3 mag., assuming that $\delta$ Cephei and $\alpha$ Persei were unreddened.

From a recent photometric investigation on the $\alpha$ Persei cluster (Harris 1956) it was found that the color excesses of the B stars varied quite uniformly over the region. These are shown on a section of the *BD* chart, Figure 1, and it is seen that our estimate of 0.12 mag. for $\alpha$ Persei appears to be quite well determined.

We were probably overly optimistic in considering $\delta$ Cephei and $\alpha$ Persei to be unreddened, a fact which should have been obvious from Roman and Morgan's (1950) discussion of the $E_1$ color excesses, and the conclusions in our earlier paper should be modified to allow for a total visual absorption of about 0.4 mag. for $\delta$ Cephei and 0.7 mag.

for $\eta$ Aquilae. The color excesses on the $V - I$ scale are very nearly the same as the total visual absorption, so that the color temperatures are significantly affected, as well as the zero point of the period-luminosity relation.

The appreciable space reddening obtained for one of the apparently brightest supergiants, $\alpha$ Persei, indicates that probably the other brightest supergiants are similarly affected, and it would be desirable to determine their color excesses in a similar manner. Unfortunately, very few cases of membership of intermediate-type supergiants in clusters exist. However, an estimate of the color excess might be obtained by studying the color excesses of the F-type stars between us and the star in question, using the technique developed by Strömgren (1954). Such a technique might well be carried out for the brighter cepheids used in the establishment of the zero point of the period-luminosity relation as well.

DANIEL L. HARRIS III

YERKES OBSERVATORY
WILLIAMS BAY, WISCONSIN

REFERENCES

Harris, D. L. III. 1954, *Ap. J.*, **119**, 297.
———. 1956, *ibid.*, **123**, 371.
Roman, N. G., and Morgan, W. W. 1950, *Ap. J.*, **111**, 426.
Stebbins, J., Kron, G. E., and Smith, J. L. 1952, *Ap. J.*, **115**, 292.
Strömgren, B. 1954, *A.J.*, **59**, 193.

## POLARIZATION IN THE JET OF MESSIER 87

It has been suggested by several investigators (Manchester Symposium 1955) that the synchrotron mechanism which beautifully explains the radiation and polarization of the continuum of the Crab Nebula (Oort and Walraven 1956) is also operative in the curious jet of Messier 87 (for discussion and illustration of the jet see Baade and Minkowski 1954). The main arguments for this suggestion are the following: Like the Crab Nebula, Messier 87 is a well-known radio source. There is every reason to believe that the remarkable jet is a part of the radio emitter. As in the amorphous mass of the Crab Nebula, the jet in Messier 87 emits a blue continuum without any absorption or emission lines. It remained only to show that the light of the jet, like the Crab continuum, is strongly polarized. Two sets of exposures which I obtained last month at the prime focus of the 200-inch telescope prove, indeed, that the light of the jet is strongly polarized.

The two sets of exposures were obtained on March 15 and 16, 1956. Each consists of four exposures, with maximum transmission of the electric vector in position angles 200°, 245°, 290°, and 335° (the position angle of the jet itself is 290°). Exposure times for the first set were 3 minutes; for the second, 6 minutes. Each plate contained two exposures, and the two plates of each set were developed together. Blue-sensitive 103*a*-O plates behind a Schott GG-13 filter were used. The analyzer was a glass-laminated polaroid filter of the HN-32 type.

Both sets of plates clearly show the polarization of the three strong condensations which lie at the end of the jet (Fig. 1). The thin jet itself is too faint on my plates. In the description of the results in Table 1, I have called the innermost of the three condensations "A," the next "B," and the outermost "C." A and B form a close pair and tend to merge into one elongated image when the seeing gets poor.

It is evident from the description in Table 1 that condensations A and C are brightest when the plane of the electric vector lies between position angles 290° and 335°, a direction which nearly coincides with that of the jet. The polarization of condensation B does not seem to be in agreement with that of A and C, since it reaches its maximum

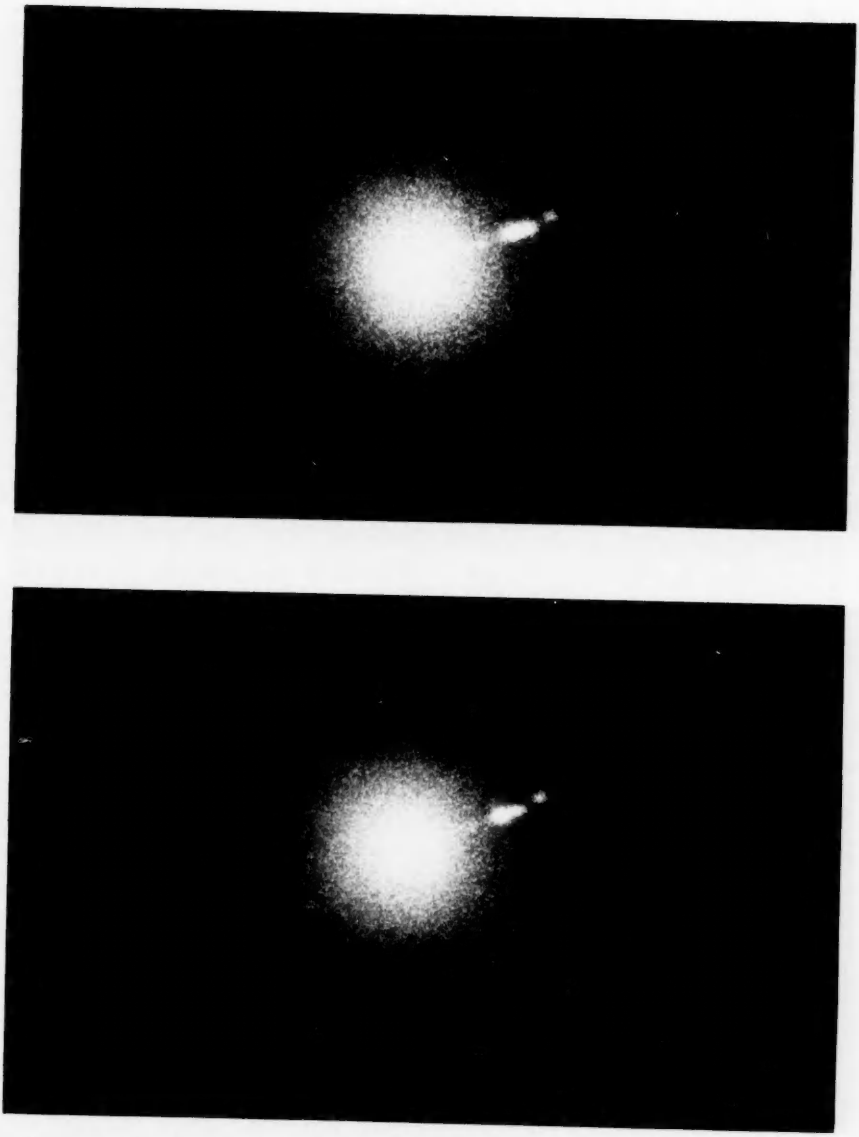

FIG. 1.—*Upper picture*: maximum transmission of electric vector in position angle 200°. *Lower picture:* maximum transmission of electric vector in position angle 290°.

intensity between position angles 200° and 245°. It is difficult to estimate on the present plates the amount of the polarization for the three condensations. However, I would guess that for A it is of the order of 30 per cent. Obviously, plates obtained under the best seeing conditions are required in order to derive quantitative data for condensations A and B. Attempts are being made at the present time by Dr. W. A. Baum to measure photoelectrically the polarization of condensation C.

TABLE 1

POLARIZATION IN THE JET OF MESSIER 87

| Position Angle of Maximum Transmission of Electric Vector by Polaroid | Description |
|---|---|
| 200° | A and B nearly equal (A perhaps 0.15 mag. brighter than B); C faint (about 0.5 mag. fainter than B) |
| 245° | Difference in brightness between A and B somewhat larger; C has brightened up by about 0.25 mag. |
| 290° | A now considerably (0.6 mag.) brighter than B; A has clearly increased in brightness, B has faded; C has further increased in brightness and is now brighter than B |
| 335° | Relative brightness of A and B nearly the same as for position angle 290°; C nearly equal to B |

W. BAADE

MOUNT WILSON AND PALOMAR OBSERVATORIES

REFERENCES

Baade, W., and Minkowski, R. 1954, *Ap. J.*, **119**, 221.
Oort, J. H., and Walraven, J. H. 1956, *B.A.N.*, No. 462.
*Proceedings of Manchester Symposium on Radio Astronomy*, 1955 (in press).

# ABSTRACTS OF ASTROPHYSICAL JOURNAL SUPPLEMENT SERIES

Supplement No. 21, Volume II

## STELLAR SPECTRA IN MILKY WAY REGIONS. V. A REGION IN MONOCEROS. VI. A REGION IN CAMELOPARDALIS

S. W. McCuskey
Warner and Swasey Observatory, Case Institute of Technology, Cleveland, Ohio

Observational data on spectral class, photographic magnitude, and red color index are given for two areas in the Milky Way. The first is in Monoceros, designated as LF9, at R.A. $6^h51^m$; Dec. $1°.3$; $l = 182°$; $b = +2°$, and contains 2290 stars. The second is in Camelopardalis, designated as LF6, at R.A. $3^h51^m$; Dec. $+56°.8$; $l = 114°$; $b = +4°$, and contains 929 stars. These are two of the regions surveyed in the program of the Warner and Swasey Observatory for studies of the stellar-luminosity function.

Identification charts and a catalogue of the data are presented for each region. The blue-red color indices have been determined photographically but are based on magnitude sequences which were established photoelectrically. The plates used were Kodak 103*a*-E and a No. 22 Wratten filter for the red magnitudes and Kodak II*a*-O for the blue magnitudes. The probable errors in each system are about $\pm 0.05$ mag. for a final determination. Analyses of the data for these two regions have been given by McCuskey (1952, 1954).

### REFERENCES

McCuskey, S. W. 1952, *Ap. J.*, **115**, 479.
———. 1954, *ibid.*, **120**, 139.

## ANNOUNCEMENT

### *A TABLE OF SOLAR SPECTRUM WAVE LENGTHS, 11984 A TO 25578 A*

The present volume (published by the University of Michigan Press) supplements and expands the solar-spectrum data previously published in the *Photometric Atlas of the Near Infrared Solar Spectrum* (University of Michigan Press, 1950; $10.00). Detailed identifications have been attempted for all lines, both solar and terrestrial in origin.

## ERRATA

In *Ap. J.*, **102**, 496, 1945, the following corrections should be made in Table 1. *For* Q 4257, *read* Q 4317; *for* Q 4317, *read* Q 4257; *for* Q 4369, *read* Q 4349; and *for* G 4845, *read* G 4945. The other tabular entries will then be correct as they are printed. I am indebted to Dr. J. A. Pearce for pointing out these errors.

Armin J. Deutsch

On page 442, Volume **115**, in Table 5, line 12, *for* $b = -33$ to $+8$ *read* $b = -3$ to $+8$.

On page 443 in Figure 4, *for* ordinate values $^{A}2$ and $^{A}4$ *read* $^{m}2$ and $^{m}4$.

*The Second Volume in a Distinguished Series*

# THE EARTH AS A PLANET

## The Solar System—Volume II

*Edited by* GERARD P. KUIPER

This is the second of four volumes designed to collect and systematize our knowledge of the solar system. Like its predecessor, *The Sun*, it is conceived as both a reference book for the specialist and a source of general information for the general reader with some knowledge of the physical sciences.

Consisting of authoritative articles written by internationally eminent specialists, *The Earth as a Planet* is a complete and fully documented handbook, covering the entire range of physics, geochemistry, oceanography, and biochemistry as they apply to the earth in its planetary aspect. Among the many topics treated are the rotation of the earth; the nature of the earth's interior; the growth of continents; current systems of oceans and atmospheres; the life-cycles of methane, carbon dioxide, oxygen, and nitrogen; the absorption spectrum of the atmosphere; the physics and chemistry of the upper atmosphere; and the appearance of the earth from interplanetary space.

*Contributions by*

SIR HAROLD SPENCER JONES
FRED L. WHIPPLE
J. TUZO WILSON
D. R. BATES
HORACE R. BYERS
LEO GOLDBERG
SIR EDWARD BULLARD
A. B. MEINEL
BRIAN MASON
CLYDE T. HOLLIDAY
ANDRÉ DANJON
SIR HAROLD JEFFREYS
J. W. CHAMBERLAIN
H. U. SVERDRUP
M. NICOLET
G. E. HUTCHINSON

*752 pages* *$12.50*

The remaining two volumes in the series will consist of *Planets and Comets, Part 1, Planets and Satellites* and *Planets and Comets, Part 2, Minor Planets, Meteorites, Comets, Origin of the Solar System.*

*from your bookseller or from*

THE UNIVERSITY OF CHICAGO PRESS

5750 ELLIS AVENUE CHICAGO 37, ILLINOIS

## THE ASTROPHYSICAL JOURNAL SUPPLEMENT SERIES

These *Supplements* are intended to provide a medium for the publication of extensive investigations, such as wave-length lists of stars of special interest, photometric data, results of numerical integrations pertaining to stellar interiors, model stellar atmosphere calculations, and original memoirs.

*Supplement No. 21*

"Stellar Spectra in Milky Way Regions"
V. A Region in Monoceros
VI. A Region in Camelopardalis

S. W. McCuskey

Spectral class data, photographic magnitudes, and blue-red color indices for 3219 stars in two areas of the Milky Way are presented in tabular form with identification charts. The limiting magnitude is about 12.3 and the areas cover 32.6 square degrees. (Published March 1956. Price $1.25)

*Subscriptions*

$8.00 per volume
Canada, $8.75. Foreign, $9.50.
To members of the American Astronomical Society, $6.00 per volume. Orders now accepted.

THE UNIVERSITY OF CHICAGO PRESS
5750 ELLIS AVENUE CHICAGO 37, ILLINOIS

# THE OBSERVATORY

**FOUNDED 1877**

* * *

A Magazine presenting current developments in Astronomy by means of Articles, Correspondence, Notes on discoveries and Reviews of important astronomical books. The papers read at the Meetings (Astronomical & Geophysical) of the Royal Astronomical Society and the discussions which follow are also fully reported.

* * *

*Annual subscription for 6 issues, post free, £1 (U.S.A. and Canada, $3.00) should be sent to*

*The Editors,* ROYAL GREENWICH OBSERVATORY
Herstmonceux Castle, Hailsham, Sussex, England